UNIVERSITY COLLEGE LONDON
Department of Chemical Engineering

Particle Engineering via Sonocrystallization: The Aqueous Adipic Acid System

OLGA NARDUCCI

Thesis Submitted to University College of London for the Degree of Doctor of Philosophy

October 2012

Supervisor: Professor A.G. Jones

I, Olga Narducci confirm that the work presented in this thesis is my own. Where information has been derived from other sources, I confirm that this has been indicated in the thesis.

Abstract

Many of the companies involved in powder processing are seeking to improve their economic performance via improved control of the physical properties of their products. Pharmaceutical manufacturers, for example, are considering the potential benefits of moving from batch to continuous operations to improve consistency. Furthermore, in recent years interest in the application of ultrasound to crystallization has received a significant impetus with the increased requirement to prepare complex chemical entities to very exacting standards. Literature reports about sonocrystallization indicate several interesting benefits, including superior crystal habit, purer and easily handled product, narrowed crystal size distribution, and prolific nucleation. The sonocrystallization literature, however, mainly focuses on batch crystallization operations, with less information relating to continuous crystallization processes.

The present thesis concerns an evaluation of the use of ultrasonic technology during batch and continuous crystallization of adipic acid crystals and compares it with common industrial operations for product particle engineering.

Firstly, the effect of a continuous sonication on a continuous crystallization process has been investigated. Cooling crystallization of adipic acid from aqueous solution is the selected case study. Analogous experiments have been carried out both under silent and continuous insonation regimes in order to investigate the effects of sonication on the time required to reach the steady state, particle size distribution (PSD), solids yield, and crystal habit. The results reveal that under continuous ultrasonic irradiation the steady state particle size distribution is achieved after shorter times than in silent continuous crystallization experiments. Continuous crystallization with ultrasonic irradiation results in significantly smaller crystal sizes, reduced agglomeration and an improved habit of crystals with highly reproducible product characteristics. Furthermore, the product yield is increased.

The crystallization kinetics, focused on both the nucleation and growth rates, has been determined using the continuous Mixed-Suspension Mixed-Product-Removal (MSMPR) crystallizer model. Kinetics have been extracted sequentially from experimental data relating the particle size distribution, using the Population Balance Equation (PBE) in terms of moments, and evaluating the effect of mean residence time,

supersaturation at steady state and ultrasonic power amplitude on the growth and nucleation rates. Application of ultrasound resulted in the most pronounced effects on the nucleation process, with rates increased by one order of magnitude with the results without sonication. The Mydlarz and Jones three parameters (MJ3) model for size dependent growth fits the non-linearity in the insonated experimental population density data for crystal sizes up to 10 μm. For larger sizes, whereas the population density plot is linear, the growth rate is deemed to be independent of crystal size.

Further analysis of the kinetics of nucleation and growth at steady state, in continuous crystallization under continuous insonation, has been developed using the commercially available software package PARSIVAL based on the fully adaptive Galerkin h-p method. The population balance has been modeled with secondary nucleation and a growth rate depending on both supersaturation and particle size, according to the MJ3 model. Numerically derived results from the population balance modelled with PARSIVAL are in reasonable agreement with experimental observations, in terms of population density values.

The use of ultrasound in the particle engineering of micron scale adipic acid crystals has been implemented by evaluating its size reducing power compared with the product of industrially established milling processes. Specifically, the steady state particles characteristics of a continuous operation under ultrasonic irradiation and the final product characteristics of batch cooling crystallization under continuous ultrasonic have been compared with hammer milling, micronization, and High Shear Wet Milling (HSWM). Ultrasound applied to batch and continuous crystallization produces particle sizes comparable with those from micronization. Continuous insonation during batch crystallization provides spherical particles, with regular surface roughness and highly reproducible results.

The use of ultrasound in the crystal product engineering has been addressed to the achievement of large particles by generating seeds crystals in-situ by means of controlled primary nucleation; the results were compared with the product of conventionally seeded crystallization.

Seeded batch cooling crystallization of adipic acid from aqueous solution has been investigated to determine the effects of the method used to produce seeds and optimize

seeding load, cooling rate, initial concentration, and supersaturation at seeding to achieve large particle sizes and mono-modal crystal size distribution.

Finally, the analysis of final particle size distributions and particle surface characteristics has demonstrated that seed crystals generated in-situ by ultrasound offer advantages comparable with conventionally inoculated seeds, eliminating the need of previous preparation and selection of seeds and the drawbacks associated with seed handling and selection of a suitable inoculation time.

Acknowledgements

I would like to thank Professor Alan Jones for his immense support throughout this PhD project: his constant encouragement to think freely and propose ideas has boosted my confidence. I feel profoundly grateful to him for all the opportunities he has offered me during my research.

I am very grateful to the Material Science team in Pfizer Pharmaceutical, Sandwich, Kent (UK) for the opportunity to collaborate with an outstanding group of scientist, for their useful advice in developing this work, and for the warm hospitality during my industrial placement during summer 2009

I owe many thanks to Dr. Paola Lettieri and Dr.Luca Mazzei for their precious guidance, the stimulating exchanges of ideas and all their good advices during my PhD.

I would like to express my gratitude to Simon Barrass and Mike Gorecki for their invaluable technical support to my research project and for providing constructive suggestions.

Many thanks also to my fellow PhD colleagues and friends, in particular Miguel, Achilleas and Valentina, who make particularly enjoyable my time at UCL, and shared joy and despair during these years.

I gratefully acknowledge the financial support from the Engineering Physical Science and Pfizer Research Council (EPSRC) and Pfizer Pharmaceutical, Sandwich, Kent (UK).

Lastly, I would like to thank my parents and my sister for all their love and endless encouragement.

A special Thank you to my loving and supportive husband Giovanni, for his constant and invaluable patience, especially in the more difficult periods of this work.

CHAPTER 1

INTRODUCTION TO CRYSTALLIZATION

1.1 Introduction

Crystallization is a technique which involves the formation of an ordered solid phase from a homogeneous gas, liquid or amorphous phase. It ranks as the oldest unit operation in the chemical engineering sense. Sodium chloride, for example, has been manufactured by this process since the dawn of civilization. Today most sections of the chemical industry, at some stage, utilize crystallization as method of production, purification or recovery of solid materials (Mullin, 2001).

Crystallization offers several advantages over other separation processes:

1. High purity solids from impure solutions: the rigid structure of the crystalline material results in a low tendency to incorporate foreign substances or solvent molecules.
2. Low level of energy consumption: this is the main advantage of crystallization over distillation.
3. Relatively mild process conditions: crystallization is a favorable unit operation for temperature sensitive or even temperature labile substances, since many crystallization processes, such as anti-solvent crystallization, reactive crystallization and so on, can be operated at relatively low temperature.
4. A safe and low cost process: as crystallization processes can be operated at low temperature, the material requirement of a crystallizer is lower than that of a distillation column and the operating environment is safer.
5. Efficiency of separation: crystallization can be used to separate mixtures, such as mixture of isomers, azeotropes, and temperature sensitive substances.
6. Less environmental pollution: normally, crystallization processes do not generate any exhaust gas, which causes environmental pollution after emission without treatment.
7. End product with many desirable properties: crystallization can produce uniform crystals, which have good flow, handling and packaging characteristics, and an attractive appearance that can be a very important sales factor.

Crystallization processes can be used in not only mass production with outputs over

1 million tons per year, as in the production of sugar and salt, but also small-scale production such as manufacture of single crystals. In addition to purity and yield, the quality requirements of crystal products include crystalline form, crystal mean size and size distribution. Some special quality standards even include the color and the degree of hardness of the chemical crystal product.

Normally, crystallization processes are distinguished into four categories: solution crystallization, melting crystallization, sublimation crystallization, and precipitation crystallization (Mullin, 2001).

Crystallizers can be operated as continuous or batch processes. The advantages of continuous crystallization are: low operational cost; low labor cost; stable process; high throughput. However, it also has some disadvantages. Generally, scale is easily to form on the wall of crystallizers, and crystal size is normally small compared to batch crystallization. Batch crystallization is used widely in some processes with long precipitation time, and in some processes to treat poisonous materials or expensive but low yield substances. The advantages of batch operation in crystallization make it the most common approach for crystallization processes in the chemical industry (Guo, 2007).

1.2 Pharmaceutical crystallization

Crystallization is a major technological process for particle formation in pharmaceutical industry and, in addition, plays an important role in defining the stability and drug release properties of the final dosage forms. Solution crystallization is widely used for manufacturing bioactive drug substances and excipients during final and intermediate stages of purification and separation. This process defines drug chemical purity and physical properties: particle habit and size, crystal structure and degree of crystal imperfection. Crystalline variations are responsible for a wide range of pharmaceutical formulation problems, such as chemical and physical instability of the solid drugs in their final dosage forms. The crystallization process requires considerable

time and energy resources with economical issues as the efficiency of solvent recycling, separation of waste (impurities) and consumption of raw materials. Over 90% of all pharmaceutical products, such as tablets, aerosols, capsules, suspensions and suppositories contain drug in particulate, generally crystalline, form (Shekunov and York, 2000).

Despite the documented influence of the crystallization process on the properties of dosage forms and products, particle formation and crystallization have often been regarded as a ′low-tech′ area of chemical production. Advances of chemical synthesis have achieved control over drug identity and purity, but control over the physical form and crystallinity remains poor. Chemically equivalent materials are commonly found to perform or behave unpredictably and impair product development or manufacture.

Table 1.1 summarizes the most important solid state and drug delivery characteristics affected by crystallization. Pre-formulation and formulation drug development stages are associated with manufacturing control, characterization and optimization of the solids. The Pre-formulation stage concerns the requirements for drug substances and excipients which include physicochemical stability, consistency and solid state-properties. This stage begins immediately after the synthesis and initial toxicity screening of a new drug. Formulation research relates more to the drug products (e.g. final composition of drug and functional excipient substances in the dosage form) and focuses on stability and drug release properties to be carried out through the phases relating the clinical evaluation. This development work, combined with results of clinical tests, culminates in a new drug application (NDA) submitted to a government regulatory body such as US Food and Drug Administration (FDA).

The newness of a drug product may arise from a new bioactive chemical form, but also from a different solid-state form (e.g. polymorphic, amorphous or chiral), combination with other solids (excipients, carriers, coating), different delivery method or even a different proportion of the drug in this combination. New drugs and any associated manufacturing and formulation aspects, including crystallization methods for a

particular solid-state form, are, in fact, typically protected by patents. These patents guarantee the future financial security of the company-sponsor; therefore, screening of all different solid state forms and the development of corresponding crystallization techniques should ideally be carried out as early as possible.

The drug substance section of an NDA must contain, among other requisites, specifications related to purity, solubility, crystal properties, morphology, particle size and surface area. Both drug substance and drug product sections of NDA require detailed investigation into the influence of structure on stability, in order to avoid negative recrystallization phenomena, and also into the relationship between structure and drug release rate.

Table 1.1 Solid-state properties defined by crystallization process and their relationship with specific characteristics of drug substances and drug products (Shekunov and York, 2000)

Solid-state properties	Effect on drug substance and/or drug product
Structural	
Crystallinity (existence of amorphous and semi-crystalline forms)	Physical and chemical stability
Polymorphs	%RH profile (hygroscopicity)
Solvates (hydrates)	Solubility profile and dissolution rate
Salts	All aspects of processing
Crystal defects	
Dimensional	
Particle size distribution	Processing behaviour: bulk density, agglomeration, flow/rheology, compaction
Particle morphology	Particle permeability (i.e. particle adsorption)
Particle surface structure	Bioavailability (drug absorption)
	Consistency and uniformity of the dosage form
Chemical	
Organic and inorganic impurities, residual solvent and decomposition products	Toxicity
Chiral forms and chiral separation	Chemical, physical and enantiomeric stability
Sterility (microbial limits)	
Mechanical	
Brittle/ductile transitions, fracture stress, indentation hardness, stress/strain relaxation, yield pressure, Young's modulus	Milling and tableting behaviour
Electrical	
Electrostatic charge distribution	Agglomeration and flow properties

The potential impact of changing crystal properties during late-stage drug

development, in terms of both cost and product delay has led to specific guidelines on the control of physicochemical properties according to the NDA requirements and further inspections. These guidelines have been developed as a result of collaboration between regulators, industry and academia. Four types of solid-state phases have been identified according the FDA charts: polymorphs, solvates (e.g. hydrates), desolvated solvates (pseudopolymorphs) and amorphous compounds. The regulations, combined with internationally accepted manufacturing rules covering current good manufacturing practices (cGMP) make the crystallization process among the most important industrial and regulatory recognized issues in pharmaceutical development. The crystallization process must be controllable with respect to the solid form produced as process determining not only for the production cost of pharmaceuticals but also for the curative effects.

Pharmaceuticals with similar components and similar molecule formula, even at very high purity, may have different effects, if the physical properties of solids, such as crystal habit, crystalline form and crystal size distribution etc. are different; viz. the quality standard of pharmaceuticals includes not only purity but also the configuration of crystals, which is important for biological effects of pharmaceuticals.

Except for some simple compounds (inorganic salts), the majority of pharmaceuticals with large molecules, particularly biological pharmaceuticals, are polymorphous compounds. The crystalline forms depend on the operational conditions during the crystallization process. The change of operational conditions may change the crystalline form of the product. As a result, the pharmaceuticals may have less effect or even become non-effective or damaging.

In the global pharmaceutical market, similar pharmaceuticals from different countries or different companies frequently have different curative effects. The main reasons are (Guo, 2007):

1. Crystal habits are different. For example, chlormycetin has three forms, but only the metastable form has curative effect. Rifamicin, a polymorphous

compound, can only be absorbed by muscle after re-crystallization from acetone or butanol. Sulfanilamide has α, β and γ forms, however, crystals with α and β forms have very high side-effects and are not suitable for use as medicine.

2. Crystal size distributions (CSD) are different. The CSD includes two parameters, viz. mean particle size and size distribution. Specific volumes of pharmaceuticals are determined by these two parameters. The change of crystal habit and crystalline form may also change the CSD. The human body also has different absorbability to crystal products with different CSD. For example, the CSD requirement of procaine penicillin is that more than 65% of crystals should have sizes between 1 and 15 μm, and crystals with size larger than 50 μm should not exist in the product.
3. Impurity contents are different. The unavoidable presence of impurities, may have passive influence on curative effect of pharmaceuticals, present in crystal product. For example, trace amounts of butanol can cause lincomycin crystals to become non-effective.

Controls of polymorphism and powder properties are often the most important issues in crystallization process development of an active pharmaceutical ingredient (API). After the crystallization process is determined, it is also very important to design an operable crystallizer and choose suitable control units. Crystallizers and the control units are vital factors for crystallization processes. The choice and design of crystallization processes are established on the basis of the phase diagrams, crystallization kinetics and fluid dynamics. The phase diagrams and crystallization kinetics are very rarely published in the open literature. So it is necessary to measure the above parameters for process design.

The composition of crystallization mother solution is always very complex (normally, it is not possible to obtain the components using normal analytical methods), and the composition, the density and viscosity of mother liquid may fluctuate during the

crystallization processes. Both the mother liquor and crystal product may decompose and lose biological activity. All of these factors require efficient controls of mass transfer and heat transfer as changes of operational parameters may breach the crystallization process, worsen quality of product and decrease the yield of production.

Because the pharmaceutical industry is always with high costs and low output, any quality and yield improvements of product may bring significant benefit to the producer.

The production of particles from solution is a very complex process, which involves mass, energy and momentum transfer. Kinetics parameters are used to describe the events of growth (growth rate), birth and death (nucleation rate, agglomeration rate and disruption rate) of a precipitation process. The interplays of these parameters and their dependence on supersaturation, hydrodynamics and mixing determine the crystal size distribution (Mullin, 2001).

1.3 Supersaturation

Crystallization can be considered as a result of three main stages: establishment of supersaturation, nucleation and subsequent crystal growth. Supersaturation, the essential pre-requisite for all crystallization operations, is the driving force for nucleation and crystal growth processes. In chemistry, the term supersaturation refers to a solution that contains more of the dissolved material than could be dissolved at thermodynamical equilibrium by the solvent under existing conditions. Methods to induce supersaturated conditions from saturated or undersaturated solution include reducing the temperature, decreasing the volume of solvent by evaporation, or by reaction.

In solution, when the condition is changed and the concentration of solute exceeds the equilibrium (saturation) solution concentration, solid crystals will not separate from the liquid phase until the concentration is increased to a certain value, commonly called “supersolubility”. Every solution has a maximum amount that can be supersaturated before it reaches the metastable limit and becomes unstable: the solid phase starts separating spontaneously. In the diagram solute concentration versus temperature, the region lying between the saturation curve and this unstable boundary is called “the

metastable zone" and is where all crystallization processes should be operated to exert a control on the process itself, hence on the final product. Supersaturated solutions in this area are called "metastable". The width of this region cannot be univocally established as it depends on the degree of agitation, the rate at which supersaturation is generated, the concentration of crystalline solids in suspension, and the degree to which other solutes are present in solution (Randolph and Larson, 1988).

The work of Miers and Isaac (1907) on the relationship between supersaturation and spontaneous crystallization indicated by Mullin (2001), led to a diagrammatic representation of the metastable zone on a solubility-supersolubility diagram as shown in Figure 1.1. The lower continuous solubility curve can be located with precision with appropriate techniques. The upper broken supersolubility curve, which represents temperatures and concentrations where uncontrolled spontaneous crystallization occurs, is not as well defined as that of the solubility curve.

Despite the fact that the supersolubility curve is ill-defined, there is no doubt that a region of metastability exists in the supersaturated region above the solubility curve. The diagram is therefore divided into three zones, one well-defined and the other two variable to some degree:

1. The stable (unsaturated) zone where crystallization is impossible.
2. The metastable (supersaturated) zone, between the solubility and supersolubility curves, where spontaneous crystallization is improbable, however, if crystallization has been artificially induced in such a metastable solution, for example by seeding, growth occurs on it.
3. The unstable or labile (supersaturated) zone, where spontaneous uncontrollable crystallization is probable, but not inevitable.

On an industrial scale, a large supersaturation driving force is necessary to initiate primary nucleation. In continuous crystallization, once primary nucleation has begun, the crystal size distribution begins to take shape.

Figure 1.1 The solubility-supersolubility diagram (Mullin 2001).

Figure 1.1 describes the progression of a cooling crystallization of a solution represented by point A, where the cooling is supposed without loss of solvent. Spontaneous crystallization cannot occur until conditions represented by point C are reached, where the solution leaves the metastable zone. Before point C is reached, crystallization may be induced by seeding, agitation or mechanical shock. Further cooling to some point D may be necessary before crystallization can be induced, especially with very soluble substances. After the nucleation process, solution comes back with the metastable zone, where nuclei continue growing with high growth rate. With the increase of crystal size, the supersaturation level decreases and the crystal growth rate becomes lower. As alternative, supersaturation can be achieved by removing some of the solvent by evaporation. Line AB′C′ represents this operation carried out at constant temperature while line AB″C″ represents a combination of cooling and evaporation, employed in practice (Mullin, 2001).

Control of supersaturation is the key to successful crystallizer operation. The local and global supersaturation ratios that are experienced over the course of a crystallization operation are critical because they determine the balance between nucleation and growth not only at the onset of crystallization but throughout the course of a batch or semi-batch operation. This balance, in turn, determines the resulting physical properties

and, in many cases, the distribution of chemical impurities between the crystals and the liquors (Paul et al., 2005).

1.4 Nucleation

Crystals are created when nuclei are formed and then grow: as anticipated, the kinetic processes of nucleation and crystal growth require supersaturation, which can generally be obtained by a change in temperature, cooling or heating, depending on the gradient the solubility curve, by removing the solvent (usually by evaporation), or by adding a drowning-out agent or reaction partners. The system then attempts to achieve thermodynamic equilibrium through nucleation and the growth of nuclei.

The mechanism of nucleation can be distinguished into primary nucleation and secondary nucleation, described in more detail in the following paragraphs. They are commonly defined as activated mechanisms as they have in common the fact that a free-energy barrier must be passed in order to form clusters of a critical size, beyond which the new phase grows spontaneously. The height of this barrier or, equivalently, the extent of penetration into the metastable zone, is different for each process due to different physical mechanisms (Mersmann, 2001).

1.4.1 Primary Nucleation

Primary nucleation involves the formation of a new solid phase from a clear solvent under supersaturated conditions. As indicated by Mersmann (2001), the classical nucleation theory dates back to the work of Volmer and Weber published on the *Zeitschrift für Physikalische Chemie* in 1926. They were the first to argue that the nucleation rate should depend exponentially on the reversible work of the formation of a critical cluster. In order for a new phase to appear an interface must be formed, which (in the absence of impurities or suspended foreign material) occurs by small embryos formed within the bulk of a metastable solution. These embryos are formed due to spontaneous density or composition fluctuations, which may also result in the

spontaneous dissolution of such clusters. The creation of nuclei can, therefore, be described by a successive addition of units A according to the formation scheme

$A + A \Leftrightarrow A_2 \qquad A_2 + A \Leftrightarrow A_{3n} \ \ldots \qquad A_{n-1} + A \Leftrightarrow A_n$ (critical cluster)

rather than resulting from the simultaneous collision of the required number of molecules, since this would constitute an extremely rare event. In fact, not only the constituent molecules have to coagulate, resisting the tendency to re-dissolve, but they also have to become orientated into a fixed lattice. In general, the number of molecules in a stable crystal nucleus can vary from about ten to several thousand (Mersmann, 2001).

The reversible work necessary to form a cluster is given by a balance of the free energy ΔG_V (being proportional to the condensed matter and, thus, to the volume of the cluster) that is gained and the free-surface energy ΔG_S needed to build the new surface.

$$\Delta G = \Delta G_V + \Delta G_S \qquad (1.1)$$

The change in positive free-surface energy ΔG_S increases with the interfacial tension γ_i between the developing solid crystal surface and the surrounding solution, as well as with the surface of the cluster. The energy change is to be added to the system and is therefore positive. On the other hand, the change in free-volume energy ΔG_V during solid phase formation is negative. The magnitude of ΔG_V is proportional to the volume of the cluster, V_c, and increases with increasing energy $RTlnS$, where $S = a/a^*$ (solute activity/solute activity in a saturated solution) that, in ideal systems, can be expressed in terms of solute concentration $S = C_s / C_s^*$, where the concentration C_S of the elementary units changes to the lower equilibrium concentration C_s^*. The free-volume energy ΔG_V is hence a function of the volume of a cluster and therefore can be correlated to the characteristic size of the cluster r (under the assumption of spherical cluster):

$$\Delta G_V \propto V_C \propto r^3 \qquad (1.2)$$

whereas the free-surface energy ΔG_S is related to the size of the nucleus in the following manner:

$$\Delta G_S \propto S_C \propto r^2 \tag{1.3}$$

The change in total energy ΔG with respect to the cluster characteristic size r passes through a maximum value as sum of two terms opposite of sign, as represented in Figure 1.2. This maximum value, ΔG_{crit}, corresponds to the critical cluster size r_c at which clusters become thermodynamically stable nuclei. The critical size can be calculated by setting

$$\frac{d\Delta G}{dr} = 0 \tag{1.4}$$

The type of nucleation investigated relates a solution containing neither solid foreign particles nor preformed crystals, defined as *homogeneous nucleation*. In industrial crystallizers, homogeneous nucleation is usually not desired at all, and for the production of large crystals in particular, it has to be avoided. Only for the crystallization of very fine or even nano-sized materials this mechanism may be useful.

Besides, it should be pointed out that solutions absolutely free of foreign particles correspond to an ideal case, which is uncommon in industrial crystallizers as it is impossible to remove completely all solid matter from a solvent or solution. In theoretically clean and particle-free solutions, spurious traces of suspended material or imperfections in the container's surfaces are believed to function as nucleation sites. Not surprisingly, the reproducibility of the nucleation behaviour in these systems is often poor (Mersmann, 2001; McCausland et al., 2001).

When foreign particles are present, nucleation is facilitated and the process is known as heterogeneous nucleation. Both homogeneous and heterogeneous nucleation processes take place in the absence of solution-own crystals as primary nucleation mechanism.

Figure 1.2 Free energy diagram for nucleation (Mullin 2001)

A crystallization operation can be dominated by either nucleation or growth, depending on how the critical variables are controlled (the amount of seeds, the size distribution and surface qualities of the seeds, and the environment in which supersaturation is created). Both nucleation and growth virtually always proceed simultaneously. In general, nucleation dominates when supersaturation, either local or global, is near to or greater than the upper limit of the metastable region. Even with a poor or absent control of supersaturation, nucleation is usually the predominating mechanism. This control may be exceedingly difficult to achieve at any scale, and particularly difficult to reproduce upon scale-up, often because of mixing problems. In addition, for a specific compound, the nucleation rate is also dependent on the solvent(s) system, impurity levels, and mixing. These factors combine to cause the extreme difficulties that are often encountered in controlling a nucleation based on crystallization process, especially scale-up.

There are several potential problems with a nucleation-driven process upon scale-up, including:

1. Fine crystals and/or wide particle size distribution (PSD);

2. High surface area;
3. Low bulk density;
4. The risk of large batch-to-batch variation;
5. Occlusion of impurities;
6. Agglomeration/aggregation;
7. Lack of control of hydrates, solvates, and polymorphs.

Crystal growth can dominate at low supersaturation and in the presence of sufficient crystal surface area. Both inherent nucleation rate and growth rate of the specific compound also play a major role in determining the dominant mechanism (Guo, 2007).

1.4.2 Secondary Nucleation

In laboratory and industrial crystallizers, it has often been observed that nuclei can be generated even at very low supersaturation, into the metastable zone, when solution-own crystals are already present, for instance in the form of attrition fragments or added seed crystals. Such nuclei are known as *secondary nuclei* as they grow under supersaturated conditions, and the mechanism is known as *secondary nucleation*. Secondary nucleation can result from contact, shearing action, breakage, abrasion, and needle fraction as schematically shown in Figure 1.3, and is mainly influenced by the prevailing hydrodynamic conditions and the suspension density (Mersmann, 2001).

Figure 1.4 illustrates the dependence of supersaturation on several types of nucleation process plotted against solubility.

Two major mechanisms are usually distinguished: firstly, a mechanical process whereby secondary nuclei are formed by attrition due to contacts among crystals themselves and crystals and parts of the crystallizer. This can occur at very low supersaturation conditions. Collision in a liquid medium can initiate complex behaviors. Mullin (2001) indicates that fractures may occur at the point of contact, but hydrodynamic forces can operate over the surface in the vicinity of the point of contact,

Figure 1.3 Various kinds of nucleation (Mersmann, 2001)

Figure 1.4 Metastable supersaturation against temperature for several types of nucleation processes (Mersmann, 2001).

giving rise to plastic and elastic deformation in the parent crystal. Due to energy absorption, a small fragment broken off a crystal by collision could be in a considerably disordered state, with many dislocations and mismatch surfaces. That could explain why these small crystalline fragments often grow much more slowly than macrocrystals, or do not grow at all, and explain the growth rate dispersion in attrition fragments.

Crystal agitator contacts are prior suspects for causing secondary nucleation in crystallizers, although only those crystals that manage to penetrate the fluid boundary layer around the blade will actually be hit. The probability of impact is directly

proportional to the rotational speed of the agitator. However, the relative hardness of the contacting bodies is a factor to consider as well, for example a metal impeller gives a much higher nucleation rate than one coated with a soft material such as polyethylene. The production of breakage fragments may not always be a direct result of crystal interactions or collisions as growing crystals, containing dislocations, defects or inclusions are prone to secondary nucleation through the development of internal stresses which lead to crack formation and produce secondary nuclei.

Secondly, an activated process known as surface nucleation, which needs a higher supersaturation than the previous one to happen, can be distinguished. There is some evidence in the literature that secondary nuclei that are not attrition fragments are formed either as preordered species or as clusters in the immediate solution vicinity of the crystal surface or on the crystal surface by dendritic growth and dendritic coarsening. These mechanisms can lead to the formation of nuclei and/or the detachment of small dendrites from the crystal surface without any fluid dynamics or mechanical shear (Mullin, 2001; Mersmann, 2001). This process can occur with seeding (breeding). Seed crystals carry very small crystalline particles to their surface. These small particles detach in solution, while the stable ones continue to grow. Surface secondary nucleation phenomenon can be violent and is difficult to control since it has non-linear kinetics (Guo, 2007).

1.5 Crystal Growth

The mechanism of crystal growth from solution requires that solute is transported to the crystal surface and then oriented into the crystal lattice, with the supersaturation being the driving force. Two successive steps are required, a diffusional step followed by a surface reaction step or integration step. Depending on the system, state of flow and supersaturation, the first or second step can determine the entire process, or both steps can control growth to different extents. Accordingly, the entire concentration gradient, $C_S - C_s^*$, is divided into two parts, and the concentration at the interface

between the layer dominated by diffusion and integration can be indicated as C_i. The first part, $C_S - C_i$, within a diffusive–convective layer causes diffusive–convective transport, whereas the second, $C_i - C_s^*$, is decisive for the integration reaction within a reaction boundary layer. The mass flux density, directed toward the crystal surface is

$$\frac{dm}{dt} = K_d A(C_s - C_i) = K_r A(C_i - C_S^*)^{r_i} \qquad (1.6)$$

where K_d is the mass transfer coefficient, K_r is the integration reaction rate constant, and r_i is the order of the integration reaction. The diffusional step is generally considered to be linearly dependent on the concentration driving force, while the validity of the assumption of a first order reaction is questionable. A general equation for crystallization based on this overall driving force is

$$\frac{dm}{dt} = K_G A(C_S - C_S^*)^g \qquad (1.7)$$

where K_G is an overall crystal growth coefficient and the exponent g is referred as the order of the overall crystal growth process. Many inorganic salts crystallizing from aqueous solution give a g value in the range 1 to 2 (Mullin, 2001).

When diffusion is the controlling mechanism, the crystal growth rate increases as the velocity of supersaturated solution relative to the crystal surface is increased. When a further increase in velocity no longer increases the growth rate, the growth is considered as surface-integration controlled.

When units of the crystallizing substance arrive at the crystal face, they are not immediately integrated into the lattice, but they merely lose one degree of freedom and are free to migrate over the crystal face, forming an absorbed layer of partially ordered solute, called “third phase”. It is possible that this layer consists of solute clusters formed in the saturated solution diffusing along the surface until oriented for incorporation into the crystal lattice at an appropriate site. This layer plays an important role in crystal growth and secondary nucleation and its thickness probably does not exceed 10 nm (Randolph and Larson, 1988; Mullin, 2001).

There are several theories relating the integration step, however they can be

categorized into three general theories: continuous growth, surface nucleation and continuous step growth. The continuous growth model assumes a rough surface, where the growth unit integrates at the site of lowest energy for its orientation. Surface nucleation growth is controlled by the formation of two dimensional nuclei on the smooth face of a growing crystal: the controlling step is the nucleation as the subsequent spread around the nucleus is much more rapid because of the lower energy requirements (birth and spread model). The continuous step model is the most used and the most often applicable in the form of the Burton-Frank-Cabrera (BFC) model. To summarize, this model incorporates the idea of a self-perpetuating kink and leads to the concept of a screw dislocation originating a spiral growth: the addition of a growth unit not only fills a kink site but creates another, which is favorable to growth (Randolph and Larson, 1988).

In addition to molecular structure and solvent system, the growth rate can be greatly modified by the presence of dissolved impurities that may either compete for growth sites or block these sites. As with nucleation rate, these differences can be so extreme as to make growth impracticably slow, or in the opposite extreme, the rate may be sufficient to achieve an essentially all growth process with careful control of supersaturation and growth area (Mullin, 2001).

In designing a crystallization process, therefore, the balance that is achieved between nucleation and growth rates is critical to particle size. Supersaturation ratio can be controlled to limit nucleation in order for growth to predominate as in seeded operations.

1.6 Agglomeration

Small particles in liquid suspension have a tendency to cluster together, leading to agglomeration, aggregation or flocculation. As indicated by Mersmann (2001), agglomeration can be considered as the unification of primary particles that are cemented afterwards by chemical forces (e.g., by a crystalline bridge between two or

more crystals). The formation of this bridge requires crystal growth, for which supersaturation is an essential prerequisite. In the case of aggregation and flocculation, the bonding forces, such as Van der Waals forces, are quite weak. A flocculate is a group of particles that consists of primary particles connected by weak cohesive forces. In the case of aggregates, the strength of the bonding forces is intermediate to agglomerates and flocculates. Aggregates and flocculates can occur in saturated or undersaturated solutions and can readily be destroyed. However, strong agglomerates are generated only in supersaturated solutions.

Two types of crystal agglomeration can be distinguished: (a) primary agglomeration as a result of malgrowth of crystals (polycrystals, dendrites, and twins) and (b) secondary agglomeration as a consequence of crystal–crystal collisions in supersaturated solutions. It is often difficult to distinguish between the different origins of particles by microscopic observation.

Secondary agglomeration (often simply referred to as agglomeration) takes place in suspended particle systems and depends on (a) mechanical and fluid dynamic processes, such as the movement of primary particles and liquid, and on particle collisions, (b) kinetic processes, mainly crystal growth in supersaturated solutions, and (c) particle properties.

Another classification among agglomerative mechanisms distinguishes (a) perikinetic agglomeration caused by Brownian motion of monodisperse, submicron primary particles that are subjected to collisions (diffusion controlled) in a solution at rest, (b) orthokinetic agglomeration induced by fluid-mechanical forces acting on particles (shear rate controlled) in a solution in motion, or (c) differential settling by gravitational or centrifugal forces. Von Smoluchowski has derived equations for the first two agglomeration mechanisms (Mullin, 2001).

Agglomeration is dominant in the submicron and micron ranges of primary species and is less important or negligible for particles larger than 50 μm, or, more generally, agglomeration in crystallizers does not occur with particles above a certain critical size

(Mersmann, 2001). This critical size depends on the suspension density, crystal growth rate, and specific power input.

For particles smaller than the critical size, it is assumed that a fraction independent of size will be converted to agglomerates: the fraction depends on the crystal residence time, the growth rate, and the time necessary to join the loosely agglomerated particles together. As a rule, agglomeration takes place after small primary particles have been formed by primary nucleation (Mersmann, 2001).

One mechanism for agglomerate growth is attributed to growing nuclei colliding and becoming "cemented" together by continuing growth between two or more crystals: the addition of a large number of nuclei to an original two-crystal agglomerate can readily occur by ongoing collisions leading to very large agglomerates.

Several investigators have developed models for the effectiveness of collisions that lead to agglomeration. This complex interaction of hydrodynamics and surface chemistry is difficult to predict or describe but can be critical to the successful operation and scale-up of a crystallization process. In particular, for reactive crystallization in which high supersaturation levels are inherently present, agglomeration is very likely to occur as the precipitate forms. Careful control may be necessary to avoid extensive agglomeration.

The difficulties that can result from agglomeration include:

1. Entrapment of solvent and/or impurities in the crystal mass;
2. Reduced effective surface area for true growth;
3. Subsequent break-up of agglomerates into small crystals that were captured during nucleation without opportunity for growth;
4. Difficulties in downstream processing;
5. Friability during dry processing (drying, solids transfer);
6. Leading to changes in PSD.

For these reasons, agglomeration is generally to be avoided. The use of additives may be considered for suppressing agglomeration. However, the use of additives in the

pharmaceutical industry–particularly for final products–is generally not considered for regulatory reasons (Guo, 2007).

The primary process variables that can be manipulated to minimize agglomeration include:

1. Operation within the metastable region;
2. Controlled rate of supersaturation generation;
3. Removal of crystallization inhibitors from the feed stream;
4. Appropriately high seed levels;
5. Solvent selection;
6. Mixing conditions.

Both the formation and disruption of agglomerates by attrition are functions of mixing conditions and local shear. Agglomerates that are formed under conditions of high supersaturation are much stronger and not subject to disruption by typical mixing conditions (Guo, 2007).

1.7 Attrition and Breakage

Attrition refers to the process by which asperities and fines are removed from the surface of parent particles suspended in solution, such that there is only a gradual change in their size. Breakage (or fragmentation) is the process by which the parent particles are broken down into smaller entities of significant size, resulting in a rapid disappearance of the original particles.

Two main mechanisms exist for this process. The first is a consequence of collisions of particles with parts of the equipment (impeller or walls) of the crystallizer (Biscans, 2004): this is the breakage mechanism expected in dilute solutions. The second is caused by inter-particles collision.

Contact secondary nucleation correspond to a breakage of attrition process under supersaturated conditions or, in other words, when attrition fragments grow in a

supersaturated solution, they are secondary nuclei and influence the particle size distribution and the population balance. The impact crystal–impeller in a stirred vessel depends on several parameters:

- the stirring intensity,
- the impact energy applied per unit energy needed to produce one attrition fragment from the crystal surface,
- the target efficiency, which is similar to impact probability between a crystal of given size and an impeller,
- the material properties of crystal and stirrer,
- the total number of parent particles in the vessel which influences the relative contribution of crystal–crystal collisions (dominant with high densities of crystals) and
- crystal–rotor collisions.

The production rate of the attrition fragments depends on the stirrer rotation rate (or the power input), the solid content of the slurry and the mechanical properties of the solid material, and on the physico-chemical properties of the liquid. Fracture may occur at the point of contact, but hydrodynamic forces can also operate over the surfaces in the vicinity of the point of contact and plastic and elastic deformation in the parent crystal can be generated. The fragment broken off from the crystal could be in a considerably disordered state (formation of dislocations) with many irregular surfaces. It is why these small crystalline fragments often grow more slowly than macro-crystals. Cases have even been reported where they do not grow at all (Mullin 2001, Garside and Davey, 1979). The probability of a fragment being non-growing increases with decreasing size. As the solubility of a particle increases with decreasing size (Ostwald ripening) for a given solution concentration, the supersaturation experienced by a crystal decreases with decreasing crystal size (Mersmann, 2001).

1.8 Ostwald ripening

When solid particles are dispersed in their own saturated or low supersaturated solution there is a tendency for the smaller particles to dissolve and the solute to be deposited subsequently on the large ones. Consequently the small particles disappear while the large particles grow larger modifying the particle size distribution. This process of particle coarsening is called Ostwald ripening after the proposer of the mechanism (Ostwald, 1986) and the reason for this behavior lies in the tendency of the solid phase in the system to adjust itself to achieve a minimum total surface free energy (Mullin, 2001).

The driving force for ripening is the difference in solubility between small and large particles, as given by the size-solubility (Gibbs-Thomson) relationship which may be expressed as

$$ln\left[\frac{c(r)}{c^*}\right]=\frac{2\gamma_i v_s}{\nu RTr} \tag{1.8}$$

Where v_s represents the molar volume of the solute, $c(r)$ the solubility of small particles of size (radius) r, c^* is the equilibrium saturation for large particles ($r \to \infty$), γ_i is the interfacial tension and v is the number of ions in a formula unit; a significant increase in solubility occurs when $r < 1\ \mu m$ (Mullin, 2001).

Ripening can change the particle size distribution of a precipitate over a period of time, even in an isothermal system, and the change can be accelerated by the use of controlled temperature fluctuation, a process known as “temperature cycling”.

On the other hand, as ripening occurs at very low supersaturation and considering the mass transfer mechanisms involved are the same in growth processes, it is supposed that the process is more likely to be controlled by surface integration reaction than by diffusion. Under these circumstances, ripening can be considerably retarded, and the suspension can be stabilized, using additives which slow down the surface reaction step. Substances as gelatin and carboxymethyl cellulose are commonly used for this purpose (Mullin, 2001).

1.9 The Population Balance Model

An important factor of continuing interest in the operation of industrial crystallizers is the dynamics of the crystal size distribution (CSD) determined by growth phenomena and birth and death mechanisms (nucleation, agglomeration, breakage processes). Therefore, a complete description of the crystal size distribution and its evolution over time requires the quantification and the combination of these processes' kinetics, and the application of the three conservation laws of mass, energy and crystal population (Mullin, 2001). The mathematical framework used to describe the crystallization process in terms of crystal population is called "the population balance". Defined a way to characterize the size of crystals, the formulation of the population balance is based on the crystal population density function that defines the number of crystals per unit size per unit volume of system (Mullin, 2001; Mersmann, 2001).

More details on the mathematical formulations of the population balance equation commonly adopted in the literature are provided in chapter 4.

1.10 Conclusions

Crystallization is a separation technique which ranks as the oldest unit operation in the chemical engineering industry and is the major technological process for solid particle production in pharmaceutical industry. It involves the formation of an ordered solid phase from a homogeneous phase, for instance a liquid solution of the crystallizing compound.

Supersaturation is the essential requisite for all crystallization operations; the amount of dissolved solute has to be greater than under thermodynamic equilibrium conditions. After establishment of supersaturated conditions, the separation of a solid phase into crystals occurs through the main stages of nucleation and crystal growth, but is also affected by phenomena such as agglomeration, breakage, dissolution and ripening, which significantly impact on the physical characteristics of the final product, especially habit and size distribution. Other variables affecting the product quality

include operating variables as impurities, mixing, and solvent systems.

The main requirements for an industrial crystallization output relate the purity level, the crystal habit, the particle size distribution and the productivity. Successful control of a crystallization process requires an understanding of the key processes (establishment of supersaturated conditions, nucleation and growth rates, agglomeration and breakage) and the possibility to manipulate them. The choice can be directed to the manipulation of supersaturation, for example by seeding, or be addressed to crystallization equipments, methods of crystallization and procedures.

1.11 Research objectives and thesis structure

The main objective of this research is the investigation of ultrasonic irradiation effects on continuous and batch crystallization, to evaluate the potential offered by ultrasonic technology in controlling size, size distribution and habit of final crystals, and productivity. The effect of ultrasonic technology on crystallization has been reported in the literature mainly for batch processes; the sonocrystallization literature reveals a noticeable improvement in the mass transfer, an enhancement in nucleation phenomena, and a reduction of agglomeration, providing crystals with better habit definition and even distribution of particle sizes than in analogous processes under silent conditions.

In the first instance, this investigation focuses on the combination influence of residence time, inlet concentration and insonation power amplitude on the time required to reach steady state operating conditions, the particle size evolution and the de-supersaturation over time during the start-up of a continuous operation. The experimental investigation focuses in particular on the physical characteristics of the steady state throughput in terms of solid recovery (concentration, supersaturation and crystal yield) and at the steady state, particle size distribution and crystal habit.

The kinetics of secondary nucleation and crystal growth at continuous steady state is modeled using the population balance equation implemented with a size dependent growth model.

The investigation is then implemented by comparison with the physical product characteristic of industrially established processes to generate both micrometer and large scale particles.

In Chapter 2, the mechanism of ultrasound on crystallization from solution is presented. Physical properties of ultrasonic waves are summarized and the acoustic streaming and cavitation phenomena are highlighted as leading effect of sonication. The chapter covers a summary about the main ultrasonic effects and benefits to crystallization documented in the literature.

Experimental apparatus, operating procedure and results of continuous crystallization are described and discussed in Chapter 3. The results include the influence of residence time, inlet composition and power ultrasound on the achievement of steady state conditions and physical properties of the steady state system in terms of habit and size distribution of produced crystals, and solid recovery. The investigation, furthermore, covers the effect of the mentioned parameters on steady state solute concentration and crystal yield, estimated by combination of conductivity measurement and mass balance equations for a continuous stirred tank reactor, and on the de-supersaturation evolution over the transient period.

The determination of nucleation and growth kinetics from experimental data is discussed in Chapter 4, coupled with the analysis of the effects induced by continuous sonication on the kinetics of both processes and the consequent produced particle distribution.

In Chapter 5, the kinetics of nucleation and growth at steady state, in continuous crystallization under continuous insonation, have been estimated using the commercial available software package PARSIVAL based on the fully adaptive Galerkin h-p method. The population balance has been modeled with secondary nucleation and a growth rate depending on both supersaturation and particle size, according to the Mydlarz – Jones three parameter model (MJ3).

Adipic acid was crystallized via batch cooling from aqueous solution under

continuous ultrasonic radiation. The product particle characteristics of continuous crystallization experiments under continuous insonation in Chapter 3 are compared firstly with those achieved at the end of a batch operation and secondly with the products of dry milling techniques, viz. hammer milling and micronization and High Shear Wet Milling (HSWM) respectively, and of batch reverse antisolvent crystallization (RAS) in Chapter 6. Off-line Malvern MasterSizer measurement, Scanning Electron Microscopy (SEM), and Atomic Force Microscopy (AFM), were used to compare particle size distributions, to investigate the difference in particle habit and to analyse the surface characteristics at sub-micron scale.

The use of ultrasonic technology in the particle engineering of adipic acid crystals is addressed to the achievement of narrow monomodal distributions of large particlesin Chapter7. The assessment is based first on the product characteristics of seeded batch crystallization. The effects of seed preparation method and operating conditions during the batch cooling crystallization of adipic acid in aqueous solution are presented. Seeds are prepared by cooling crystallization with and without ultrasound and by grinding commercial crystals. The effects of cooling rate, initial concentration, seeding load, and supersaturation at the point of seeding on the crystal size distribution and crystal habit of the final product are studied to characterize conditions for the achievement of a growth-dominated operation.

The investigation is then focussed on the use of a short ultrasonic burst at the beginning of a cooling crystallization to achieve a growth dominated process and produce crystals with regular habit without the requirement of inoculation of seeds. In Chapter 8, the seeded crystallization of adipic acid from aqueous solution is compared with the unseeded cooling crystallization coupled with an initial short ultrasonic burst interrupted after the nucleation onset.

Chapter 9 concludes the work with a summary of the thesis content with recommendations for future works in sonocrystallization.

CHAPTER 2

PRINCIPLES OF SONOCRYSTALLIZATION

2.1 Introduction

"The application of ultrasound to crystallizing systems offers a significant potential for modifying and improving both the processes and products" (McCausland at al., 2001) Research into the influence of ultrasound on crystallization processes has revealed that the crystallization of solid crystals (from a number of liquids ranging from organic fluids to metals) is affected by the presence of ultrasonic waves. The use of ultrasound offers a method for modifying and improving both products, in terms of crystal habit, size distribution and purity (Devarakonda et al. 2003**,** Ruecroft et al. 2005, Manish et al.2005, Luque de Castro and Priego-Capote, 2007), and processes (controllability and reproducibility) with broad applications in crystallization, product recovery and purification processes. The requirement for environmentally clean processing and the use of relatively inexpensive equipments contributes in making ultrasound an intensifying technology. Furthermore, ultrasound seems to provide a distinct alternative to more traditional techniques of controlling the crystallization process as seeding strategies (McCausland et al. 2001**,** Ruecroft et al. 2005).

Ultrasound technology has been available for many years in research and diagnosis; however, its application to chemical processes has developed rapidly only in the last two decades as high intensity systems that can deliver power ultrasound on industrially relevant scales have become available. Furthermore, sonocrystallization literature focuses on batch crystallization operations, with lack of data relating to continuous processes. The range of applications for the use of ultrasound includes synthesis, environmental protection (the destruction of biological and chemical contaminants), chemistry (Mason, 1997) and improvements in extraction, emulsification, filtration, extrusion and fermentation in the food industry (Patist and Bates, 2008). Besides, ultrasound offers an interesting method in selecting the desired polymorphic form in process engineering (Gracin et al, 2004 and 2005, Louhi-Kultanen et al., 2006). When ultrasound is applied to a crystallization system, it may influence nucleation and crystal growth rates, agglomeration and breakage, with significant influence on the crystal

production.

The driving force for sonocrystallization are the so called cavitation phenomena, presented in section 2.2.6, coupled with acoustic streaming mechanism, and so a general requirement is that at least one of the phases involved in the process should be a liquid.

In this chapter, the mechanism of ultrasound on crystallization from solution is presented. The first section details the physical properties of an ultrasonic wave, with cavitation phenomena highlighted as leading effect of sonication. In the second part, the chapter presents an overview about the main ultrasonic effects and benefits to crystallization documented in the literature.

2.2 Physical properties of ultrasonic irradiation

2.2.1 Ultrasonic wave

Ultrasound is defined as a sound with frequency beyond the limit of human ear response. As illustrated in Figure 2.1, the normal range of hearing is between 16 Hz and about 18 kHz while ultrasound is generally considered to lie between 20 kHz to beyond 100 MHz. Frequencies in the range between 20 kHz and 40 kHz are commonly used in laboratories. However, since acoustic cavitation can be generated well above this frequency range, researchers use recently a much broader range. High frequency ultrasound from around 5 MHz and above does not produce cavitation: this is the frequency range used in medical imaging (Mason, 1997). Table 2.1 lists the comparison between the features of ultrasound and normal sound (Guo, 2007).

Being a sound wave, ultrasound is transmitted through any substance, solid, liquid or gas, which possesses elastic properties. As a consequence, unlike electromagnetic radiation, acoustic energy cannot be transmitted through a vacuum. The movement of the vibration body (the sound source) is communicated to the molecules of the medium, each of which transmits the motion to an adjoining molecule before returning approximately to its original position. For liquid and gases, particle oscillation takes place in the direction of the wave producing longitudinal waves, as shown in Figure

2.2a. Solids, however, since they also possess shear elasticity, can also support tangential stresses giving rise to

Figure 2.1 Frequency ranges of sound **(**Mason, 1997**)**

Table 2.1 Features of ultrasound which distinguish it from sound in water (Guo, 2007)

Ultrasound	Normal sound
Transmitted by means of waves	Transmitted by means of waves
Beyond the range of human hearing	A periodic disturbance stimulating the ear
Wavelength between cm and μm	Wavelength between m and cm
Frequency between 20 000 and 10^{13} Hz	Frequency between 20 to 20 000Hz
With high sound pressure	With low sound pressure
With cavitation phenomenon	Without cavitation phenomenon

transverse waves, in which particles movement takes place perpendicular to the direction of the wave (Figure 2.2b). An example of longitudinal wave can be seen when a coiled spring, anchored at one end, is given a sharp push from the other end, as represented in Figure 2.3. The action causes a disturbance in the spring which can be seen to "run" through the whole length. If an individual coil is identified, as the wave passes the coil it will be seen firstly to move forward in the direction of the wave and

Figure 2.2 Wave particles movement: (a) longitudinal waves; (b) transverse waves (Mason and Lorimer 2002).

subsequently to return to its original position. For a series of consecutive waves, the motion will be the one of oscillation.

Focussing on the vibration of an individual molecule of medium, its displacement from the mean rest position at any time t is given by

$$x = x_0 \sin(2\pi ft) \tag{2.1}$$

where x_0 is the displacement amplitude, or maximum displacement of the molecule, while f is the frequency of the sound wave. Differentiation of the equation (2.1) leads to an expression for the molecule velocity:

$$v = \frac{dx}{dt} = v_0 \cos(2\pi ft) \tag{2.2}$$

Figure 2.3 The compression and expansion cycle of ultrasound (Guo, 2007).

where v_0, including the product fx_0, is the maximum velocity of the medium molecule. Besides the variation in the molecules' position, there is a variation in pressure. At the point where the molecules are compressed ($x = 0$), the pressure is the highest whereas the rarefaction regions correspond to lowest pressure values.

As with displacement, the pressure P_a at any instant is time and frequency dependent.

$$P_a = P_A \cos(2\pi ft) \tag{2.3}$$

Displacement and pressure are out of phase as the maximum displacement appears at the point of minimum pressure, as represented in Figure 2.4.

The ultrasonic waves include continuous wave, gated (amplitude-modulated), and acoustic-burst pulsed waves. A continuous wave at a single frequency is a simple sinusoidal wave having constant amplitude. The pressure of an amplitude-modulated wave changes with distance, at a fixed instant of time, or as a function of time at a fixed point in space. For the pulsed wave, the pressure amplitude is not constant and is zero for part of the time. No acoustic energy is being emitted between pulses and the ultrasound propagates through the medium as small packages of acoustic energy (Mason and Lorimer, 2002).

2.2.2 Ultrasonic wavelength and propagation velocity of sound

The wavelength λ corresponds to the distance between two consecutive points of maximum compression or rarefaction. For any sound wave, the wavelength of sound in a medium is correlated to the the propagation velocity through the medium c (the speed at which ultrasonic vibrations are transmitted through a medium), and the frequency f.

$$c = \lambda f \tag{2.4}$$

For frequencies in the range of 20-50 kHz, usually employed to influence chemical processes, the wavelength produced in the liquid are in the range 7.5 to 3.0 cm, while with greater frequencies (1-100 MHz) the wavelength range is 0.15-0.0015 cm . These values are considerably longer than molecular (bonds) length values; therefore

Figure 2.4 Displacement graph(x) and pressure graph (Mason and Lorimer, 2002).

sonochemical effects are not the result of a direct interaction between reagents and the wave (Mason and Lorimer, 2002).

2.2.3 Ultrasonic intensity

The ultrasonic field produced by a transducer obeys all the physical laws of wave phenomena. It can be thought as being produced by many small point sources making up the transducer face and thus producing a characteristic interference pattern at any point in the field. As indicated by Mason and Lorimer (2002), sound is a form of energy. In fact, under ultrasonic irradiation the particles of the medium are set into vibration motion and thereby posses kinetic energy. This energy is derived from the wave itself. Using this principle we can deduce the energy, hence the intensity, associated with an applied ultrasonic field.

Considering the movement, with velocity v, of a layer of medium of area *A* and thickness *dx*, hence volume *Adx*, under the action of the ultrasonic wave (Figure 2.5), then the kinetic energy ($mv^2/2$) of the layer is given by

Figure 2.5 Relationship between sound source and ultrasonic wave (Mason and Lorimer, 2002).

$$k = \frac{1}{2}(\rho A dx)v^2 \tag{2.5}$$

The energy for the whole wave, E_w, can be derived by integration, for example between 0 and x:

$$E_w = \frac{1}{2}(\rho A x)v^2 \tag{2.6}$$

while the energy per unit time, or energy density, E, is given by

$$E = \frac{1}{2}\rho v^2 V_t \tag{2.7}$$

If the sound energy passes through unit cross sectional area (A=1) with a velocity c, then the volume swept out in unit time (V_t) is c, and the energy flowing in unit time corresponds to Ec. Since intensity I is defined as the amount of energy flowing per unit area A per unit time,

$$I = Ec \tag{2.8}$$

or

$$I = \frac{1}{2}\rho c v^2 \tag{2.9}$$

As ultrasound is propagated from the transducer, the sound field is divided into two main zones as depicted in Figure 2.6. The region close to the transducer, defined the *near field* or *Fresnel zone*, is a zone where the overall beam size remains relatively constant, though there are many variations of intensity within the zone itself, both across and along the beam axis (www.olympus-ims.com/en/ndt-tutorials/transducers/characteristics/). The near field ends at the last on-axis maximum at

distance N_f from the face. Near field distance N_f represents the natural focus of the transducer and, considering a circular transducer, is a function of the transducer's frequency and diameter D_t, and the sound velocity in the test medium, and it may be calculated as follows

$$N_f = \frac{D_t^2 f}{4c} = \frac{D_t^2}{4\lambda} \tag{2.10}$$

Higher frequency values (or shorter wavelength values) and larger diameter values will result in longer near field distances.

The near zone is followed by a zone where the beam diverges and becomes more uniform, called the *far field* or *Fraunhofer region*. In the far field of any transducer, the acoustic intensity is proportional to the square of the acoustic amplitude (Mason and Lorimer, 2002):

$$I = \frac{P_A^2}{2\rho c} \tag{2.11}$$

Figure 2.6 Ultrasonic beam from a circular transducer element. Pressure amplitude varies in a complex way in the near field while it monotonically decreases in the far field (www.olympus-ims.com/en/ndt-tutorials/transducers/characteristics/)

2.2.4 Sound Attenuation and Absorption

During the propagation of a sound wave through a medium the intensity of the wave decreases as the distance from the radiation source increases. The intensity at some distance *d* from the source is given by

$$I = I_0 \exp(-2\alpha d) \tag{2.12}$$

where α is the *adsorption* or *attenuation coefficient*. The attenuation may arise as result of reflection, refraction, diffraction or scattering of the wave, or it may be the result of converting some of the mechanical (kinetic) energy of the wave into heat. For chemical applications, which usually take place in the gaseous or liquid phase, it is the latter process which is the most important. As the molecules of the medium vibrate under the action of the sound wave, they experience viscous interactions that degrade the acoustic energy into heat. The adsorption of this degraded acoustic energy by the medium gives rise to the observed bulk heating effect during the application of high power ultrasound. In practice the experimental temperature often rises very quickly (approximately 5 °C) during the first few minutes of applying ultrasound. After this initial period, the temperature remains effectively constant provided the vessel is effectively thermostated (Mason and Lorimer, 2002).

As the forward-directed intensity distribution falls-off with increasing distance from the tip, in regions away from the forward scatter zone, the insonation energy may be close to zero determining a sort of dead zone. Vessel containing such zones must be stirred to ensure a reasonably uniform insonation of the working volume (Cains et al. 1998). The intensity distribution varies even along the axis of a transducer with an axial intensity peak occurring at some distance from the transducer, in the so called *Focal zone*, as shown in Figures 2.7 and 2.8. This peak is a common feature of both focused and non-focused fields, and its existence is an important factor in characterizing ultrasound fields. Apart from the distance from the transducer, the intensity attenuation is increased by less homogeneous medium to traverse, because of high acoustic

Figure 2.7 Pressure gradients in both the transverse and axial directions in the ultrasonic beam: red represents areas of highest energy, while green and blue represent lower energy (**www.olympus-ims.com/en/ndt-tutorials/transducers/characteristics/**).

impedance mismatch, and by higher frequency (or shorter wavelength) values (AACA Pre-conference Workshop Perioperative Ultrasound, Nov. 2006).

A common intensity measurement is the energy dissipated by the probe tip per unit area of probe surface, expressed as $W \cdot cm^{-2}$.

Finally, the intensity of the ultrasonic field produced by the transducer also varies with time, if the ultrasound is pulsed, and intensity averaging can be carried out in the time domain and it is therefore necessary to distinguish between time average (such as the average over the total time or over the pulse duration) and spatial peak intensities (Guo, 2007).

Figure 2.8 The intensity distribution in the ultrasonic field and the flows caused by ultrasound (Guo, 2007).

2.2.5 Acoustic Impedance, Reflection and Refraction

The *acoustic impedance*, *Z*, is a parameter indicating the opposition of a medium to the passage of sound waves, and depends on the density ρ of the medium and the propagation velocity of ultrasound through the medium *c*

$$Z = \rho c \tag{2.13}$$

When an ultrasound wave encounters an interface between two media (heterogeneous medium), part of the wave will be reflected back into the first medium with the same speed while the rest of the wave will be transmitted or refracted into the medium beyond the interface and will travel with the velocity of propagation in that medium. The amount reflected depends on the difference in acoustic impedance between the media traversed by the beam. A large difference in acoustic impedance is referred to as *acoustic impedance mismatch* and the greater the acoustic mismatch the greater the percentage of ultrasonic beam reflected. Because the significant difference between the acoustic impedance of liquids and gas or air, the latter forms a virtually impenetrable barrier to ultrasound (AACA Pre-conference Workshop Perioperative Ultrasound, Nov. 2006, Guo 2007).

2.2.6 Cavitation

Ultrasonic cavitation is commonly recognised as the most important mechanism by which ultrasonic irradiation can influence crystallization. According to McCausland et al. (2001) and Mason and Lorimer (2002), the application of ultrasound on a continuum fluid imposes an oscillatory pressure that, at low intensity, induces motion and mixing within the fluid. This process is known as *acoustic streaming* and enhances both heat and mass transfer processes. As described by Eckart in the work published in 1948, acoustic streaming consists of strong currents of liquid appearing in front of the vibrating surface of the piezoelectric generators, and frequently great enough to disturb its free surface. Such currents, as they involve circulation of the fluid, could not arise in the absence of friction.

The effect of insonation are of three kinds: (2) those that can be ascribed to the inertia of acoustic energy, (2) those arising from radiation pressure, and (3) those caused by the variable compressibility of the medium. All of them result in the production of overtones of the fundamental vibration. In certain cases, this distortion can become very large.

The pressure gradient is expected to produce an acceleration of the fluid, whose velocity would thus increase until the viscous forces balance the pressure gradient. The end result would be fluid streaming at a velocity proportional to the acoustic energy gradient and inversely proportional to the coefficient of viscosity. Eckart argued that those gradients are balanced not only by the viscous forces, but by the elastic forces as well.

Mason and Lorimer (2002) refer to the tensioning effect on the fluid considering a series of compressions and rarefaction waves induced in the molecules of the medium. At higher, but still moderate, acoustic intensities, in addition to acoustic streaming the local pressure in the expansion phase of the cycle falls below the vapor pressure of the fluid, causing minute bubbles or cavities to grow (growth phase in cavitation phenomena). Suslick et al. (1990) indicate that at moderate intensities three processes occur with equal rates: the growth of bubble during rarefaction, the contraction during compression and change of the sound field from rarefaction to compression, specifying that the intrinsic properties of the liquid (viscosity, density, and surface tension) determine the rates of expansion and compression of the bubble in the liquid. In these conditions, a small gas bubble can be long lived and may undergo many oscillations, driven by the sound field. This oscillation of bubble size around a mean equilibrium size in a weak to moderate acoustic field is defined as *stable cavitation*. A resonating bubble in an acoustic field can grow by a process called *rectified diffusion*. In fact, growth occurs because the rate of diffusion of gas in and out of a bubble is dependent on the surface area of the bubble. Thus, more gas diffuses into the bubble during rarefaction, when the bubble is large, than diffuses out of the bubble during compression, when it is

small. Bubbles can grow substantially by this process over many acoustic cycles. Rectified diffusion is most commonly observed in near saturated liquids.

At sufficiently high power, negative transient pressures cannot only enhance preexisting bubbles growth but the rarefaction cycle may exceed the attractive forces of the molecules of the liquid and cavitation bubbles will form. The latter define the nucleation stage in the cavitation phenomenon. Small bubbles will grow over a few cycles taking in some vapor or gas from the medium by rectified diffusion to an equilibrium size which matches the frequency of bubble resonance to that of the sound frequency applied and, in the compression phase, the increase in pressure either contracts the void or bubble to a smaller size, or eliminates it by implosion. However, at high acoustic intensities, the inertia of a large bubble prevents it from responding rapidly enough to the sound field to maintain resonance. The rate of expansion can be sufficiently high than the bubble can expand until the next rarefaction phase without recompressing, accelerating the bubble growth (the diameter can almost double in a single expansion). Once the bubble has overgrown, it can no longer efficiently absorb energy from the sound field and can no longer sustain itself. At this point the bubble is very unstable, the forces that cause the bubble to contract (surface tension and static pressure) start to dominate, the surroundings liquid rushes in, and the cavity implodes. These cavitation bubbles, with a lifetime of only a single cycle, are defined *transient cavitation* (Mason and Lorimer, 2002).

The generation and collapse of a cavitation bubble is schematized in Figure 2.9. Stable and transient cavitation bubbles are both important mechanisms for ultrasonic effects on chemical and physical processes. In many experiments, they occur simultaneously, but in certain situations only stable cavitation occurs. Generally, these processes are non-linear, in that the changes in the radius of the void are not proportional to the variations in acoustic pressure.

When these cavities collapse, the energy for chemical and mechanical effects is generated. The implosion of gas-filled cavities generates a number of smaller bubbles,

Figure 2.9 Generation of an acoustic bubble
(http://www.sonochemistry.info/Research.htm)

while vapor-filled bubbles collapse with considerable violence, since there is no residual compressible gas present to cushion the mechanical effect. However, the principal effect of imploding transient cavities is the release of large amount of energy into small and spatially resolved regions, i.e., the cavitation bubble can be seen as a localized microreactor which, in aqueous systems, generates extreme temperatures and pressures, according to the hot spot theory. In addition to this, there are mechanical effects: cavitation is responsible for the formation of large shock waves which produce a variety of physical events, such as microstreaming and particle acceleration. Microstreaming is the localized turbulence of the solid-liquid film which accelerates the rate of mass transfer through the film by increasing the intrinsic mass transfer coefficient (Thompson and Doraiswamy 2000).

The value of a resonant size is determined by the frequency of the ultrasound. As a rough guide, the resonant diameter of a cavitation bubble in water at 20 kHz is about 170 μm, the liquid reaction zone extends about 200 nm from the bubble surface, with an effective lifetime of less than 2 μs (Suslick, 1990).

2.2.6.1 The Hot-Spot Theory

The dominant theory in explaining the effect of insonation is a thermal theory. It is based on the heat generation associated to a compression of a gas. The rapid compression of gas and vapor during a cavitational collapse leads to nearly adiabatic heating of the content of the bubble, because thermal transport is slower than the collapse. Thus a short lived, localized hot-spot is formed. This theory best account for the large body of data and the majority of workers in the area interpret their data in terms of this thermal theory.

The theoretical development of the hot-spot theory is focused on the equations of bubble motion in an acoustic field: these equations and derived others have been used to calculate the temperatures reached upon cavitation. Several studies have been carried out, all starting with the adiabatic collapse of a gas filled bubble, then applying different corrections for parameters that affect the maximum temperature, such as thermal conductivity of the gas, condensation of the vapor, reactions of the gas and radial distribution of the temperature inside the bubble.

Considering an ideal gas, the temperature, pressure and volume before (i) and after (f) adiabatic compression are correlated by

$$\frac{T_i}{T_f} = \frac{P_i}{P_f} = \left(\frac{V_i}{V_f}\right)^{\gamma} \tag{2.14}$$

where γ represents the ratio of the thermal conductivities at constant pressure and constant volume, $\gamma = C_p/C_v$.

The final temperatures calculated for bubbles filled with various gases initially at 297 K and adiabatically compressed by various amounts are listed in Table 2.2. The calculations indicate that significant temperatures can be reached by modest compression ratios, and that γ has a significant effect on the final temperature.

The results coincide for the noble gases as γ is assumed the only significant parameter of the dissolved gas that determines the temperature of the cavitation event. However, this is not the observed behavior. In fact, the bubble collapse is not completely adiabatic,

and the thermal conductivity of the gas in the bubble affects the rate of heat transferred to the surroundings during compression.

A bubble contains not only the gas dissolved in the liquid, but also vapor from the liquid itself, depending on the vapor pressure of the liquid, hence on the temperature of the bulk liquid. As the temperature increases, the solvent vapor increases, decreasing the efficacy of the cavitational collapse.

The vapor pressure of the liquid is thought to affect the temperature of the cavitation event in different ways. First, liquid vapor will, in general, decrease the γ of the bubble content, since polyatomic molecules have $\gamma < 1.2$. Secondly, vapor in the bubble decreases the maximum temperature of the cavitation event because the vapor is compressible and vapor condensation to liquid requires energy, which is therefore unavailable for heating. In the case of sonochemical bond cleavage, an endothermic process, the maximum cavitational temperature is decreased as well (Suslick et al. 1990).

In terms of experimental evidence, measurement of the conditions generated during bubble collapse is not possible by conventional methods because of the transient and

Table 2.2 Theoretical temperatures after adiabatic compression (Suslick et al, 1990)

		Theoretical temperatures (K) Compression ratios, V_i/V_f [r_i/r_f]		
Gas	$\gamma = C_p/C_v$	2 [1.26]	4 [1.59]	10[2.15]
He	1.67	945	3007	13892
Ar	1.67	945	3007	13892
H_2	1.41	789	2097	7634
O_2	1.40	784	2068	7460
N_2	1.40	784	2068	7460
NH_3	1.31	736	1826	6064
CO_2	1.30	731	1801	5926
C_2H_6	1.20	682	1568	4707

localized nature of the cavitation event. However, Dokticz and Suslick (1990) carried a series of experiments to estimate the maximum temperature reached during interparticle collision under ultrasonic irradiation at 20 kHz and 50 W/cm^2. A series of transition metal powders were irradiated as slurries in decane. Ni powder (mp 1453 °C) and Cr powder (mp 1857 °C), with sizes varying between 5 and 10 μm, were irradiated for 30 min and SEM micrographs relating initial and after insonation conditions were compared. After irradiation, extensive interparticle fusion occurred, resulting in the agglomeration of initially separated particles. Repeating the experiment with Molybdenum (mp 2617 °C) gave similar but noticeably lessened effect, even after 4 h of irradiation. Finally, ultrasonic irradiation of tungsten (mp 3410°C) produced not appreciable effect. It was concluded that the peak temperatures reached fall between 2600 and 3400 °C.

2.2.6.2 Cavitational effects in liquid-solid systems

Cavitation near extended liquid-solid interfaces is different from cavitation in pure liquids. In fact, the bubble collapse near to a large solid surface cannot occur in a symmetrical way as the solid surface hinders liquid movement from its side; thus, the major liquid flows into the collapsing bubble from the solid-free side. The result is a liquid jet targeted at the solid surface, with velocities greater than 100 m/s, as represented in Figure 2.10. The mechanical effect of this, coupled with the shock-waves created by cavity collapse in the liquid, is equivalent to a high pressure jetting, and the produced impact produces pitting of the surfaces, de-aggregation of loosely held clusters, removal of surface coatings by abrasion, and is responsible of the effectiveness of ultrasound in cleaning. Besides, this effect can increase mass and heat transfer to the surface by disrupting the interfacial boundary layers (www.sonochemistry.info/Research.htm).

Bubble collapse will be distorted by a solid surface only if the surface is several times larger than the resonant bubble size. Thus, for solid particles smaller than ≈ 200

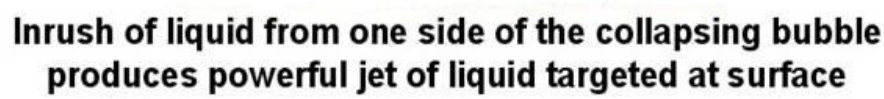

Figure 2.10 Asymmetric collapse of a cavitational bubble near to an extended solid surface (www.sonochemistry.info/Research.htm)

μm, jet formation cannot occur with ultrasonic frequencies of ≈ 20 kHz. In the presence of small particles, only normal cavitational collapse will occur, with shock waves propagating from the produced hot-spots. Such shock waves cause small particles to collide into one another with great force. Interparticles velocities depend, in fact, on various experimental parameters, including particle size, liquid viscosity and solid fraction in the slurry. Large particles are less accelerated by the cavitation shock and, in sufficiently viscous liquids, the velocity is expected to be diminished. In the experiments carried by Dokticz and Suslick (1990), summarized in the previous paragraph, for metal particles of ≈ 10 μm, the estimates impact velocities range from 100 to 500 m/s and can cause agglomeration by means of localized melting at the site of impact. For powders of brittle refractory materials, such collisions induced particle fragmentation. The comparison among large and small particles is schematized in Figure 2.11.

Figure 2.11 Acoustic cavitation in a liquid with a suspended powder (www.sonochemistry.info/Research.htm)

2.2.6.3 Effect of Frequency on Cavitation

Acoustically induced cavitation occurs above a threshold level of insonation intensity that suffices to create voids by shearing effect on a continuum fluid. However, the application of ultrasound at sub-cavitational intensities may induce mixing effects. In general, intensity refers to the mechanical-power density supplied by the insonation device, and may vary spatially, depending on the geometry of the container and the configuration of the point at which ultrasound is delivered (Cains et al.1998).

It is difficult to define a theoretical or mechanistic criterion for the onset of cavitation. However, as the most dramatic effects of cavitation are due to unstable cavities and their collapse, it may be more accurate to associate the threshold with the onset of transient cavitation that can be detected by the effect of pitting a coupon of metal foil placed in the liquid (McCausland et al. 2001).

Figure 2.12 illustrates the frequency dependence of the intensity required to induce cavitation, for degassed water at room temperature. The intensity threshold to produce vaporous cavitation presents a rapid increase only after 100 kHz and, at frequency from around 5 MHz and above, cavitation does not occur: this is the frequency range used in

medical imaging (Mason and Lorimer, 2002).

Figure 2.12 Cavitation threshold *vs* frequency for degassed water at room temperature (www.sonicsystems.co.uk/tech_paper.html)

2.3 Power Ultrasound: generation and equipment

The design of sonoprocessing equipment is set by the need to develop intensity values above the cavitational threshold throughout a defined volume of liquid. The first requirement for sonochemistry is a source of ultrasound and whatever type of commercial instrument is used the energy will be generated via an ultrasonic transducer- a device by which mechanical or electrical energy can be converted to sound energy (Mason, 1997; McCausland et al.2001). There are three main types of ultrasonic transducer used in sonochemistry:

1. liquid-driven transducers. Liquid is forced across a thin blade which causes the blade to vibrate. For each vibrational movement the leading face of the blade produces a pressure wave and the blade works as a powerful source of ultrasound.

2. Magnetostrictive transducers. Magnetostrictive transducers are based on the

reduction in size of ferromagnetic metals, e.g. nickel, when placed in a magnetic field. Magnetostrictive transducers are electromechanical devices; repeated rapid switching on and off of the current generates the mechanical vibrations, which works as the source of ultrasound.

3. Piezoelectric transducers. Piezoelectric transducers are constructed of piezoelectric ceramics. These are brittle and so it is normal practice to clamp them between metal blocks for protection. The overall structure is known as a piezoelectric 'sandwich'. Usually two ceramic elements are combined so that their overall mechanical motion is additive. Piezoelectric transducers, the most commonly used equipment for sonochemistry and sonocrystallization, are very efficient (around 85% electrically efficient according to Patist and Bates, 2000) and, depending on their dimensions, can be made to operate over the whole ultrasonic range (Mason, 1997; Guo, 2007).

There are numerous different pieces of ultrasonic equipment available for use as sonochemical reactors. The differences between them are in the design of the power generator, the ultrasonic device used and the reactor or cell used in conjunction with the source of ultrasound.

The ultrasonic cleaning bath is by far the most widely available and cheapest source of ultrasonic irradiation for the chemical laboratory. Although it is possible to use the bath itself as a reaction vessel this is seldom done because of problems associated with corrosion of the bath walls and containment of any evolved vapors and gases. The normal usage therefore involves the immersion of standard glass reaction vessels into the bath which provides a fairly even distribution of energy into the reaction medium.

The amount of energy which reaches the reaction through the vessel walls is low-normally between 1 and 5 W cm^{-2}. In fact, ultrasonic bath are of rather low power in order to avoid cavitation damage to the tank walls and the power density is low because the volumes of liquid in the tanks are generally large. Temperature control in commercial cleaning baths is generally poor and so the system may require additional

thermostatic control (Mason, 1997).

A common laboratory equipment for high intensity insonation is the ultrasonic probe. The apparatus allows acoustic energy to be introduced directly into the system rather than rely on its transfer through the water of a tank and the reaction vessel walls. The power of such systems is controllable and the maximum can be several hundred W cm^{-2}. The probe system is more expensive than the bath and it is slightly less convenient in use if the horn is to be used in reactions which involve inert atmospheres or pressures above (or below) ambient, in which case special seals will be needed (Mason, 1997).
The use of a single probe can result inefficient in large vessel, with unavoidable large uninsonated regions, nevertheless it can be extended to large volumes by incorporating it into a flow cell with a proper designed flow systems. The effective insonation volume, defined by the probe geometry and the ultrasonic path length, and the required insonation time determine the maximum flow rate through the cell, with arrangement able to operate at elevated pressure (to 10 bar) . The insonation unit can be connected via a pump in a recirculation loop from a large crystallizer (McCausland et al., 2001). However, the disadvantage is the uncontrolled attrition of particles in the pump necessary for the circulation (US2003/0051659 A1 patent).

Probe systems operating at typical face intensities of 5×10^4 to 10^6 W/m^2 and at frequencies of 20–60 kHz suffer the disadvantage that the intense cavitation field cannot be transmitted for more than a few centimeters beyond the end of the probe. Even banks of probes have been found incapable of transmitting cavitation through distances of 100–700 mm. To achieve high-density fields in large volumes, it is preferable to operate at lower face intensity (~104 W/m^2) but over extended areas. As a single transducer will only transmit a maximum total power of around 50 W, therefore it is necessary to place multiple transducers around the medium to attain high-power density. Transducers can be mounted circumferentially around a cylindrical duct, fitted in rows and spaced equidistantly, and the ultrasonic energy is transmitted from the transducer to the duct via a non-cavitating fluid acoustic-matching section. Moreover this arrangement effectively

concentrate ultrasonic intensity towards the central axis of the cylinder and away from the vessel walls preventing erosion of the metal surfaces at the point of delivery and making the process suitable for pharmaceutical applications, with strict limitations on particle shedding and metal contamination. The transducer electronics are furthermore built to a spark-proof specification suitable for flammable solvents. The unit provides a reasonably uniform insonation intensity above the cavitational threshold throughout its working volume of 4.5 L, with relatively little energy dissipated in the barrier fluid (Ruecroft et al., 2005). A metal casing contains the transducers and restricts noise release to the operating environment. With this type of system, based on a flow-through operating mode, power densities of up to 70–80 W/L are achievable in large volumes (McCausland et al., 2001; Ruecroft et al., 2005).

2.4 Ultrasonic effect on crystallization processes

Crystallization is one of the oldest unit operations in the pharmaceutical industry; however, crystallization processes still exhibit design and operational problems. These problems are mainly related to product quality requirements such as filterability, caking behaviour (the inclusion of mother liquor during subsequent re-crystallization may cause particulate agglomerate formation, a process referred to as caking of particles), purity and tablet behaviour of pharmaceuticals on the one hand, and process requirements, such as capacity. Pharmaceutical crystallization frequently produces crystals which do not satisfy the required quality and crystal size distribution. Moreover, although a significant portion of the problems encountered in crystallization processes are operational, crystallization involves few control parameters that can be adjusted to drive the processes of nucleation and growth towards the desired yield and product properties.

Sonocrystallization consists in the use of power ultrasound to control the course of a crystallization process. The application of power ultrasound to crystallizing systems appears to offer significant potential for modifying and improving both processes and

products as power ultrasound offers an additional and highly flexible method of control. Particularly, ultrasound can be used to solve some problems during crystallization processes that cannot be solved by other methods. Generally, the application of ultrasound to a crystallization operation process may bring the following advantages:

1. Narrowing of the metastable zone width.
2. Controlling initiation of nucleation.
3. Improvement in crystal shape and habit.
4. Selection of desired polymorph.
5. Processing time reduction.
6. Improving filtration characteristics.
7. Improving product properties including handling, bulk density and appearance.
8. Reduced agglomeration of crystals and fewer imperfections.
9. Increased process reproducibility.
10. Products already within a tight specification without the need for extra milling or micronisation.
11. Mixing of immiscible liquids by production of emulsion at their boundary.
12. Homogenisation.
13. Elimination of the need to add seed crystals
14. Accelerating catalytic reactions and solid/liquid separations.

Cavity collapse under heterogeneous conditions, such as near a liquid-solid interface, corresponds to an asymmetrical collapse and inrush of liquid on one side of the bubble gives rise to a violent liquid jet targeted at the surface. The net effects are surface cleaning, the destruction of boundary layers, and concomitant mass and heat transfer improvements. Bubble collapse on the surface of a particle forces it into rapid motion and collision with vicinal solid matter. Overall, such effect accounts for dispersion, erosion, and size reduction, which represents driving forces in the activation of solid reagents and catalysts. As further mentioned insonation effects, a high

ultrasonic power irradiation can cause scrubbing of the catalyst from the surface of the substrate; a higher amount of catalyst was found on the surface of the substrate when the catalyst bath was sonicated; the mechanical effect induced by cavitation enhances dissolution of a solid reactant or catalyst by renewal of the liquid at the solid liquid interface (Handbook on Application of Ultrasound: Sonochemistry for sustainability, 2012).

The main reason why ultrasound can significantly influence crystallization process is mainly on account of the cavitational effects on nucleation, crystal growth, agglomeration and breakage during crystallization process.

2.4.1 Effect of Ultrasound on Nucleation

The pre-ordering of solids in a supersaturated solution during nucleation, in particular via hydrogen bonding motifs, is important in determining what solid forms are produced. There is good experimental evidence that applying ultrasound can induce primary nucleation in nominally particle-free solutions and, noteworthy, at much lower supersaturation levels than would otherwise be the case, with a significant increase in reproducibility.

The reasons why the local and transient energy concentrations produced by cavitation phenomena correlate with nucleation events have not yet been fully explained. In one sense, the effect is counter-intuitive, in that a local temperature increase will reduce or eliminate the supersaturation in the immediate vicinity, effectively removing the driving force to nucleation. However, the cavitational shock waves may contribute to nucleation in the regions of the supersaturated solution somewhat remote from the cavitation event. Other postulates suggest (i) subsequent rapid local cooling rates, calculated at $10^7 - 10^{10}$ K/s, play a significant part in increasing de-supersaturation rates; (ii) localized increases of pressure reduced the subcooling required for the onset of crystallization, and (iii) the cavitation events allow the attivation energy barriers

associated with nucleation to be surmounted (Ruecroft et al., 2005).

Ultrasound can even induce nuclei in some systems when nucleation processes are extremely difficult to occur. In fact, ultrasound is used popularly in sugar industry to form nuclei at the initial stage of sugar crystallization. Sugar solution always has high viscosity and the nuclei are difficult to form and ultrasound irradiation can increase the nucleation rate at low supersaturation and the dispersion of nuclei is much easier than sugar seeds produced by grinding (Guo, 2007).

Ruecroft et al. (2005) suggest the possibility that ultrasound may also induce secondary nucleation (by contact) by mechanically disrupting crystals or loosely bound agglomerates that have already formed while, according to McCausland et al. (2001), continuing insonation of a solution in which solid has already separated appears not to cause mechanical disruption and breakage, but to create further nucleation and inhibit crystal growth. This results in smaller crystal sizes. It is possible that the further nucleation at this stage may be secondary (surface), resulting from cavitationally induced disturbances at the solid surfaces.

There is clearly a need for further investigation on the relationship between cavitation and nucleation.

2.4.2 Effect of Ultrasound in inducing Supersaturation

In the work presented in 2000, Thompson et Doraiswamy. investigated the effect of ultrasound in inducing supersaturation of a sparingly soluble solid in a liquid system. Such supersaturation was observed with two different types of solid-liquid systems: sodium sulfide in acetonitrile and calcium citrate in water. In the presence of ultrasound, the concentrations of these solutes in their respective solvents were increased at least 1.4 times the corresponding equilibrium saturation values.

The rate of dissolution of a solute A in a solvent depends upon the intrinsic mass transfer coefficient K_m, the interfacial area A_i, and the driving force $C_A^* - C_A$:

$$-\frac{dC_A}{dt} = K_m A_i (C_A^* - C_A) \qquad (2.15).$$

Their study demonstrated that the use of ultrasound increases the driving force for mass transfer, with the added benefit of simultaneously increasing both the intrinsic mass transfer coefficient and the interfacial area.

In a system exposed to high-power ultrasound, several simultaneous events occur that may enhance the dissolution rate of a sparingly soluble solute in a solvent. At temperatures and pressures above the critical point, the solvent is neither a distinct liquid nor a distinct gas, and is present as a supercritical fluid. The solubility of a solute in this fluid may be significantly greater than at ambient conditions, and solid particles which are typically insoluble or only slightly soluble in a solvent at ambient conditions may have very high solubilities in the same solvent when this is in the supercritical state (Mullin, 2001). Another mechanism may be the Gibbs-Thompson or Ostwald ripening effect, i.e., the enhanced solubility of very small (<1.0 μm) particles due to the increased pressure difference between the bulk fluid and the curved interface of the small solid particle. In both cases, the enhanced solubility of each system is retained even after the sonication is discontinued (Thompson and Doraiswamy, 2000**)**.

2.4.3 Effect of Ultrasound on the Metastable Zone Width

The possibility of both carrying out and controlling a crystallization process can be linked to the knowledge of the metastable zone (MZ) relating to the investigated system. For a cooling crystallization, the width of this zone (MZW) can be described as the temperature drop below the solubility curve at which the solid starts to separate spontaneously for a given concentration value and cooling rate (supersolubility limit). Reduced MZW is associated with better product quality in terms of size and habit, and a lesser propensity for the solute to “crash out” with the extensive formation of fines. Figure 2.13 shows the effect of high-intensity 20 kHz ultrasound on the crystallization of sorbitol hexacetate from methanol. When a saturated solution at 40°C was cooled (at 0.5 K/min) without ultrasound, the solution remained clear down to 33.2°C, where nucleation occurred and the solid separated out. When the experiment was repeated with

Figure 2.13 Induction of nucleation by ultrasound at reduced MZW; crystallization of sorbitol hexaacetate from methanol (McCausland et al, 2001).

insonation, the solid separation occurred at 36.8°C. Ultrasound thus reduced the metastable zone width from 6.8 K to 3.2 K (McCausland et al., 2001). Very similar effects have been recorded for a variety of small molecules where the MZW is fairly narrow and crystallization occurs quite readily.

The ultrasound effect on crystallization of sugars from water appears of significant interest. Such systems exhibit MZWs of tens of K under conventional conditions. Table 2.3 shows the reduction in MZW observed in laboratory-scale experiments for a range of sugars. For d-lactose, the MZW reduction appeared small; however, the crystals obtained with ultrasound were smaller and more uniform in appearance than those in the non-insonated control. For d-glucose a broad MZW was usually observed; if ultrasound was not used, the solution remained metastable down to 22 °C or less, while well-defined crystals of d-glucose monohydrate were obtained by sononucleation at 70 °C and managing the growth process accordingly whilst cooling to ambient temperature

(Ruecroft et al., 2005).

Table 2.3 Ultrasonic crystallization of mono- and disaccharides from aqueous solutions (Ruecroft et al., 2005).

solute	quantity dissolved in 10 mL water (g)	temp (°C) at which solid appeared	
		without ultrasound	with ultrasound
D-xylose	25.0	36	43
D-sucrose	18.0	<40	47
D-lactose	5.5	41	43
D-maltose	13.0	<20[b]	40
D-glucose	100.0[c]	<30	75
D-cellubiose	2.0	<20[b]	42

[a] Saturated solutions are prepared at 50 °C and cooled at 0.2 °C/mn: 20 kHz ultrasound applied for 30 s for every degree drop in temperature at power input density ~35 $W \cdot L^{-1}$. [b] No crystals appeared at 20 °C. [c] Solution prepared at 85 °C.

2.4.4 Effect of Ultrasound on Induction time and Nucleation rate

The induction time, t_{ind}, is defined as the time elapsed between the creation of supersaturated conditions and the appearance of crystals, and usually decreases as supersaturation increases. In the work proposed in 2002, based on cooling crystallization of potassium sulphate from aqueous solution, Lyczko et al. demonstrated that the induction time is dramatically reduced by the presence of ultrasound. At an absolute supersaturation of 0.0156 g K_2SO_4/g water, the induction time in the absence and presence of ultrasound was found to be 9000 and 1000 s respectively (with ultrasonic power of 0.05 and 0.12W/g solution and frequency of 20 kHz). Moreover, the concentration seemed to decrease faster with ultrasonic irradiation suggesting that more crystalline surface was formed. Interestingly, the ultrasonic effect on t_{ind} was especially significant at low absolute supersaturation levels (<0.014g K_2SO_4/g water), becoming less significant at high supersaturation levels, when nucleation is very fast anyway. When ultrasound is applied to the solution, a lower wall temperature is required to

maintain the same reactor temperature in order to allow the ultrasonically generated heat power to be removed by the jacket. Therefore, the absolute supersaturation at the wall is higher when ultrasound is applied, and this could contribute in a shortening of the induction time. Lyczko et al. (2002) compared the specific contribution of ultrasound and its thermal effect, concluding that the strong effect on nucleation cannot be explained by the wall temperature effect.

Finally, they investigated the relationship between induction time and supersaturation ratio S analysing the slope of the plot $ln(t_{ind})$ versus $ln(S^{-2})$: the low numerical values of the slopes suggested that the main mechanism is heterogeneous primary nucleation. Kordylla et al. (2009) developed this point suggesting that the nucleation work is reduced, possibly because a low wetting angle between the cluster and the bubble surface area, or due to the induced energy of ultrasonic waves, which decreases the activation energy and therewith the critical cluster radius.

In crystallization processes induced by the addition of an antisolvent, where high supersaturation levels may be produced very rapidly, it has been shown that the application of ultrasound reduces not only the induction times of nucleation but also the spread of variability in induction times at a given level of supersaturation. Figure 2.14 illustrates the effects for the anti-solvent crystallization of roxithromycin in an acetone–water mixture (Guo, 2005), and similar results have been achieved with Barium sulphate in a reactive crystallization. As can be seen, the induction time decreased as supersaturation increased, whether or not ultrasound was applied. However, ultrasound significantly reduced the induction time, particularly at low supersaturations, confirming the effect of ultrasound on nucleation is stronger at low supersaturation levels.

Induction time has an inverse proportional relationship with nucleation rate that can be expressed by

$$B_0 = K_p t_{ind}^{-1} \tag{2.16}$$

Figure2.14 Influence of ultrasound on the induction time of roxithromycin: (▲) with ultrasound, (■) without ultrasound, (Guo et al, 2005).

where B^0 is the nucleation rate, defined as the number of nuclei formed per unit time and volume and K_p is a coefficient of proportionality. Combining this relationship with the commonly used correlation between nucleation rate and supersaturation

$$B^0 = K_N \Delta C^b \tag{2.17}$$

where K_N is the nucleation rate constant and b is apparent nucleation order, and taking the natural logarithm of both sides of resulting equation, the following equation is produced :

$$ln\, t_{ind} = ln\left(\frac{K_p}{K_N C_S^{*b}}\right) - b\, ln(\sigma) \tag{2.18}$$

where C_S* is the solubility concentration, and σ the relative supersaturation $\left(\sigma = \frac{C_S - C_S^*}{C_S^*}\right)$.

The plot of $ln(t_{ind})$ versus $ln(\sigma)$ for experiments with and without ultrasound are depicted in Figure 2.15. The values of the slope, that coincide with the apparent nucleation order, are very close so ultrasound does not increase significantly the apparent nucleation

order under the assumption of homogeneous nucleation. On the other hand the intercepts are very different, that implies that the nucleation coefficient k_N is significantly increased: in this particular case it was increased 4.25 times. The increase of k_N is hence the main reason for the increase of nucleation rate.

2.4.5 Ultrasound and Seeding

As controlling method for crystallization operations, ultrasound can be compared with seeding. Intentional seeding is common in industrial crystallization processes, including the crystallization of APIs, but they usually require operator intervention to add the seeds, which may entail additional engineering to control the seed addition. Seeding operations induce decay in the solute concentration at low supersaturation values, in the metastable zone. The effects of intentional seeding include narrowing of the MZW, shortening of induction times, and, most importantly, the control of particle sizes and distribution. In a batch process, seeds have to be added at precisely the correct time during the development of the supersaturation profile. Addition too soon to a

Figure 2.15 Induction time as a function of relative supersolubility: (♦) without ultrasound, (■) with ultrasound (Guo et al, 2005).

solution that is undersaturated will result in the seeds dissolving. Seeding too late will also be ineffective because the solute material may already have rapidly (and possibly disastrously) crystallized as a result of high supersaturation levels with ensuing high nucleation rates, or because the metastable limit can be crossed during the early stage of cooling after seeding, with consequent prolific and uncontrolled nucleation, giving a product of inferior physical characteristics. Furthermore, grinding processes are often employed to produce crystal seeds, hence the mean size and size distribution of seeds are commonly unsatisfactory, while grinding processes may introduce impurities into seeds and may pollute the environment and, when added into solution, seed particle often agglomerate and are difficult to disperse. Extremely small seed crystals generated by insonation offer all the advantages of conventional seeding without many of the drawbacks such as handling, actual physical size of the seeds, when to add to a batch process, and quality of the seed. The exact point of nucleation (in terms of supersaturation) can be well controlled, with the number of nuclei generated as a result of the prevailing supersaturation level (Ruecroft et al., 2005).

2.4.6 Effect of Ultrasound on Crystal Growth

The effects of ultrasound on crystal growth does not appear as dramatic as those on nucleation and arise largely from enhanced bulk-phase mass transfer due to mechanical disturbances via cavitation and acoustic streaming. Such effects will alter the fluid dynamics and increase bulk-phase mass transfer of solute to the surface of the growing crystal. In most cases, however, the surface nucleation and integration effects at the crystal faces will determine the growth rate of each individual face and, hence, the habit of the crystal. The magnitude of the supersaturation can affect the influence of ultrasound on crystal growth rate. In a study indicated by Ruecroft et al. (2005), at low supersaturation, with growth velocities at the crystal faces around 10^{-10} m/s, the application of ultrasound doubled the growth rate, while at higher supersaturation, with growth velocity around 10^{-7} m/s, there appeared to be no effect. The ultrasonic effect is

explained by the hypothesis that, at low supersaturation, the quantity of available growth units in the vicinity of the crystal surface is small. Under these conditions, bulk-phase mass transfer becomes rate limiting in supplying growth units to the crystal surface, and its ultrasonic enhancement will enhance the growth rate.

2.4.7 Ultrasonic effects on Agglomeration and Breakage

Ultrasound has been shown to significantly influence agglomerative phenomena. Doktycz and Suslick (1990) showed that metal microparticles under ultrasonic irradiation can bond together by means of neck of melt material and form agglomerates. However, works carried out on non-metallic particles reveal a reduction of agglomeration. According to Luque de Castro and Priego-Capote (2006), three ultrasonic effects may contribute to this phenomenon. First, the shock wave caused by cavitation can shorten contact time between crystals. Therefore crystals do not have enough time to bond together. Secondly, some agglomeration invariably occurs at the nucleation stage as nuclei possess a high surface area to volume ratio: that results in a high surface tension which nuclei tend to lower by adhering to one another. The surface tension decreases as crystals grow larger and become more stable, which hinders agglomeration. Finally, the enhanced mixing conditions created by ultrasound application also reduce agglomeration through control of the local nucleus population.

Poor mixing conditions increase the nucleation rate locally. An example can be an anti-solvent crystallization: when the anti-solvent is added into the solution, it does not disperse immediately and produces high localized supersaturation regions. Poor-mixed conditions are unavoidable when the process uses mechanical agitation only. That increases the possibility for nuclei to agglomerate

Compared with mechanical agitation, ultrasound induces a great advantage as the mixing is improved and the local nuclei population is controlled. As a result, the agglomeration is also significantly depressed.

The ultrasound also has breakage effect to crystals. The phenomenon is on account

of the velocity increase and the collision between particles after ultrasound is applied to the system. The mechanical effects (shock wave, liquid jet and acoustic streaming) of ultrasound can produce interparticle collisions with high levels of kinetic energy. Moreover, liquid jet acoustic streaming can erode crystal surface directly, which will increase both secondary nucleation rate and breakage rate during crystallization.

Guo et al. (2005) reported that ultrasound has a significant effect on depressing agglomeration and breaking crystals as shown in Figure 2.16.

Figure 2.16 SEM photos of roxithromycin crystals (Guo et al., 2005)
left: without ultrasound
right: with ultrasound

2.4.8 Ultrasonic effects on Crystal Size Distribution and Crystal Habit

Ultrasonic irradiation over a crystallization operation makes it possible to "tailor" a crystal size distribution between the extreme cases of a short burst of ultrasound to nucleate at lower levels of supersaturation and allow growth to large crystals, and the production of small crystals via continuous (or perhaps a longer single burst) insonation throughout the duration of the process, which can facilitate prolific nucleation at higher levels of supersaturation at the expense of some crystal growth. Pulsed or intermittent application of ultrasound can give intermediate effects with the optimum to be determined by experimental investigation. Figure 2.17 illustrates the effects of ultrasound on the overall shape and size of crystals of adipic acid. The continuous application of ultrasound narrows the particle size distribution and gives generally a

mono-modal distribution.

Moreover, insonation at different stages of crystallization may be used to modify and tailor product properties to meet requirements. Applied only at the early stage, insonation induces primary nucleation, and enables crystallization to be carried out at moderate MZWs, producing large and well formed crystals with minimum fines while ultrasound may be applied univocally in the final stages to break up agglomerates.

An initial burst of ultrasound gives an even lower bulk density that is easy to filter, but not ideal for packaging while a finely divided product obtained from continuous insonation yields excellent bulk density that is difficult to filter, but convenient for packaging (McCausland, 2001).

A molecule of an active pharmaceutical ingredients (API) exhibiting troublesome behaviour in terms of crystal habit has shown significant improvement in crystal habit. When high (labile) levels of supersaturation were reached in a standard cooling crystallization, high nucleation rates, along with concomitant poorly controlled crystallization, led to the proliferation of a distinct needle habit, with poorly stirred slurries and variable product bulk density. Conversely, when a solution was treated with ultrasound at much lower levels of supersaturation, a highly desired rhombic-/plate-type habit was easily produced. In addition to controlling the habit, careful insonation regimes allowed the particle size to be controlled consistently as shown in Figure 2.18. Importantly, large particles and agglomerates >1 mm in size were avoided (Ruecroft et al., 2005).

Figure 2.17 Cooling crystallization of adipic acid from water: (left) noninsonated control experiment; (center) short ultrasound burst at 48 °C; (right) continuous insonation (Ruecroft et al.2005).

The specification of crystal habit is usually determined by the physical properties required of the product, both in terms of further processing and of end-use. Two reasons may cause the change of crystal habit by ultrasound. For one thing, crystal growth does not occur isotropically, and the faces that are exhibited by a crystal are those that grow more slowly. Extreme crystal habits form when the growth rate at a particular crystal face (or faces) occurs significantly more rapidly than the growth at other faces. These anisotropic effects are most marked when the driving force for growth, i.e. the supersaturation, is high. Crystals produced with ultrasound usually exhibit moderate and regular habits, because the process operates under conditions of low or moderate supersaturation.

2.5 Conclusions

The physical processes associated with ultrasonic irradiation bring several

Figure 2.18 The effects of ultrasound on particle size distribution for a small-molecule API: (1) single burst at low supersaturation, (2) multiple bursts with cooling at low supersaturation, (3) multiple bursts with cooling commencing at medium-high levels of supersaturation, (4) as (3) but with improved stirring with baffles (Ruecroft et al.2005).

beneficial effects in crystallization. Ultrasonic energy consists of mechanical vibrations occurring above the upper frequency limit of human audibility (generally accepted as about 20 kHz). Ultrasound consists of a propagating disturbance in a medium that causes subunits (particles) of the medium to vibrate. Its power induces the phenomenon of stress and acoustic streaming in fluids, a driving force for mass transfer: after ultrasound is applied to a system, the mass transfer rate can be accelerated significantly in both diffusion process and convection process. Above a threshold of intensity, depending on the frequency, it initiates an important phenomenon known as cavitation. The cavitation produces strictly localized and transient regions of extreme conditions of temperature and pressure, and the release of a powerful shock wave.

Cavitation results particularly effective as a means of inducing supersaturation of sparingly soluble solutes, modeling the crystal size distribution, producing particles with improved habit and reducing agglomeration. The most relevant benefit of sonocrystallization relates to the nucleation stage: ultrasound has been demonstrated to reduce the induction time, narrow the metastable zone width and increase the nucleation rate. Furthermore ultrasonic irradiation results particularly effective in inducing nucleation in otherwise non nucleating systems. As fundamental benefit, ultrasound consistently improves the reproducibility.

Cavitation is also responsible for mechanical disturbances by which ultrasound may induce secondary nucleation (by contact) and mechanical disruption of loosely bound agglomerates that have already formed.

Using ultrasound provides a well-defined starting point for the control and monitoring of crystallization processes, including factors as product purity, product bulk density and powder characteristics. Thus, the application of power ultrasound to crystallization systems appears to offer significant potential for modifying and improving both processes and products. Sonication can eliminate the requirement to add seed crystals, and this can be particularly advantageous in sterile crystallization.

The main reason why ultrasound can bring such a significant influence to

crystallization processes is on account of its effects on crystallization kinetics. Ultrasound can influence the kinetics of nucleation, crystal growth, agglomeration and breakage during crystallization processes.

CHAPTER 3

CONTINUOUS CRYSTALLIZATION OF ADIPIC ACID WITH ULTRASOUND

3.1 Introduction

Continuous crystallization is an attractive method for large-scale production of crystalline powdered materials. Many of the companies involved in continuous processing are looking towards this technology to improve their economic performance and the controllability on the physical properties of the product. Furthermore, in recent years interest in the application of ultrasound to crystallization has received a significant impetus with the increased requirement to prepare complex chemical entities to very exacting standards.

"The application of ultrasound to crystallizing systems offers a significant potential for modifying and improving both the processes and products" (McCausland at al., 2001). Ultrasound technology has been available for many years in research and diagnostics, however its application to chemical processes has developed rapidly only in the last two decades as high intensity systems that can deliver power ultrasound on industrially relevant scales have become available. Research into the influence of ultrasound on crystallization processes has revealed that the crystallization of solid crystals (from a number of liquids including organics and metals) is affected by the presence of ultrasonic waves. The use of ultrasound offers a method for modifying and improving products in terms of crystal habit, size distribution and purity (Ruecroft et al. 2005, Luque de Castro and Priego-Capote, 2007) and processes (controllability and reproducibility) which has broad applications in crystallization, product recovery and purification processes. The requirement for environmentally clean processing and the use of relatively inexpensive equipment contributes in intensifying the interest on ultrasound technology and in developing its applications. Furthermore, ultrasound seems to provide a distinct alternative to more traditional techniques of controlling the crystallization process such as seeding strategies (McCausland et al. 2001, Ruecroft et al. 2005).

Coupling ultrasonic irradiation to a crystallization process has proven to influence nucleation and also affect crystal growth rate, agglomeration and breakage, thus can significantly influence crystal production.

Ultrasonic cavitation is commonly recognized as the most important mechanism by which ultrasonic irradiation can influence crystallization (Young, 1989, McCausland et al., 2001: Mason and Lorimer, 2002; Patist and Bates, 2008).

The principal effect of imploding transient cavities is the release of large amount of energy into small and spatially resolved regions. The violent collapse generates extreme local temperatures and pressures, apart from mechanical effects: large shock waves are produced in the region of the liquid remote from the cavitational event, causing a variety of physical events, such as microstreaming (localized turbulence of the solid-liquid film which accelerates the rate of mass transfer through the film itself) and particle acceleration (Thompson and Doraiswamy 2000).

The sonocrystallization literature mainly focuses on batch crystallization operations, currently prevailing in pharmaceutical industry, with less information relating to continuous crystallization processes. However, the greater pressure to reduce manufacturing costs, the lure of reduced process variability and a regulatory environment supportive of manufacturing modernization are leading companies to consider continuous processing in their strategies. Continuous crystallizers are generally more economical in operating and labor costs than batch units are, require smaller sizes and can reduce the degree of scale-up issues because of the greater replicability of results. Process conditions can be more stable through achieving a steady state, offering an improved controllability compared to batch processing. Nevertheless, these advantages are counterbalanced by the slowness in attaining the steady state and encrustation issues on heat-exchanger surfaces (Randolph and Larson, 1988; Pellek and Arnum, 2008; Mullin, 2001).

The present chapter concerns an experimental investigation on the effect of a continuous sonication on a continuous crystallization process. Cooling crystallization of adipic acid from aqueous solution is the selected case study. Analogous experiments have been carried out both under silent and continuous insonation regime in order to investigate the effects of cavitation on the solid recovery and the physical properties of crystals at steady state operating conditions. A separate analysis focuses on the influence

of residence time on the time required to reach the steady state, theoretical yield and supersaturation/ solute concentration at steady state, particle size distribution (PSD) and crystal habit.

3.2 Physical properties of the system under investigation

3.2.1 Materials

The working substances selected for this work are adipic acid (>99.5% pure, Sigma-Aldrich) and deionized water (conductivity < 0.2 μS/cm).

Adipic acid has chemical formula $COOH(CH_2)_4COOH$ and is one of most significant aliphatic dicarboxilic acids. Its primary industrial use is the production of nylon 6,6 polyamide but it also has many other commercial uses such as flavoring, leavening, and pH control agent in food production . Adipic acid imparts a slowly developing smooth, mild taste in supplementing foods with delicate flavors. Furthermore, it is practically non hygroscopic, a property that has the advantage of prolonging the shelf life of powdered products (e.g. drink, cake mixes, and instant pudding) in which it is incorporated. Finally, it is an excipient used in the pharmaceutical industry (tablet lubricant, acidulant in effervescent tablets and a constituent of tablet coating films) (Clydesdale et al, 2005).

The physical properties of Adipic acid are listed in Table 3.1:

Table 3.1.Properties of pure adipic acid: data from NIST chemistry WebBook.

Molecular weight g mol^{-1}	Solid density at 20 °C g/ cc	Melting point K	Specific heat (solid) Kcal Kg^{-1} $°C^{-1}$
146.14	1.36	425	1.59

Regards to the acidity of adipic acid, Christensen et al., 1976, indicate a second acidity constant Ka_2 of 5.4 at 25°C. Accordingly, it may be considered as a monoacid with dissociation reaction in the form of

$$HR \Leftrightarrow H^+ + R^-$$

The acid dissociation constant, k_a for such reaction,

$$k_a = \frac{[H^+][R^-]}{[HR]}$$

is equal to 4.42 at 25°C.

Adipic acid normally crystallizes from aqueous solutions as flat, slightly elongated, hexagonal, monoclinic plates (Clydesdale et al., 2005; Caputo et al., 2008). According to Michaels and Colville (1960), the two predominant faces are [001] and [001] (crystallographic family {001}- face (C) as shown in Figure 3.1), whilst the two elongated side faces are $\{\overline{1}\ 02\}$(faces (B)), and the four end faces are {110} (faces (A) in Figure 3.1). The linear, six-carbon dicarboxylic acid molecules are aligned end-to-end in a parallel array in the crystal, with their long axes parallel to the B face; therefore the C faces are made up entirely of carboxyl groups, whereas the B and A faces contains both carboxylic and hydrocarbon portions of the molecules. According to Clydesdale et al (2005), the water molecules tend to block the growth of the dominant faces (001), made up entirely of carboxyl groups: the growth rates of these faces are determined more by water desorption than the addition of new growth slices.

The solubility of the adipic acid–water system, in the temperature range 0-100 °C,

Figure 3.1 Morphology, faces, and orientation of the adipic acid molecules with respect to the faces of adipic acid crystals. The linear six-carbon chains are perpendicular to the C face so that the face is made up entirely of carboxylic groups (Caputo et al., 2008).

Figure 3.2 Solubility of adipic acid in water (data from Mullin, 2001)

is shown in Figure 3.2. Solubility data are taken from the literature (Mullin, 2001) and the trend shows a strong dependency on the temperature above 20°C, therefore cooling crystallization or flash-cooling crystallization from higher temperatures is the most efficient method of crystallization for this binary system.

3.2.2 Experimental set-up

The experiments were carried out in the experimental apparatus shown schematically in Figure 3.3. The crystallizer consists of a flat bottomed jacketed glass reactor (1; 300 ml, *ID* = 80 mm) equipped with four baffles. The content was stirred using a four-blade marine-type propeller (d_p= 32 mm), and the clearance between the blade axis and the vessel bottom was 1/7 of the whole height of the liquid in the vessel. In non insonated experiments, the stirrer speed was maintained at 800 rpm to ensure complete particulate suspension and avoid the formation of bubbles. For insonated experiments, adequate stirring was provided by a combination ultrasonic probe-magnetic stirring bar at a speed value of 200-250 rpm to ensure an effective suspension. Feeding solution from the feed tank (2) was realized by means of a peristaltic pump (5) whose rotational speed could be set at different values in order to select the desired

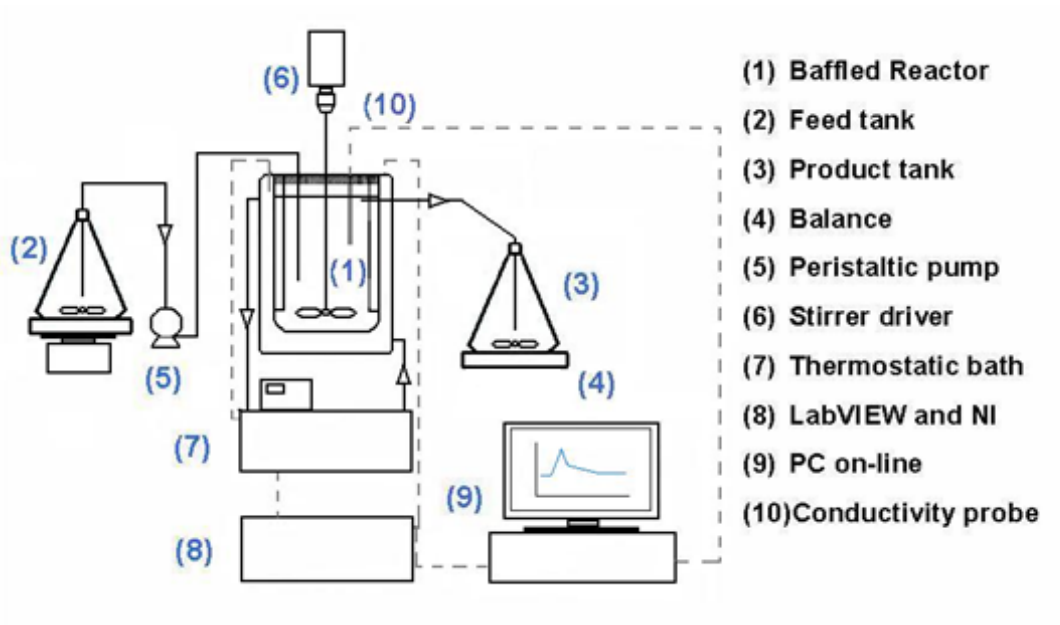

Figure 3.3 Experimental set-up: Continuous Laboratory-scale crystallizer.

flowrate value. The feed tank was heated using a hot plate magnetic stirrer and insulated to reduce thermal losses. The withdrawing of the product from the reactor to the product tank (3) was obtained by means of an overflow pipe, and the discharge was operated in an intermittent way, using a valve, to achieve high withdrawal velocity levels and prevent classification: this precaution ensured that the discharge size distribution and liquid phase composition were the same as they were in the crystallizer (Randolph and Larson, 1988). In each cycle about the 10% of the vessel volume was removed. A balance (4) was used to control the speed of the pump and therefore the desired feed rate by checking the weight of the product tank during the run. The reactor jacket was thermostated using a Haake thermostatic bath (7) and the vessel temperature was controlled by means of a Labview -National Instrument hardware.

Conductivity measurements were carried out during the experiments to monitor the desupersaturation trend over time. In a set-up menu, the main process parameters such as temperature, eventual cooling or heating rates, and the duration of the experiment were chosen.

The PSD was determined using Malvern MasterSizer-S (Malvern Instruments Ltd, Worcestershire WR14 1XZ0, UK), based on the principle of laser ensemble light

Figure 3.4 Schematic diagram of the classical laser diffraction technique (Abbas et al.,2002).

scattering. The instrument is categorized as a non-imaging optical system, as sizing is accomplished without forming an image of the particle on a detector. The optical configuration is shown diagrammatically in Figure 3.4. The light from a low power helium–neon laser is transmitted to the crystal sample. The crystal particles within the sample scatter this laser light: the scattering angle is a function of the crystal's size, shape, refractive index, and the wavelength of the incident light. The particles are introduced to the analyser beam by the sample cell. The light scattered by the particles and the unscattered remainder are incident on a Fourier transform lens and focused on a detector, which gathers the scattered light over a range of solid angles of scatter (0.01 - 135 degrees) . The information gathered by the detector is, via a deconvolution step, translated into a Crystal Size Distribution (CSD). An important note to make is that the measured size distributions and characteristic length refer to spherical particles with volume equivalent to the detected particles and their diameter respectively (Malvern Mastersizer S Manual, Chapter7).

The morphology of the crystals at the steady state was investigated using a light microscope (Olympus IX50), with magnification selected within the range 100-400. In addition, some morphological investigation was carried out using a scanning electron microscope (SEM), with magnifications up to 1000.

A 750 W ultrasonic processor with the frequency of 20 kHz (Cole-Parmer Instruments, Illinois, USA) was used for the experiments with insonated control. It

consists of three major components: an ultrasonic power supply (generator), a converter and a probe. The ultrasonic power supply converts 50/60 Hz voltage to high frequency electrical energy. This energy is transmitted to the piezoelectric transducer within the converter where it is changed to small mechanical vibrations. Finally, the converter's longitudinal vibrations are amplified by the probe and transmitted to the liquid as ultrasonic waves consisting of cycles of alternate compressions and rarefactions (www.innocalsolutions.com). The intensity of sonication is proportional to the amplitude of vibration of the ultrasonic source and, as such, an increment in the amplitude of vibration will lead to an increase in the intensity of vibration and to an increase in the sonochemical effects (The Power Ultrasound from http://www.wiley-vch.de/books/sample/3527319344_c01.pdf).

The probe, with a diameter of 12 mm, was immersed of approximately 15 mm in the liquid. The acoustic intensity of the probe was adjusted by regulating the power amplitude.

3.2.3 Operating procedure

The experiments were carried according two different operating procedures. In the first case, the experiments were carried out initially by cooling down a slightly undersaturated solution from a temperature up to 5ºC higher than the solubility value to a final temperature of 20 ± 0.5 ºC, and, only once stable conditions were attained, the continuous run was started with constant feed and discharge rate. During the continuous run, the temperature of the inlet stream was approximately equal to the value set for the beginning of the cooling. In this latter procedure, an extreme fouling on the cooling surfaces (vessel walls) occurred, reducing the effectiveness in the temperature control. However, as most deleterious effect, the encrustations caused obstruction in the outflow pipe and a consequent overflow of the reactor, requiring a premature interruption of the experiment, showing similarities with the operation of a 20 L bench-scale KCl crystallizer reported by Randolph and Larson in their book "Theory of Particulate Processes" (1988).

In an effort to avoid extreme fouling conditions, a second operating procedure was tried to carry out this investigation. The crystallizer was initially filled with a saturated solution at the temperature set as steady state value of 20 ºC, and the continuous run was started by admitting hot concentrated feed solution and initiating the product discharge. In this start up mode the crystallizer was operated for long times without extensive cooler fouling and a steady state PSD was obtained. The results achieved in this work have been obtained following the latter operating procedure.

Experiments were carried at three different values of mean residence time, τ, defined as

$$\tau = \frac{V}{Q_{feed}} \tag{3.1}$$

where V is the bulk volume, and Q_{feed} is the volumetric feedstock flowrate. The objective was to examine the influence of τ on the time required to reach steady state operating conditions, final supersaturation and yield, particle size distribution, and particle morphology. A set of three mean retention time values was selected, fixed at 10,

Table 3.2 Experimental conditions for insonated experiments

T_{feed}, °C	T_i, °C	% of Power amplitude	τ, min
40	20	40	10
40	20	40	20
40	20	40	30
40	20	60	15
40	20	60	20
40	20	60	30
50	20	60	15
50	20	60	20
50	20	60	30

20 and 30 minutes. Two inlet concentration values were chosen, 5 and 9.2 g solute/ 100 g of water, corresponding to a solubility temperature of 40 and 50 °C respectively (Mullin, 2001). Insonated experiments were performed at 40% and 60% of the maximum nominal value as reported in Table 3.2. Whenever the power amplitude was set at 60 %, the minimum residence time value investigated was 15 min: such a precaution ensured isothermal operating conditions throughout the continuous run, not guaranteed at lower values of τ under continuous insonation.

3.2.4 Running of the experiments

The first part of each experiment consisted in the preparation of the feed stock solution before starting the experiment; the feed solution was kept at temperature values slightly higher than the solubility value for at least 1 hour, in order to delete the thermal history of adipic acid crystals.

The feed tank temperature was regulated at a value ensuring that the inlet solution was slightly undersaturated to prevent crystallization before entering the crystallizer. The continuous run was started only after the desired values of reactor temperature and inlet temperature were reached.

During the experiment, samples of product were taken at different times, quickly weighed and filtered using a vacuum filter, to reduce the time for possible alteration of the sample characteristics. The conductivity of filtered mother liquor was measured and recorded to monitor the concentration-supersaturation evolution over time. In some cases, the just-filtered filter cake was analyzed in the Malvern Mastersizer to determine the particle size distribution and investigate its temporal evolution. In other cases the filter cake was washed several times, using saturated solution at the same operating temperature of 20 °C, to reduce the solid content in the entrainment, namely the amount of mother liquor retained on the crystal surfaces (Yang and Randolph, 1999).

Particles sampled both during and after the experiments were also visually analyzed to investigate the crystal habit.

3.3 Results and Discussions

3.3.1 Crystal habit

Figure 3.5 shows two SEM photomicrographs of adipic acid crystals obtained under steady state conditions. Pictures refer to a cooling experiment from 40 °C to 20 °C, with a mean residence time of 30 min, without sonication (a) and with sonication at 40% amplitude (b). A massive presence of agglomerated particles (particles grown into each other) and a hexagonal-like geometry for the crystals can be recognised in picture (a).

Crystals produced under continuous ultrasonic treatment present a noticeably reduced particle size than those produced under silent conditions; in particular, picture (b) reveals elongated crystals with hexagonal-prismatic geometry, and particles sizes smaller than 10 μm. These particles appear more regularly and evenly shaped, with a cylindrical symmetry rather than a plate geometry and the amount of agglomerates is visibly reduced. Several reasons are suggested to explain this phenomenon. First, the

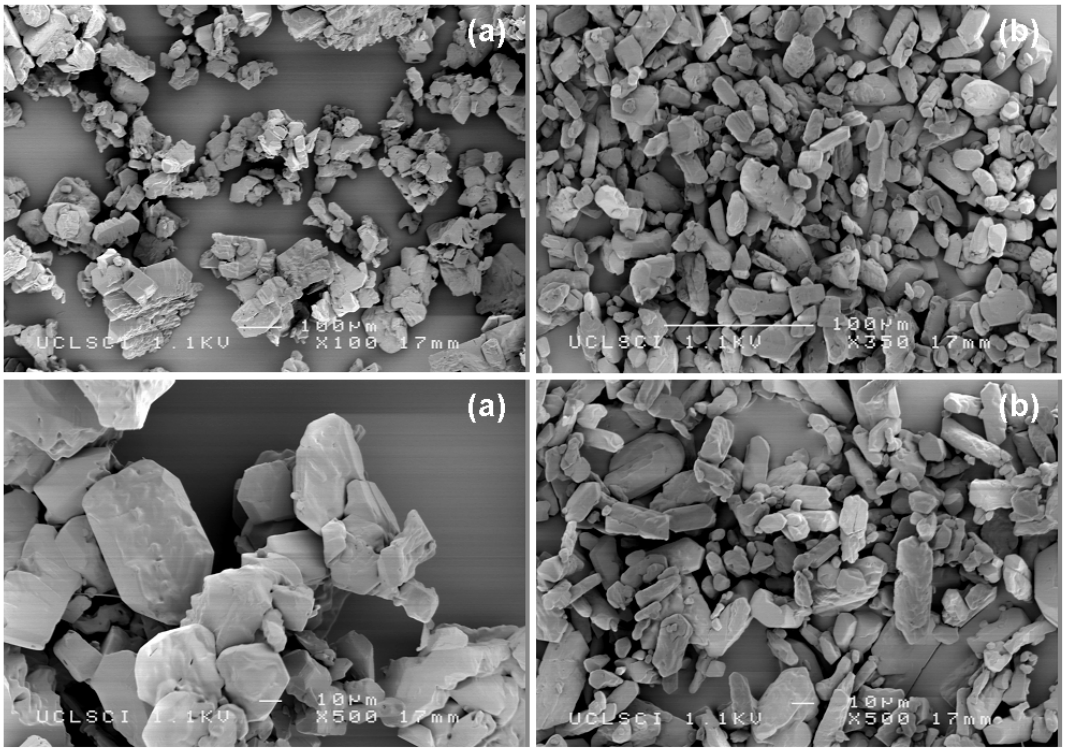

Figure 3.5 SEM photomicrograph of adipic acid crystals at steady state: (a) without sonication; (b) with sonication.

shock wave caused by cavitation can shorten the contact time between crystals to an extent precluding their bonding together. Second, some agglomeration invariably occurs at the nucleation stage, when nuclei possess a high surface area to volume ratio, hence a high surface tension tends to lower their propensity to adhere to one another. The enhanced mixing condition created by ultrasound application reduces agglomeration through control of the local nuclei population (Ruecroft et al., 2005). Finally, a system of single separated particles of higher energetic state is favoured under a continuous energy supply due to ultrasonic irradiation.

On the other hand, ultrasound may also induce secondary nucleation by mechanically disrupting crystals or loosely bound agglomerates that have already formed. In fact larger solute particles have an increased opportunity to collide with each other because of microstreaming induced by cavitation and high kinetic energies, that could justify the presence of fragments (Ruecroft et al., 2005; Luque de Castro and Priego-Capote, 2007).

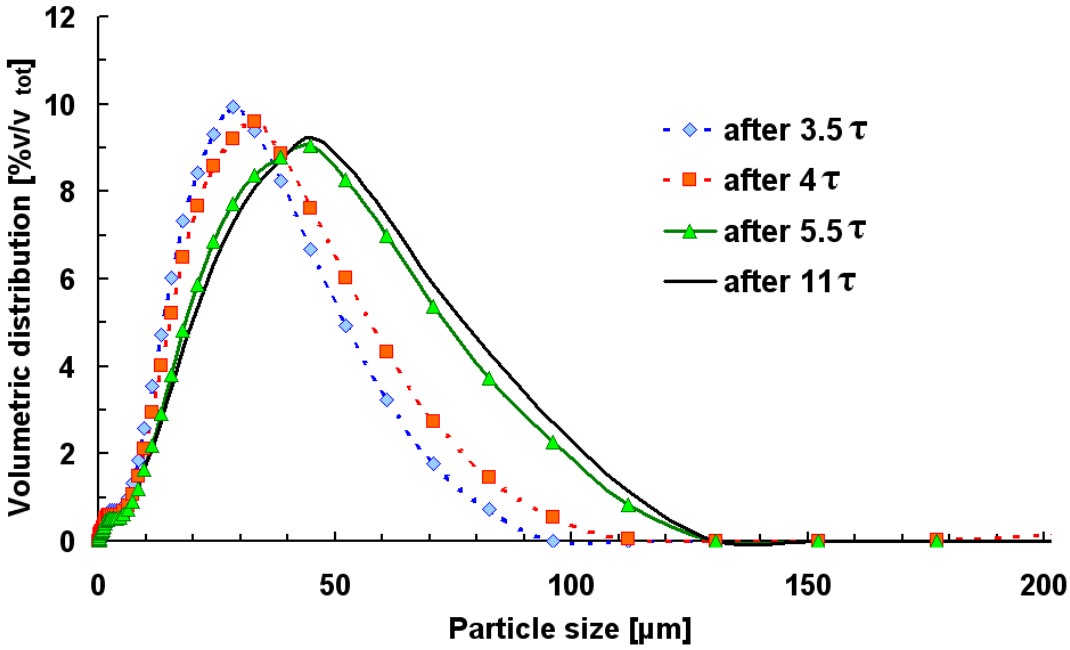

Figure 3.6 Crystal Size Distribution evolution over time. Operating conditions: cooling from 40 °C to 20 °C, τ = 30 min, sonication at 60% of nominal power

3.3.2 Steady state determination

The achievement of steady state conditions was determined by monitoring the temporal evolution of the particle size distribution. Samples of crystals from the outflow product were taken at different times, quickly filtered to reduce the time for eventual alteration of the sample characteristics, finally analyzed with Malvern MasterSizer instrument. Exemplifying results are depicted in Figure 3.6, referring to a case of cooling crystallization from 40 °C to 20 °C, sonication at 60% power amplitude, and 30 min as residence time.

To check no classification occurred at the withdrawal, and the size distribution of crystals in the product reflected the conditions in the crystallizer, a further investigation was carried out to compare the PSD from the product with the PSD of the total crystallizer content at the end of the experiment, after steady state was reached. The results, as can be seen in Figures 3.7, mostly show a good agreement, however, the curve relating the vessel content presents an extension for higher values of characteristic length. The fouling formed on the internal walls of the vessel and on the surfaces of baffles, impeller and probes, composed of crystals retained for longer than the liquid residence time distribution, is considered a plausible cause. For this reason, this study focused on the size distribution of particles solely collected from the product slurry.

Figure 3.8 illustrates the effect of mean residence time on the duration of transient period, τ_{tp}, expressed in terms of ratio of τ_{tp} / τ. The application of ultrasound clearly reduces the time requirement to achieve steady state operating conditions. That could be ascribed to the rise in the nucleation rate, as will be explained in a separate chapter, and the corresponding reduction of the temporal scale of several following phenomena involved in the crystallization process. The power amplitude does not seem significantly to affect the duration of the transient period in the range of τ values investigated. It is notable that continuous insonation throughout the duration of a continuous experiment markedly reduces the influence of residence time on the length of the transient period.

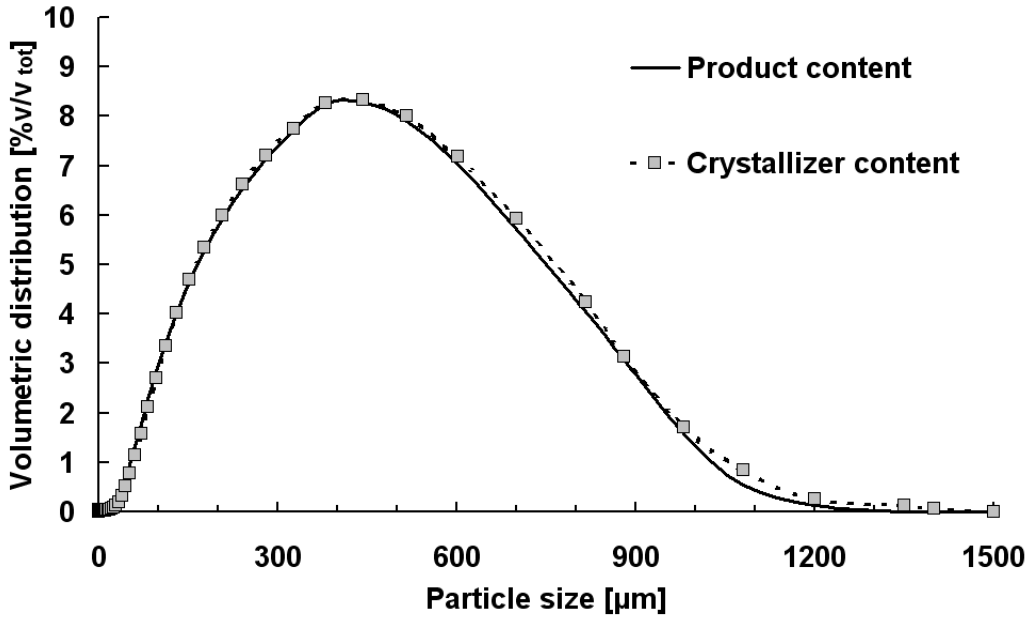

Figure 3.7 Comparison among the crystal size distributions of the product and the vessel content at steady state. Operating conditions: silent conditions, cooling from 40 °C to 20 °C, τ = 10 min.

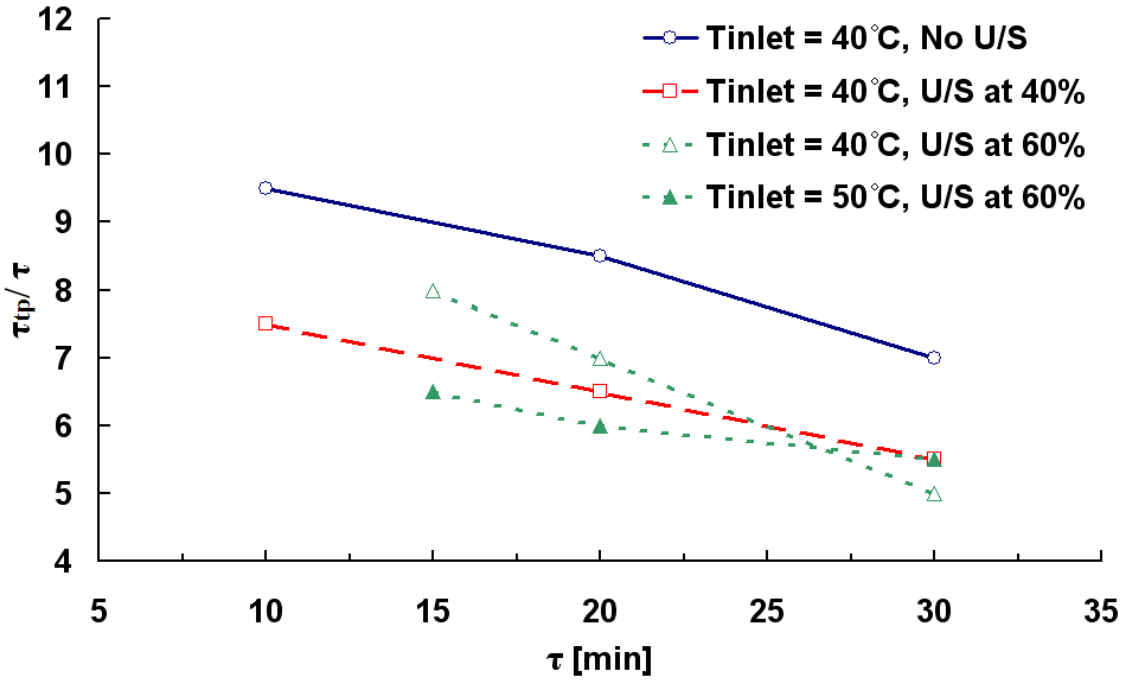

Figure 3.8 Effect of mean residence time on the transient period duration

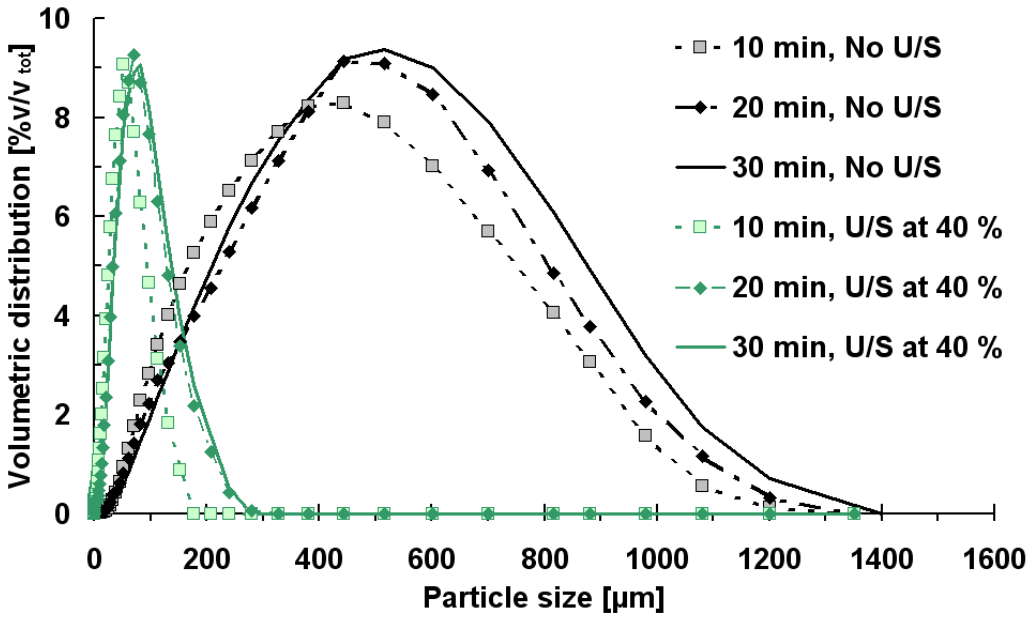

Figure 3.9 Effect of mean residence time on the crystal size distribution, under silent conditions and with sonication at 40 % of power amplitude

3.3.3 Particle Size Distribution at steady state

According to Ruecroft et al. (2005), "a continuous insonation throughout the duration of a batch crystallization process, can facilitate prolific nucleation at the expense of some crystal growth leading to the production of small crystals". Figure 3.9 shows the Crystal Size Distribution at steady state in a continuous process, for different values of the mean residence time, with and without sonication. As can be seen, the crystals produced under continuous sonicated control present a noticeably reduced size and a more narrow size distribution, confirming the results achieved during batch operations. Increasing residence time values lead to larger particles both with and without sonication. This could be explained considering that the residence time is inversely proportional to the flowrate of undersaturated inlet solution introduced per unit time, viz. the amount of adipic acid introduced per unit time as dissolved phase undergoing crystallizing conditions. At lower flow rates the entering molecules of dissolved solute tend to act as growing unit on previously formed nuclei because the large extent of time involved, while higher flow rates correspond to high de-

supersaturation rates at the beginning of crystallization, given the higher amount of solute introduced per unit time (and exposed to cooling conditions as soon as solute molecules enter a vessel at lower temperature); therefore, high flow rates favour nucleation phenomena, simulating conditions of higher cooling rates in batch cooling crystallization processes. Therefore, "as residence time is shortened, more particles are formed" (Randolph and Larson, 1988), and smaller sizes are produced. The application of ultrasound attenuates the influence of the residence time on the crystal size distribution, as the curves at 20 and 30 min tend to overlap.

Figure 3.10 compares the CSD achieved for two different values of ultrasound power intensity at different residence time values. The increase of ultrasound intensity induces a further reduction in the particle sizes while the size distributions at different τ values become comparable. The effect of inlet concentration was investigated as well. The results are shown in Figure 3.11. The experiments have been carried out under continuous insonation at 60% of the nominal power. Higher values of the inlet concentration produce larger particle sizes, however, not to a marked extent. Higher

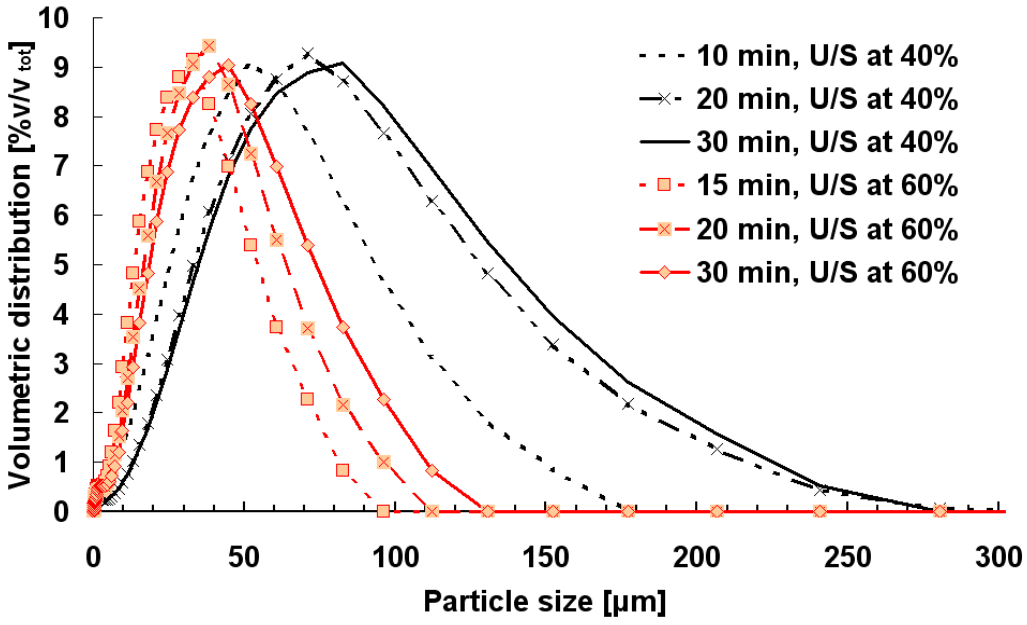

Figure 3.10 Effect of power amplitude on the crystal size distribution; ultrasonic intensity set at 40% and 60% of the power amplitude.

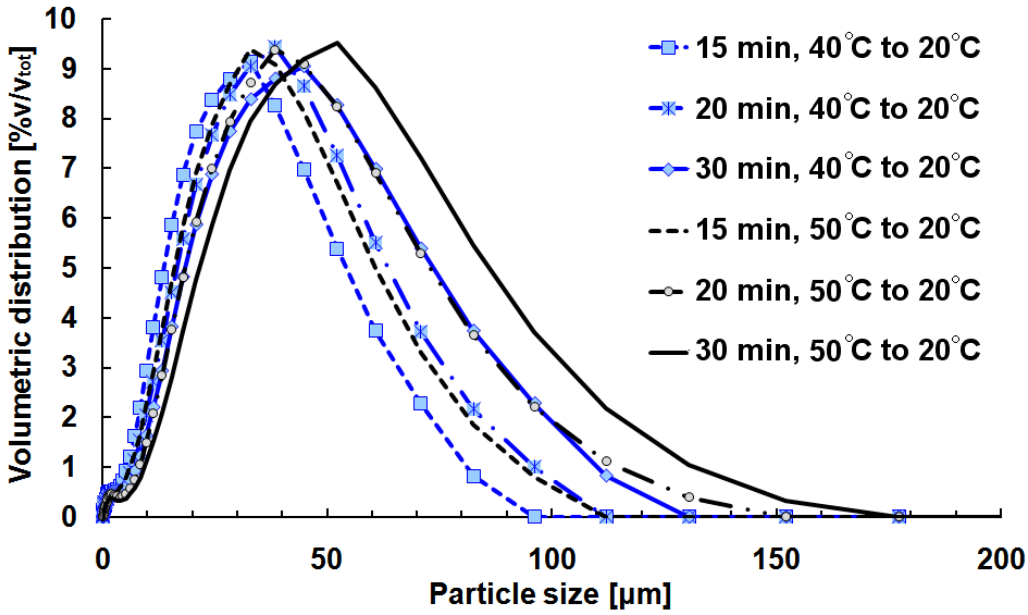

Figure 3.11 Effect of inlet temperature on the crystal size distribution at 40% and 60% of ultrasonic power amplitude

initial compositions mean higher amount of solute involved in the whole crystallizing process and supersaturated conditions extended over a broader range of temperature during cooling, favouring the growth of crystals. Furthermore, higher compositions favour agglomerative phenomena due to the increased magma density in fact, the agglomeration rate increases with .both supersaturation and magma density (Tai and Chen, 1995), and both are increased at higher inlet concentration values, both during the transient period and at steady state .

The investigation does not cover the effect of ultrasonic irradiation on Ostwald ripening, however localized hotspots related to cavitational phenomena are supposed not to induce ripening of produced crystals because of their transient and local nature; the duration of cavitational event has in fact been estimated of the order of microsecond (Suslick, 1990) and to occur within the liquid phase. While the rapid cooling following the cavitational collapse has been mentioned in the enhancement of primary nucleation, the effect on already present crystals is mainly ascribed to acoustic streaming and shock waves propagating in remote areas from the cavitational collapse and resulting in increased kinetic energy. Finally, the reason for the Ostwald ripening lies in the

tendency of the solid phase to adjust itself to minimize the total surface energy (Mullin, 2001), while ultrasonic irradiation favors a system of separate particles at high surface tension as mentioned above.

3.3.4 Concentration

The electrical conductivity of sparingly soluble electrolytes in water depends on concentration and temperature (Mullin, 2001). Therefore conductivity measurements can be used to determine concentration values and its trend at constant temperature. A number of experiments have been carried out to work out the relationship between

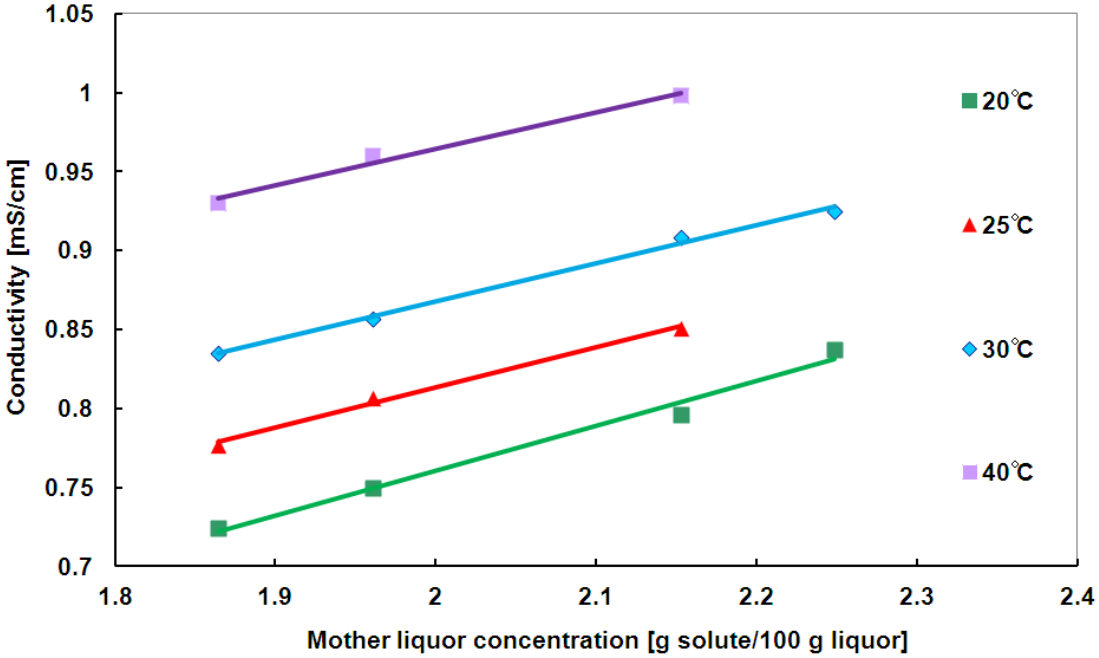

Figure 3.12 Electrical conductivity vs solute concentration in the adipic acid aqueous system.

electrical conductivity and concentration of dissolved adipic acid in the mother liquor in the temperature range between 20 and 40 °C. The results are illustrated in Figure 3.12: in this range of temperature, the electrical conductivity increases linearly with increasing concentration values of concentration and temperature and the slopes are very close to each other.

Conductivity measurements however present the limit of being unreliable in near-saturated or slightly supersaturated solutions: the massive presence of crystals (as every other solid element) alters the conductivity reducing its values. For this reason, after crystallization started, the conductivity measurements were carried out on filtered mother liquor from product samples of 30-40 g.

Figure 3.13 shows the concentration trends determined during a non sonicated experiment and insonated experiments at 40% and 60% of nominal power amplitude.

The plots refer to 30 min residence time. Before starting the continuous run, the concentration was stable at the solubility value at 20 °C. As the run was started the conductivity (and the concentration) increased very sharply until the beginning of the crystallization. Plots refers to the same flowrate value, consequently the similarity in the slope in the ascending segment indicates the same increase in the concentration of dissolved material due to an effective mixing in all cases. Concentration started decreasing as the instrument detected the onset of crystals appearance: the acid in solution turned into crystals. Such a decrease, very marked at the beginning of crystallization, became more and more gradual over time until a stable plateau was reached. De-supersaturation trends indicate a more relevant decrease of supersaturation at the beginning of crystallization for experiments coupled with sonication; that could be indicative of higher primary nucleation rates. In the first 10 minutes of crystallization , the reduction in supersaturation appears more marked when ultrasound was applied, suggesting secondary nucleation phenomena at the expense of growth processes. On the other hand, the supersaturation/ concentration decreased more gradually without ultrasonic application: the driving force for both nucleation and growth is expected to be more evenly distributed by both processes. The kinetics of secondary nucleation and growth in both insonated and not insonated cases will be estimated in Chapter 4.

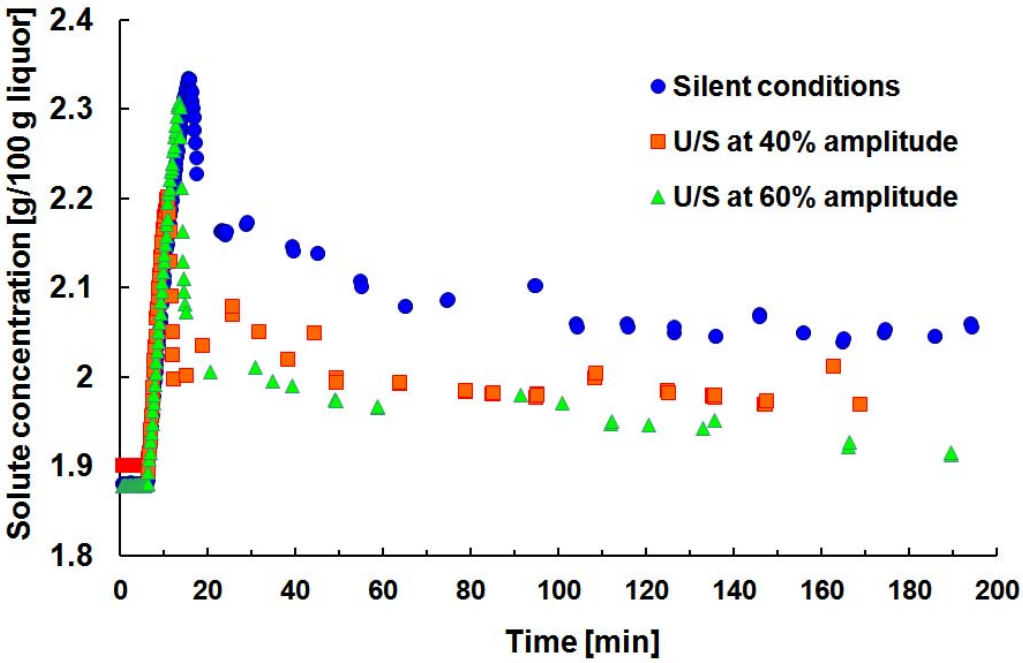

Figure 3.13 Adipic acid concentration vs. time; comparison between sonicated and silent operating conditions. Experimental conditions: cooling from 40 °C to 20 °C, τ = 30 min.

The start point for the concentration decrease corresponds to the detection of first crystals: after the continuous run was started, the first crystals appeared after a minimum of 4.66 minutes to a maximum of 10 minutes without ultrasound. The appearance of crystals was detected after shorter times during continuously insonated experiments: at inlet temperature of 40 °C the appearance was detected after 3.5-4.67 minutes at 40% of power amplitude and after 5.34-6.84 minutes at 60% of power amplitude. At inlet temperature of 50 °C the first crystals were detected after a time varying between 3.3 and 4 minutes. The delay for the onset of nucleation generally increased as the residence time increased, since the residence time is inversely proportional to the inlet flow rate, hence the amount of solute introduced in the crystallizer per unit time, as mentioned before. Furthermore, a wider variability in the "induction times" has been recognized in the case of non sonicated experiments.

During experiments without ultrasound the first visible crystals were easily recognized on the surfaces of baffles, probes and impeller while in the sonicated ones crystals appeared as a cloud of minute particles evenly distributed in the whole volume

bulk since the beginning of crystallization.

Figure 3.14 illustrates the relative supersaturation calculated at steady state conditions from conductivity measurements. In general, the steady state concentration/ supersaturation decreases as the residence time increases and increases with higher inlet concentration values, as could be intuitively explained considering the mass balances involved. In fact, higher τ values means longer periods for both nucleation and growth processes, with final results closer to solubility conditions at isolation temperature, while a higher solute content in the feed stream results in a global higher supersaturation value throughout the crystallization process, hence correspondingly higher nucleation and growth rates. The solid recovery from the dissolved phase is enhanced by cavitation and micromixing phenomena due to continuous insonation; in fact the energy provided by sonication activates a prolific nucleation of crystals assisting the clusters to pass the thermodynamic activation energy barrier of nucleation while cavitation bubbles can act as heterogeneous surfaces for nucleation processes

Figure 3.14 Effect of residence time on the relative supersaturation value at steady state

(Lyczko et al, 2002; Kordylla et al. 2009).

A second method was used to estimate concentration values and monitor the concentration trend over time. During the continuous run, samples of product were taken at different times, quickly weighted and filtered using a vacuum filter. The filter cake was washed several times, using saturated solution at the same operating temperature (close to the room temperature), then dried.

The mass concentration of adipic acid crystals produced in a given interval of time Δt, m_c, can be determined from the mass balance equation for a CSTR reactor:

Input = Output (3.2)

where the solute mass in the inlet stream corresponds to the input term and the adipic acid in the product stream to the output. Equation (3.2) can be arranged as:

$$m_c = m_{feed} - m_{ml} \tag{3.3}$$

as difference between the adipic acid mass concentration in the feed stream and the adipic acid mass concentration in the mother liquor over Δt. This equation can also be written as:

$$G_{feed} w_{feed} = m_c + G_{ml} w_{ml} \tag{3.3.1}$$

where G_{feed} and G_{ml} are the inlet mass and the mother liquor mass in the product discharge , over Δt, respectively, w_{feed} is the mass fraction of adipic acid at the inlet and w_{ml} is the mass fraction of adipic acid in the product mother liquor. G_{ml} can be easily calculated by applying the global mass balance equation for a continuous crystallizer

$$G_{ml}(t) = G_{feed}(t) - m_c(t) \tag{3.4}$$

where G_{feed} is known and m_c is estimated as mass of the filter cake after drying. Therefore the concentration of adipic acid in the liquor can be determined in terms of mass fraction from equation (3.3.1).

The concentration values determined using the two adopted methods show good agreement at steady state, as can be seen in Figure 3.15, nevertheless, the concentration

values from conductivity measurements result 1.5-4.2% lower than the corresponding ones evaluated by weight measurements. A plausible reason could be that dried filter cake includes the solid separated from the entrainment during the drying process. Comparing the weight of dried filter cakes with their weight just after filtration, and assuming that the entrainment solvent is completely removed during drying, the estimated weight of solid from entrainment varies between 1.93 and 2.22 % of the total weight of the filter cake.

3.3.5 Yield

The theoretical crystal yield refers to the quantity of pure crystals deposited from the solution. The actual yield of a solid material may be slightly different. In fact, crystal masses invariably retain some mother liquor even after filtration, increasing the calculated value, while the washing on a filter, aimed to reduce the amount of mother

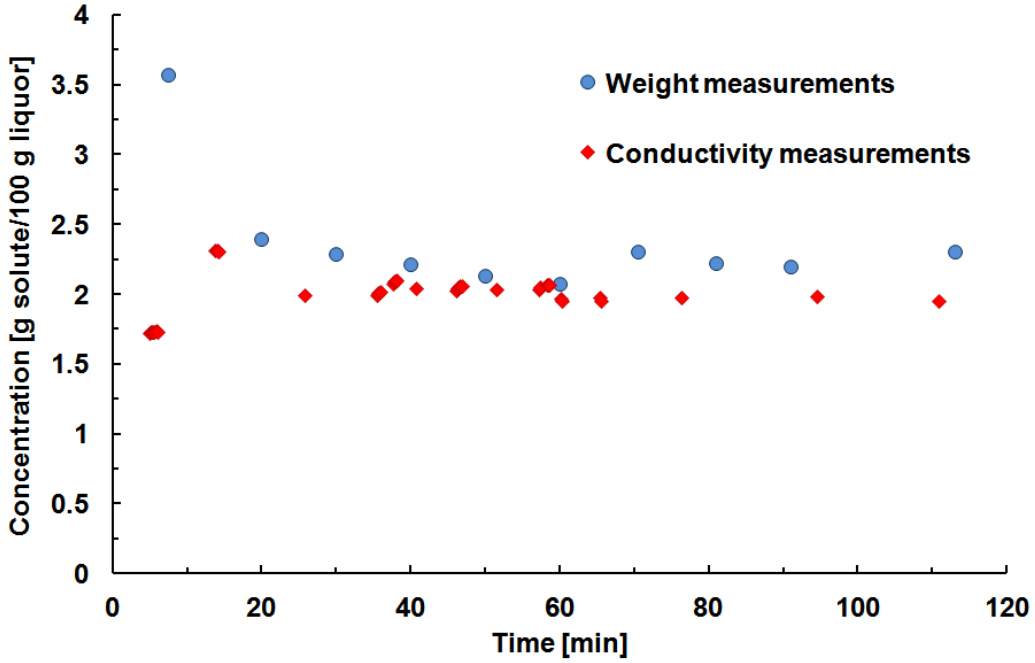

Figure 3.15 Comparison between the concentration trends from conductivity measurements and from measurement of slurry and dried crystals mass. Experimental conditions: cooling from 40 °C to 20 °C, ultrasonic intensity at 40% of nominal value, τ = 20 min.

liquor retained, may reduce the final yield by dissolution of crystals. Furthermore the calculation can be complicated if some the solvent is lost (Mullin, 2001). For a cooling crystallizer the crystal yield is defined as the weight percentage of crystals product in mother liquor after an operation between initial and final temperature.

Assuming no loss of solvent, no dissolution of crystals during washing and considering the amount of retained mother liquor and impurities as negligible, the crystal yield is calculated as

$$Y\% = \frac{C_1 - C_2}{C_1} * 100 \qquad (3.5)$$

where Y% represents the weight percentage of adipic acid crystals produced over the adipic acid content in the feed stream, C_1 and C_2 are the inlet solution concentration and the outlet solution concentration, expressed or converted in terms of g adipic acid /100 g solvent. Calculated results are reported in Figure 3.16. As can be expected, the yield increases with the residence time and the inlet concentration. An increase in inlet concentration leads to a higher yield value as it enhances the solid recovery. In fact, as the initial concentration was increased from 5 to 9.5 g solute/100 g water (increase by 84%) , the solid recovery was more than doubled (increased by 116% to 124.5%). This can be ascribed to a higher supersaturation, therefore to an enhanced driving force for crystallization, throughout the continuous process. The application of ultrasound induces interesting benefits in terms of improved yield values. For given operating temperatures and the residence time, sonication can lead to an increase in the yield up to 34 %. This benefit is more marked for the lowest values of τ investigated while it reduces to a minimum of 4% increase for a residence time of 30 min. In addition, the crystal yield has been evaluated in terms of percentage of the maximum allowable yield value, calculated from the solubility data of both inlet and vessel temperature (final)

$$Y\,max\% = \frac{C_1 - C_2^*}{C_1} * 100 \qquad (3.6)$$

Interestingly, while the maximum absolute solid recovery is achieved by increasing the inlet temperature/concentration, as intuitively expected, the maximum productivity

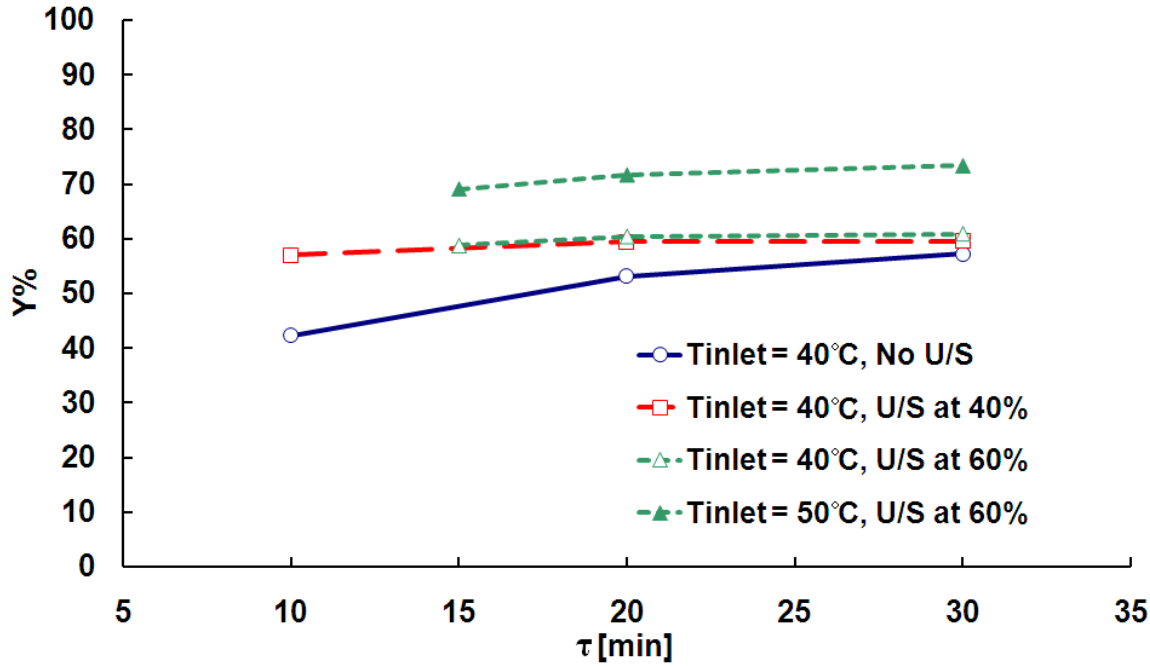

Figure 3.16 Effect of power ultrasound and residence time on the theoretical crystal yield value at steady state

(where the solid recovery is related to the solubility limit, viz the crystal yield *Y%* is compared with its thermodynamic limit Y_{max}*%*) is achieved for the lower inlet temperature considered, under insonation, as revealed in Figure 3.17.

3.3.6 Classification at the withdrawal

In order to meet the conditions of well-mixed reactor the slurry discharge must be accomplished so that the discharge suspension density, size distribution and liquid-phase composition are the same as they are in the crystallizer: i.e. there should be no size classification at the discharge point. On the other hand, laboratory crystallizers are commonly operated with 15 to 60 min retention times; consequently the average outflow rates are too low to assure that no classification of the suspended solid occurs.
It is therefore necessary to adopt an intermittent product withdrawal in order to achieve high withdrawal velocities (Randolph and Larson, 1988). For this reason a valve was used to realize an intermittence in the discharge stream. Experiments carried without

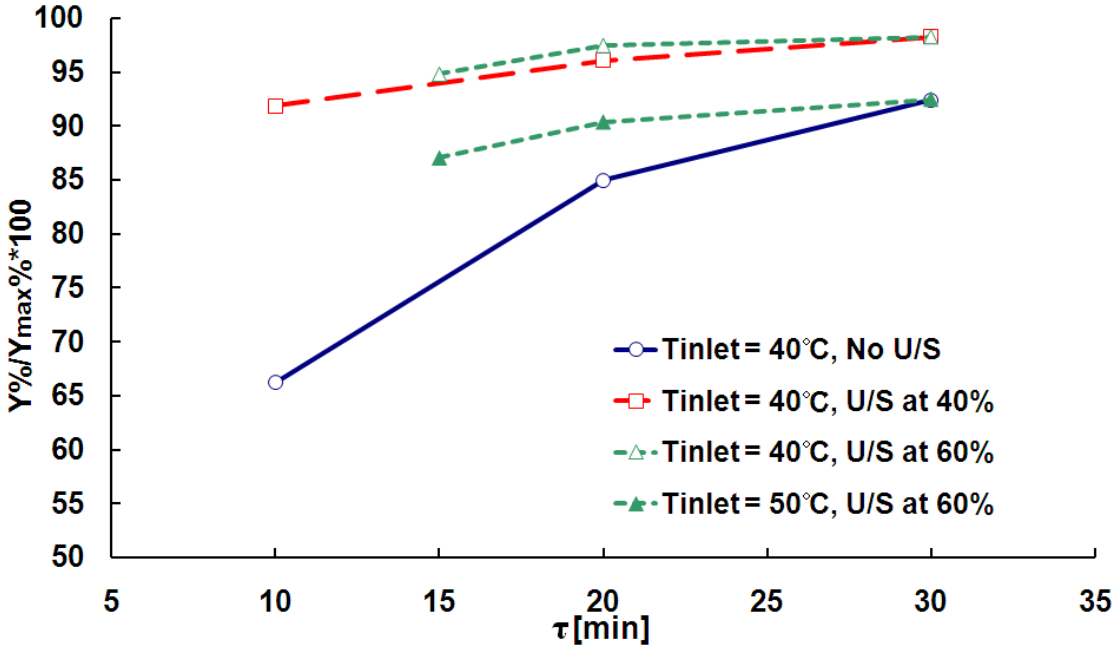

Figure 3.17 Effect of power ultrasound and residence time on the percentage of maximum allowable yield value at steady state.

this device gave usually reduced crystal size values for the product while bigger particles were retained in the vessel. The phenomenon appeared more significant for higher values of mean residence time, corresponding to lower values of the outflow rate. In consequence, the trend in the particle size distributions revealed an inverse behaviour than expected because the particle sizes decrease with increasing values of retention time, both with and without sonication. The results are presented in Figure 3.18.

3.3.6 Fouling

In a cooling crystallization, fouling commonly occurs on the cooling surfaces, as the temperature gradient is at the maximum level. An extreme vessel fouling hinders the temperature control and can obstruct the outflow pipe requiring a premature interruption of the test. The experiments carried with sonication presented a visible reduction of encrustations on non cooling surfaces like baffles and probes, as shown in Figure 3.19.

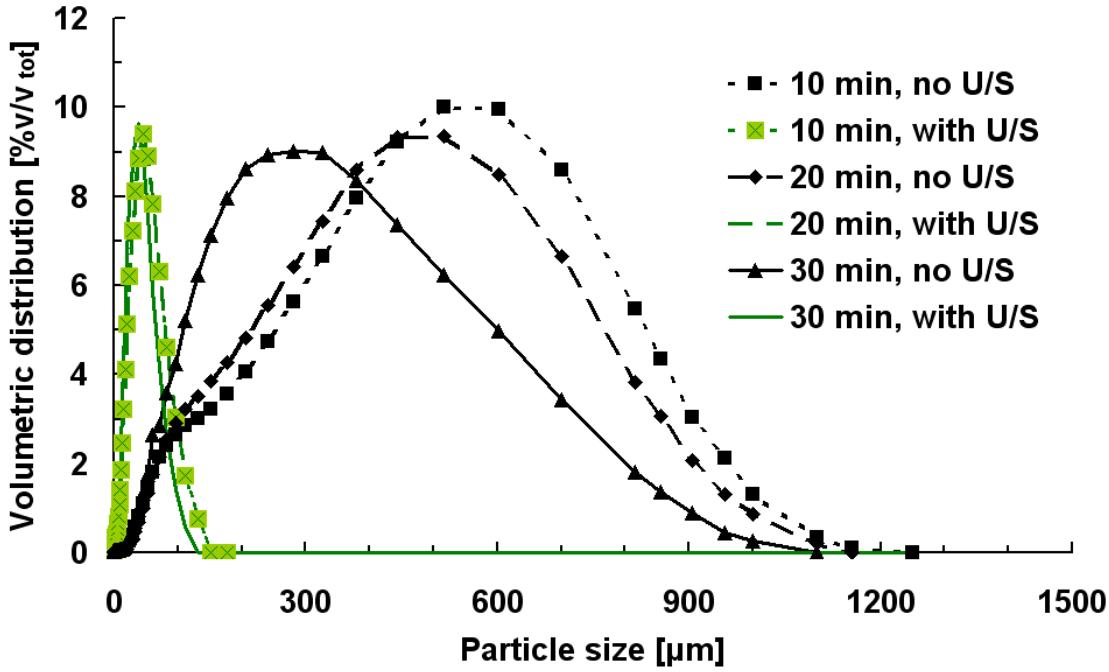

Figure 3.18 Effect of classification at the withdrawal on the crystal size distribution, under silent conditions and with sonication at 40 % of power amplitude.

On the other hand, the fouling on cooling surfaces appeared comparable in both non sonicated and sonicated experiments, although insonated experiments needed lower cooler liquid temperatures, with temperature gradient of about 15-20°C at the walls, to keep the slurry thermostated at 20°C. To explain this phenomenon it should be considered that ”If cavitation bubbles are formed at or near to any large solid surface the bubble collapse will not be symmetrical. The large solid surface hinders liquid movement from that side and so the major liquid flow into the collapsing bubble will be from the other side of the bubble. As a result, a liquid jet will be formed which is targeted at the surface with speeds in excess of 100 m/s. The mechanical effect of this is equivalent to high pressure jetting and is the reason why ultrasound is so effective in cleaning” (Mason, 1997).

The ultrasonic device used for this study falls in the category of sonotrodes that provide sonic field with high intensities. As main limit, the ultrasonic energy is dissipated longitudinally from the tip of emitting surface. While in bench scale vessels agitation of the solution can effectively ensure all of the solution is exposed to ultrasonic action, high-density fields can be achieved in large volumes by a lower face

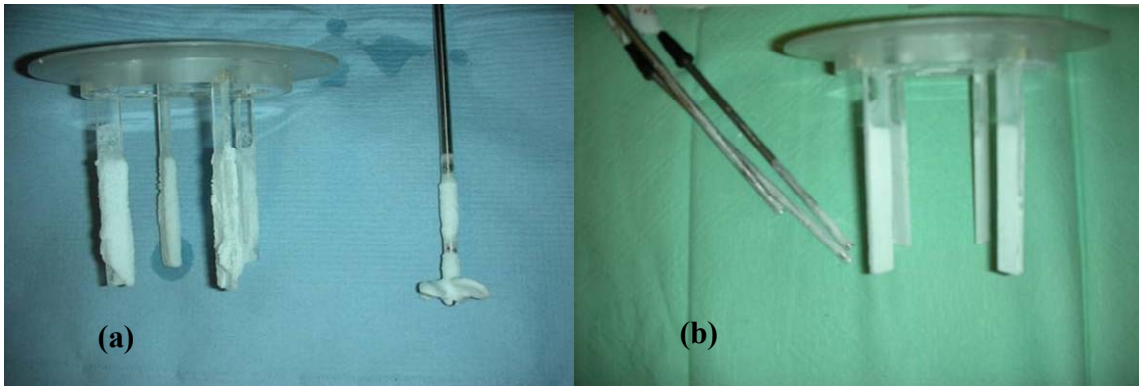

Figure 3.19 Effect of sonication on fouling formation on :
(a)the surface of baffles and impeller surfaces (without sonication);
(b)the surface of baffles and probes (with sonication)

intensity ultrasonic devices (~104 W/m^2) over extended areas. Multiple transducers mounted circumferentially around a cylindrical duct, fitted in rows and spaced equidistantly, have been designed to transmit ultrasonic energy from the transducer to the duct via a non-cavitating fluid acoustic-matching section. The unit provides a reasonably uniform insonation intensity above the cavitational threshold throughout its working volume, with relatively little energy dissipated in the barrier fluid, and can be implemented in a recirculation loop, or directly attached to the walls of the vessel, providing power densities of up to 70–80 W/L in large volumes (McCausland et al.2001, Ruecroft et al. 2005).

3.4 Conclusions

Continuous cooling crystallization experiments with and without ultrasound irradiation (silent regime) were performed at different mean residence times, inlet feedstock solute concentrations and ultrasound power amplitudes. The study investigated the influence of mean residence time and ultrasonic power on the time required to reach steady state operating conditions, yield and relative supersaturation at steady state, particle size distribution and crystal habit. Continuous ultrasonic irradiation throughout the continuous cooling crystallization process resulted in a shortening of time required to reach steady state PSD and relative supersaturation leading to improved

product yields. The influence of ultrasound on the crystal habit and particle size distribution of adipic acid was significant. Adipic acid crystals produced under ultrasound irradiation had a more uniform crystal habit (of elongated prismatic crystals compared to hexagonal plates from silent control experiments), and smaller crystal size when compared to silent continuous cooling crystallization experiments. SEM images also revealed a significant reduction in crystal agglomeration confirming results from batch cooling crystallizations. The continuous cooling crystallization under ultrasonic irradiation could be operated at much lower supersaturation levels. Crystal encrustation on baffles, impeller and monitoring probes was significantly reduced in insonated experiments. Fouling on the cooling surfaces appeared comparable in both silent and sonicated experiments, although insonated experiments needed lower coolant liquid temperatures with temperature gradients up to 20°C at the walls.

In conclusion, ultrasound technology provides an interesting tool that was coupled with continuous cooling crystallization for the first time, enabling a greater flexibility to be achieved in terms of influencing crystal habit, crystal size and size distribution of adipic acid from aqueous solution.

CHAPTER 4

ESTIMATION OF THE KINETICS OF SECONDARY NUCLEATION AND GROWTH

4.1 Introduction

"The unit operation of crystallization is governed by some very complex interacting variables. It is a simultaneous heat and mass transfer process with a strong dependence on fluid and particle mechanics. It takes place in a multiphase, multicomponent system and it is concerned with particulate solids whose size and size distribution, both incapable of unique definition, vary with time. The solids are suspended in a solution which can fluctuate between a metastable equilibrium and a labile state, and the solution composition can also vary with time" (Mullin, 2001). For a complete description of the crystal size distribution (CDS) it is necessary to quantify the nucleation, growth, agglomeration, breakage processes and to apply the three conservation laws of mass, energy and crystal population. In this chapter the kinetics of nucleation and crystal growth are estimated separately from the particle size distribution experimental data, by means of equation of moment applied to the population balance. The investigation focuses on the effect of ultrasound intensity, mean retention time, and steady state supersaturation on the rate of secondary nucleation and crystal growth at steady state operating conditions.

4.2 The Population Balance Equation

The mathematical framework used to describe the crystallization process in terms of crystal population is called "the population balance".

Recognised a characteristic crystal size L, the formulation of the population balance is based on the crystal population density, n, that defines the number of crystals per unit size per unit volume of system (Mullin, 2001; Mersmann, 2001):

$$n(L) = \lim_{\Delta L \to 0} \frac{\Delta N}{\Delta L} = \frac{dN}{dL} \qquad (4.1)$$

where ΔN is the number of crystals in the size range ΔL, per unit volume of suspension. The value of n depends on the value of L at which the interval dL is taken, i.e. n is a function of L. Hence the number of crystals in the size range L_1 to L_2 is given by

$$\Delta N = \int_{L_1}^{L_2} n(L) dL \tag{4.2}$$

The equation of population balance, based on a statistical mechanical formulation, was introduced by Hulburt and Katz (1964). The main problems treated were mainly those of particle nucleation and growth, but also agglomeration. Later, Randolph and Larson (1962) investigated in the details the modelling of crystal size distribution using population balance, and developed the mixed-suspension mixed-product removal (MSMPR) model for continuous crystallization. They distinguished the variables characterizing a generic particle in "external" coordinates, referring to its physical location, and "internal" coordinates, referring to properties independent of position, and quantitatively measuring the particle state, such as size, temperature, composition and energy content. Both coordinates define the so called "particle phase space".

The population balance is generally derived as particle-number continuity equation. Considering a generic sub region of volume R in the particle phase space of volume V, the population balance can therein stated as

Accumulation = Input – Output + Net generation (4.4)

Therefore, taken the Lagrangian viewpoint (Accumulation = Net Generation), the population balance equation can be written as

$$\frac{d}{dt}\int_R n dR = \int_R (B - D) dR \tag{4.5}$$

where n is a function of time and of all phase space coordinates and B and D are the birth and the death density functions, respectively. B and D take into account the possibility of particles suddenly appearing or disappearing in the internal particle phase space region investigated. From the (4.1), the former term of the (4.5) may be expanded to

$$\frac{d}{dt}\int_R n dR = \int_R \left[\frac{\partial n}{\partial t} + \nabla \cdot \left(\frac{d\mathbf{x}}{dt} n \right) \right] dR \tag{4.6}$$

where x is the set of internal and external coordinates comprising the phase space *V*, and $\frac{d\boldsymbol{x}}{dt}$ is the *substantial derivative* (also called *material derivative* or *derivative following the motion*) (Bird et al.2002). Recognizing that

$$\frac{d\boldsymbol{x}}{dt} = \boldsymbol{v} = \boldsymbol{v_i} + \boldsymbol{v_e}, \tag{4.7}$$

where v is the vector particle phase-space velocity, with internal component v_i and external component v_e, then the population balance can be written as

$$\int_R \left[\frac{\partial n}{\partial t} + \nabla \cdot (\boldsymbol{v_e} n) + \nabla \cdot (\boldsymbol{v_i} n) + D - B \right] dR = 0 \tag{4.8}$$

The internal velocity includes the contribution of the change in particle size or particle volume while the external velocity includes the contribution due to the fluid velocity in the reactor.

As the region *R* was arbitrarily chosen, the integrand must be independent on *R* and identically null:

$$\frac{\partial n}{\partial t} + \nabla \cdot (\boldsymbol{v} n) - B + D = 0 \tag{4.9}$$

Equation (4.9) is a number continuity equation in particle phase space, analogous to the continuity equation derived for the conservation of mass

$$\frac{\partial \rho}{\partial t} + \nabla \cdot (\boldsymbol{v} \rho) = 0 \tag{4.10}$$

Equation (4.9) is completely general and is used when the particles are distributed along both external and internal coordinates in the particle phase space. However, as many engineering problems involve dispersed-phase particulate systems that are carried in regions that can be considered to be well mixed, only the distribution of particles in the internal coordinates space can be taken into account. In the simplified case of a back-mixed system, one can choose a suitable volume $V_e(t)$ in the external phase having an arbitrary number of inputs and outputs of flow rate Q_k and population density n_k, and integrate the population balance over this region. The population balance for this case can be derived multiplying Eq.(4.9) by dV and integrating over $V(t)$

$$\int_{V_e}\left[\frac{\partial n}{\partial t}+\nabla\cdot(\boldsymbol{v_e}n)+\nabla\cdot(\boldsymbol{v_i}n)+D-B\right]dV=0 \tag{4.11}$$

Being the suspension mixed, n, D and B are functions only of time and the internal coordinates, thus they can be taken out of the integration

$$\frac{\partial n}{\partial t}+\nabla\cdot(\boldsymbol{v_i}n)+D-B+\frac{1}{V_e}\int_{V_e}\nabla\cdot(\boldsymbol{v_e}n)dV=0 \tag{4.12}$$

By application of the divergence theorem, assuming as positive the outward-directed normal vector to the moving surface S_m of $V_e(t)$, the integral over the volume of the spatial divergence of the population flux can be converted into a surface integral of the population flux flowing through S_m:

$$\int_{V_e}\nabla\cdot\boldsymbol{v_e}ndV=\int_{S_m}v_N ndS_m \tag{4.13}$$

Where v_N is the average fluid velocity normal to the surface S_m, and S_m is the sum of all moving surfaces of the system. The term S_m may be considered to be composed of three contributions: the first contribution is related to the k input and output streams to the volume V_e. The integral of $v_N ndS_m$ over these streams represents the inflow and outflow of slurry to the system.

$$\int_{S_m}v_N ndS=\sum_K Q_k n_k \tag{4.14}$$

According the convention assumed for the normal vector to S_m, Q_k is taken as positive for flow out of V_e and negative for flow into V_e.

The second contribution is correlated to the changes in system volume due to accumulation at a free interface. Assuming n independent of position, this term can be expressed as

$$\int_{S_s}v_N ndS=n\int_{Ss}v_N dS=n\frac{dV_s}{dt} \tag{4.15}$$

where S_s is the free surface of liquid in the vessel and dV_s is the change, at the free surface, of the solids-free volume of liquid.

The last contribution is due to the change in void fraction of solids in the system: for a mixed suspension it becomes

$$n\int_{S_e} v_N dS = -n\frac{dV_e}{dt} \tag{4.16}$$

where V_e is the volume occupied by the solid phase and S_e is the total particle fluid interface. The last two contributions can be grouped together referring to a total rate of change of slurry volume (total volume of the solid-liquid system):

$$\frac{dV}{dt} = \left(\frac{dV_s}{dt}\right) - \left(\frac{dV_e}{dt}\right) \tag{4.17}$$

Thus, the total contribution of the spatial flux divergence term is given as

$$\int_V \nabla \cdot \mathbf{v_e} n dV = \sum_k Q_k n_k + n\frac{dV}{dt} \tag{4.18}$$

and the spatial averaged balance becomes

$$\frac{\partial n}{\partial t} + \nabla \cdot (v_i n) + D - B + n\frac{1}{V}\frac{dV}{dt} = -\frac{1}{V}\sum_k Q_k n_k \tag{4.19}$$

that could be arranged as

$$\frac{\partial n}{\partial t} + \nabla \cdot (\mathbf{v_i} n) + n\frac{d(\log V)}{dt} = B - D - \frac{1}{V}\sum_k Q_k n_k \tag{4.20}$$

or, expressing the internal velocity in terms of crystal growth rate,

$$\frac{\partial n}{\partial t} + \frac{\partial (Gn)}{\partial L} + n\frac{d(\log V)}{dt} = B - D - \frac{1}{V}\sum_k Q_k n_k \tag{4.21}$$

Equation (4.20) represents the macroscopic population balance, averaged in external phase and distributed in the internal phase space. It is commonly used to describe both transient and steady state particle-size distribution in well mixed vessels.

4.2.1 Moment transformation of the Population Balance Equation

In many systems of engineering interest, the knowledge of the complete particle size distribution is unnecessary. Some average or total quantities, for example average size and mass concentration are sufficient to represent the particle distribution. Such properties can be obtained in terms of moments of the distribution, whereas the *j-th* moment of the distribution is defined as

$$m_j = \int_0^\infty nL^j\, dL \tag{4.22}$$

with $j = 0, 1, 2,\ldots$

As indicated by Mullin in his book Crystallization (2001), the number of crystals up to a characteristic size L (cumulative distribution), $N(L)$, is given by

$$N(L) = \int_0^L n(L)dL \tag{4.23}$$

while the *zeroth moment* of the distribution, for large values of L ($L \rightarrow \infty$)

$$m_0 = \int_0^\infty n(L)dL = N_T \tag{4.24}$$

gives the volume-related total number of crystals in the system N_T (Mullin, 2001; Mersmann, 2001).

The first moment of the distribution is the cumulative length L_T:

$$m_1 = \int_0^\infty n(L)LdL = L_T \tag{4.25}$$

The *second moment* of the distribution gives the cumulative surface area A_T:

$$m_2 K_a = K_a \int_0^\infty n(L)L^2 dL = A_T \tag{4.26}$$

where k_a is the surface shape factor, defined by the correlation

$$S_p = K_a L^2 \tag{4.27}$$

with S_a representing the effective surface of a particle of characteristic size L.

The *third moment* of the distribution gives the cumulative mass of crystals M_T per unit volume of slurry (M_T is also defined as *slurry density*):

$$m_3 K_v \rho_c = K_v \rho_c \int_0^\infty n(L)L^3 dL = M_T \tag{4.28}$$

where ρ_c is the crystal density *and* k_v is the volume shape factor, defined from the correlation between the effective volume of a particle V_p and its characteristic length L:

$$V_p = K_a L^3 \tag{4.29}$$

The transformation of the population balance in terms of moments leads to a loss of information about the distribution of the variables with the particle size and other internal coordinates and reduces the dimensionality of the relating equation to that of customary transport equations. As consequence, the mathematical effort to solve the population balance decreases considerably.

The moment transformation can be applied directly to the spatially averaged, or macroscopic, form of the population balance. Multiplying the macroscopic balance by $L^j dL$ and integrating on (0, ∞) it can be obtained

$$\int_0^\infty L^j \left[\frac{\partial n}{\partial t} + \frac{\partial (Gn)}{\partial L} + n \frac{d(\log V)}{dt} + D - B + \frac{1}{V} \sum_k Q_k n_k \right] dL = 0 \qquad (4.30)$$

where the single internal particle coordinate L can be considered as particle size. Assuming the growth rate G vary no more than the first power of size L and the birth and death terms can be expanded in terms of the first k moments (j = 0, 1, 2, …≥ k) the macro-moment form of the population balance is given as (Zauner, 1999)

$$\frac{dm_j}{dt} + m_j \frac{d(\log V)}{dt} = 0^j B^0 + jGm_{j-1} + \overline{B_j} - \overline{D_j} - \sum_k \frac{Q_k n_k}{V} \qquad (4.31)$$

It can be noted that only ordinary derivatives with respect to time remain. At steady state, these equations reduce to a set of non-linear algebraic equations.

4.2.2 Population Balance for the Mixed-Suspension Mixed-Product-Removal (MSMPR) Crystallizer

Kinetic data needed for crystallizer design purposes (effective growth and nucleation rate) can be conveniently measured on the laboratory scale in a so called Mixed- Suspension Mixed-Product-Removal (MSMPR) crystallizer model operated continuously in the steady state. The MSMPR model is analogous to the continuous stirred tank reactor (CSTR) model. The following assumptions lead to the basic definition of an ideal MSMPR crystallizer (Mullin 2001, Zauner 1999):

• continuous steady state of operation,

• well-mixed system,

• no agglomeration or disruption,

• crystal growth rate independent of crystal size,

• no classified withdrawal of the product,

• no seed crystals in the feed.

Under these conditions, the following simplifications can be made:

- $\frac{\partial n}{\partial t} = 0$ steady state
- $n\frac{d(\log V)}{dt} = 0$ constant volume
- $\frac{\partial (Gn)}{\partial L} = G\frac{dn}{dL}$ size-independent growth
- $B = 0, D = 0$ no agglomeration, no breakage
- $n=0$ in the inlet stream no seeds in the feed
- $\sum_k \frac{Q_k n_k}{V} = \frac{Qn}{V} = \frac{n}{\tau}$ mixed suspension discharge

τ is the mean residence time, defined as

$$\tau = \frac{V}{Q} \tag{4.32}$$

where V represents the crystallizer volume and Q is the slurry withdrawal rate. The population balance equation of a MSMPR therefore reduces to

$$G\frac{dn}{dL} + \frac{n}{\tau} = 0 \tag{4.33}$$

whose integration gives

$$n = n_0 \, exp\left(-\frac{L}{G\tau}\right) \tag{4.34}$$

where n_0 is defined as *population density of nuclei* assumed as zero sized crystals.

The population density distribution is usually shown within a semi-logarithmic coordinate plot where equation (4.26) is represented by a straight line of slope $-\frac{1}{G\tau}$ and intercept n_0.

Defined the nucleation rate as

$$B^0 = \left.\frac{dN}{dt}\right|_{L=0} \qquad (4.35),$$

corresponding to the number of nuclei crystals generated per unit volume of slurry, and the linear growth rate as

$$G = \frac{dL}{dt} \qquad (4.36),$$

the following correlation can be found for a MSMPR crystallizer

$$B^0 = \left.\frac{dN}{dt}\right|_{L=0} = \left.\frac{dN}{dL}\right|_{L=0} \frac{dL}{dt} = n_0 G \qquad (4.37).$$

For a MSMPR crystallizer, the resolution of equations (4.23) to (4.27) gives

$$m_0 = N_T = n_0 G\tau \qquad (4.37.a)$$

$$m_1 = L_T = n_0 (G\tau)^2 \qquad (4.37.b)$$

$$m_2 k_a = A_T = 2k_a n_0 (G\tau)^3 \qquad (4.37.c)$$

$$m_3 k_v \rho_c = M_T = 6k_v \rho_c n_0 (G\tau)^4 \qquad (4.37.d)$$

4.3 Evaluation of the kinetics of Growth and Secondary Nucleation

The aim of the work proposed in this chapter is to deduce the growth rate G and the nucleation rate B^0 from the experimental particle size distribution. It is notoriously difficult to extract kinetic data using the population balance. In fact, being strongly non linear, the population balance equation does not possess an analytical solution in most cases, requiring the development and adaptation of numerical techniques. The equation of moments (4.31) for a well mixed crystallizer can be manipulated in such a way to determine the growth and nucleation kinetics the determination of (Zauner and Jones, 2000).

Assuming steady state, size-independent growth, conservation of the mass (corresponding to the third moment) in the agglomeration and breakage processes, the equation of moment (equation 4.31), for j = 3 (to consider a mass balance) , reduces to

$$0 = 3Gm_2 - \frac{m_3}{\tau} \tag{4.38}$$

Consequently, knowing the moments of the distribution, the growth rate G can be easily calculated as

$$G = \frac{m_3}{3m_2\tau} \tag{4.39}$$

while the nucleation rate can be calculated as

$$B^0 = n_0 G \tag{4.40}$$

n_0 can be evaluated from the intercept of the experimental distribution with the abscissa at $L = 0$.

4.4 Results and Discussion

An investigation over the growth and nucleation rates has been carried out under the assumption of MSMPR operating conditions. In the first instance, the effect of the residence time was determined, both with and without sonicated control. Then the investigation was focused on the influence of power ultrasound with amplitude values varying between 40 and 60% of the maximum allowable power value of 750 W. In the case of continuous sonication at 60 % amplitude, two different inlet concentration/temperature values were considered. In Figure 4.1 and 4.2 the growth and nucleation rate are plotted versus the residence time for all conditions investigated. The values of growth and nucleation rates were calculated from equation (4.39) and (4.40) respectively.

Under all conditions, a decrease in both the growth and the nucleation rate values is observed as the residence time increases. This is an expected result considering that the driving force for both processes, the supersaturation at steady state, decreases with increasing values of τ. The effect on G appears more relevant for results obtained under non-sonicated conditions, where G values varies between 3.07×10^{-8} and 5.27×10^{-9} m/s and are reduced 2.2 ÷2.6 times as τ increases of 10 min. Under sonicated control, as the

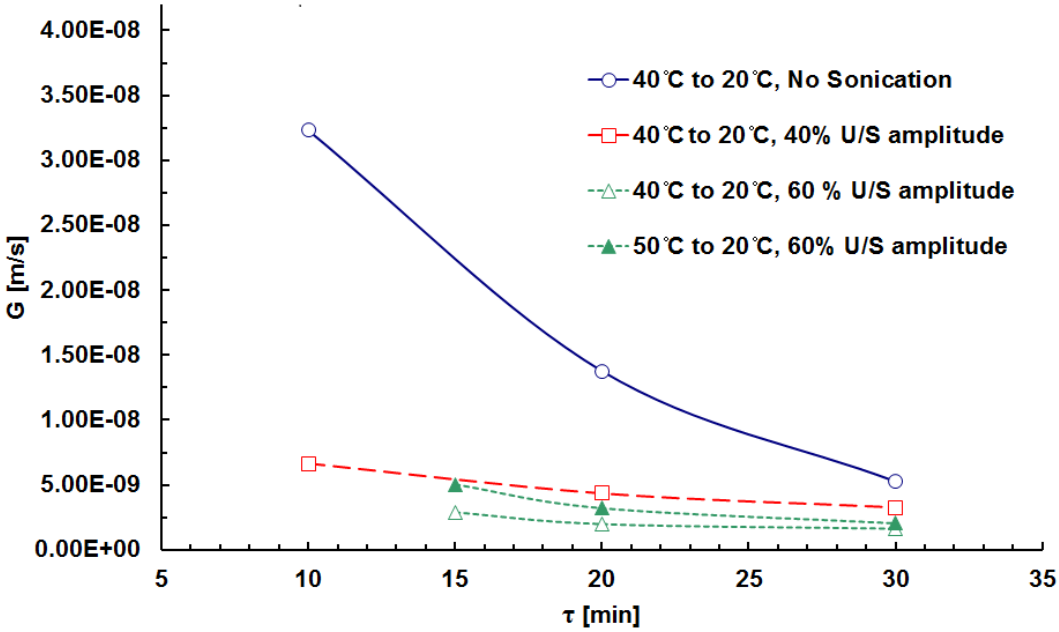

Figure 4.1 Growth rate vs. residence time

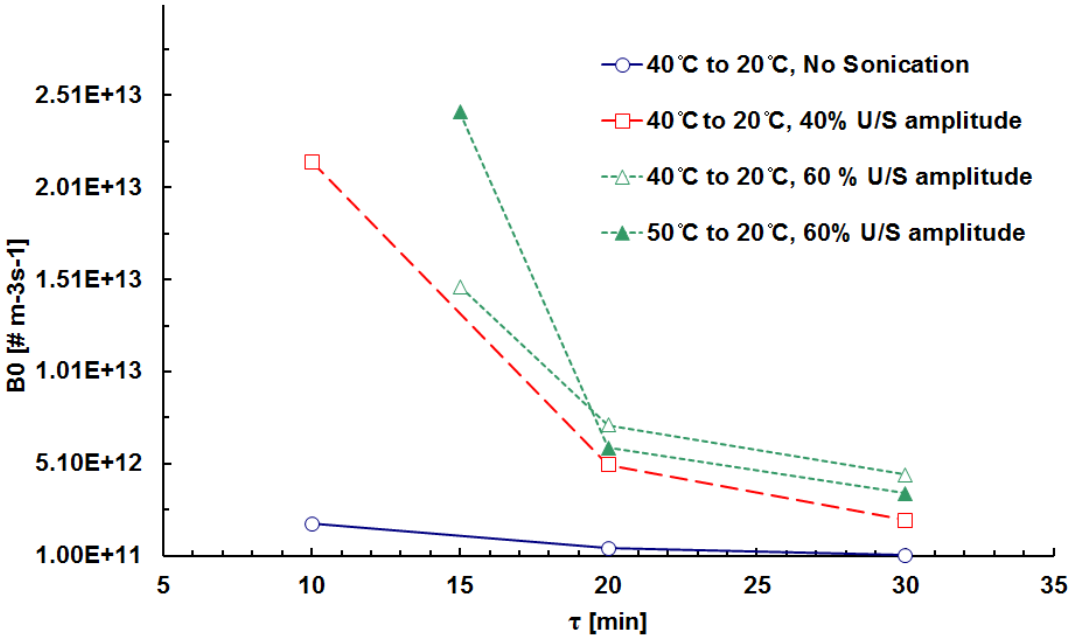

Figure 4.2 Nucleation rate vs. residence time

residence time increases at a regular interval of 10 minutes, the maximum recognized reduction for *G* is of 1.8, achieved only for the lowest values of τ investigated.

For fixed inlet conditions, vessel temperature and residence time, the growth rate is reduced by application of ultrasound, with increasing extent as the ultrasound power increases. Higher values of the inlet concentration lead to higher *G* values, but without remarkable difference.

The *G* values determined for all sonication control conditions investigated cover a range from 1.63×10^{-9} to 6.15×10^{-9} m/s.

The application of ultrasound results in relevant effects in terms of nucleation: the nucleation rate values are increased at least by 1.7 fold comparing the results without sonication with those with ultrasound. The effect of residence time on the nucleation rate is more marked in the case of non-sonicated conditions with B^0 values varying in the range from 1.47×10^{11} to 1.86×10^{12} #/(m^3s) and reduced by 3.4-3.7 fold for every increase of 10 min in τ. B^0 values corresponding to sonicated conditions are one order of magnitude higher than those from uninsonated crystallization, varying between 2.02×10^{12} and 2.42×10^{13} #/(m^3s) in total, and with a maximum reduction by 4.25 fold as τ increases from 10 to 20 min. The increase of power ultrasound leads to a further increase in the nucleation rate values at residence time values shorter than 20 min, while comparable results appear for longer time values where the experimental data reveal higher values at lower insonation intensity. The effect of solute content in the feed stream appears more interesting than in the growth rate case but only for the lowest residence time values investigated. In fact, the higher the solute content of the solution, the higher the supersaturation throughout the continuous operation, resulting in even higher nucleation during the transient period and at steady state. The explanation for the ultrasonic influence on the nucleation process is normally ascribed to the "mechanical disturbances" caused by cavitation phenomena. It is suggested that ultrasound irradiation provides energy raising the number of clusters able to pass the thermodynamic barrier of nucleation per unit time for primary nucleation phenomena. Furthermore, cavitation bubbles can act as heterogeneous surfaces for nucleation or activate other surfaces, such as dust particles already present in the system. In addition,

the presence of particle smaller than 10 μm can reveal secondary nucleation, considered as the dominating nucleation phenomenon at steady state in a continuous operation, with low supersaturation levels and crystals of the solute already present (Garside and Davey, 1979; Mullin, 2001). Ultrasound may, in fact, induce mechanical disruption of crystals or loose bound agglomerates already formed and increase the kinetic energy of particles favouring the collision among particles and their erosion, as already indicated for batch experiments. However, when continuous insonation is applied during a crystallization process, crystals undergo cavitational effects for longer times in batch rather than in continuous operations; the mean residence time corresponds to the average insonation time for crystals in continuous crystallization under continuous insonation.

The correlation between both nucleation and growth rates and the supersaturation has been analyzed as well. Considering the expression of supersaturation in terms of concentration driving force, the rates of nucleation and growth can be conveniently written in terms of supersaturation as

$$B^0 = K_N\left(\frac{C-C^*}{C^*}\right)^b = K_N\sigma^b$$
$$G = \frac{k_a}{3k_v\rho_c}k_G\left(\frac{C-C^*}{C^*}\right)^g = K_G\left(\frac{C-C^*}{C^*}\right)^g = K_G\sigma^g \qquad (4.41)$$

where C is the steady state concentration, C^* is the solubility concentration at operating vessel temperature, both referred to the solute mass concentration in the clear liquor, σ represents the supersaturation ratio, K_N is the nucleation rate coefficient, K_G the overall mass transfer coefficient, and b and g the apparent order of nucleation and growth respectively. The value of exponent g is given by the slope of the linear plot of lnG versus $ln(\sigma)$ while K_G can be evaluated from the intercept value. The results are depicted in Figure 4.3.

Theoretical considerations show that spiral growth at very low supersaturations results in $g = 2$ and for large supersaturations, $g = 1$. This represents the two limiting cases of the Burton Cabrera and Frank (CBF) kinetic theory of growth, and is also a

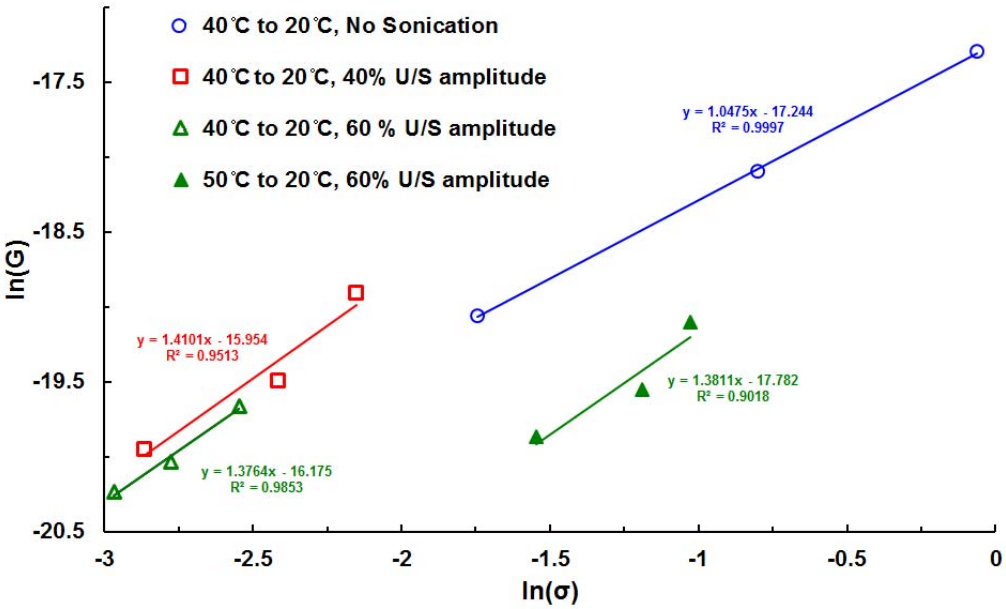

Figure 4.3 Growth rate vs. supersaturation

good approximation for the intermediate regime $1<g<2$. Therefore, the g values in the range 1-2 can be explained by the BCF growth theory based on spiral growth mechanism from screw dislocations, as already indicated in the work relating batch operating conditions. Michaels and Colville (1960) indicate that adipic acid crystal growth can proceed by propagation by dislocation. The probability that a dislocation develops in a growing crystal face increases with the length of time the crystal have been growing or, in other words, larger crystal are likely to contain more dislocations than smaller ones, and large-area faces more than small area ones.

On the other hand, the unitary close value of g estimated under non sonicated conditions could reveal a diffusion controlling mechanism for crystal growth. The higher values for the g coefficient due to sonication application (between 1.38 and 1.41) can consequently confirm an enhancement of the diffusional mass transfer of additional units from the bulk to the surface of growing crystals. The order with respect to supersaturation indicates that both diffusion and surface reaction exert some influence of the growth rates. Plots of $\ln(G)$ versus $\ln(\sigma)$ correspond to straight lines appearing almost parallel, indicating no relevant influence of power amplitude on the apparent

order of growth. The difference among the slopes could be ascribed to the experimental variability in data (with standard deviation equal to 0.02) and a single value for g, calculated as averaged value, can be considered. The results indicate that, given the inlet and isolation temperature values, K_G is slightly increased by sonication, while, fixed the isolation temperature and the 60 % ultrasonic amplitude, K_G is reduced as the inlet concentration increases from 5 to 9.2 g of solute/ 100 g of solvent. Two opposing effect can be considered: ultrasound accelerate the mass transfer and the mass deposition process accelerating the diffusion and enhancing micromixing phenomena while the massive presence of crystals due to higher inlet concentration hinder the macromixing and the bulk mass convective transfer. Thus, the influence of the inlet conditions on K_G appears significant in the case of sonocrystallization operations.

The empirical coefficients b and K_N can be estimated using an analogue procedure. It should be pointed that the population density has been calculated from steady state particle size distribution experimental data using the correlation:

$$n(L) = \frac{\Delta m_S(L)}{m_{tot}} \frac{M_T}{\Delta L k_v \rho_c L^3} \qquad (4.42)$$

where Δm_s represents the mass of crystals in the size range ΔL and M_T is the magma

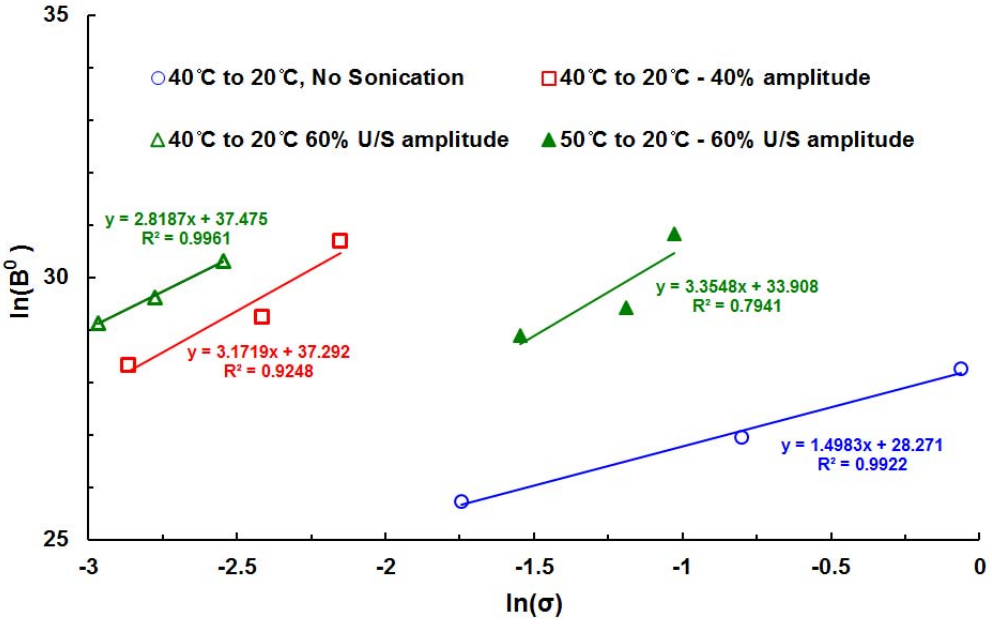

Figure 4.4 Nucleation rate vs. supersaturation: aqueous adipic acid system

density, defined as mass of crystals per unit volume of slurry. Thus the coefficient K_N includes the proportionality between the nucleation rate of zero sized crystals and the magma density.

The plots of $\ln(B^0)$ against $\ln(\sigma)$ are shown in Figure 4.4. Ultrasound noticeably enhances the apparent order of nucleation increased from a value 1.49 without sonication to a value between 2.81 and 3.35 with sonication. At constant inlet concentration and isolation temperature values, the sonication effect increases K_N by around 1.32 with the 40% of amplitude and the 60 % of maximum ultrasonic power.

Ultrasonic continuous irradiation affects both primary and secondary nucleation processes. As regards to primary nucleation, arguments whether the nucleation phenomenon under ultrasound irradiation is dominantly of homogeneous or of heterogeneous nature were opposed. Lyczko et al. (2002) suggested that ultrasound changes the activation energy. At fixed temperature, the ultrasonic energy input can work as nucleation impetus, which is converse of the activation energy of nucleation, reducing the activation energetic barrier and the critical radius to turn clusters into stable nuclei. Therefore, according to the heterogeneous nucleation model, ultrasound affects either the surface energy for the crystal-solution interface or the wetting angle. It should be pointed out that in the heterogeneous approach cavitational collapsing bubbles are regarded as active nucleation sites. As a consequence, sonication induces prolific nucleation. Kordylla et al. (2009) confirm the heterogeneous approach and indicate a reduction in the nucleation work under insonation due to lower wetting angle values between the cluster and the bubble surface area. On the other hand, Guo et al. (2006) suggest a homogeneous approach indicating that ultrasound significantly accelerates the diffusion process, increasing the mass deposition rate, and in turn the number of clusters able to cross the activation size barrier.

Ultrasonic cavitation also induces secondary nucleation phenomena by mechanical disruption of produced crystals or by loosing weekly bounded crystals in the already formed agglomerates. In fact, the solute particles have an increased opportunity

to collide with each other because of both enhanced microstreaming and high kinetic energies provided by the cavitational bubble collapse. The bimodality in the crystal size distribution (CSD) produced under continuous ultrasonic irradiation, for crystal size values under 10μm, and the SEM pictures revealing the presence of fragments in the same size range, can confirm the occurrence of secondary nucleation from attrition.

In the current study, the increase in the K_N value due to a higher ultrasound power at inlet temperature of 40°C can reassert the role of microstreaming and mass transfer enhancement due to ultrasonic irradiation. On the other hand, fixed the ultrasonic power at the maximum value investigated, the increase in the inlet composition reduces the value increase of coefficient K_N: a possible justification can be that the convective bulk mass transfer to the interface of the crystal boundary layer is hindered by the massive density of suspended particles. Interactions with surrounding particles and increase in the apparent suspension viscosity and density occurs as the concentration of solids increases, in analogy with the effect of surroundings on the settling of solids (Chapter 10 of Handbook of industrial mixing, 2004).

To compare the effect on nucleation rate with those on the growth rate, the empirical expressions (4.37) have been combined to give

$$B^0 = K_R G^i \qquad (4.43)$$

where i is the *relative order of crystallization*:

$$i = \frac{b}{g} \qquad (4.44).$$

The plots of ln(B) versus ln(G) gives straight lines and the coefficient i coincides with their slopes. i values are increased from 1.43 without ultrasound to 2.03 – 2.55 with ultrasound at 40% and 60% and inlet temperature of 40°C. As shown in Figure 4.5, the apparent order of nucleation is higher than the corresponding order of growth in every experimental condition investigated and the continuous application of ultrasound enhances more the apparent nucleation order than the growth order.

The results indicate also a negligible effect of power amplitude and of inlet concentration as *i* values under sonicated conditions are comparable. The results can confirm the convective bulk mass transfer as the controlling mechanism for the higher inlet composition. In fact, such phenomenon affects both nucleation and growth in a comparable manner and its effect is annulled when the ratio between nucleation and growth rate is considered resulting in parallel lines at different solid concentration values as obtained in Figure 4.5.

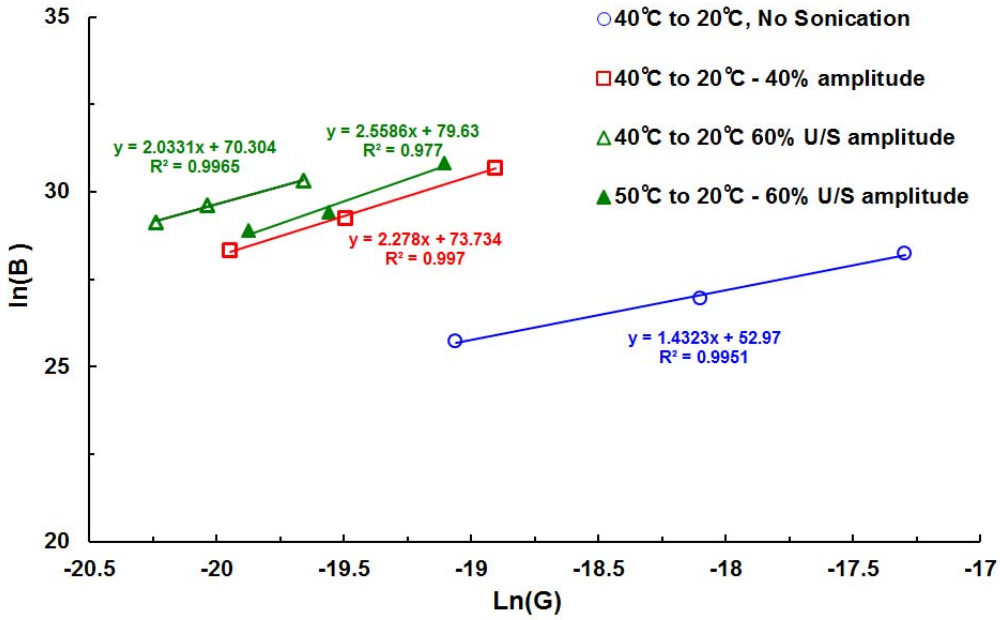

Figure 4.5 Nucleation rate vs. Growth rate

4.4.1 Size dependent Growth Rate

A non-linearity in the log population density distribution is often experienced in the works published in the crystallization literature. In some cases a curvature is observed over a wide size range, while in other cases a sharp upward curvature is recognized for small crystal size values.

Also in this case, the plot of the population density versus the characteristic crystal size shows a non-linearity trend with a deviation from the McCabe's ΔL law. The deviation from the linear trend is recognized for small crystal sizes, as presented in

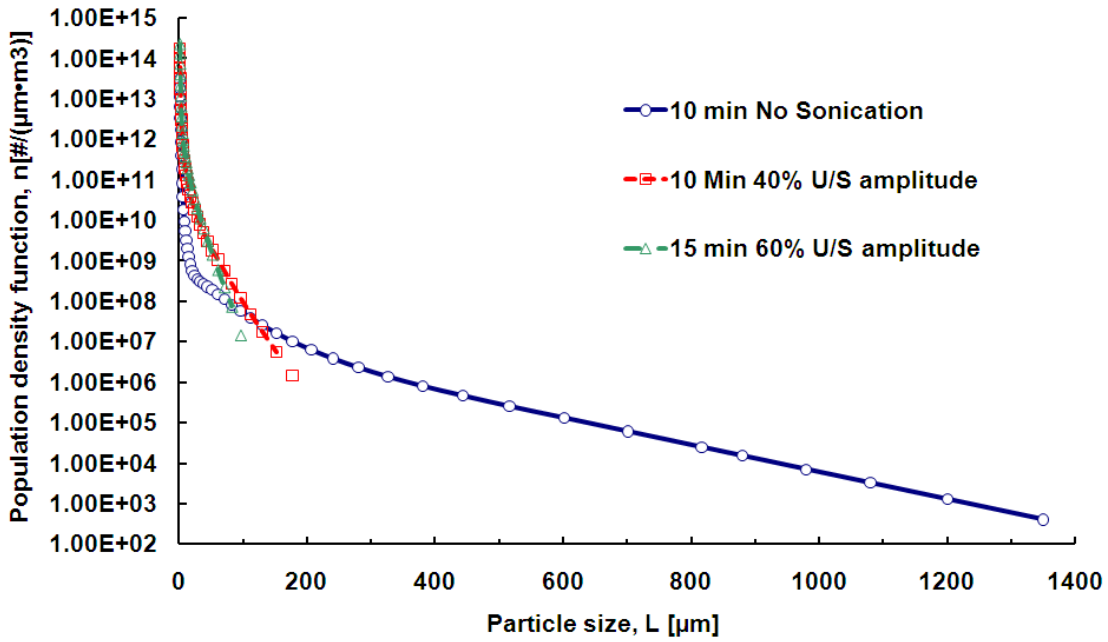

Figure 4.6 Population density distribution from experimental data: T_{inlet} = 40 °C, T_{vessel} = 20 °C

Figure 4.6. The possible reasons include size-dependent growth (SDG) or growth rate dispersion (GRD), agglomeration and/or breakage. In this work SDG was modelled using the Mydlarz-Jones three parameter (MJ3) model. Mydlarz and Jones proposed an exponential model, which has been successfully applied in modelling SDG rates both for systems which hold and which violate McCabe's ΔL law. The authors defined a SDG model in the form

$$G(L) = G_m\{1 - exp[-a(L+c)]\} \qquad (4.45),$$
$$a > 0, c \neq 0$$

Where G_m is the limiting growth rate for large crystals, L is the crystal size and a and c empirical parameters. $G(L)$ approaches limited value of G_m as $L \rightarrow L_{max}$ and the value of the parameter a should be positive since only positive size-dependent crystal growth rates are observed in practice.

Under steady state operating conditions, assuming constant crystallizer volume, no crystal breakage neither agglomeration, no crystals in the feed stream(s), size dependent

growth rate, and a well-mixed crystallizer, the population balance equation can be written as

$$\frac{d[G(L)n(L)]}{dL} + \frac{n(L)}{\tau} = 0 \qquad (4.46).$$

Using the *MJ3* model, equation (4.46) can be integrated analytically to give the following expression of the steady state MSMPR population density distribution:

$$n(L) = n^0 \exp(aL)\left\{\frac{\exp(ac)-1}{\exp[a(L+c)]-1}\right\}^{\frac{1+a\tau G_m}{a\tau G_m}} \qquad (4.47)$$

Equation (4.45 and 4.40) permit simultaneous estimation of the growth and nucleation kinetics in a relatively simple way.

Size dependent growth of crystals at steady state was modelled by direct fitting method to the population density function. The size-dependent exponential model was fitted to the experimental data using the curve fitting software program DataFit version 9. The inlet G_m value for the regression was evaluated directly from the experimental population density distribution as maximum value estimated, applying the method proposed by White et al. (1976). Defined the cumulative number of oversize distribution of particles above size *L*, *N(L)*, as

$$N(L) = \int_L^\infty n(L)dL \qquad (4.48)$$

The authors estimated the size-dependent growth rate as

$$G(\overline{L}_{i+1}) = \frac{L_{i+1} - L_i}{\tau \cdot ln\left(\frac{N(L_{i+1})}{N(L_i)}\right)} \qquad (4.49)$$

where $\overline{L}_{i+1}$ is the arithmetic average crystal size in the range L_i, L_{i+1} and L_i and L_{i+1} are two consecutive sizes ($L_i < L_{i+1}$).

n(L) regression results were compared with experimental data. The results were satisfying only in the case of sonication at 40% of maximum power input. One example is shown in Figure 4.7. The comparison reveals a good agreement for $L < 10$ μm, underestimation of experimental data in the range 10-100 μm and an overestimation for

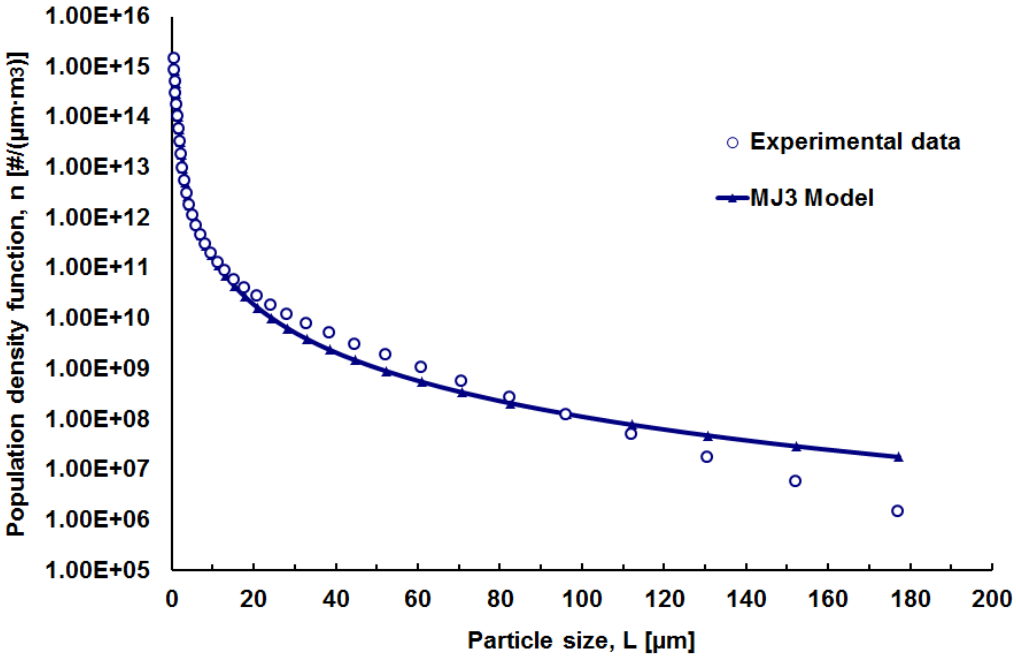

Figure 4.7 Comparison between experimental steady state distribution data with MJ3 model

larger particles. As a result, the crystal growth may be considered strongly size-dependent for smaller crystal sizes, whereas the growth rate values are extremely low. Attrition fragments can act as secondary nuclei and grow at different rates. For crystal larger than 40-50 µm the population density data present a linear trend in the semi-logarithmic plot, thus, for larger particle size the growth rate can be easily estimated from the slope of the population density data plot ($-1/\tau G$) and the mean residence time.

The direct fitting of experimental population density data to the *MJ3* model resulted in G_m values varying between 2.31×10^{-6} and 4.94×10^{-6} m/s, a and c values varying from $1.23\times10^{-4}$and 3.25×10^{-4} μm^{-1} and from 0.44 and 0.54 µm respectively.

4.5 Volumetric shape factor

The particle size distribution was determined using Malvern MasterSizer-S that refers to spherical shaped particles with equivalent volume. The characteristic crystal size L is therefore a diameter. For this reason the volume shape factor k_v, defined as

$$k_v = \frac{V}{L^3} \qquad (4.50),$$

has been introduced. k_v can be estimated using the correlation

$$m_3 K_v \rho_c = M_T \qquad (4.51),$$

Where m_3 was calculated from the particle size distribution, M_T was determined from conductivity measurements and ρ_c is the density of adipic acid at room temperature (from NIST chemistry WebBook). The values obtained varied from 0.6 to 0.63 both with and without sonication; these numerical values are intermediate between those corresponding to a spherical particle (k_v = 0.524) and an hexagonal prism (k_v = 0.867) (Mersmann, 2001)

4.6 Mean Size and Coefficient of Variation

In crystallization and precipitation, the size distribution information can be compressed into two terms that best describe the distribution (in this case the population density function *n(L)*) in a qualitative sense. These terms are the *mean size* and the *coefficient of variation*, that indicate how large the particles are and how much size variation they have relative to the mean size. The *arithmetic mean size* and related *coefficient of variation* are respectively defined in terms of a normalized density function as

$$\bar{L}_{10} = \frac{\int_0^\infty L n(L) dL}{\int_0^\infty n(L) dL} \qquad (4.52)$$

and

$$c.v. = \frac{\sigma}{\bar{L}_{10}} \qquad (4.53)$$

where the variance is given as

$$\sigma^2 = \int_0^\infty (L - \bar{L}_{10})^2 n(L) dL \qquad (4.54)$$

Equation (4.52) shows that the arithmetic mean size is given by the ratio of the first moment of the distribution to the zeroth moment of the distribution. Properties

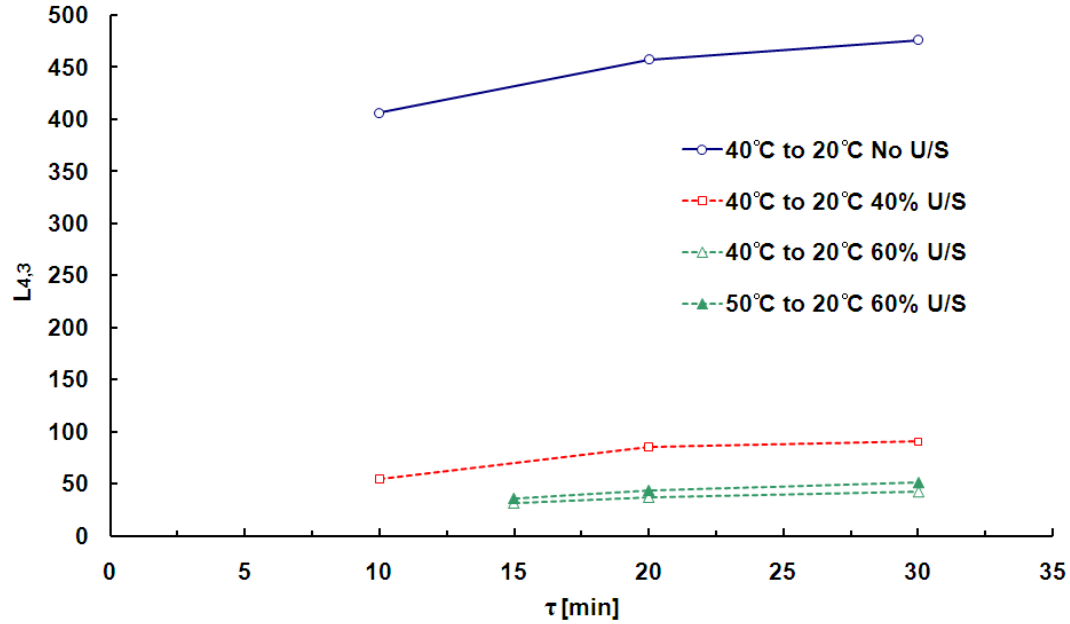

Figure 4.8 Volume mean diameter vs. mean residence time

expressed in terms of moments could be found for the weight –size distribution by simply incrementing 3 in the order of moments and the *coefficient of variation* can be expanded in terms of the first three moments (Randolph and Larson, 1988, Zauner, 1999). As a consequence, given a numerically defined population density function, then

$$\overline{L}_{wt} = \overline{L}_{43} = \frac{m_4}{m_3} = \frac{\int_0^\infty L^4 f(L) dL}{\int_0^\infty L^3 f(L) dL} \tag{4.55}$$

and

$$c.v._w = \frac{\sigma_3}{L_{43}} = \left(\frac{m_3 m_5}{m_4^2} - 1 \right)^{\frac{1}{2}} \tag{4.56}$$

The volume/ mass mean diameter L_{43} and the coefficient of variation *c.v.* have been investigated as function of mean residence time. As shown in Figure 4.8, the volume mean diameter generally increases with the residence time. In fact, the occurrence of larger particles is more likely with longer residence times due to growth and eventual agglomeration. The ultrasonic application visibly reduces both the values of L_{43}, and the effect of residence time on L_{43}. Increasing values for ultrasonic power influence the

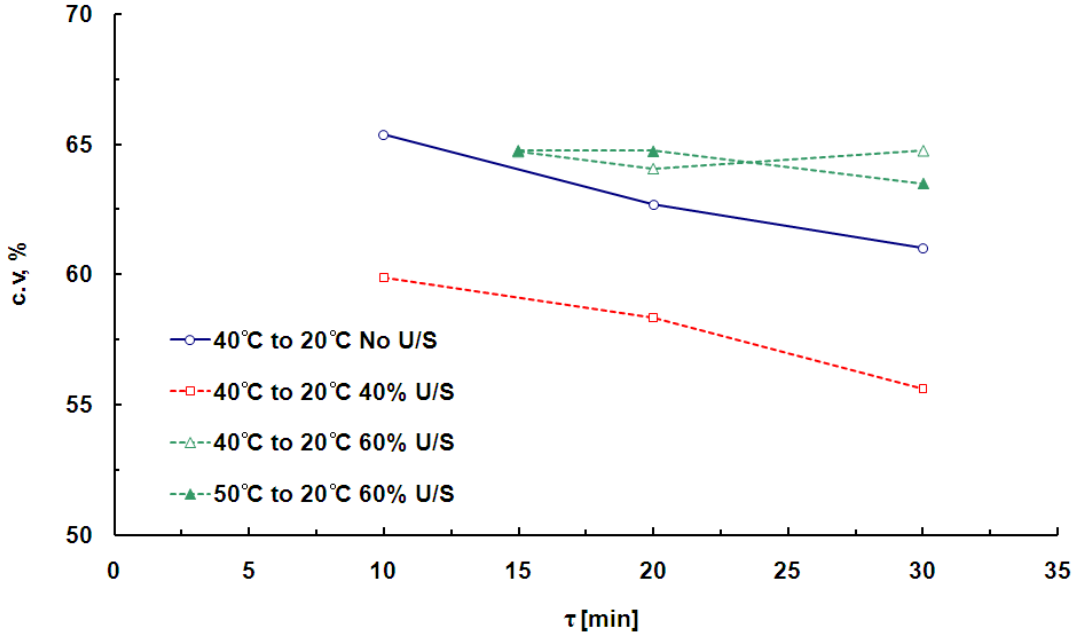

Figure 4.9 Coefficient of variation vs. mean residence time

volume mean diameter leading to a further reduction, while the inlet concentration shows a negligible influence under sonicated conditions.

Finally, the results in term of coefficient of variation are depicted in Figure 4.9; the coefficient of variation decreases as the residence time increases in the case of non sonicated control and with sonicated control at 40% of amplitude. Although higher values of τ lead to larger particles, the residence time shows a negligible effect on the width of the particle sizes distribution. In the case of continuous sonication at 60% of amplitude both the effect of residence time and of inlet concentration appear negligible. The reason for the decrease in the mean particle size and the narrowing of the crystal size distribution due to ultrasound application may be explained in terms of enhanced macromixing rates.

In the absence of sonication, slow mesomixing mechanisms can generate volumes with high supersaturation (around the inlets) and volumes with low supersaturation (bulk). Therefore, areas with high nucleation rates will generate, opposite to areas with high crystal growth rates resulting in the broadening of the PSD. With micromixing and enhanced mass transfer due to insonation, distributed supersaturation will be more

evenly distributed, therefore nucleation and crystal growth rates will have reduced deviations in the bulk volume. The result will consist of a narrowed span in the particle size distribution.

4.7 Conclusions

The equation of moments applied to the population balance has been used to estimate the kinetics of both nucleation and growth crystallization processes at steady state in the continuous cooling crystallization of adipic acid from aqueous solution. The investigation has been addressed to the effect of residence time, ultrasound power amplitude, and inlet concentration and has been carried under the assumption of Mixed-Suspension and Mixed-Product-Removal operating conditions.

In a first instance, the effect of the residence time was determined, both with and without sonicated control. Then the investigation was focused on the influence of power ultrasound with amplitude values varying between 40 and 60% of the maximum allowable nominal power value (750 W). In the case of continuous sonication at 60 % amplitude, two different inlet concentration/temperature values were investigated.

Under all operated conditions, a decrease in both the growth rate and the nucleation values was observed as the residence time increases. This result can be easily explained considering that the driving force for both processes, the supersaturation at steady state, increases with decreasing values of τ.

The effect of residence time on the kinetic of crystals 'growth appeared more relevant in the case of non-sonicated conditions. The results indicate a reduction of the growth rate as continuous insonation is applied, with increasing extent as the power ultrasound increases. In addition, higher values of the inlet concentration resulted in only slightly increased growth rate.

The application of ultrasound resulted in more relevant effects on the nucleation process, in fact the nucleation rate values resulted increased by 10-30 folds comparing the values with ultrasound with those calculated in absence of sonication. The effect of

residence time on the nucleation rate appears more marked in the case of non-sonicated conditions and reduced by 3.4-3.7 folds for every increase of 10 min in τ. The estimated values of nucleation rate of zero-sized crystals, B^0, under continuous sonicated conditions result one order of magnitude higher than those achieved without sonication.

Increasing the power ultrasound leads to a further increase in the nucleation rates values, but not significant in the range of values considered. The effect of solute content in the feed stream appears more significant on the kinetic of nucleation rather than on the growth rate: that could be linked to the higher solute content in the solution, resulting in higher supersaturation and nucleation rates both at steady state and before reaching steady operating conditions, especially at the beginning of the continuous experiment. However the influence of inlet concentration resulted significant only for the lowest values of residence time investigated.

The explanation for the ultrasonic influence on the nucleation process is normally ascribed to the "mechanical disturbances" induced by cavitation phenomena that induce mechanical disruption of crystals or disaggregation of loosely bound agglomerates that have already formed. In fact, larger solute particles have an increased opportunity to collide with each other because of the microstreaming while the shock wave generated by ultrasonic irradiation increase the kinetic energy of particles in suspension.

In the second part, the correlation between both the rates of nucleation and growth and the supersaturation has been examined. The values of the apparent order of growth g estimated under non-sonicated conditions are close to the unity. That suggests a diffusion controlling mechanism for the growth of crystals. The values for the g coefficient under sonication application are higher but still in the range 1-2, indicating that both diffusion and surface integration reaction exert some influence of the growth rates but with a sonicated enhancement of the diffusional mass transfer of additional units from the bulk to the surface of growing crystals. Ultrasound noticeably enhances the apparent order of nucleation almost doubled from a value 1.49 without sonication to a value between 2.81 and 3.35 with sonication, whilst the effect on the apparent order of

growth seems to be less remarkable. The results indicate a negligible effect of power amplitude and inlet concentration.

In the third part the Mydlarz and Jones three parameters (MJ3) model for size dependent growth has been considered to fit the experimental population density data. A non-linearity in the population density distribution is experienced with a sharp upward curvature in for small crystal size values, but the model prediction fitted well the experimental data only in the case of sonication at 40% amplitude and for crystal size values under 10 μm. As a result, the crystal growth could be deemed strongly size-dependent for smaller crystal sizes, whereas the growth rate values are extremely low. Attrition fragments can act as secondary nuclei and grow at different rates. For larger size values, the growth rate could be evaluated as size independent from the slope of the linear portion of the population density plot.

Finally, the volume/ mass mean diameter L_{43} and the coefficient of variation *c.v.*, were estimated as function of the mean residence time. The results indicate the volume mean diameter generally increases with the residence time. In fact, the occurrence of larger particles is more likely with longer residence times due to growth and possible agglomeration. The L_{43} values are visibly reduced by ultrasonic application as well as the influence of residence time on L_{43}. Increasing values of ultrasonic power affect the volume mean diameter leading to a further reduction, while the inlet concentration shows a negligible influence under sonicated conditions.

CHAPTER 5

MODELING THE KINETICS OF SECONDARY NUCLEATION AND GROWTH USING PARSIVAL

In the third chapter, continuous cooling crystallization was operated with and without ultrasound to assess the effect of sonocrystallization on the product control at steady state. The analysis was focused, in particular, on de-supersaturation evolution, theoretical yield, particle size distribution and habit of crystals in the steady state product. In the present chapter, the population balance modeling software Parsival is used to evaluate both nucleation and growth rates directly from experimental population density distribution data, referring to the case of continuous crystallization with continuous insonation. The effect of the parameters residence time, inlet concentration and power ultrasound on the kinetics of nucleation and growth are investigated. The population balance equation (PBE) has been modeled with secondary nucleation and a size dependent growth module, the latter according to the Mydlarz-Jones three parameter model. Nucleation and growth kinetics parameters have been evaluated using the Parameter Estimation (PE) function in Parsival.

5.1 Introduction

The crystal size distribution (CSD) of the product from a continuous crystallizer is determined by a direct relationship between both nucleation and crystal growth rates with the magma residence time distribution. Since *a priori* prediction of crystallization kinetics is not yet possible, experimentally determined and statistically correlated nucleation and growth rates are needed for the design and analysis of industrial crystallizers. Analysis of the CSD from continuous MSMPR (mixed-suspension, mixed-product-removal) crystallizers has proved to be a popular way of inferring such crystallization kinetics but reported kinetic data often vary considerably, even for the same substance, limiting the general adoption of this technique (Mydlarz and Jones, 1993).

The MSMPR model permits simultaneous determination of both nucleation and size-independent growth by extrapolation of the *number density* (or *population density*) function from crystal size distribution (CSD) data at given mean residence time during steady-state operation (Mydlarz, 1994). According to the model assumption, all crystals have equal and constant growth rate and all nuclei are formed at or near zero size, therefore a linear semi-logarithmic relation is predicted between crystal population density and crystal size L. However, population density plots from experimental data

often show an increase in the population density for small particles; the number of crystals per unit size per unit volume of suspension is greater than would be expected under MSMPR conditions. The estimation of both nucleation and growth rate becomes then more difficult (Mydlarz, 1994).

The population density data relating continuous crystallization under continuous ultrasonic irradiation shows an upward curvature below circa 20 μm, as presented in Chapter 4, with consequent effects on kinetic parameters. An upward curvature for micrometer particle sizes and the interaction among crystals present in the suspension provides circumstantial evidence for secondary nucleation mechanisms and can give some indication about the nature of the crystal contacts responsible for production of secondary nuclei. The most important mechanism of secondary nucleation in industrial crystallizers would appear to be *contact nucleation*, sometimes referred as *collision nucleation* or *collision breeding* (Garside and Davey, 1980). Contact nuclei result from contact between a growing crystal and the walls of the container, the stirrer or other crystals. However, it has been also suggested that secondary nucleation can be caused by fluid shear, that is, by flow of the supersaturated solution relative to the growing crystal surfaces. The forces required to obtain nuclei in this way seem to be comparatively large but the contribution of such mechanism to secondary nucleation in crystallizers is uncertain (Sung et al, 1973). Hydrodynamic interactions between suspended crystals, solution and rotating stirrers or impellers will clearly be important if contact nucleation, or a secondary nucleation induced by fluid shear, is an important mechanism.

This chapter presents an investigation on the kinetic of crystallization in a continuous process under continuous irradiation of ultrasound, where different experiments have been operated using the same coated impeller to minimize secondary nucleation by impact crystals-impeller.

Secondary nucleation rates in suspension crystallizers have been found to depend on supersaturation but also on a number of other variables; the two most important are the amount of crystals in suspension and the crystallizer hydrodynamics. The former has usually been represented by the concentration of crystals in suspension M_T (also called the “magma density” or “suspension density”) which is proportional to the third moment of the size distribution of the CSD (Garside and Davey, 1980).

In a literature review presented by Garside and Davey (1980) evidence is provided that micro attrition of parent crystals may be the mechanism by which secondary nuclei are detached. It is also indicated that the size of initial fragments is substantially greater than the critical size for stable nuclei and the initial size distribution appears to vary directly with the supersaturation; attrition of the crystal surface with an instantaneous production of nuclei has a spectrum of sizes which changes directly with the supersaturation.

Different studies provided confirmation of the fragmentation of growing crystals to produce smaller new crystals by secondary nucleation during sonocrystallization, as mentioned in Chapters 2 and 3; collapsing cavitation bubbles generate shock waves that enhance the shear on the surface of existing crystals, or increase the kinetic energy of pre-existing particles favouring secondary nucleation by collisional events.

The non-linearity in log population density vs. size plot, with an upward curvature for smaller sizes, can arise also from anomalous crystal growth mechanisms (size dependence, dispersion) or hydrodynamic classification. One way of modeling this behavior is to adopt a size-dependent growth function such that an "effective" crystal growth rate can be determined for design purposes (Garside and Davey, 1980; Mydlarz and Jones 1994).

In this chapter, the population balance equation has been modeled by combining a secondary nucleation term with a size and supersaturation dependent growth model. A finite distribution of secondary nuclei is considered for this work and the Mydlarz-Jones three-parameter model has been selected to tailor a size –dependent growth rate, as the model was proved to offer a good curve fitting of population density data on a large size range, both in conditions that hold and violate McCabe's ΔL law (Mydlarz and Jones 1994).

5.2 PARSIVAL

The commercial available software package PARSIVAL (PARticle SIze eVALuation) uses the fully adaptive Galerkin h-p method. It is based on a generalized finite-element scheme with self-adaptive grid-and order construction (Wulkow, 2001).
The discrete Galerkin h-p method (h-p: variable grid-variable order), initially developed for the simulation of polymerization reactions, has been transferred to a continuous

property coordinate (here: particle size). The method is based on a time discretization by means of a Rothe's method. The idea is to discretize the population balance as an abstract differential equation in an appropriate function space. Given a time step τ_s, and defined as $u(L)$ an approximation the solution $u(L, t + \tau_s)$ and as $\eta_1(L)$ the estimate of the time error $u(L)- u(L, t + \tau_s)$, whenever a time step with (old) step size τ_s has been performed with the adopted scheme (semi-implicit Euler scheme), a new step size τ_{new} can be computed by

$$\tau_{new} = \tau_s \sqrt{\frac{TOL}{\|\eta_1(L)\|}} \qquad (5.1)$$

with "TOL" representing the desired overall accuracy (default value:10^{-2}) and $\|\cdot\|$ being an appropriate norm (M. Wulkow et al.,2001).

The algorithm has been implemented in the Parsival program package with a full graphical user interface. The goal of the development was the complete, flexible and efficient solution of particle processes of very different kinds, so that PARSIVAL is capable of treating models with

- an arbitrary number of fluid components and particle size distributions,
- an arbitrary number of operators including arbitrary kernels,
- no restriction on the form of the particle size distributions.

Furthermore PARSIVAL allows the input of recipes, estimation of parameters from given experimental results and the treatment of additional differential equations.

The input is supported by a user-friendly Workshop. A process representation in PARSIVAL consists of six types of components, which can be defined by the user: reactors, coefficients, fluids, distributions, streams and modules. All processes can be combined in terms of basic modules such as nucleation, growth, agglomeration, breakage, attrition etc to be implemented. When a module is pre-selected, an equation pattern is shown to check whether the selected module meets the requirements (M. Wulkow et al.,2001).

It is worth pointing that while MSMPR models generally use a series of simplifying assumptions such as no classification of particles, only nucleation and growth but no

agglomeration, attrition and breakage, the Galerkin h-p method is not bound to any of these assumptions.

5.2.1 Population Balance modeling with Parsival

In the population balance model the number density function of particles of size L is denoted usually by $n(L,t)$, representing the number of particles per system volume with characteristic size L at time t . Solute and solvent are treated as different compounds; adipic acid represents the component 1, whose mass has been denoted by $m_1(t)$ (water is component 2). The concentrations (densities) in the fluid phase are $\rho_i = m_i / V_{fluid}$ (i = 1, 2). The main fluid mass balance has been applied for the component 1. Assuming constant volume, the population balance equation for the particle-size distribution of this component, taking into account secondary nucleation and both supersaturation and size dependent growth, becomes

$$\frac{\partial n(L,t)}{\partial t} + \frac{\partial [G(\rho_1, L) n(L,t))]}{\partial L} = B(\rho_1, n) - \frac{1}{V_{fluid}} Q n \qquad (5.2)$$

5.2.2 Growth and Nucleation Kinetics

The growth rate mathematical expression considered in this work includes the dependence from the supersaturation and a size dependent expression tailored on the Mydlarz-Jones three parameter model (Mydlarz and Jones 1994):

$$G(\rho_1, L) = G(\rho_1) G(L) = k_g \left(\frac{\rho_1 - \rho_1^*}{\rho_1^*} \right)^g \{1 - exp[-a(L + c_{MJ})]\} \qquad (5.3)$$

$$a > 0, c_{MJ} \neq 0$$

where k_g is a growth velocity coefficient, ρ_1^* is the solute saturated concentration at the operating (constant) temperature, g is the dimensionless apparent order of growth, a and c_{MJ} empirical parameters. The value of parameter a should be positive as only positive growth rates are observed in practice (Mydlarz and Jones 1994). Since the supersaturation is expressed in terms of relative supersaturation, kg coefficient has the same units of measurements than the growth rate, m/s, independently from the value of g.

The supersaturation implemented MJ-3 model is capable of describing systems which obey the McCabe ΔL law, in fact, as a→∞, G = constant. On the other hand, it

has been demonstrated that, with c_{MJ} = 5 μm, for values of a in the range 10^3-10^4 m^{-1} the empirical MJ-3 model predicts almost invariant growth rates over most of the size range (apart from smaller sizes); the c_{MJ} parameter affects the growth rate mainly in the size range close to zero (the larger the crystal size, the smaller is the influence of this parameter on the growth rate). Furthermore, as the value of the parameter a decreases, the deviation of the population density function from a straight line becomes more consistent (Mydlarz and Jones 1994).

The nucleation rate $B(\rho_1, n)$ depends on the supersaturation and on the number density and the representing function has been written as (Garside and Davey, 1980):

$$B(\rho_1, n) = K_N \left(\frac{\rho_1 - \rho_1^*}{\rho_1^*} \right)^b \frac{M_T}{\tau} \tag{5.4}$$

with a nucleation rate constant K_N and apparent order of nucleation b.

Figures 5.1 and 5.2 show the dialogue window for the secondary nucleation and the particle growth modules, which involve the dependence from supersaturation and particle size respectively. Parsival requires a file to input the initial shape of the nuclei distribution.

The form of the nuclei is prescribed by a normalized distribution $n_0(L)$ as recommended in the software manual (data file requested for "File 2" in Figure 5.1):

$$\int_0^\infty n_0(L)dL = 1 \tag{5.5}$$

Parsival provides a nucleation rate in terms of number of nuclei per unit volume of slurry, per unit of time, but also per unit length of crystals (the idea of zero sized crystals has been removed, thus nuclei are characterized by a range of size values). For this reason, it is important to define the interval of time to run the simulation; in this particular case it was run for a time interval corresponding to the mean retention time $\tau = V_{fluid}/Q$, and τ has been taken into account in the mathematical expression for the nucleation rate module (equation 5.4).

Finally, the volume exit stream V_{exit} is controlled in Parsival by an algebraic equation such that the volume V is kept constant (Wulkow, 2007).

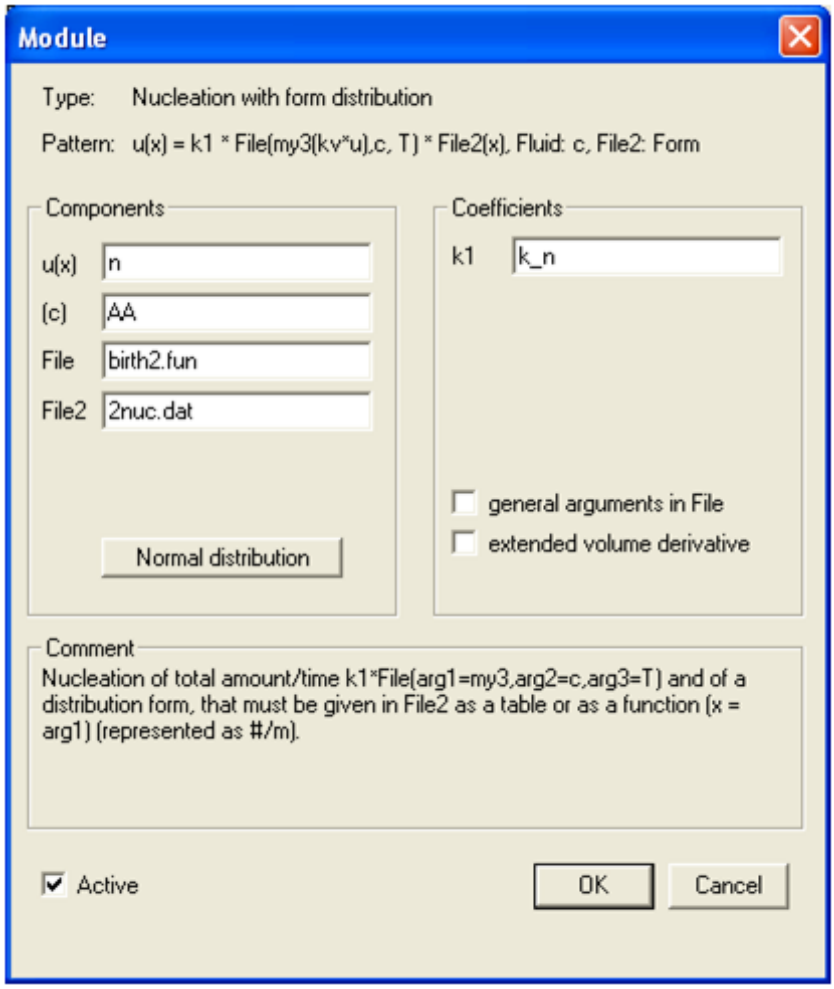

Figure 5.1 Nucleation module in Parsival. Nucleation kinetics depends on solute concentration c, temperature T, and the third moment of the particle size distribution my3, corresponding to the magma density.

5.2.3 Experimental data

Figure 5.3 presents two particle size distributions at steady state from experimental data, measured using Malvern Mastersizer S. The plots refer to a cooling crystallization at 40°C inlet temperature and 20°C vessel temperature, with continuous insonation at nominal power of 95W/100 g of slurry, and mean retention time of 10 min and 30 min. The plots show small peaks for particle size smaller than 10µm , which may correspond to secondary nuclei. It is worth pointing that it is no problem for PARSIVAL to resolve multi-modal distributions which are drastically changing their form with time, since the form and the smoothness of the distributions are automatically adapted by the algorithm (Wulkow, 2007).

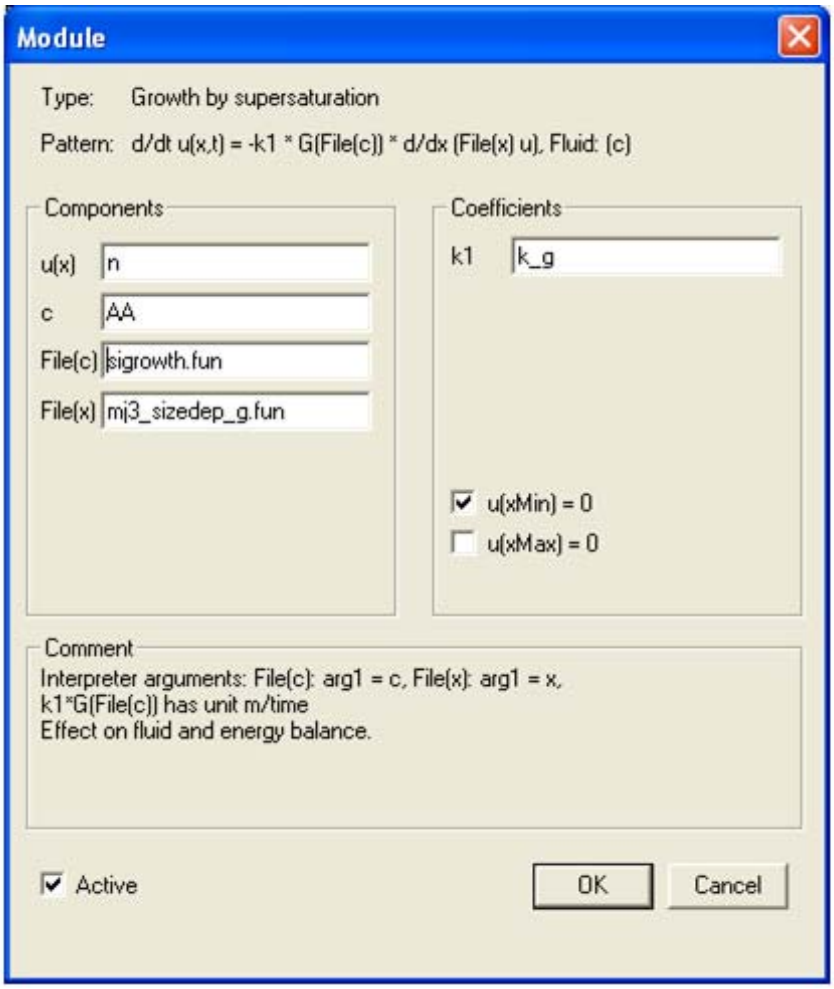

Figure 5.2 Size-dependent growth module in Parsival. The growth kinetics function $G(\rho_1)$ depending on supersaturation is written in File (c) while the code of size dependent term G(L) is written in File (x). In Parsival, x indicates the characteristic size. Fluid: adipic acid (AA).

Visual analysis of SEM photomicrographs showed in Chapter 3 suggests that agglomeration phenomena can be neglected, therefore no agglomeration kernel has been considered for this model.

The input number density function to start the simulation has been calculated from experimental measured particle size distribution data and from the slurry or magma density M_T. Particle size distribution data have been measured using a Malvern Mastersizer instrument, and it was provided in terms of volumetric percentage of particles of size L as function of L ($\%\Delta V_s(\Delta L)/V_{tot} = \%m_s(\Delta L)/m_{tot}$). M_T values were measured from concentration data estimated by conductivity measurements (Chapter 3). The formula used to determine the experimental population density function is:

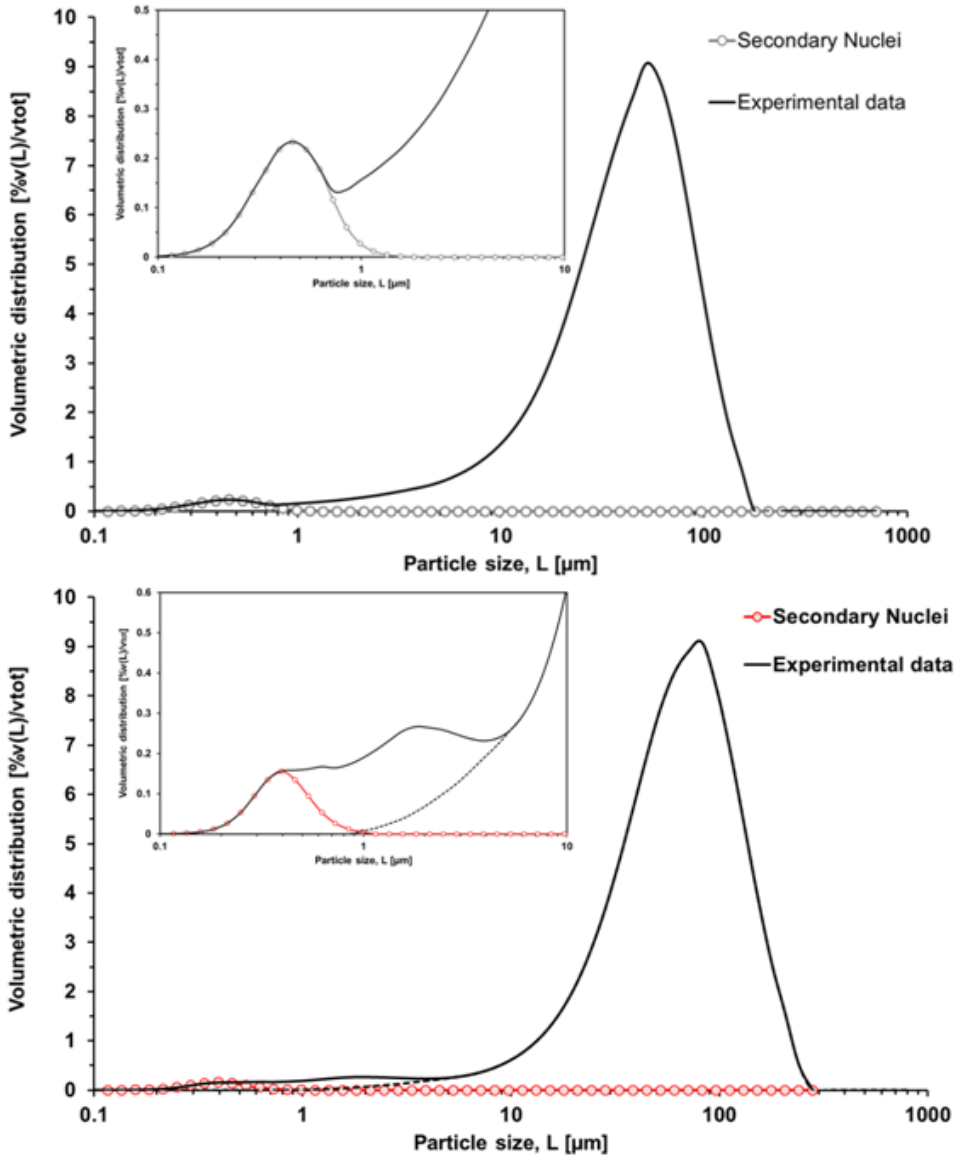

Figure 5.3 Particle size distribution at steady state of adipic acid crystals and secondary nuclei distribution chosen for the nucleation module in Parsival. Operation conditions: 40°C inlet temperature, 20°C vessel temperature, continuous insonation at nominal power of 95W/100 g of slurry. Mean retention time: 10 min (Top figure), 30 min (Bottom Figure).

$$n(L) = \frac{\%\Delta m_S(\Delta L)}{100 * m_{tot}} \frac{M_T}{\Delta L k_v \rho_c L^3} \qquad (5.6)$$

The distribution $n_0(L)$ has been extrapolated from the PSD of finest particles ($L < 2$ µm), as a distribution with the same mode and coefficient of variation. The total volume of these particles does not reach the 2% of the total volume of solid particles at steady state.

5.2.4 Parameter Estimation function in Parsival

In this work, PARSIVAL has been used to estimate the kinetics parameters for secondary nucleation (*b, k_n*) and supersaturation and size dependent growth (*g, k_g, a, c_{MJ}*). It is worth pointing that, whereas the number density function requires a good resolution for the smaller particles, the mass density function (~ $n(L)\cdot L^3$) has to be represented accurately for larger particles. This is adaptively done by the algorithm using the previously mentioned sophisticated error control mechanism (Wulkow, 2007).
The input values for the growth rate parameters *g* and k_g were estimated from the linear portion (G_{lin}) of the population density plot (experimental data) using the common relationship

$$slope = -\frac{1}{G_{lin}\tau} \tag{5.7}$$

where

$$G_{lin} = k_g \sigma^g = G_{exp}\,. \tag{5.8}$$

Differently from the MSMPR model, the input values for the nucleation parameters where not estimated from the y-intercept (L= 0) as a finite distribution of nuclei is used (and recommended) in Parsival; these value were estimated from the population density plot as

$$n(L_{nuclei}) = k_n \sigma^b = B_{exp} \tag{5.9}$$

with L_{nuclei} corresponding to the mode of the secondary nuclei distribution.
Finally the input values of *a* and c_{MJ} were set as 3000 m^{-1} and 5 µm respectively. These reference values were chosen in the range of values listed in the works presented by Mydlarz and Jones in 1993 and 1994.
Table 5.1 presents the parameters used for the model equation with corresponding input values. Parsival offers a Parameter Estimation (PE) module to adapt the selected coefficients/constants in such a way that the difference between the computed values and the experimental data is as small as possible. This option offers the optimization of input parameters providing the best fitting between numerical solution and experimental data. This work adopted the PE in Parsival to estimate the value of kinetic parameters *b, k_n, g, k_g, a, c_{JM}.*

Table 5.1 Kinetic parameters for the secondary nucleation and growth modules with corresponding input values.

	Cooling from 40 ºC to 20 ºC 40% power amplitude			Cooling from 40 ºC to 20 ºC 60% power amplitude			Cooling from 50 ºC to 20 ºC 60% power amplitude		
Mean retention time, min	10	20	30	15	20	30	15	20	30
K_n, $kg^{-1}m^{-1}$	1.97E+19	1.97E+19	1.97E+19	9.59E+19	9.59E+20	9.5E+20	6.83E+18	6.83E+18	6.83E+18
b, #	3.56	3.56	3.56	3.47	3.47	3.47	3.45	3.45	3.45
k_g, m/s	4.94E-7	4.94E-7	4.94E-7	2.9E-7	2.9E-7	2.9E-7	2.94E-8	2.94E-8	2.93E-8
g, #	1.36	1.36	1.36	1.33	1.33	1.33	1.32	1.33	1.33
a, m^{-1}	3000	3000	3000	3000	3000	3000	3000	3000	3000
c_{MJ}, μm	5.0	5.0	5.0	5.0	5.0	5.0	5.0	5.0	5.0

5.3 Results and Discussion

The population density (PD) plots from continuous cooling crystallization experiments of adipic acid with ultrasound are presented in Figures 5.4 (a), (b), (c). Experimental plots are fitted by the corresponding model simulations obtained after parameter estimation. Experimental PD data exhibits a marked upward curvature for particles smaller than 20 μm and a quasi linear trend for larger sizes in any investigated case; for L < 20 μm, data trend exhibit greater number density values than would be expected on the basis a MSMPR crystallization model.

In the case of 40% power amplitude (the lowest ultrasonic intensity in this investigation), the model simulation fits well the experimental data, both in the non-linear portion of the PD plot and in the linear part, where a size independent growth rate can be considered; the model satisfactorily reproduce the experimental data points in the whole size range. However, in the case of 60% of ultrasonic amplitude and high initial concentration, the model developed in Parsival overestimates the experimental data at steady state for L > 20 μm. The high ultrasonic intensity combined with dense concentration of solids can enhance breakage processes generating particles with negligible growth (hence not nuclei particles). Neglecting breakage phenomena can explain the model overestimation for large particle sizes.

The parameter estimation based on direct fitting of population density data results in the parameters values listed in Table 5.2. The table lists also the *residual*, viz. the square error *Sn*, which is calculated according to the equation:

Table 5.2 Kinetics parameters for the secondary nucleation and growth modules with corresponding PE values.

	Cooling from 40 ºC to 20 ºC 40% power amplitude			Cooling from 40 ºC to 20 ºC 60% power amplitude			Cooling from 50 ºC to 20 ºC 60% power amplitude		
Mean retention time, min	10	20	30	15	20	30	15	20	30
K_n, $kg^{-1}m^{-1}$	1.98E+19	2.01E+19	1.96E+19	9.53E+20	9.65E+20	9.71E+20	6.94E+18	6.69E+18	6.85E+18
b, #	3.44	3.22	2.97	3.48	3.24	3.63	2.60	3.72	3.36
k_g, m/s	5.06E-7	4.94E-7	4.77E-7	2.35E-7	2.88E-7	2.00E-7	1.6E-8	2.94E-8	2.93E-8
g, #	1.27	1.36	1.32	2.01	1.36	2	1.95	1.33	1.34
a, m^{-1}	3077	3201	2763	2433	2983	2142	1944	3020	3011
c_{MJ}, µm	5.13	5.0	4.61	4.06	4.97	3.57	2.74	4.98	5.02
Residuals	0.28	0.15	0.14	0.47	0.48	0.25	0.27	0.21	0.44
B, $\#/(m \cdot m^3 \cdot s)$	1.53E+13	1.94E+12	4.30E+11	1.23E+14	5.17E+13	4.25E+10	5.2E+14	5.17E+13	1.33E+12
G, m/s	2.63E-8	1.55E-8	1.02E-8	8.99E-9	7.21E-9	5.22E-9	1.5E-8	7.21E-9	2.76E-10

$$Sn = \left\{ \frac{\sum_{i=1}^{n_i} \left[\left(n_{exp}(L_i) - n_{sim}(L_i) \right) / n_{exp}(L_i) \right]^2}{n_i} \right\}^{1/2} \tag{5.10}$$

where $n_{exp}(L_i)$ represents the experimental value of $n(L)$, $n_{sim}(L_i)$ is the results of simulation after PE and n_i is the number of experimental points.

Table 5.2 also lists the growth and nucleation rate obtained from the parameter estimation B_{sim} and $G_{sim.}$ It is important to note that Parsival provides a nucleation rate in terms of nuclei generated per unit length, per unit volume of suspension, but also per unit time, while the experimental value $n(L_{nuclei})$ is per unit length and per unit volume of suspension only. Both nucleation and growth rate values confirm the trend observed in the previous chapter; an increase in the mean retention time reduces both growth and nucleation rate values. Furthermore, an increased insonation intensity leads to increased nucleation rate values and reduced growth rates.

Parameter estimation values are in general comparable with the corresponding input values listed in table 5.1, however the coefficient g values are closer or equal to the one indicating a growth process controlled by surface integration (g = 2) rather than

diffusional mass transfer (g = 1). The values for the g coefficient appear slightly lower than those determined in the previous chapter at 40% of power amplitude while , the parameter estimation provided g = 2 (or close values) for 60% of power amplitude. These values can consequently confirm an enhanced diffusional mass transfer of additional units from the bulk to the surface of growing crystals, and a growth process controlled by surface integration (Mullin, 2001). The order of growth rate values resulting from the parameter estimation appear comparable with those determined in Chapter 4, while nucleation rate values estimated in Parsival are reduced by one to two orders of magnitude. The population model in Parsival is based on a finite distribution of nuclei and the nucleation rate is provided as average value of a distribution while the MSMPR approach considers only zero sized nuclei. In fact nucleation rate is provided in Parsival as number of nuclei per unit volume of suspension and per unit time (like in the MSMPR modeling), but also per unit length of particle. It should be also pointed that the nucleation rate is proportional to the intercept of the number density distribution with the abscissa at L = 0 in the MSMPR model. Due to the sharp upward curvature for smaller sizes, the order of magnitude for these intercept values is up to $10^{21}(\#/m^3)$.

5.4 Conclusions

The commercial software package PARSIVAL (PARticle SIze eVALuation) has been used to estimate the kinetic of nucleation and growth at steady state in the continuous sonocrystallization of adipic acid from aqueous solution. The mathematical expression chosen for the rate of crystal growth includes both the dependence from the supersaturation and a size dependent expression tailored on the Mydlarz-Jones three parameters model.

Parsival uses the fully adaptive Galerkin h-p method and it is based on a generalized finite-element scheme with self-adaptive grid-and order construction. It uses an automatic error control for the time discretization as well as for the discretization of the property coordinate. The method is implemented in a dynamic flow sheet simulator that allows the combination of all different kinds of processes (e.g., agglomeration, breakage, nucleation, growth, erosion), which runs on a standard personal computer. The kinetic coefficients have been evaluated using the Parameter Estimation (PR) module in Parsival.

In the case of 40% power amplitude (the lowest ultrasonic intensity in this investigation), the model satisfactorily reproduce the experimental data points in the whole size range, both in the non-linear portion of the population density plot and in the linear part, where a size independent growth rate can be considered. It should be noted that the model tend to overestimate the experimental data produced at higher ultrasound intensity values for $L > 20$ μm, predicting population density values up to 10 times greater than the experimental ones.

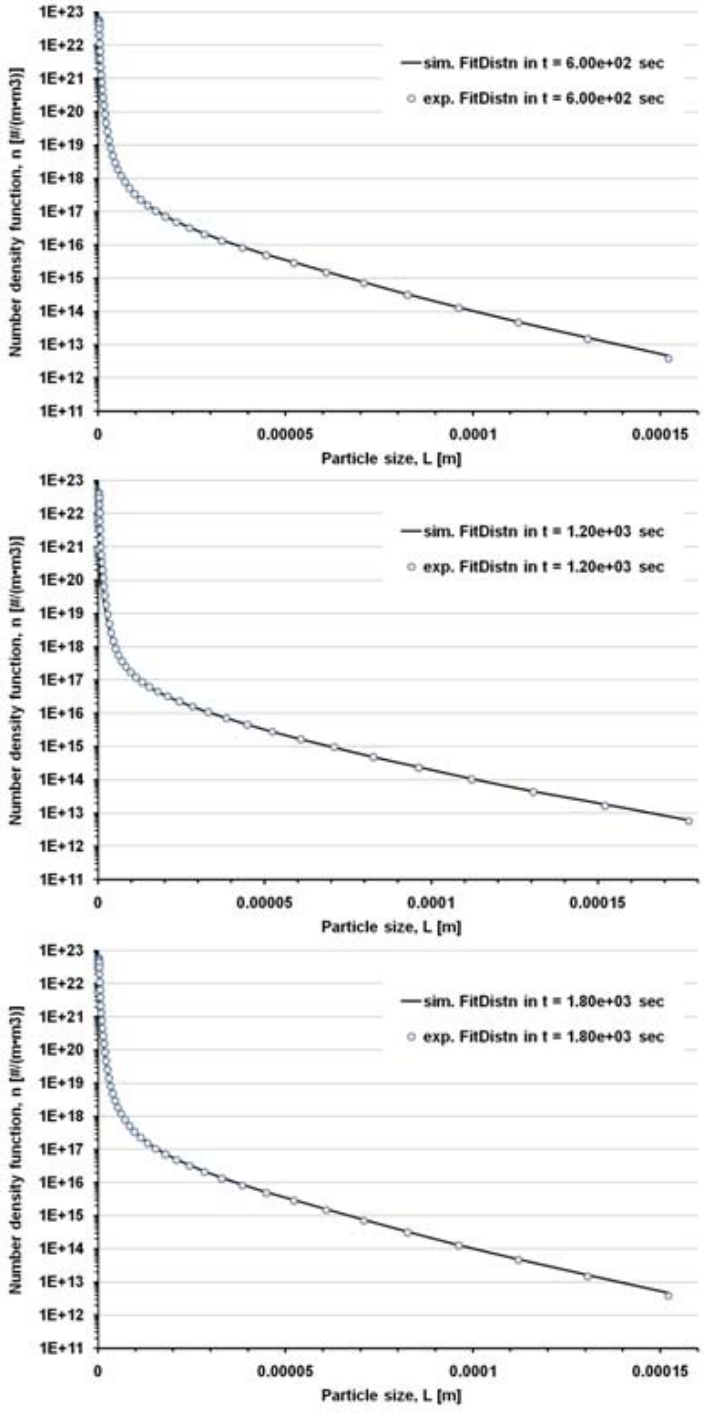

Figure 5.4a Steady state population density data for adipic acid. Comparison between experimental data and fitted data after Parameter Estimation with Parsival. Operating conditions: 40°C inlet temperature, 20°C vessel temperature, continuous insonation at nominal power of 95W/100 g of slurry (.sonication at 40 % of power amplitude). Mean retention time: 10 min (Top), 20 min (Center), 30 min (Bottom).

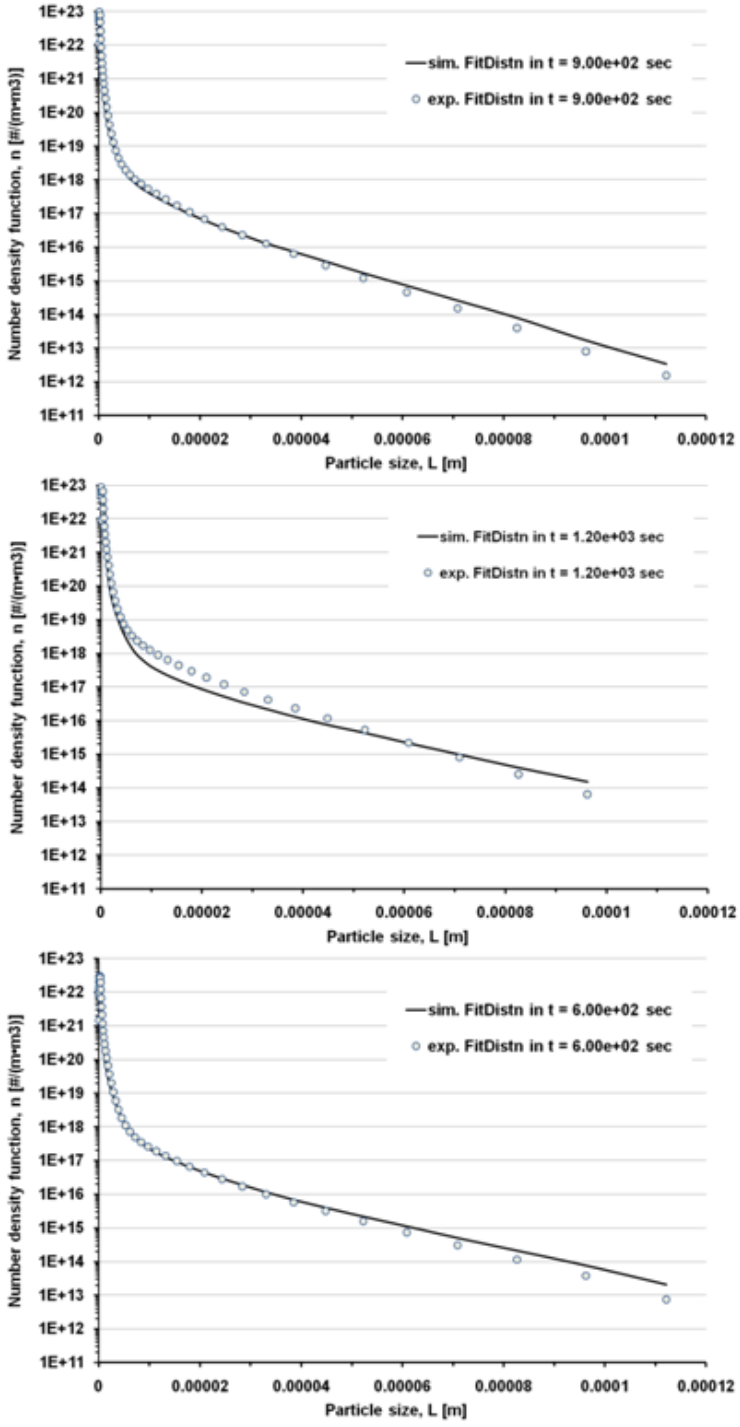

Figure 5.4b Steady state population density data for adipic acid. Comparison between experimental data and fitted data after Parameter Estimation with Parsival. Operating conditions: 40°C inlet temperature, 20°C vessel temperature, continuous insonation at nominal power of 127W/100 g of slurry (.sonication at 60 % of power amplitude) Mean retention time: 15 min

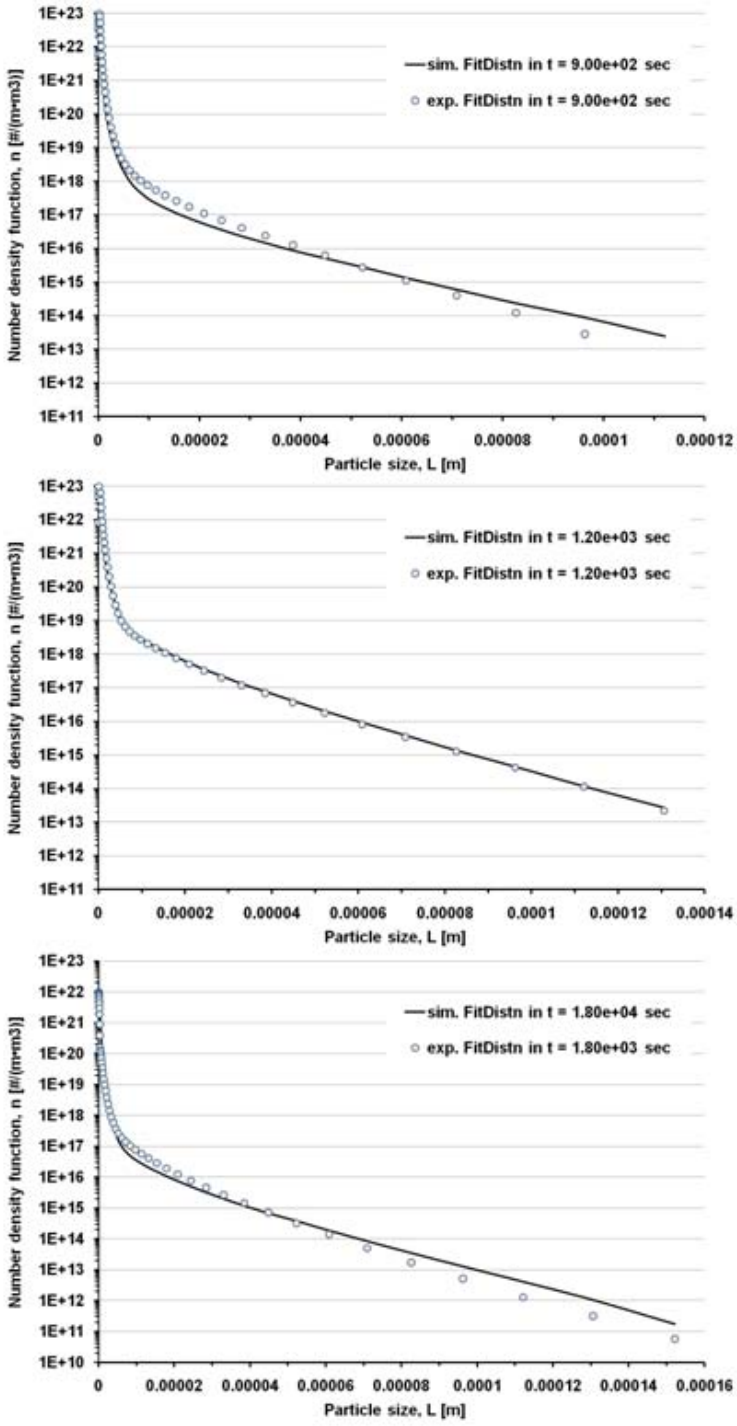

Figure 5.4c Steady state population density data for adipic acid. Comparison between experimental data and fitted data after Parameter Estimation with Parsival. Operating conditions: 50°C inlet temperature, 20°C vessel temperature, continuous insonation at nominal power of 127/100 g of slurry (.sonication at 60 % of power amplitude). Mean retention time: 15 min (Top), 20 min

CHAPTER 6

USING ULTRASOUND IN THE PARTICLE ENGINEERING OF MICROMETER SCALE ADIPIC ACID CRYSTALS

6.1 Introduction

Crystallization from solution of active pharmaceutical compounds or their intermediates is the commonest method of purification used in industry. The integrity of the crystal structure, the size distribution and surface properties of solid-state particles in the end product are important considerations in the crystallization process, which often requires further processing to achieve the required particle form. Such parameters have been shown to play a critical role in the behaviour of active ingredients in a variety of pharmaceutical solid dosage forms affecting both delivery characteristics and therapeutic efficacy. High bioavailability and short dissolution time are desirable attributes of the pharmaceutical product (Midler et al., 1994).

An effective active pharmaceutical ingredient (API) for oral administration needs to be dissolved in the gastrointestinal tract, then diffuse through the intestinal wall and absorbed into the body. The first step in that process is the disintegration of the dosage form followed by dissolution of the active ingredient. For relatively insoluble compounds the rate limiting step in the overall absorption process is generally the rate of dissolution. Particle size reduction increases the specific surface area of the powders, resulting in modifications of dissolution rate (Mosharraf and Nystrom, 1995; Am Ende and Rose, 2006). Johnson and Swindell (1996) mapped out the effect of particle size typically found in a dosage form on absorption over a range of doses, solubilities and absorption rate constants to provide guidance in setting particle size specifications. The results showed that the greatest improvement due to particle size reduction is for low-solubility and low-dose drugs, with a little effect at high dose.

The control of particle size is generally required also to ensure that uniform distribution of particles is obtained in a solid dosage formulation (often referred to as content uniformity). Tablets and capsules are produced in equipment that controls the mass of the API and excipients and ultimately blend composition by volumetric filling. Solid materials with different particle size and shape have different flow and packing properties, giving rise to potential segregation within the formulation blends. Content uniformity is usually achieved through careful selection of the particle size distribution

especially important for highly potent APIs where, for example, precise milligram quantities are required in each tablet during manufacturing. Increasing the number of particles of the API and decreasing the particle size will increase the probability of achieving the needed content uniformity in the formulation (Am Ende and Rose, 2006). Particle shape also influences the surface specific dissolution rate by affecting both the average and the distribution of hydrodynamic boundary layer thickness around the undissolved solid surface, where diffusion dominates. This explains the importance of geometrical form (size and shape) of the particles in all discussions that concern the dissolution rate of fine particulate sparingly soluble drugs.

Crystallization of small sized, high surface area particles requires a high supersaturation, which often results in material of low purity, high friability and decreased stability due to poor crystal structure formulation. Conversely, slow crystallization increases product purity and provides more stable crystal structure but produces large particles with low surface area that frequently require an additional processing step to reduce particle size characteristics to the desired range (Midler et al., 1994). Product quality, reproducible particle-size control, contamination probability and process validation are among the considerations to select appropriate size-reduction systems to yield product crystals of the required specification. Industrially, particle size reduction is typically accomplished by either wet or dry grinding processes.

Conventional size reduction of dry pharmaceutical powders is accomplished by impact techniques. The equipments commonly used fall into two main categories: fluid energy impact mills and mechanical impact mills. Micronization is a type of fluid energy impact milling normally used for pharmaceutical powders. The technique involves the acceleration of particles in a fast gas stream so that grinding occurs by particle-to-particle impact, or by impact against a solid surface, with particle velocities in the range of 300-500 m/s (Am Ende and Rose, 2006).

A hammer (or Fitz) mill is a commonly used mechanical impact mill. It operates by rotating a series of hammers hinged on a central rotating shaft enclosed in a cylindrical housing. The high-speed rotating hammers impact with the particles or facilitate

particle-to-particle collisions (Hajratwala, 1982).

A convenient alternative to dry milling in reducing particle size of APIs consist of a high-shear wet milling (HSWM) integrated into the final step of a crystallization operation.

These destructive-based techniques have been shown to adversely affect a range of highly important physicochemical properties. The high-energy input requirements of mechanical processing will inevitably introduce varying degrees of disorder within the crystal lattice, with formation of crystal defects (point defects, edge and screw dislocations). If the degree of disorder is localized, domains of amorphous material may be generated and, due to the three dimensional nature of crystal defects, these disordered regions can be ubiquitously present on the surfaces of processed particles. The associated increase in surface free energy with the formation of amorphous states will directly influence interfacial interactions. Although disordered regions may occupy only an insignificant percentage of the total mass of the bulk powder, the impact on a typical formulation involves the overall stability, batch-to-batch performance, and therapeutic efficacy of active pharmaceutical ingredients. The amorphous component likely absorbs greater quantities of water than its crystalline counterpart, leading to reduced glass transition temperature values and increased molecular mobility with consequent greater physical and chemical instability at any given temperature than the crystalline counterpart (Mullin, 2001; Kaerger and Price, 2004).

These issues are forcing many pharmaceutical manufacturing companies to investigate alternative methods of producing small particles, with a greater control of the surface characteristics and surface geometry of active compounds while maintaining high throughput, low cost, and industrial scalability (Swarbrick, 2007).

A standard crystallization procedure in the particle engineering of micron-scale sizes is the Reverse Antisolvent Crystallization technique, which involves reverse addition of saturated solution to an antisolvent miscible with the solvent of the original solution. In this way, high supersaturation values and, in consequence, high primary nucleation rates are obtained giving rise to sub-micron sized particles of narrow size

distribution (Midler et al., 1994; Am Ende and Rose, 2006).

Crystallization of solid crystals is affected and can be manipulated by the presence of ultrasonic waves as indicated in the previous chapters. Ultrasonic technology offers a method for modifying and improving both products in terms of crystal habit, size distribution and purity and processes (controllability and reproducibility). As part of these benefits, continuous ultrasonic irradiation applied throughout the duration of the process can facilitate prolific nucleation at higher levels of supersaturation at the expense of some crystal growth leading to the production of reduced particle sizes (McCausland et al., 2001; Devarakonda et al., 2003; Ruecroft et al., 2005).

The work presented in this chapter investigates the size reduction potential of a single stage process based on batch and continuous crystallization of adipic acid from aqueous solution under continuous ultrasonic treatment. Final products characteristics in terms of particle size, habit of crystals, surface roughness are compared with those produced from dry and wet milling techniques and reverse antisolvent crystallization.

6.2 Experimental

6.2.1 Materials

Adipic acid (>99.5% pure) was supplied by Alfa Aesar. Deionized water (conductivity < 0.2 μS/cm) was used as solvent for crystallization experiments. Heptane (>99.0 % pure) and acetone (>99.5 % pure) used for antisolvent crystallization were supplied by Sigma Aldrich.

6.2.2 Batch and Continuous insonated crystallization

Crystallization experiments were mainly performed in a 300 mL jacketed vessel (ID = 80 mm). Stirring was provided by means of a cylindrical magnetic stir bar (length = 60 mm, breadth = 10 mm). The reactor jacket was thermostated using a Haake thermostatic bath (accuracy of ± 0.5 °C) and the vessel temperature was controlled by means of Labview-National Instrument hardware. Stirrer speed was set at 200 rpm to ensure well mixed crystal suspension and avoid vortexing and bubble formation.

Batch experiments were carried in a jacketed 500 mL flat bottomed reactor with HEL automate platform. The composition of the initial solution was chosen between 5 and 18 g of solute/ 100 g of solvent, corresponding to a solubility temperature of 40 and 60 °C (Mullin, 2001) respectively. The initial temperature was set at the solubility value increased by 5 °C. The undersaturated aqueous solution was then cooled at linear cooling rate to 20 °C, and aged for at least 90 minutes to ensure stable conditions, in terms of particle size distribution, were achieved. At the end of the run, the suspension was drawn from the crystallizer and product crystals were separated by filtration under suction and dried in oven overnight.

For continuous crystallization experiments, a hot plate magnetic stirrer was used to stir and overheat the feed solution , but ensuring the desired inlet temperature value for the clear solution entering the crystallizer. The feed tank was insulated to reduce thermal losses. Inlet solution was fed using a peristaltic pump, while slurry withdrawal from the reactor to the product tank was obtained through an overflow pipe, with discharge operated in an intermittent way to prevent classification. About 10% of the vessel volume was removed in each cycle.

A 750 W ultrasonic processor with the frequency of 20 kHz (Cole-Parmer Instruments, Illinois, USA) was used for both batch and continuous crystallization experiments with insonated control at power input range from 82.79 to 95.23 W/100 g suspension as nominal value, while a Sonic Processor P100 with nominal power of 100 W was used to insonate at lower nominal power of 8.47 W/100 g of slurry. Insonation was started just before the beginning of cooling, to allow the adjustment in temperature control and ensure the heat release due to insonation did not alter the set cooling profile.

6.2.3 Dry and Wet Milling

A MC One® Fluid Jet Mill (by JETPHARMA) was used for micronization treatment. The spiral jet mill, commonly used micronizer, is simple in design; it consists of a flat cylindrical chamber with several nozzles arranged tangentially around the periphery of the chamber, a pneumatic feed injector and a feed funnel, as shown in

Figure 6.1 Design characteristics of a micronizer air-jetmil. (www.sreenex.com/html/double-cone-blender-suppliers-delhi-india-bulk_airjetmill.htm).

Figure 6.1. Powder particles are fed into the flat cylindrical milling chamber tangentially through a venturi system by pressurized air or nitrogen, then accelerated in a spiral movement inside the milling chamber by means of nozzles. Particles are subjected to two opposing forces inside the grinding chamber: the free vortex created by centrifugal force (mass force) imparted by the nozzles, and the drag force created by the airflow as it spirals toward the centre of the mill. Large particles are affected by a greater degree by the mass force, while finer particles affected by a greater degree by the drag force. Consequently, centrifugal force retains the larger particles at the periphery of the milling chamber while the smaller particles exit with the exhaust air

from the centre of the chamber. The micronizing effect results from the collision between the incoming particles and those already accelerated into the spiral path. The particle size distribution is controlled by adjusting a number of parameters, two of the main ones being: pressure and feed rate. Pressure acts as the energy used to micronize; increased pressure increases the micronization effect, whilst the feed rate refers to concentration of product fed into the milling chamber. The greater the feed rate, the less the micronization effect because particles must have space to achieve proper acceleration before collision occurs (www.jetpharma.com; www.pharmpro.com).

Experiments were run by feeding batches of 2-3 grams and selecting a mill pressure of 3 bars.

Hammer mills operate by rotating a series of hammers (typically four or more)

Figure 6.2 Design characteristics of a hammer mill.
(www.gec.jp/JSIM_DATA/WASTE/WASTE_2/html/Doc_363_1.html).

hinged on a central rotating shaft enclosed in a cylindrical housing as shown in Figure 6.2. The particle size reduction is related to the rotational speed, the size of the screens used for discharge, and the size of the particles undergoing impact. The screen size

contributes to the residence time of the particles within the mill head. The smaller the screen mesh, the longer the particles will tend to stay within the high-intensity region of the mill. Hammer mills generally produce relatively narrow size distributions, with a minimum of fines due to the self-classification of the screens and the reduced fracture potential as the particles reduce in size. As the particles reduce in size, the inertia of particles impacting with the hammers decreases and the subsequent particle size reduction is decreased (Hajratwala, 1982; Swarbrick, 2007).

A Fitz L1A Dry Mill instrument (Federal Equipment Company) was used for hammer milling experiment, operated with an output screen size of 0.5 mm and hammer speed of 9120 rpm. Raw supplied material was fed, like in micronization experiments, however with higher feeding portions of 30 g.

High shear wet milling processes involve the use of high-speed rotor blades within a work head to exert suction and draw liquids and solids into a rotor-stator assembly (Figure 6.3). Centrifugal forces drive the materials into the work head where milling occurs in the area between the rotor and stator. The technique offers a number of advantages over dry milling operations such as reduced potential occupational exposure and reduced number of handling operations as the unit operation is performed directly on the reactor slurry, typically through a recirculation loop, therefore saving time in the overall processing cycle (Am Ende and Rose, 2006).

A Silverson High Shear Wet Milling (7000 rpm) was integrated into the final stage of both seeded and unseeded crystallization experiments.

6.2.4 Reverse Antisolvent Crystallization

Reverse antisolvent batch crystallization was operated isothermally at 20 °C by addition of saturated solution of adipic acid in acetone (solvent) to heptane (antisolvent). Experiments were run at two values of mass ratio saturated solution: antisolvent, viz. 1:1 and 1:4. Inlet flow-rate and stirring were set at the same conditions (three blade marine type glass stirrer rotated at 200 rpm).

Figure 6.3 Basic working principle of a Rotor-Stator unit in a High Shear Wet Mill (http://pdf.directindustry.com/pdf/silverson-machines/silverson-corporate-brochure/15561-163714-_4.html).

6.2.5 Solid product characterization

Particle Size Distribution measurements were made using Malvern Mastersizer

2000, that detects sizes in the range 0.02μm to 2000μm. Each sample was analysed three times at least.

The morphology and microscopic surface properties of raw material and produced particles were investigated using both optical and scanning electron microscope (SEM). Atomic force microscopy (AFM) measurements were also made to analyse surface topography, amplitude and roughness, using a Park Systems XE-120 AFM. Non contact silicon cantilevers with a nominal spring constant of 42 N/m, 125 μm nominal length and nominal thickness of 4 μm were used for AFM imaging in air with nominal resonant frequency of 330 kHz. The radius of curvature of the pyramidal tip was lower than 10 nm. The non-contact mode vibrates a cantilever at a high resonant frequency, and measures the force gradient by the amplitude and phase change due to the interaction between the probe and the sample, which yields the topography of the sample. Images were processed by XEI software.

Variations in the surface of processed particles were computed by root-mean-square roughness measurements, *Rq*, given by

$$Rq = \sqrt{\frac{\sum_{n=1}^{N} (z_n - z_{av})^2}{N-1}} \qquad (6.1)$$

where z_{av} represents the average of the vertical distance values (z) within a given area of N data points and z_n is the current z value (Boussu et al., 2005). The roughness was measured for different scan areas, varying between 5×5 $\mu m^2$and 10 × 10 μm^2; each measurement was done at least ten times to obtain a mean value of the *Rq* roughness.

6.3. Results and Discussion

6.3.1 Batch and Continuous crystallization with Ultrasound

Figure 4.4 presents a comparison among particle size distribution (PSD) produced after batch cooling crystallization. The plots refer to two different initial concentration values of 5 and 18g of solute per 100 g of solvent, corresponding to a saturation temperature of 40 and 60 °C (Mullin, 2001), and two values of linear cooling rate, 0.1 and 0.5 K/min. Continuous insonation at 40% of nominal power was started just before

the beginning of cooling, to allow the adjustment in temperature control and ensure the heat release due to insonation did not alter the defined cooling profile, then continued throughout the duration of the experiment. Plots are compared with the product size distribution from non-insonated cooling experiment of 5 g of solute per 100 g of solvent at linear rates of 0.1 and 0.5 K/min.

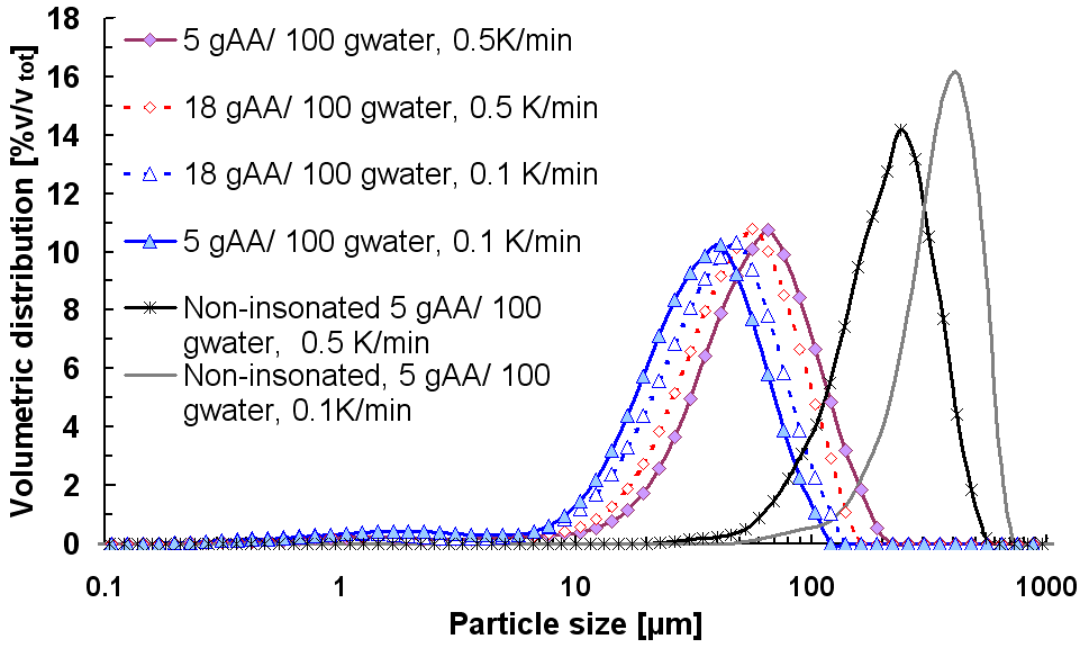

Figure 6.4 Effect of initial concentration and cooling rate on the final crystal size distribution of batch cooling crystallization of adipic acid (AA) under continuous insonation.

Continuous insonation applied from the beginning of cooling period until the end of the experiment produced rounded shaped crystals, with a massive presence of spherical particles, and uniformity of habit. In this regard, small spherical particles have a higher dissolution rate than large, irregular particles. Furthermore, spherical geometry reduces contact area among particles and consequent adhesional interaction (Mosharraf and Nystrom, 1995; Kaerger and Price, 2004).

Slower cooling rates combined with continuous insonation contribute to reducing particle sizes, being opposite to silent conditions, where larger particles were obtained after slower coolings.

The size reducing effect due to ultrasonic irradiation also affects the size increasing effect of initial concentration. Given the same values of final cooling temperature and cooling rate for both insonated and non-insonated experiments, higher initial compositions arising from cooling from higher initial temperatures leads to larger particle sizes. In fact, higher amount of solute are involved in the whole crystallizing process and supersaturated conditions are extended over longer times, favouring the growth of crystals, especially in the case of low cooling rates. Cooling at given rate from higher temperatures, however, also results in longer times for size reduction potential due to ultrasonic irradiation. The results show that, after continuous insonation, the largest particles are produced by selecting the lowest initial solution composition and the faster cooling investigated. The smallest particles were obtained from the same composition but at slower cooling rates. Data relating non insonated experiments show the opposite trend, while the plots referring to the highest investigated composition demonstrate that ultrasound counterbalances the growth effect due to highest initial concentration and dampens the size-increasing effect due to slow cooling.

Figure 6.5 illustrates optical microscope images produced after cooling 5 g of solute/ 100 g of solvent at 0.5 K/min, while scanning electron micrographs of crystals produced after continuous insonation under continuous ultrasonic treatment, at mean retention time of 20 min, are shown in Figure 6.6. The pictures reveal elongated crystals with hexagonal-prismatic geometry, and the presence of particles sized below 10 μm. Continuous provision of ultrasonic energy combined with flash cooling from inlet to vessel temperature favours nucleation phenomena. Particles appear evenly shaped, with a cylindrical symmetry and without a significant presence of agglomerates. Several phenomena are suggested to explain these results; the shock wave caused by cavitation enhances mixing condition and increase the opportunity of particles to collide with each other because of high kinetic energies (Ruecroft et al., 2005; Luque de Castro and Priego-Capote, 2007) thereby promoting secondary nucleation and providing particle size reduction under isotropic conditions. Continuous and homogeneous provision of energy promotes a system of discrete separate particles with high surface tension. This

phenomenon would be more significant for batch experiments where crystallizing particles undergo ultrasonic effects for significantly longer times.

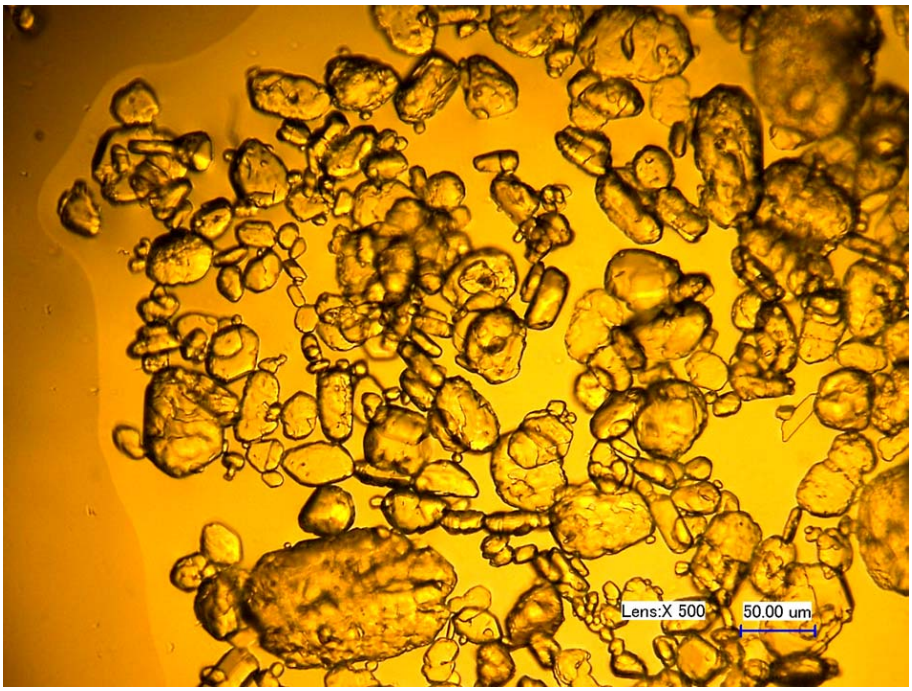

Figure 6.5 Optical microscope image of adipic acid crystals produced after continuously insonated batch cooling crystallization in aqueous solution continuous insonation.

6.3.2 Dry and Wet Milling

Particle size reduction was operated in one operational stage by micronization and hammer milling of the raw material as supplied. A comparison between SEM micrographs of both feed material and product is presented in Figure 6.7. Micronization mostly produces rod-shaped particles but also coarse blocks that are reflected in the wide size distribution from Malvern Mastersizer measurements, shown in Figure 6.8. Hammer milling produced material with poor habit and larger sizes than from the micronization treatment but with a narrower particle size distribution than in the latter (U = 41.6% as opposed to 88.8% after micronization). High shear wet milling was integrated in an unseeded batch crystallization experiment after a stable particle size distribution was achieved at the final temperature.

Figure 6.6 SEM photomicrograph of adipic acid crystals at steady state in continuous crystallization with continuous insonation.

Figure 6.9 illustrates the evolution in size reduction. Particle reduction resulted effective mostly within the first 20 minutes, reducing the mean volumetric size by 86.5%, then the particle size plot levels-out to a steady state as it presents a good agreement with the size distribution after longer milling times. A practical lower limit exists on particle size reduction with conventional rotor–stator mixer technology requiring additional or alternate methods of further particle size reduction or crystallization control. The tendency of the particles to break is ascribed to various material properties, including brittleness, shape, plasticity, and availability of fracture planes (Hajratwala, 1982). As the particles reduce in size, the inertia of particles impacting with the blades decreases and the subsequent particle size reduction is decreased, with analogous reduction of fracture potential than in hammer mills (Johnson and Swindell, 1996; Hajratwala, 1982). Furthermore, the technique involves applying a force on the particles that probably acts at imperfections in the crystal surface by initiating crack propagation through the particle.

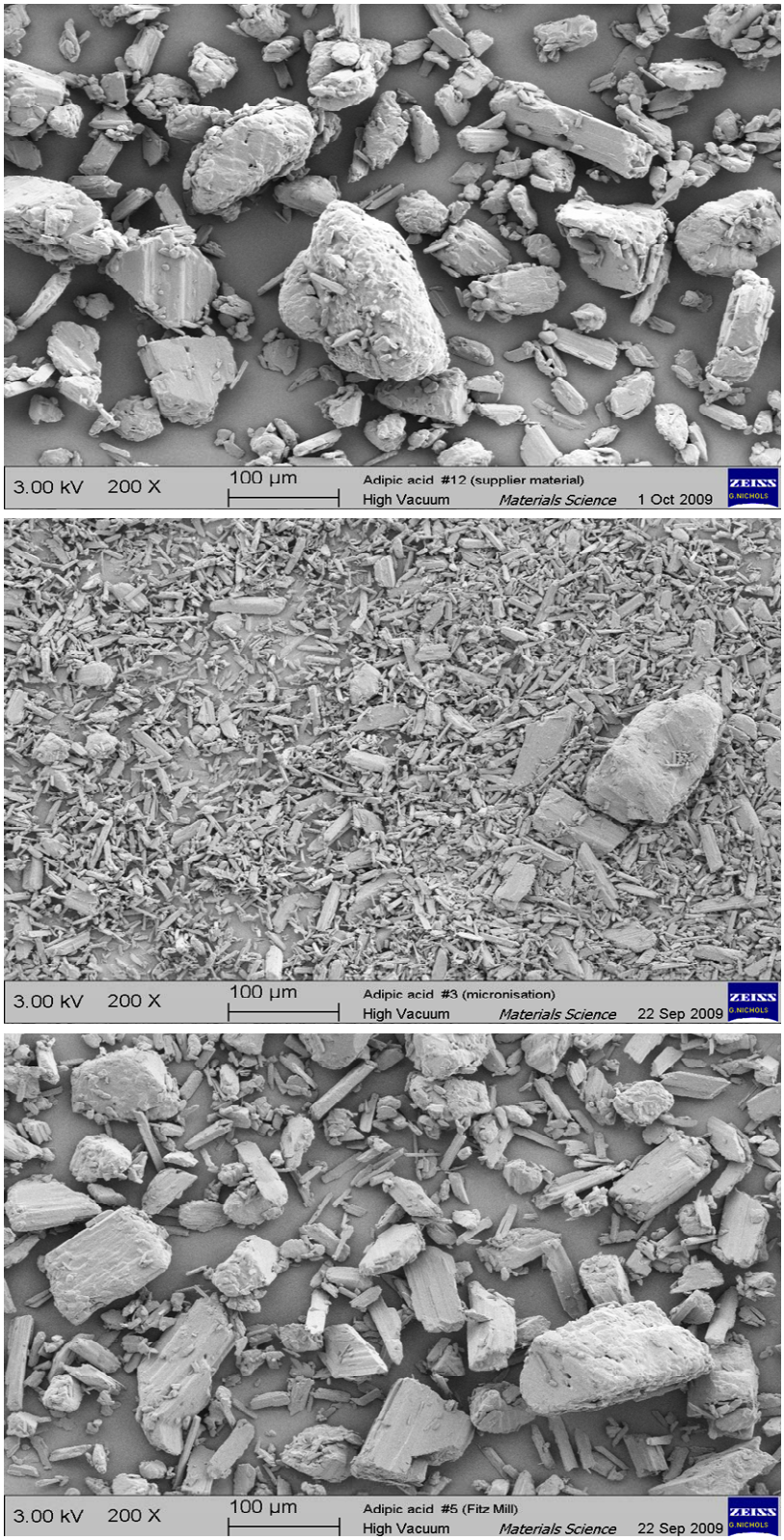

Figure 6.7 SEM phtomicrographs of commercial adipic acid raw material from supplier (top), micronized material (centre), hammer milled material (bottom).

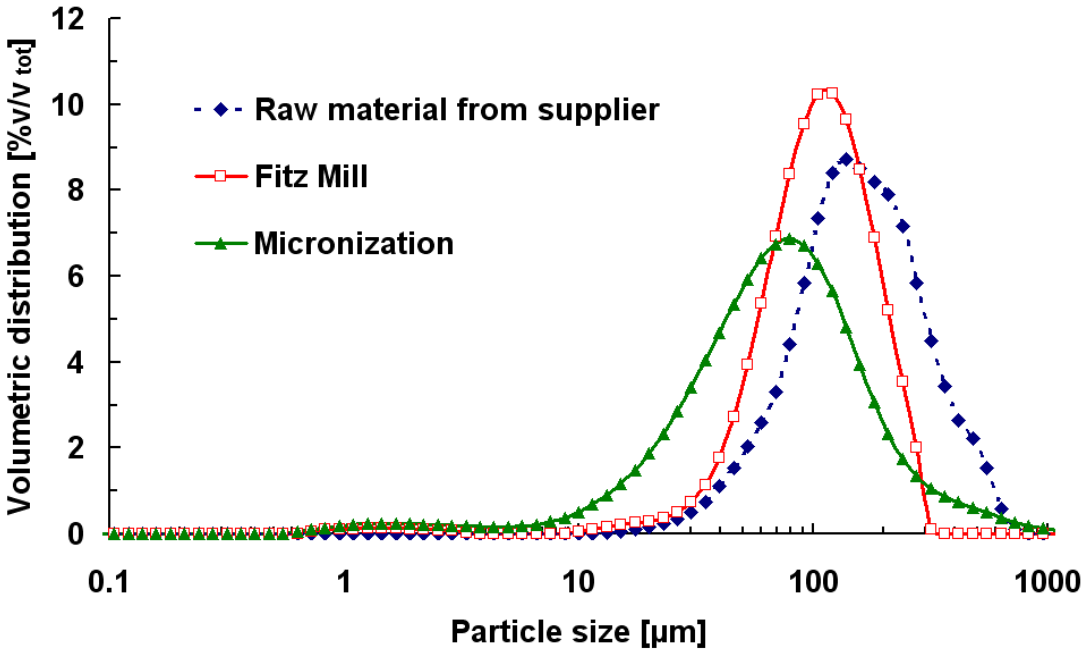

Figure 6.8 Particle size distribution of commercial adipic acid milled by micronization and hammer milling and comparison with fed material.

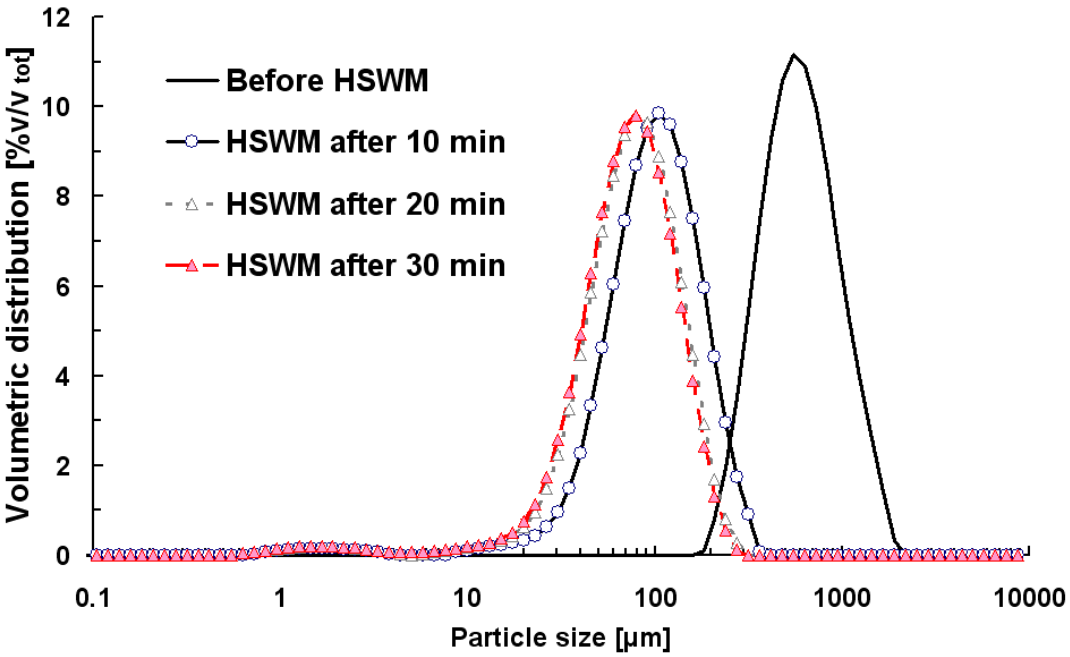

Figure 6.9 Evolution over time of commercial adipic acid particle size reduction by HSWM.

As the size of the particle decreases, the number of imperfections decreases,

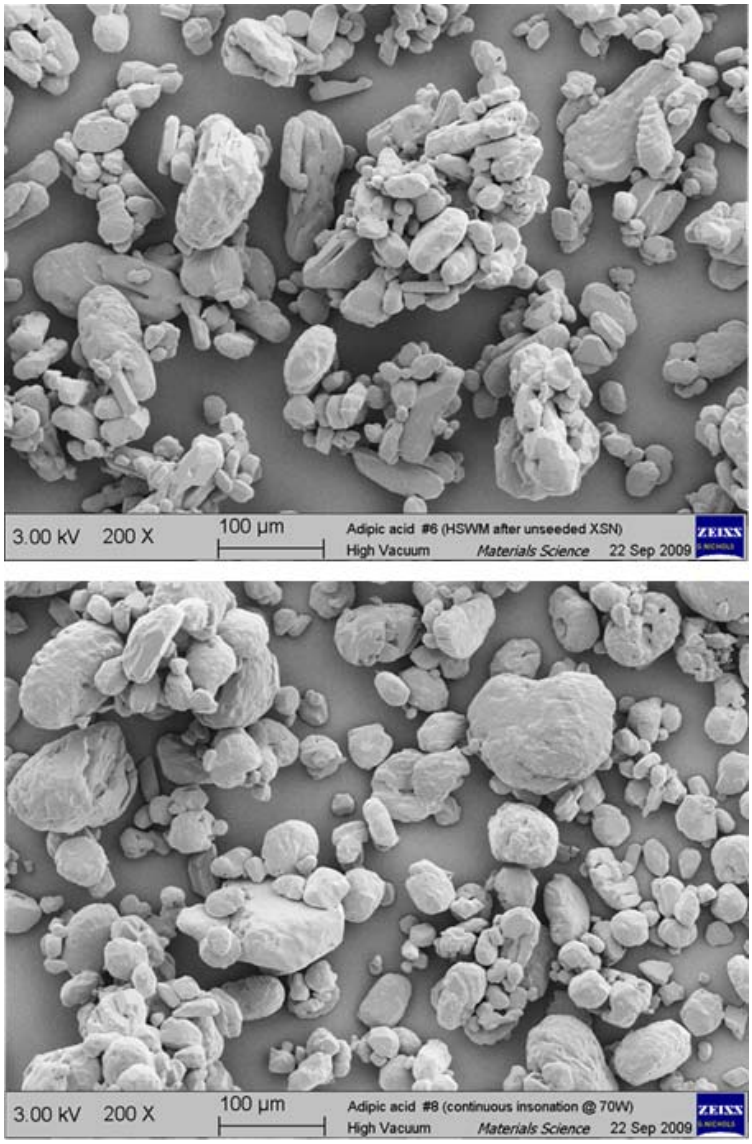

Figure 6.10 SEM photomicrographs of commercial adipic acid crystals after HSWM (top) and after batch cooling crystallization at 0.3 K/min of 60 g solute/ 100 g solvent, under continuous insonation at 8.47 W/100 g of slurry (bottom).

thereby making particle size reduction more difficult (Swarbrick, 2007). Milled particles generated by HSWM present rounded-like crystal habits similar to the product of continuously insonated batch experiments, but with a slightly more elongated shape (Figure 6.10).

A specific experiment was run to evaluate the size reduction potential of insonation; 300 g of saturated aqueous solution of adipic acid was held at 20 °C under continuous ultrasonic irradiation at 40% of maximum power amplitude. 10 g of crystals from the

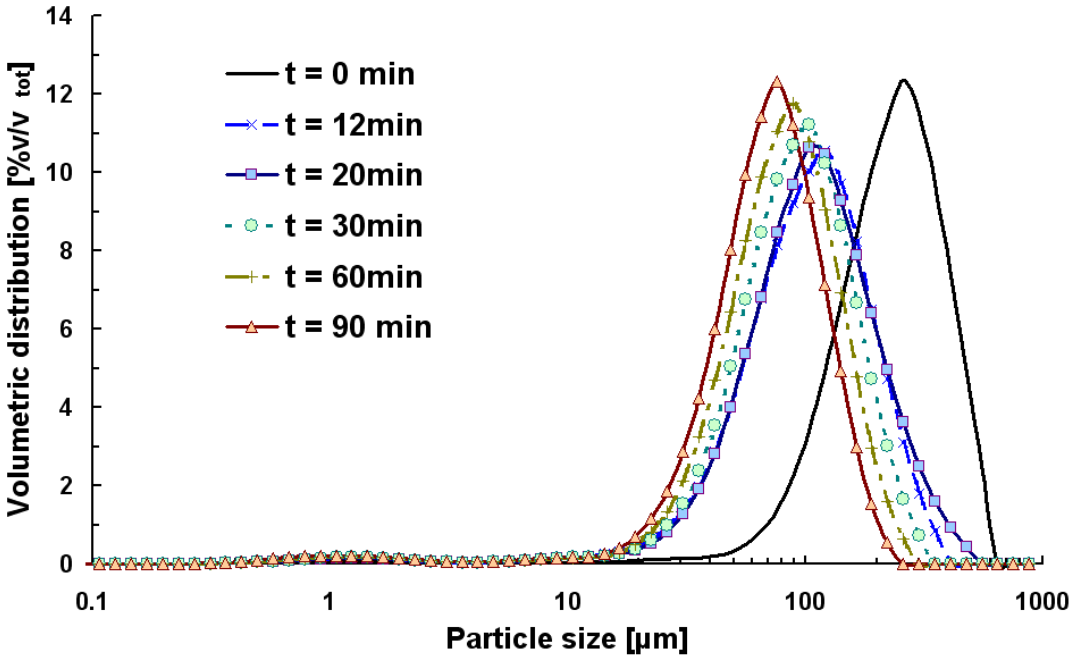

Figure 6.11 Evolution over time in adipic acid particle size reduction due to continuous insonation.

crop of unseeded initially insonated (ultrasound was stopped 3 minutes after the nucleation visible onset) batch crystallization were inoculated after the establishment of isothermal conditions under ultrasonic action. Wet crystals were inoculated, using saturated solution at 20 °C to ensure particles were added close to the stirrer, easily dispersed and avoid floating material. The evolution of particle reduction is shown in Figure 6.11, while the habit of inoculated crystals can be compared with crystals after 90 min of insonation in Figure 6.12. Particle size distribution resulted visibly shifted towards smaller particles, with reduction of 69% in the mean volumetric size, and comparable uniformity values (40.43 - 43.40 %). The final product consisted of rounded shaped particles and the same habit was obtained when the experiment was repeated inoculating particles of supplied material with poor and uneven habit. This case of "size reduction by insonation" is discussed later below.

The experiment was finally repeated with the product of seeded crystallization (L_{43} = 843 µm, C.V. = 39.8%) leading to rounded shaped particles and size reduced by 88.5% in 90 minutes.

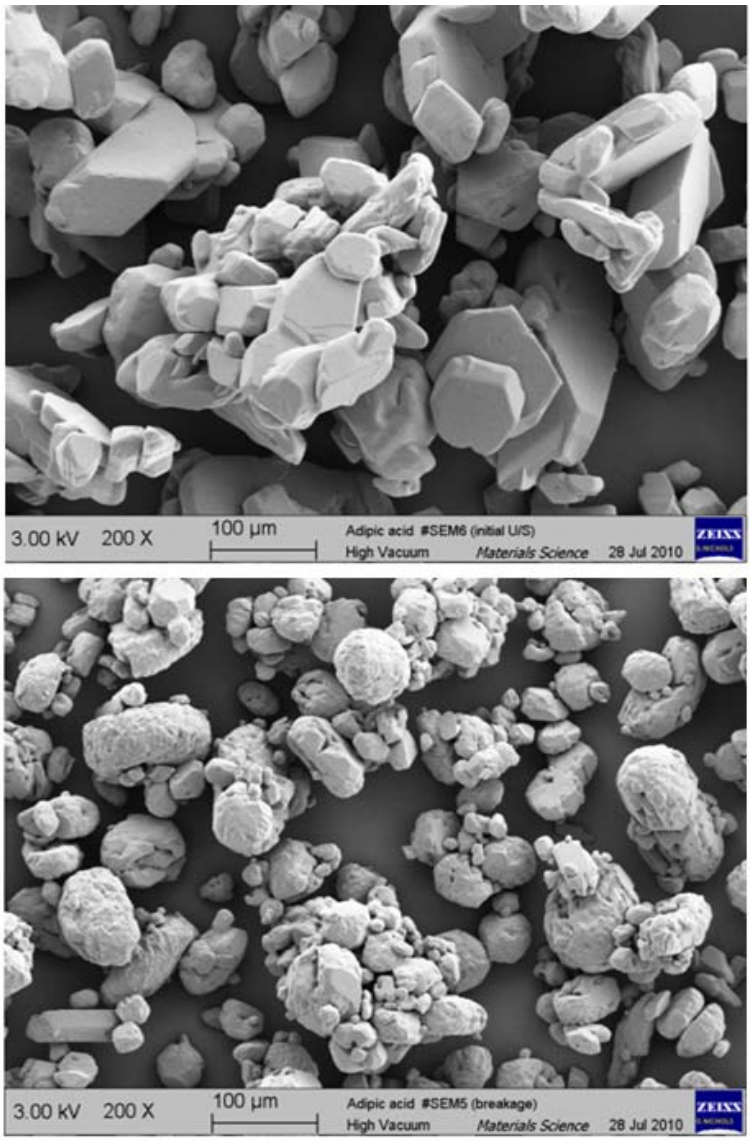

Figure 6.12 Rounded-shaped adipic acid particles obtained after continuous ultrasonic irradiation under isothermal saturated conditions; SEM photomicrograph of original particles (top) and of final product after 90 min of insonation (bottom).

6.3.3 Reverse Antisolvent Crystallization

Figure 6.13 presents bi-modal populations of particles obtained after reverse

antisolvent crystallization. The scanning electron photomicrograph in Figure 6.14 shows aggregates of submicron particles with undefined shape. Larger particles were produced when the highest amount of saturated solution was introduced; suggesting that feeding the saturated solution for longer times favours growth processes. In the other case, both

populations appeared comparable having bi-modal but narrower size distributions, indicating aggregation favoured by the smaller particle sizes.

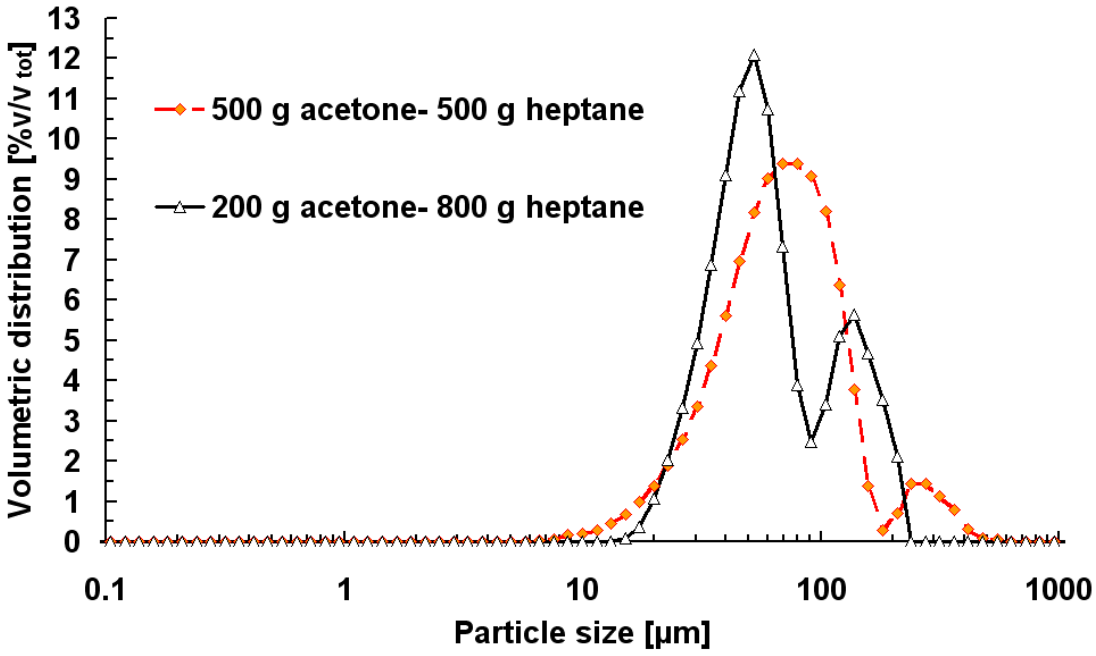

Figure 6.13 Bi-modal adipic acid particle size distributions produced after reverse addition of a saturated solution of adipic acid in acetone (solvent) in heptane (antisolvent).

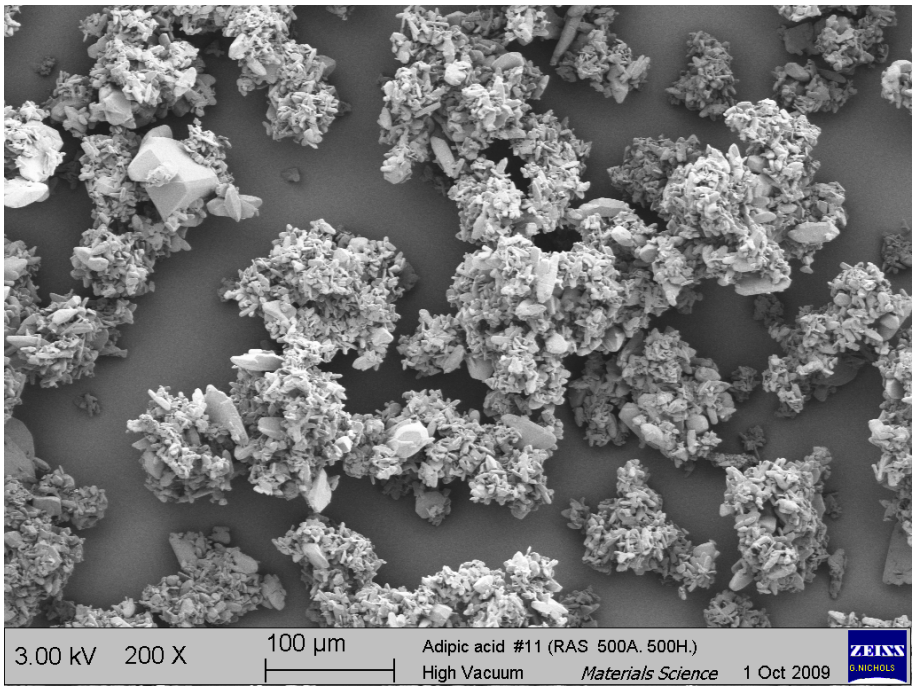

Figure 6.14 Scanning electron photomicrograph of adipic acid particles obtained after Reverse Antisolvent crystallization.

Finally, the maximum amount of solid collected was comparable with batch and continuous crystallization experiments under continuous insonation, however in the latter ones only one third of solvent was required.

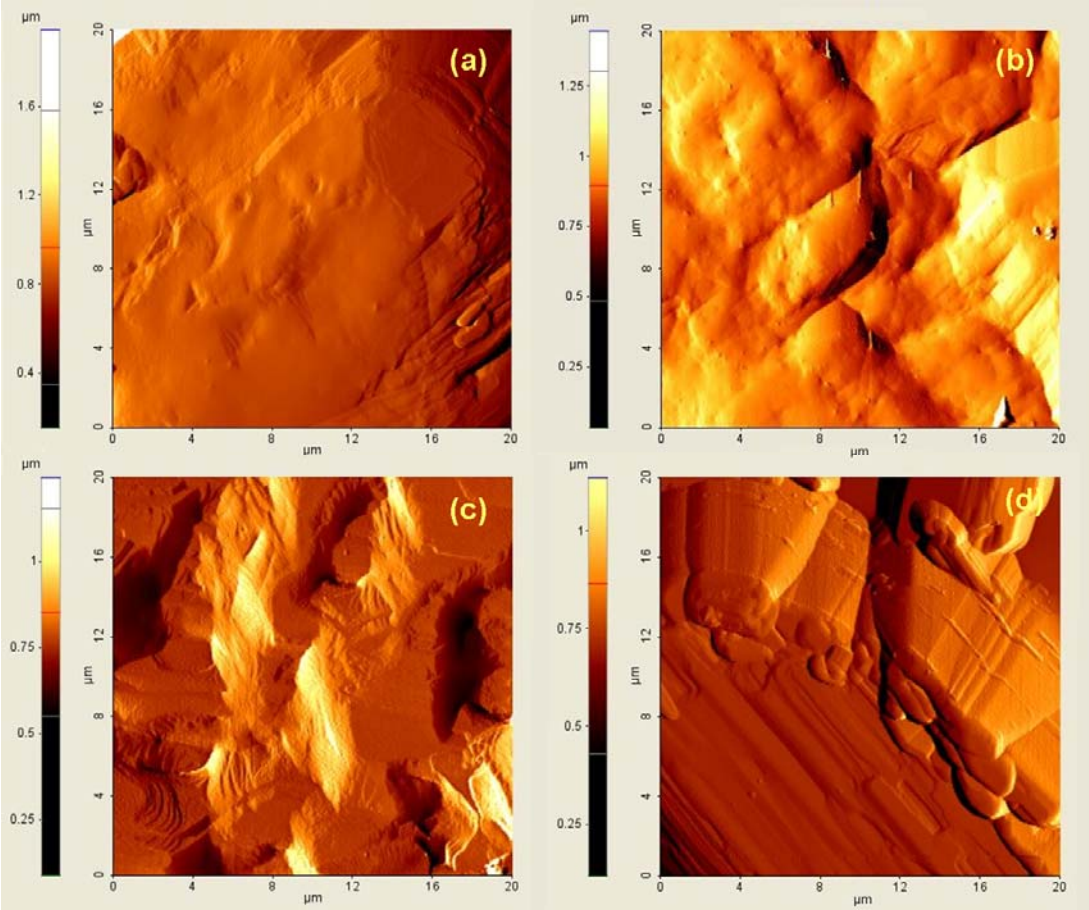

Figure 6.15 AFM amplitude images of adipic acid particles produced after batch cooling crystallization under continuous insonation at (a) 8.47 W/100 g of slurry, (b) ultrasonic treatment to reduce the particle size at supersaturated conditions, (c) high shear wet milling, and (d) micronization.

6.3.4 AFM results

The series of images shown in Figure 6.15 shows the surface geometry of particles produced: (a) after batch cooling crystallization under continuous insonation at 8.47 W/100 g of slurry, (b) ultrasonic treatment to reduce the particle size at supersaturated conditions, (c) high shear wet milling, and (d) micronization.

In the first case, pits and craters are evenly distributed on large surface areas alternated with areas characterised by overlapping layers. Both cavitational collapse and

the enhanced collisions among particles with increased kinetic energy generate attrition and dissolution may explain the wide areas with craters and hillocks. The surfaces of crystals after size reduction by ultrasound and high shear wet milling present similar characteristics; although in the latter case, the area with crystalline terraces seems to dominate. The mechanical effect due to blade-impact appears more localised that the corresponding produced by cavitation.

Comminution by micronization provided extended area with relatively smooth profile alternating with rough surface where the fracture occurred.

Passing from a planar surface to a curved surface dramatically reduces the radius of contact. Nanometer surface asperities may aid in the minimization of the contact area but also maintain large separation distances between the main bodies of contiguous surfaces. The increased separation between two surfaces may directly affect particle adhesion by reducing the short-range attractive Van der Waals force, which decays as a function of radius (Kaerger and Price, 2004).

Figure 6.16 shows a comparison of roughness profiles over a cross section line of 10 μm, while Table 1 reports a comparison of roughness data and the corresponding coefficient of variation over a scanned area of 10 × 10 μm^2, from at least 10 measurements per technique. Smoother areas, with Rq < 50 nm, and average roughness indicated as Rq_{min}, were distinguished from rougher ones with roughness up to 116 nm and average roughness value Rq_{max}. An increased roughness was generally achieved when ultrasound was applied continuously, including the case when ultrasound was applied only at the end of a crystallization operation carried under silent conditions, after stable PSD conditions were established, to reduce the size of final crystals ("size reduction by insonation"),

The highest uniformity in roughness distribution over the investigated crystal surfaces resulted from continuous insonation applied over the entire crystallization process. Conversely, micronized particles present the highest variability in the results, especially for smoother areas.

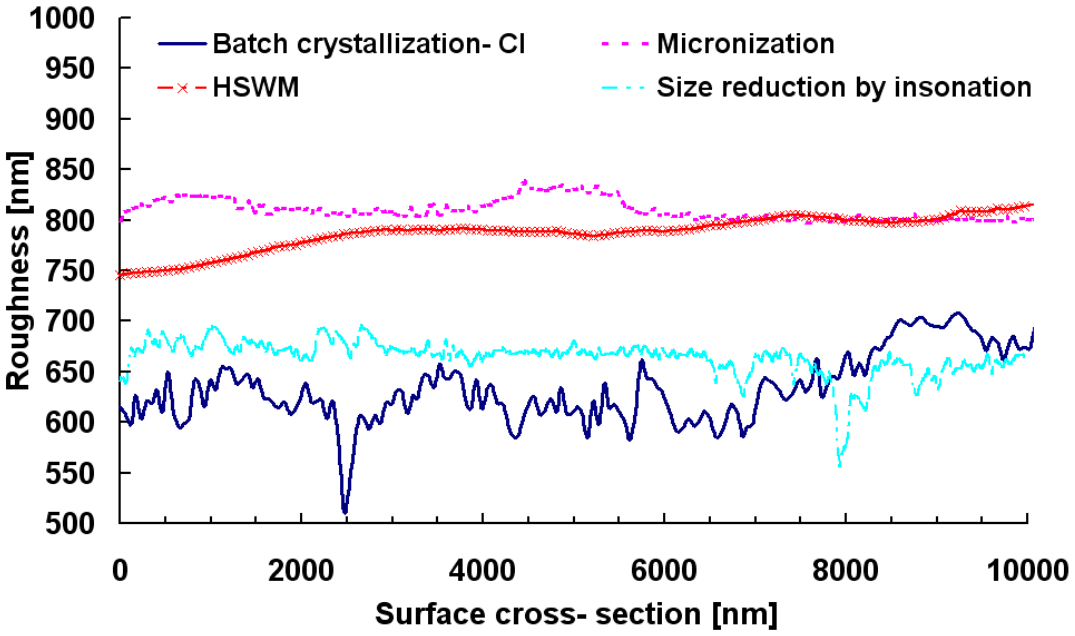

Figure 6.16 Roughness profiles of adipic acid particles produced after batch cooling crystallization under continuous insonation at 8.47 W/100 g of slurry, ultrasonic treatment to reduce the particle size at supersaturated conditions, high shear wet milling, and micronization.

Table 1 Roughness data of adipic acid crystals from scan areas of 10 × 10 μm^2.

	Rq_{max} [nm]	**Coefficient of variation for Rq_{max} [nm]**	**Rq_{min} [nm]**	**Coefficient of variation for Rq_{min} [nm]**
Batch Crystallization - continuous insonation	99.33	10.07	32.57	8.07
Micronization	80.33	20.43	19.00	14.47
Size reduction by continuous insonation	100.04	16.72	16.52	4.393
HSWM	79.43	15.32	12.384	9.605

6.4 Conclusions

Batch and continuous cooling crystallization of adipic acid from aqueous solution was carried under continuous irradiation of ultrasound in order to investigate the effect

of sonication on the final product habit, size distribution and surface roughness. High power ultrasound combined with low initial solution concentrations resulted in the production of particle sizes comparable with the product of micronization, together with narrower size distribution and highly reproducible results.

Scanning electron photomicrographs of the particles produced showed that spherical habits are always obtained from continuously insonated crystallization. Furthermore, spherical particles are obtained even after insonation, under isothermal conditions, of supplied commercial material, with poor and irregular habit. Conversely, micronization and hammer milling yielded irregular crystal habits and a massive presence of rod-shaped particles.

High Shear Wet Milling at the end of batch crystallization produced rounded shaped elongated particles and provided significant particle reduction, however final particles were larger than those obtained after micronization and batch sonocrystallization at the highest power input investigated.

Reverse antisolvent crystallization of adipic acid in acetone (solvent) and heptane (antisolvent) provided the smallest particle size, but of undefined shape. Aggregation resulted favoured by smallest produced sizes resulting in a bi-modal population in the final product.

The application of ultrasonic waves with batch and continuous crystallization produces micron sized spherical particles in a single-step operation from solution to particles. By removing the need of milling, the process avoids associated problems of dusting and reduction of yields, saves the time and expenses required for milling, eliminates the personnel contact with the produced agent and provides highly reproducible results. Surface analysis and roughness measurements revealed an increased surface roughness in crystals produced after continuously insonated batch crystallization compared to those from micronization and high shear wet milling, again with higher reproducibility in the results. Ultrasonic energy can be used to yield advantageous control of the mean size and size distribution of resulting crystals, providing regular shapes and even distribution of crystal surface roughness.

CHAPTER 7

CRYSTAL PRODUCT ENGINEERING IN THE SEEDED COOLING CRYSTALLIZATION OF ADIPIC ACID FROM AQUEOUS SOLUTION

7.1 Introduction

Crystallization processes in the pharmaceutical industry are mainly carried out in a batch-wise manner for greater flexibility and shorter process development times (Ward et al., 2006). In unseeded crystallization systems, the spontaneous formation of crystals usually occurs at high supersaturation with consequent high nucleation and poor reproducibility in the product as a result (Beckmann, 2000).

Inoculation of seeds in supersaturated solutions is commonly employed to control the final product characteristics by acting on the nucleation process and circumventing uncontrolled spontaneous primary nucleation. Furthermore, adding seeds is an appropriate way to operate under reproducible conditions. Four major circumstances can be identified as candidates for seeding: i) to initiate crystallization if the system crystallises with difficulty, ii) to control the crystal size distribution, in most cases to produce large crystals with a narrow size distribution and to avoid fines, iii) to achieve a "single-crystal-growth", where seeding is necessary to obtain crystals of high purity, iv) to avoid encrustation through spontaneous nucleation, and the control of the polymorphic crystal form(Beckmann , 2000).

In the case of adipic acid crystallization from water, where the system does not crystallize with particular difficulty, and is reported to exhibit different polymorphic forms below 136 K (Srinivasa Gopalan et al., 1999; Fun and Chantrpromma, 2009), seeding policies can be directed to the production of large-size product crystals of unimodal distribution, to improve downstream processing efficiency and total separation economics (Ward et al., 2006).

The efficacy of seeding depends on the growth propensity of the seed crystals. Origins, purity, temperature for inoculation and amount of seeds are all influencing parameters. Seed crystals should have a large surface area, so that the use of fines is often preferred, for example in the form of milled material, and the amount of seeds should be the smallest possible, so as to ensure predominance of growth and narrow size distributions in the final product (Beckmann, 2000). However, small particles tend to

agglomerate, decreasing their effective surface area, while grinding processes can introduce impurities, with negative consequences in sterile operations required for pharmaceutical applications.

In the case of seeding targeted to yield only grown seeds crystals in the product with no new nuclei, the final crystal size is given by McCabe's ΔL law (Mullin, 2001). The seed loading can be defined as the ratio of inoculated seeds' mass, Ws, to the amount of solute dissolved in the nurturing solution before inoculation. However, the concentration of seeds is often referred to as ratio between the mass of inoculated seeds and the mass theoretical yield, Y_t, (Beckmann, 2000; Doki et al. 1999; Doki et al., 2003) calculated from mass solubility data at initial and final temperature; the mass concentration of seeds C_{seed} can be expressed as

$$C_{seed} = W_s/Y_t \tag{7.1}$$

where W_s is the amount of added seed .

The final mass of crystals produced, W_f, includes the contribution of the mass of seeds (W_s) and the total mass of dissolved solute turned into crystals, defined as Y_t :

$$W_f = W_s + Y_t \tag{7.2}$$

Under the assumption of pure growth of seeds, with virtually no nucleation, and spherical particles, the number (N) of seed crystals is assumed to be conserved. Defining a characteristic size L_s for original seeds and L_{sp} for product crystals, the ratio between the final mass of crystals and the mass of inoculated seeds becomes

$$\frac{W_f}{W_s} = \frac{N\rho_s L_{sp}^3}{N\rho_s L_s^3} = \left(\frac{L_{sp}}{L_s}\right)^3 = \frac{Y_t + W_s}{W_s} = \frac{Y_t(1 + C_{seed})}{Y_t C_{seed}} = \frac{1 + C_{seed}}{C_{seed}} \tag{7.3}$$

where ρ_s is the density of solids. Therefore, equation (3) can be rearranged as

$$\frac{L_{sp}}{L_s} = \left(\frac{1 + C_{seed}}{C_{seed}}\right)^{\frac{1}{3}} \tag{7.4}$$

L_s can be chosen as the mean mass size of the original seeds and L_{sp} as expected mean mass size of grown seeds, that can be evaluated from this equation and compared with the effective mean mass size of product crystals L_{wp} measured experimentally

(Doki et al. 1999; Doki et al., 2003). A good agreement between L_{wp} and L_s validates the assumption of pure growth of seed, while $L_{wp} > L_{sp}$ can be attributed to agglomerative phenomena with consequent decrease in the number of seed crystals during crystallization. In the latter case, agglomeration among seed crystals can be reduced by selection of a large seed size (Doki et al. 1999).

At a low seed concentration the transient supersaturation profile is expected to have an initial high peak; reduced (total) surface of the seeds will cause low deposition rates of solute, and a massive production of nuclei. On the other hand, at a high seed concentration, the transient supersaturation profile should present a lower supersaturation peak at the beginning, corresponding to fewer nuclei produced.

The amount and the effectiveness of seeding are directly correlated to the rate of cooling. Two opposing effects are involved; the added seeds cause a flux of mass out of the solution, hence decreases the supersaturation via their growth, which is directly proportional to the amount of surface of seeds, while the cooling increases the supersaturation. These processes have to be balanced in such a way that supersaturation does not reach or cross the limit of the metastable zone and no spontaneous nucleation occurs (Ward et al., 2006; Beckmann, 2000; Mullin, 2001).Typical values for the amount of seed are given as Cs ≈ 10% (Beckmann, 2000).

As the cooling rate affects the increase in supersaturation, the faster the cooling, the greater the amount of seeds is required to avoid spontaneous nucleation. Slow cooling rates, such as 0.1 K/min, offer the use of a smaller amount of seeds but are not economically attractive due to the longer time required for cooling (Beckmann, 1998). A convex cooling program may be used to optimize this aspect while a linear rate at the cost of more seeds can be a simpler compromise (Jones, 1974).

Finally, inoculation of seeds has to be operated at a correct time during the development of the supersaturation profile, within the metastable limits to avoid uncontrolled conditions. Early inoculation, viz. when the solution is still undersaturated, will result in at least partial dissolution of seeds, while a late operated seeding, when the

metastable limit has been crossed, will result ineffective as the solute material may already have crystallized at high nucleation rates (because of high supersaturation levels), with consequent prolific and uncontrolled nucleation, giving a product of inferior physical characteristics (Beckmann, 2000; Ruecroft et al., 2005). Besides, the border of the metastable zone is not a physical constant but depends on a number of parameters, including the degree of purity of the investigated compound, cooling rate and presence of foreign entities in solution (Beckmann, 2000).

This present chapter concerns an experimental investigation on the effect of cooling rate combined with seeding load, initial concentration and supersaturation at seeding on the production of large crystals in the cooling crystallization of adipic acid from aqueous solution. Two different sources of seeds have been used: commercial adipic acid after grinding treatment and rounded shaped adipic acid particles from batch insonated experiments. The metastable zone limits are measured in the first instance to determine the operating limits for an effective seeding. A comparison with unseeded experiments at the same values of initial concentration and cooling rates is proposed to highlight the benefits of seeding.

7.2 Experimental

7.2.1 Materials

Adipic acid (>99.5% pure) was supplied by Sigma Aldrich. Deionized water was used as solvent.

7.2.2 Apparatus and operating procedure

Lasentec(R) FBRM and Mettler Toledo Multimax 50 ml crystallizers were used to determine both solubility of adipic acid in aqueous solution and the metastable zone limit. Lasentec technology allows in situ monitoring of particle chord length counts throughout the experiment. To estimate the solubility conditions, a batch of defined composition was heated up at 0.1 K/min: the temperature of full dissolution was

established as indicative of the solubility temperature. The metastable zone limit was instead characterised by determining the temperature value at which spontaneous nucleation occurred in cooling experiments of solution of defined compositions. For this purpose, two different cooling rates were selected, 0.1 and 0.5 K/min.

Batch crystallization experiments were mainly performed in Mettler Multimax vessels (ID = 32 mm) equipped with a three blade marine-type glass stirrer. Stirrer speed was set at just suspension speed of 500 rpm to ensure well mixed crystal suspension avoiding both vortexing and bubble formation. Experiments with the highest initial composition investigated were carried in a jacketed 500 ml flat bottomed reactor with HEL automate platform as explained in the following section.

Typically, an aqueous undersaturated solution of adipic acid was cooled down to 20 °C by linear cooling and aged for at least one hour to ensure stable conditions, in term of particle counts, were achieved. At the end of the run the suspension was drawn from the crystallizer and product crystals were separated by filtration under suction and dried in an oven overnight. Malvern Mastersizer 2000 was used to measure the volumetric Particle Size Distribution (PSD), but also the volumetric mean diameter L_{43} and the uniformity U, defined as the absolute deviation from the median of the distribution. The instrument provides particle size measurements referring to spherical particles with equivalent volume as the measured ones, that makes convenient to use equation (3) valid for spherical shapes. Each sample was analysed three times at least. Measurements were made on wet material to ensure an adequate obscuration value and all particles were detected.

The shape of crystals was investigated using a Nikon ECLIPSE E600 POL optical microscope. Pictures were recorded by means of an Olympus video camera module attached to the microscope. Further morphologic investigation was carried out using a scanning electron microscope (SEM), using magnifications up to 1000.

Seeds used for the experiment were mainly derived by grinding raw material from supplier to reduce both sizes and narrow the seeds PSD. However a number of

experiments were carried using as seeds the crop of batch experiments continuously insonated with a nominal ultrasonic power of 8.47 W/100 g slurry.

Three values were selected for the amount of seeds, corresponding to 1%, 5% and 10% of the total amount adipic acid dissolved at the beginning of the experiment.

7.3. Results and Discussion

7.3.1 Operating Challenges

Dry seed crystals were used in the initial experiments. Under these conditions, seeds tended to float on the liquid surface. Crystal formed and aggregated on the liquid surface in form of an encrustation on the top of a clear solution, with greater visible segregation. For effective seeding experiments, seeds were added as wet crystals, using a saturated solution at room temperature as carrier liquid: this procedure ensured that seeds were added close to the stirrer and easily dispersed.

It is suggested (Beckmann, 2000) to activate the surface of seeds by preparing slurry in which dissolution of the outer layer causes the surface activation. Furthermore, slurry is easier to handle than powder and does not create dust. However, as the carrier mother liquor is introduced in hot solution, it is expected that its temperature increases causing partial dissolution of the seeds. This procedure induces activation of seeds and it is expected that eliminates the fines, characterised by higher dissolution rates. The amount of seeds added, W_s, was increased by a quantity corresponding to the expected dissolved mass (estimated as the difference of solubility values at the temperature before and after the inoculation).

Finally, when a Multimax vessel was filled with 50 ml of solution and the initial concentration was chosen higher than 9 g solute/100g solvent, the stirring visibly appeared inefficient with crystals forming an encrustation layer on the top of a clear mother liquor. The phenomenon was ascribed to the high ratio H_{50} /ID (=1.9), where H_{50} is the height of liquid for 50 ml of solvent, coupled with rotational speed of 200 rpm. Adequate stirring without visible segregation of crystals within the suspension was

achieved by increasing the rotational speed to 500 rpm and reducing the content of the vessel to 40 ml of solvent (H_{40}/ID = 1.5). Hovewer, in the case of highest initial composition investigated, the encrustation on the top of the liquid was often observed even at increased rotational speed and reduced ratio *H/ID,* therefore, the experiments at 18 g solute/100g solvent were carried out in a crystallizer with comparable values of height of liquid and internal diameter ($H/ID \approx 1$) and 500 ml volume. In scaling up agitated tanks, mixer speed generally decreases and tip speed increases resulting in lower average shear and maximum shear rate at the blade tip, with a wider distribution of shear rates on scale-up. For crystallization, the average size can be larger and size distribution wider in the large tank. However, at high Reynolds numbers, the concepts of shear, mean shear, and the impeller rotational speed, *N*, become unimportant relative to the impeller tip velocity as viscosity is no longer the mechanism by which momentum is transferred (Paul, 2004). Size distribution measurement from the different scales adopted, at same operating conditions, revealed comparable values of mass mean diameter L_{43} (difference up to 0.6 %) and difference in the uniformity not greater than 7%. For this reason, the comparison in size distribution results based on the different scales adopted is deemed to be consistent.

7.3.2 Solubility and Metastable Zone Width

Measured solubility concentration data were compared with the literature (Mullin, 2001). The units used are mass of solute on a solvent basis, and the results are presented as a function of the temperature in Figure 7.1. The nucleation temperature corresponds to a sharp increase in the particle count per unit time, in the chord size range 1-1000 μm, monitored by Lasentec(R) FBRM. Measured values present a good agreement with the literature ones, with difference in solubility temperatures with literature data provided by Mullin (2001) lower than 1.5 °C within the investigated range of concentrations.

The onset of crystallization was also detected from the trend of the difference between the reactor temperature, T_r, and the coolant temperature in the vessel jacket, T_j,

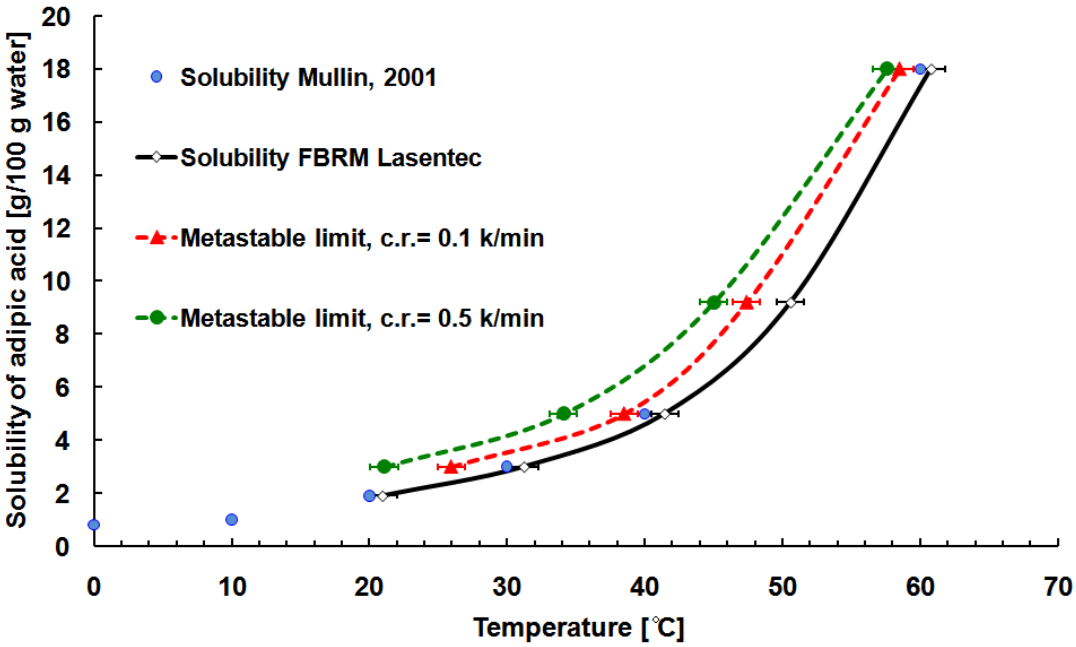

Figure 7.1 Solubility and metastable limit of adipic acid in water with standard error bar.

as the exothermicity of the nucleation process is compensated by an increased temperature difference T_r-T_j (Figure 7.2). The difference in temperature between reactor and jacket presents a peak when crystallization starts. The method provided measureable data, in agreement with FBRM results, but only for the highest (absolute) values of cooling rate.

The global trend of results revealed that spontaneous nucleation occurred at low subcoolings, varying between 3 K at the highest concentration investigated (18 g solute/100 g solvent), and 10 K for the lowest one (3 g solute/100 g solvent). The narrow width of the metastable region could be correlated with the high purity level of adipic acid (>99.6%). Impurities in the solute can hinder the nucleation considerably, thus increasing the width of metastability while the MZW decreases when using material with high purity degree (Beckmann, 2000).

7.3.3 Unseeded batch crystallization

The influence of cooling rate and initial concentration on the final crystal size distribution and crystal habit was first evaluated in an unseeded crystallization operation.

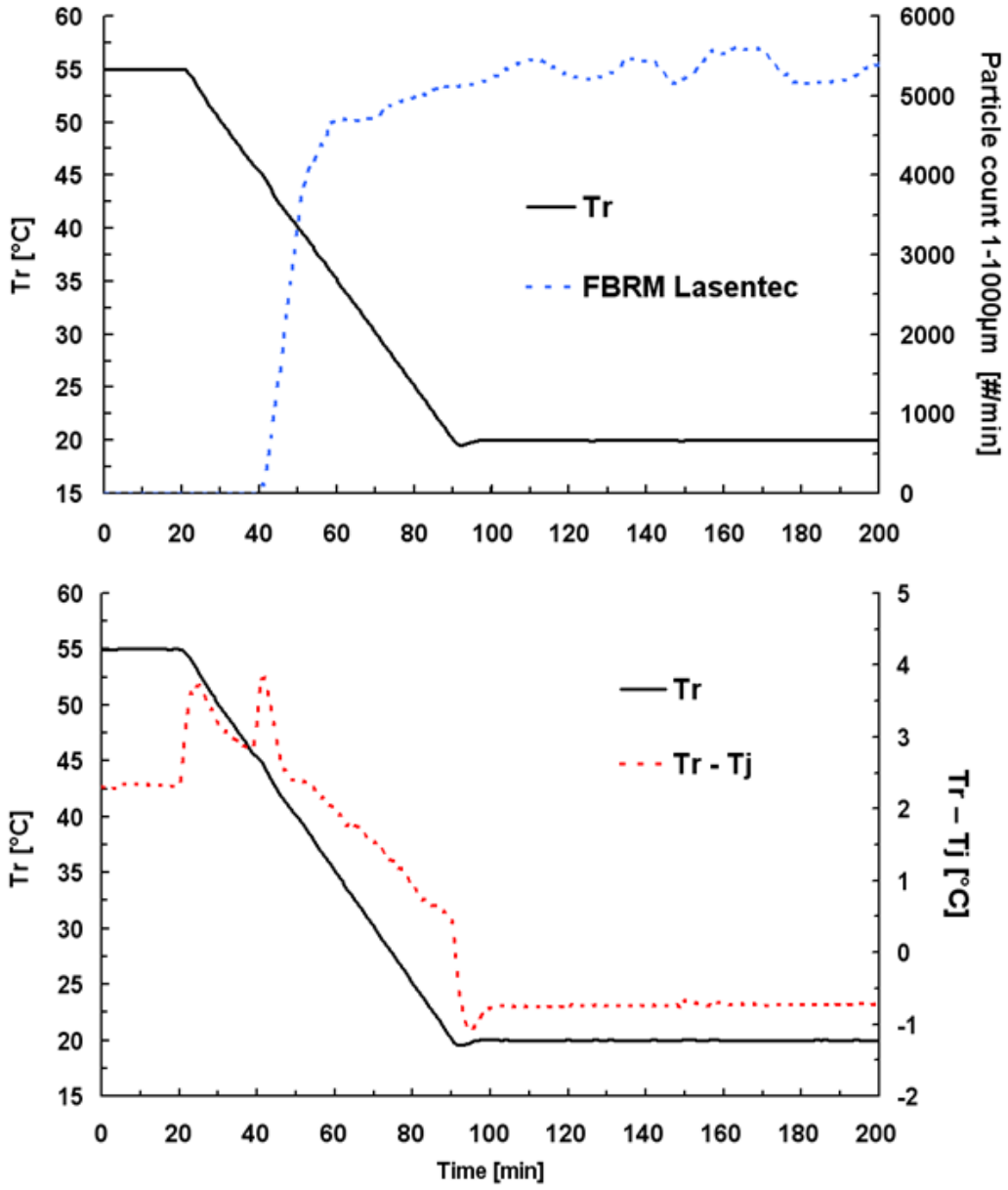

Figure 7.2 Measurement of metastable limit with Lasentec(R) FBRM (top) and Mettler Multimax (bottom) technology.

Three different values were chosen for both parameters with cooling rates set at 0.1, 0.3 and 0.5 K/min and initial concentration at 5, 9.2 and 18 g of solute/ 100 g of purified water. Figures 7.3 illustrate the results in terms of volumetric particle size distribution of the final product of crystallization.

Higher cooling rates lead to smaller particles and lower uniformity in sizes for every value of initial concentration; in fact, faster cooling induces high supersaturations

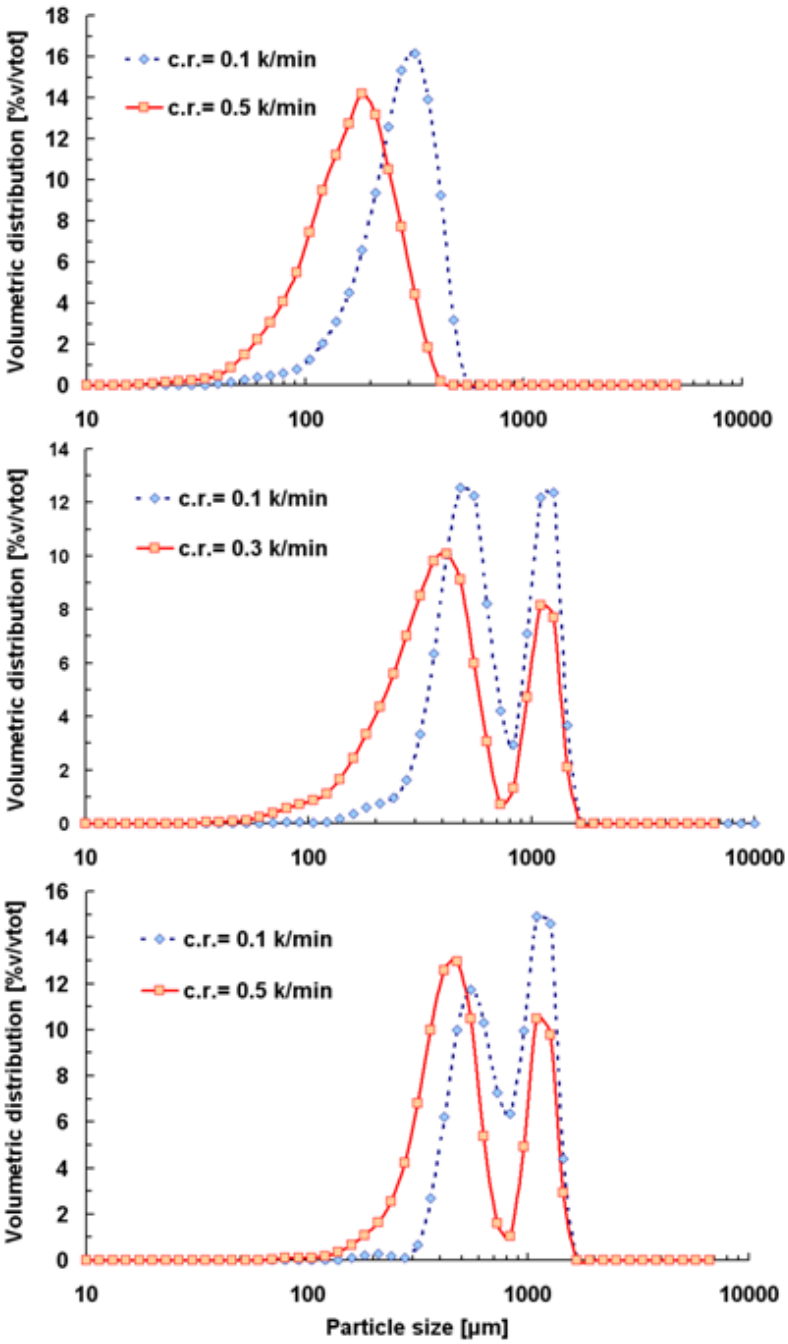

Figure 7.3 Effect of initial concentration and cooling rate on the final crystal size distribution. Concentration values: 5 g AA/100 g water (top), 9.2 g AA/100 g water (centre), 18 g AA/100 g water (bottom).

inducing high nucleation rates, hence a wide spread of the particle size distribution.

Larger particles are produced for 9.2 and 18 g solute/ 100 g water with a bimodal particle size distribution that could be ascribed to the agglomeration of smaller flat

shaped crystals with hexagonal geometry, shown by the SEM photomicrograph in Figure 7.4. The extreme cases of 5 g adipic acid/100 g of water cooled from 40 °C to 20 °C at 0.5 K/min and 18 g adipic acid/100 g of water cooled from 60 °C to 20 °C at 0.1 K/min are shown in Figure 7.5. Faster cooling combined with low initial concentration produced more elongated crystals with faceted edges whilst higher inlet concentration and slower cooling rates produced a more regular shape with rounded edges, with presence of fragments indicating the occurrence of breakage phenomena favoured by the massive presence of large particles.

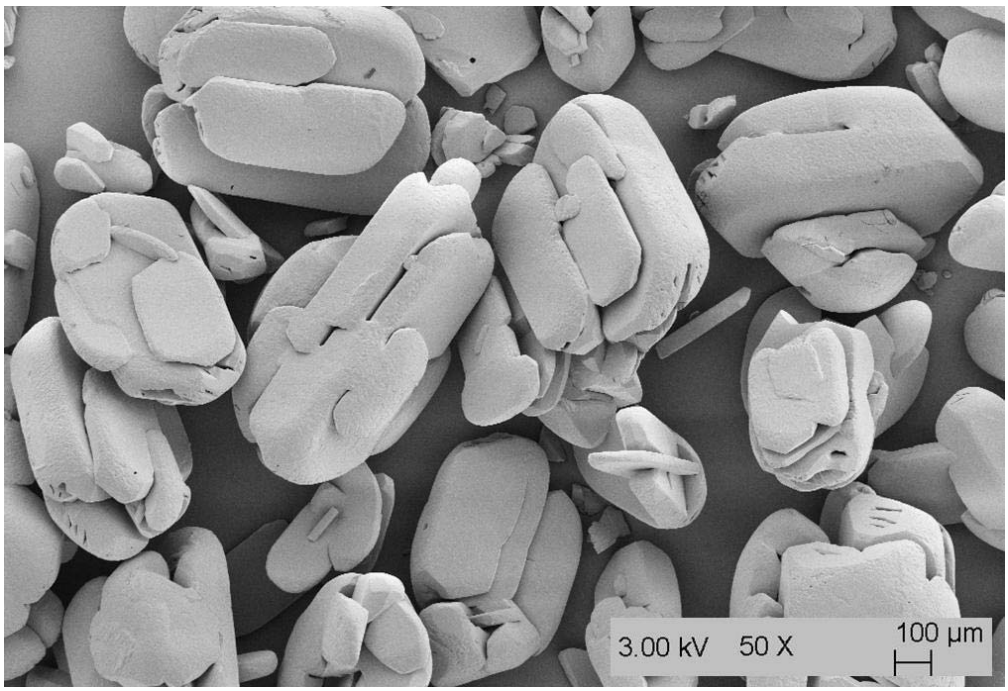

Figure 7.4 SEM photomicrograph of agglomerated adipic acid crystals from unseeded cooling crystallization.

7.3.4 Seeded batch crystallization: effect of seeding load and cooling rate

Figure 7.6 compares product particle size distributions at three different values of seeding load from ground row material. The plots refer to the cooling crystallization from 40 °C to 20 °C at 0.5 K/min, and seeding operated as the reactor temperature reached 39 °C; at this point the temperature was held constant for 60 minutes before resuming the cooling. Crystals produced with low values of seed concentration (1% and

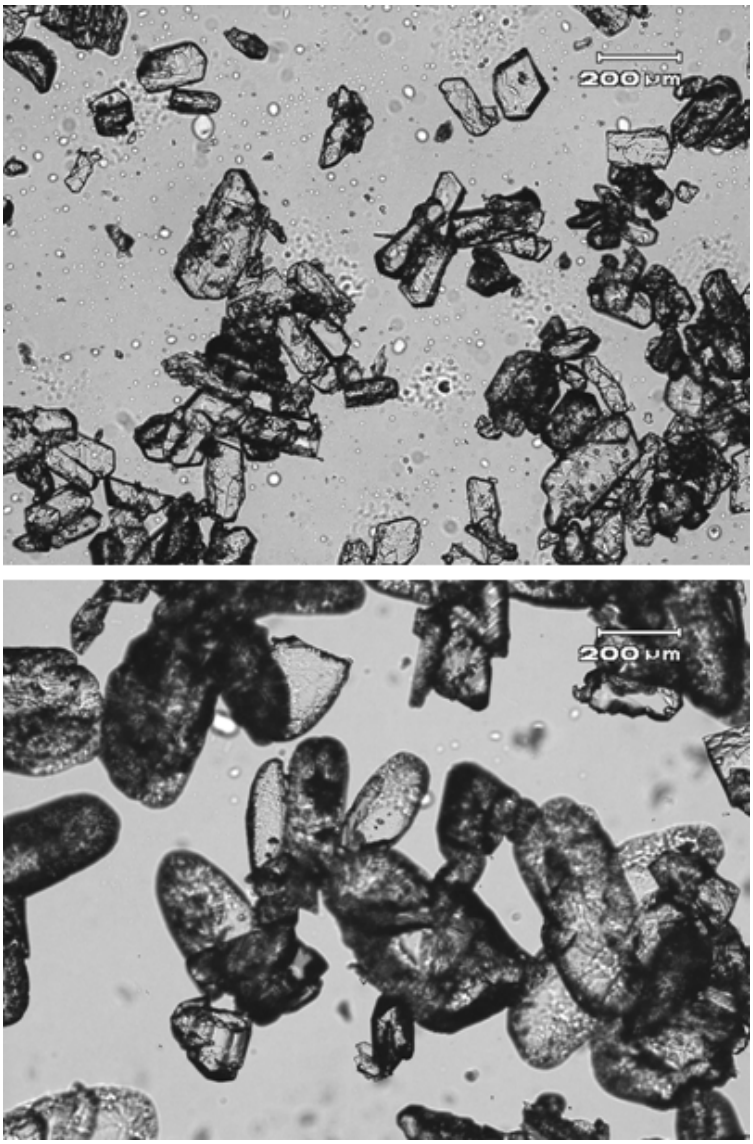

Figure 7.5 Optical micrograph of adipic acid crystals from unseeded cooling crystallization. Operating conditions: cooling 5 g AA/100 g water from 45 °C to 20 °C, at 0.5 K/min (top); cooling 18 g AA/100 g water from 65 °C to 20 °C, at 0.1 K/min (bottom).

5%) present widespread and bimodal PSD. The smaller part of the distribution is inferred to be crystals generated by secondary nucleation mechanisms, while the larger part may be classified as grown seed crystals and agglomerates. The results indicate that at the highest seed concentration considered for this study, corresponding to C_{seed} = 11%, the PSD was unimodal and narrower. The values of volumetric mean diameter and uniformity were smaller in the last case, with $L_{43} = L_{sp}$ = 238 μm and U = 34%. Largest

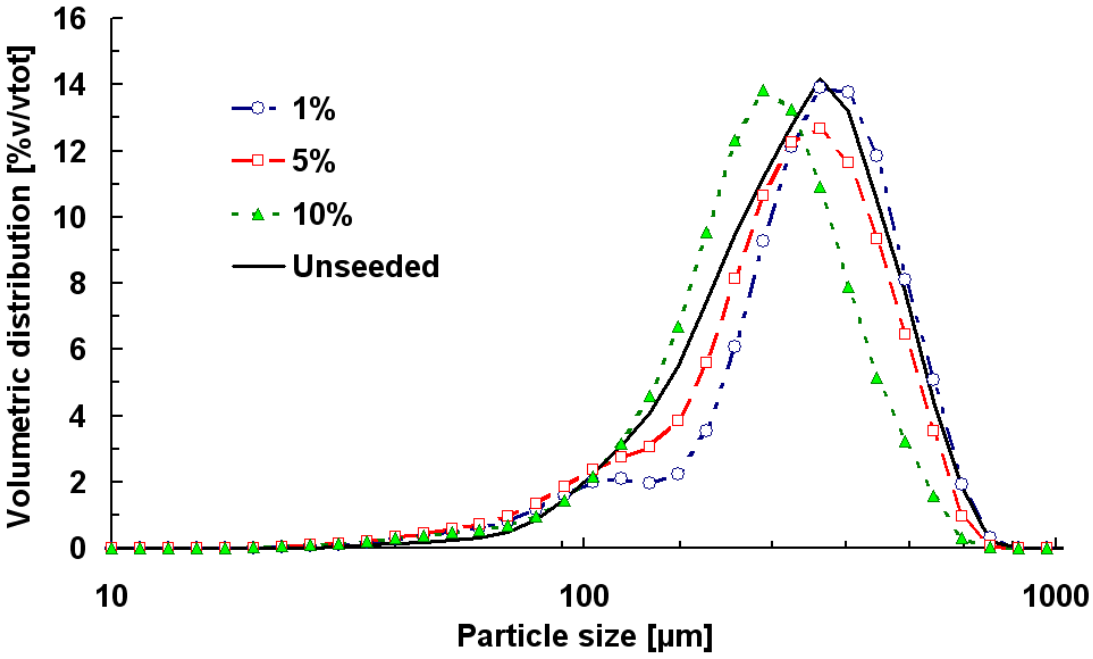

Figure 7.6 Effect of the amount of seeds on the final particle size distribution. Operating conditions: cooling 5 g AA/100 g water from 45 °C to 20 °C, at 0.5 K/min.

particles are produced in the case of 1% of seeds load (L_{43} = L_{sp} = 336 µm) while a wider uniformity (39%) is obtained in the case of unseeded crystallization. C_{seed} = 11% corresponds to L_{sp}/L_s = 2.16 that resulted similar to L_{wp}/L_s = 2.14, indicating a growth dominated process. When the amount of seeds was set at 5% of dissolved material, Malvern Mastersizer measurements indicate a high presence of fines (from the PSD plot) and provided L_{wp}/L_s = 2.44, slightly higher than L_{sp}/L_s = 2.38 (C_{seed} = 8.3%), suggesting some agglomerative phenomena of fine particles. The experiment with 1% of seed load produced a bimodal size distribution and gave L_{wp}/L_s = 2.64, lower than L_{sp}/L_s = 3.98 (C_{seed} = 1.6%) suggesting the occurrence of secondary nucleation phenomena.

Figure 7.7 shows the PSD after seeded crystallization of 18 g of adipic acid from 100 g of purified water. The amount of seeds corresponds to the 10% of the total mass of adipic acid dissolved before seeding, and seeded crystals have been produced under continuously insonated unseeded batch cooling crystallization from the same composition/ temperature. Seeding temperatures were reached by cooling at 0.5 or 0.7

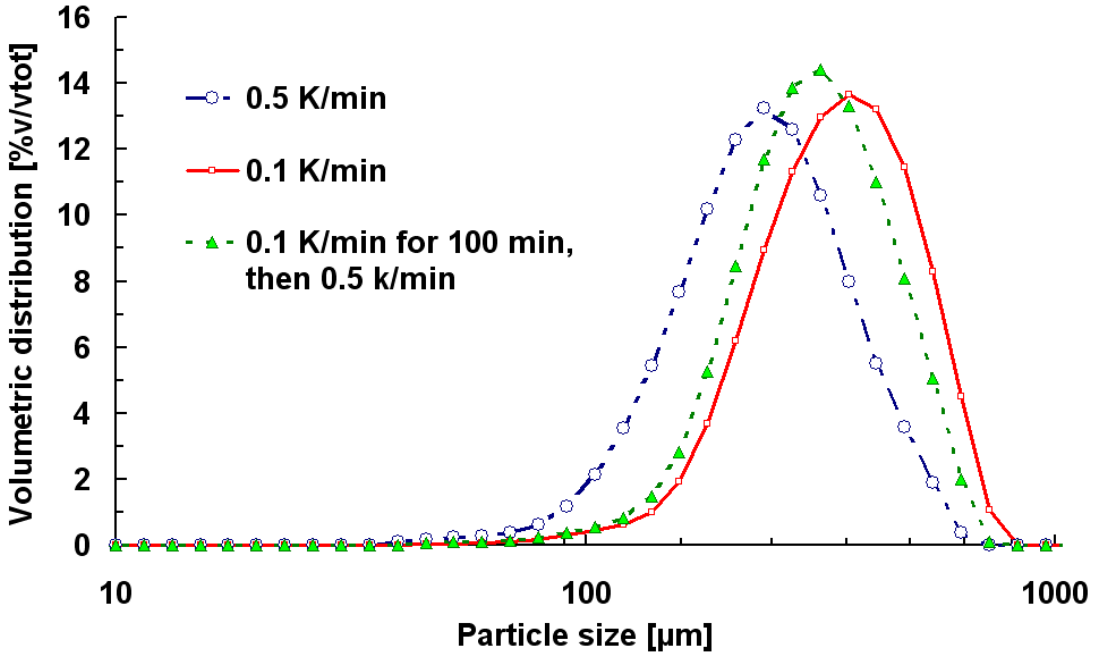

Figure 7.7 Effect of cooling rate on the final particle size distribution. Operating conditions: cooling 18 g AA/100 g water from 65 °C to 20 °C, 10% of seed loading.

K/min to ensure a wider metastable zone; the temperature was then held for 60 minutes before resuming the cooling down to 20 °C at linear rate. Two different cooling rates have been chosen after seeding: 0.1 K/min and 0.5 K/min. It can be seen that the higher cooling rate gives smaller particles with wider PSD (uniformity of 34.4%) while bigger particles are produced for linear cooling rate of 0.1 K/min, with narrowed PSD. In a third case the system was cooled first at 0.1 K/min for 100 minutes, then cooled at 0.5 K/min; the resulting PSD lies between the two previous cases, and results the narrowest produced (uniformity of 30.5%).

Figure 7.8 illustrates temperature and Lasentec(R) FBRM data over processing time for cooling crystallization of 5 g of adipic acid from 100 g of purified water from 40 °C to 20 °C at 0.1 K/min, with 10% of seeding load at a supersaturation ratio of 1.05. It can be seen a continuous decrease in the total count of particles, with a slight increase in the number of larger particles (200-1000 µm) during cooling. The normalized product mean volumetric size ($L_w/L_s \geq 2.5$, with $L_{wp}/L_s = 2.5$ without dissolution of seeds) is higher

than the expected value in case of pure growth of seeds crystal (L_{sp}/L_s = 1.93) indicating the occurrence of agglomeration of small units

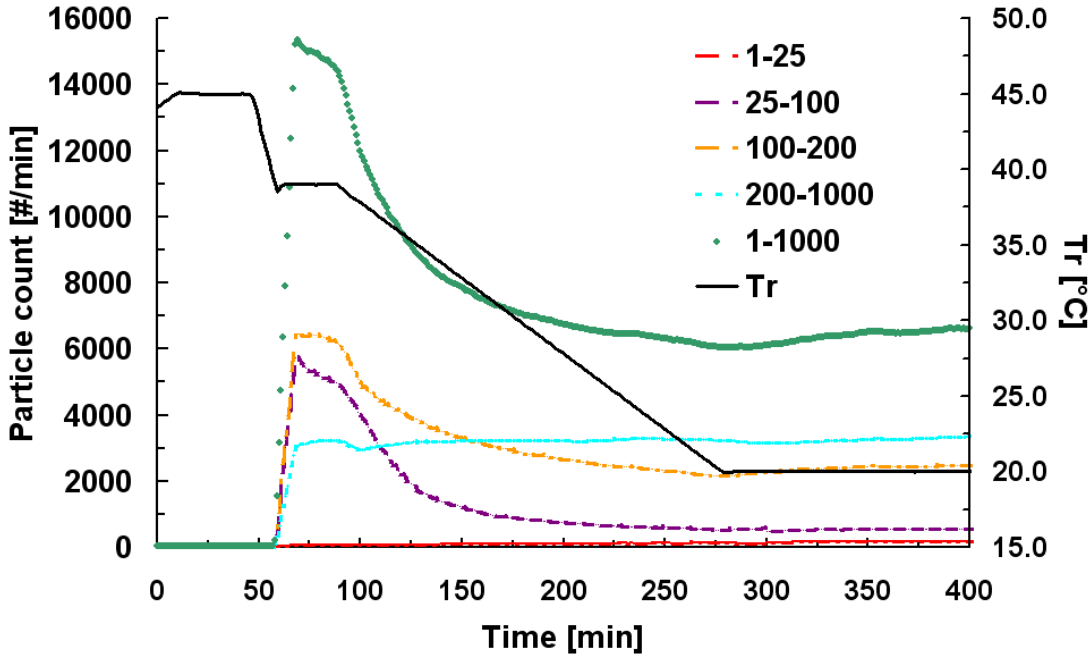

Figure 7.8 Particle count evolution over time in seeded batch cooling crystallization of 5 g solute/100 g water from 40 °C to 20 °C at 0.1 K/min, with 10% of seed loading.

7.3.5 Effect of initial concentration and origin of seeds

Figure 7.9 shows the PSD for the lowest and the highest values chosen for the initial concentration of adipic acid. The trends refer to the 10% of seeds load (from ground raw material), to avoid bimodality in the size distribution, and a cooling rate of 0.5 K/min. As in the unseeded cooling crystallization, higher initial compositions lead to larger particles with narrow PSD (uniformity reduced from 34.3 to 30.3%). However, the increase of inlet concentration favours secondary nuclei formation by attrition due to the narrower metastable zone, and the likelihood of breakage due to the larger sizes and the longer times involved.

The volumetric distributions of both kinds of seeds used for the present investigation are comparable, as shown in Figure 7.10, however the habits revealed by

the SEM photomicrograph in Figure 7.11 (a) and (c) appear significantly different. Seeds

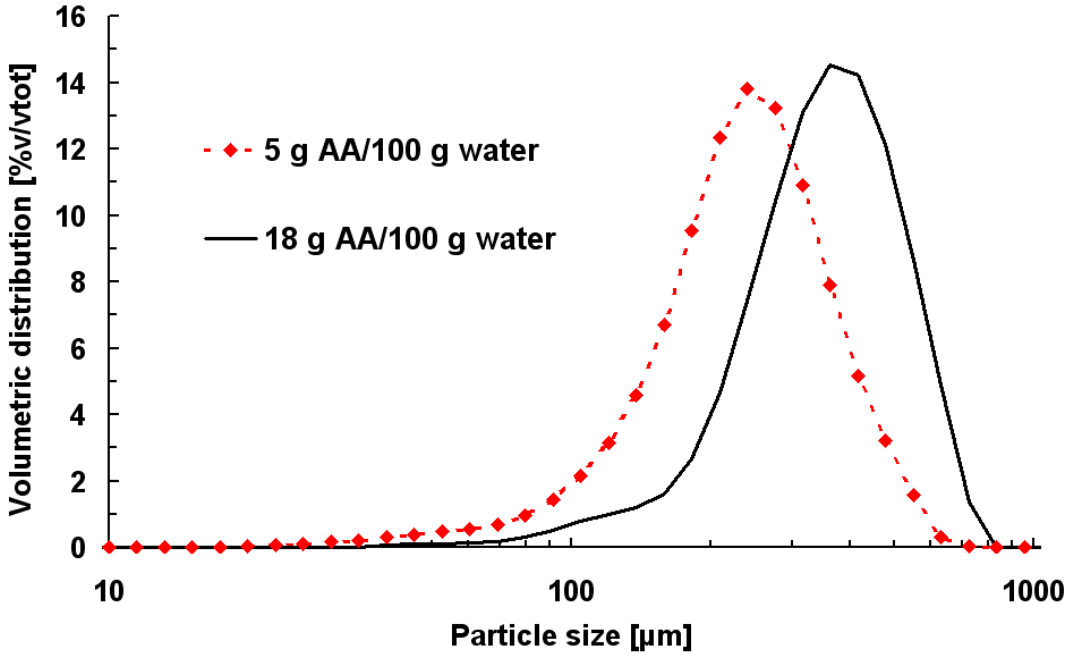

Figure 7.9 Effect of initial concentration/temperature on the final particle size distribution. Operating conditions: 10% of seed loading, cooling rate of 0.5 K/min.

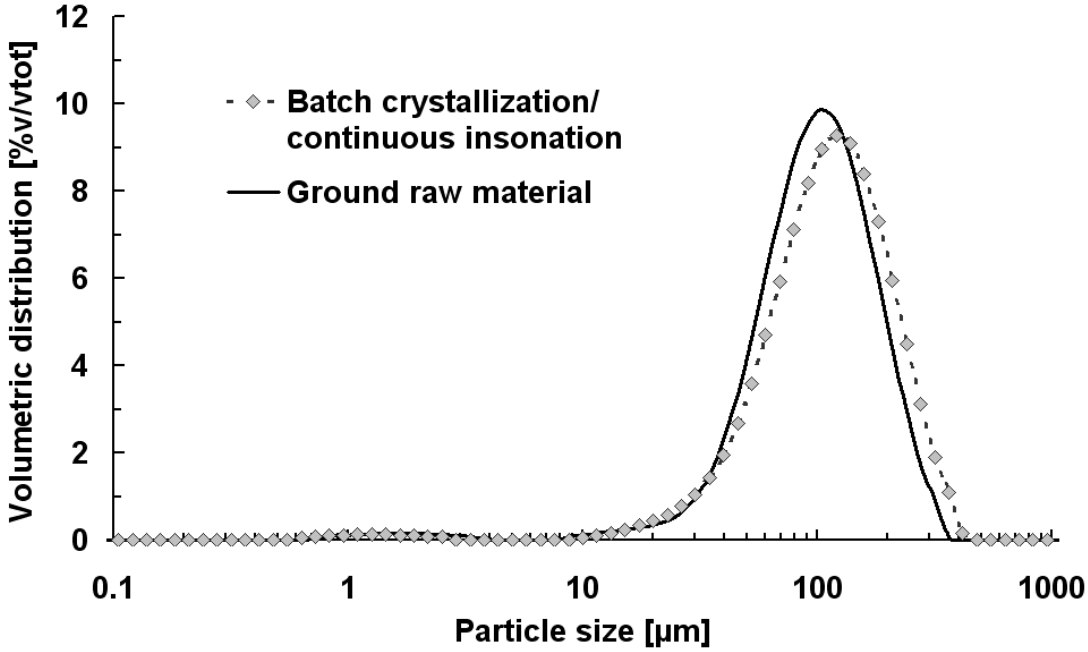

Figure 7.10 Particle size distributions of seed particles.

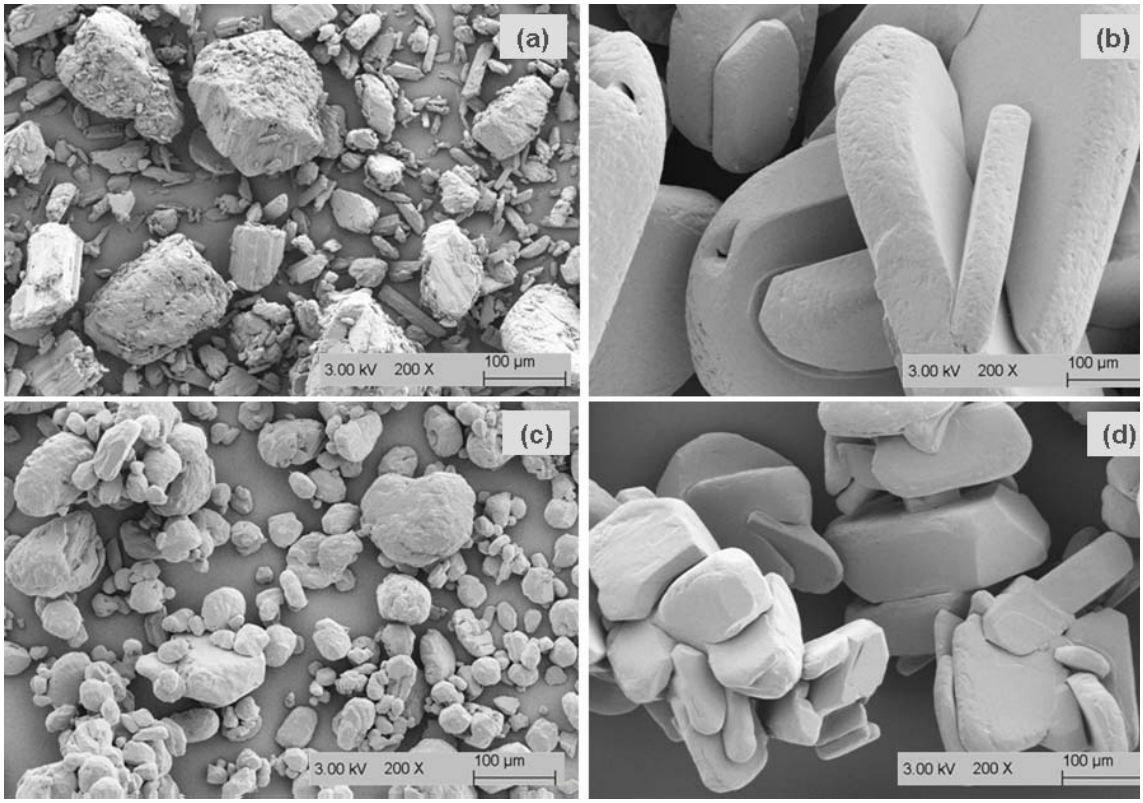

Figure 7.11 SEM photomicrograph of: (a) raw material after grinding, (b) final crystals after seeding with (a), (c) rounded shaped particles from batch sonocrystallization, (d) final crystals after seeding with (c). Operating conditions: cooling 18 g AA/100 g water from 65 °C to 20 °C, at 0.3 K/min.

produced by grinding the raw commercial material present elongated shape in smallest particles while crystals produced in batch cooling experiments under continuous insonation present a rounded shape due to the continuous pitting caused by cavitational effects.

Crystals produced from both kinds of selected seeds yields particles grown into one another: small particles tend to agglomerate, decreasing the effective surface area for crystal growth. However, in the first case elongated and flat particles were produced, while the product of the latter case present reduced elongation and increased thickness, with a more symmetric habit (Figure 7.11- right hand side). The surfaces of the latter crystals appear smooth, hence without the pitting effect as in the originating seeds.

7.3.6 Effect of supersaturation at seeding

In a cooling crystallization, as mentioned above, seeds have to be added under

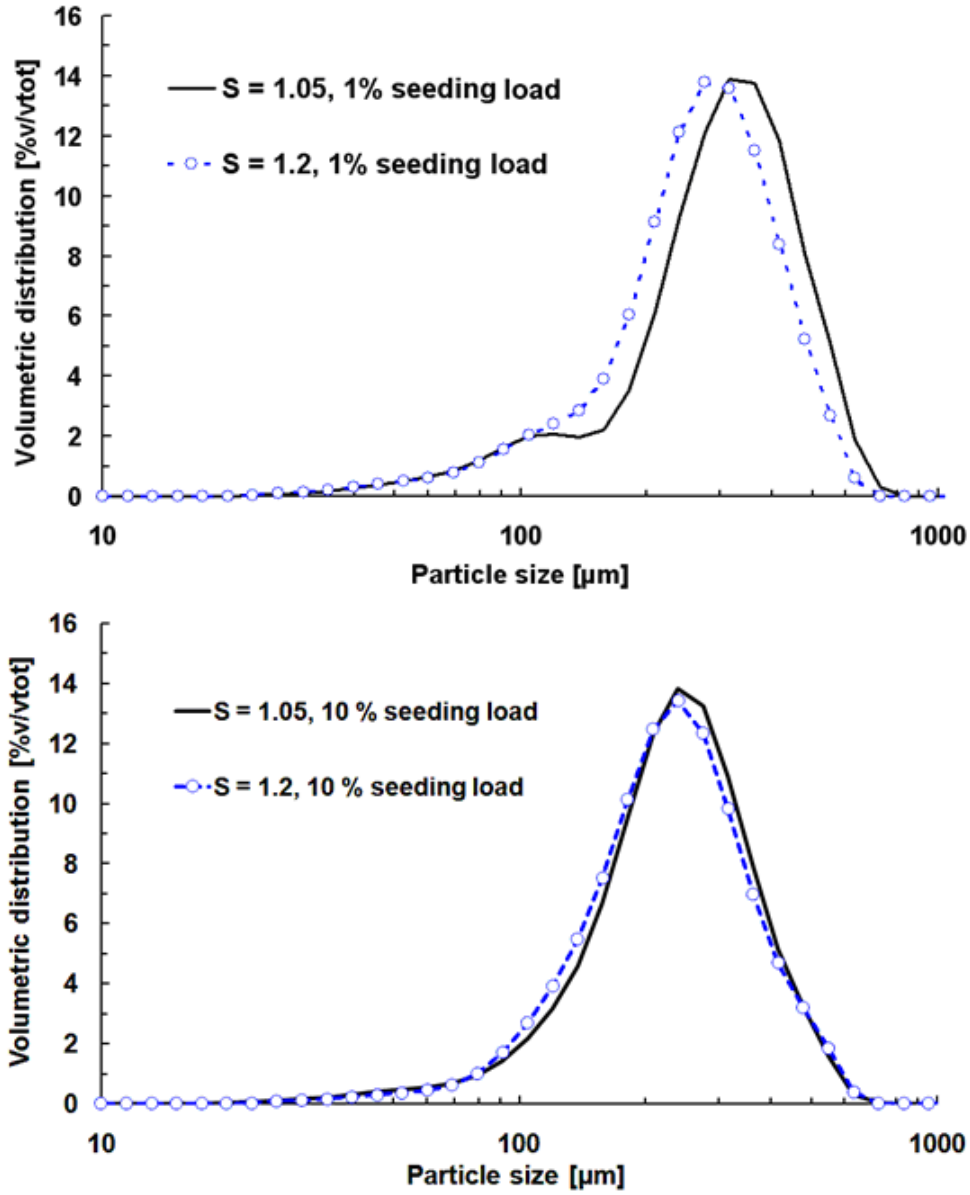

Figure 7.12 Effect of supersaturation at seeding on the final particle size distribution. Operating conditions: cooling 5g AA/100 g water from 45 °C to 20 °C, at 0.5 K/min.

supersaturated conditions and before the limit of the metastable zone is crossed. The metastability limit is not an exactly defined quantity but depends on a number of parameters and keeping well within the value estimated experimentally is advisable. For this reason, the seeding point should be fixed near to the solubility line and to a maximum of 1/4 to 1/2 into the metastable zone (Beckmann, 2000).

The effect of supersaturation at seeding was investigated at initial composition of 5 g

solute/100 g water, corresponding to a wider metastable zone, at cooling rate of 0.5 K/min, and supersaturation ratio at seeding chosen values at 1.05 (39 °C), and 1.2 (37.5 °C). The results are depicted in Figures 7.12. For a low seeding amount, where spontaneous nucleation appears more likely to occur, the difference between two different supersaturations at seeding is more evident, with a more pronounced nucleation for the highest supersaturation value at seeding and a higher peak for fine particles at reduced supersaturation. For the highest levels of seeding load, a less marked difference appears between the final product crystal size distributions after seeding at different levels of supersaturation, since the growth of seeds is the dominant process.

7.4 Conclusions

Seeded batch cooling crystallization of adipic acid from aqueous solution was investigated to determine the effects of method used to produce seeds, seeding load, cooling rate, initial concentration, and supersaturation at seeding on the final crystal product habit and size distribution. Seeds were inoculated as a slurry of adipic acid crystals in purified water to ensure they were efficiently dispersed and their surfaces activated.

An effective seed loading of 10% ensured unimodal distribution of product crystal particles, while the largest sizes were achieved by cooling at 0.1 K/min. Increasing the inlet concentration, hence the temperature, also favours the achievement of larger crystals, but a narrow metastable zone increases the probability of nucleation thereby requiring faster cooling to reach the temperature for seeds inoculation. An initial cooling rate of 0.1 K/min for 10 °C, followed by 0.5 K/min provides large product crystal particles and reduced nucleation with shorter operation times. Seeding with ground commercial material gives elongated and flat particles, while seeding crystals with regular rounded habit obtained from batch sonocrystallization provided reduced elongation and increased thickness in the final crystal product.

CHAPTER 8

SEEDING *IN SITU* THE COOLING CRYSTALLIZATION OF ADIPIC ACID USING ULTRASOUND

8.1 Introduction

The most documented benefits of ultrasound in crystallization relate to the primary nucleation stage; ultrasound has been demonstrated to reduce the induction time, to narrow the metastable zone width, and to increase the nucleation rate, as documented in chapters 2, 3, and 6. Furthermore, ultrasonic irradiation has proved to be particularly effective in inducing nucleation in otherwise non-nucleating systems (Ruecroft et al. 2005, McCausland et al., 2001). These effects on both nucleation processes and product characteristics invite comparison with other controlling techniques, *viz.* with seeding, frequently employed in crystallization to exert control over the product size and size distribution, as documented in Chapter7, and select the desired polymorph.

Intentional seeding is commonly applied in industrial crystallization processes to narrow the metastable zone width, shorten the induction time, and control the particle size distribution in the final product. However, in a batch process, seeds have to be added at a precise timing during the development of the supersaturation profile to achieve effective results (Beckmann, 2000).

The amount and effectiveness of seeding are directly correlated to the rate of cooling. In fact, the deposition of growth units on the surface of seeds, which is directly proportional to the amount of surface of seeds, causes a flux of mass out of the solution and decreases the supersaturation, while cooling rate values are correlated to the supersaturation profile created over time and can thus be related to the average level of supersaturation. The amount of inoculated seeds and cooling rate have to be balanced in order to: i) avoid that supersaturation reaches or crosses the limit of the metastable zone and no spontaneous nucleation occurs; ii) produce crystals with even and regular habit; iii) avoid economically unattractive longer time for cooling. Typical values for the amount of seed are given as Cs ≈ 10% (Beckmann 2000).

This chapter presents an investigation on the use of ultrasound to generate seeds directly within the bulk of a supersaturated solution, to yield a growth dominated crystallization. The target is to achieve the benefits of conventional seeding eliminating the problems connected to both inoculation procedures and treatment of seeds prior inoculation. Batch cooling crystallization of adipic acid from aqueous solution is the selected model system

The investigation focuses on the quantity of crystals acting as seeds generated *in situ* using ultrasound to achieve a comparable particle size distribution with that from

conventional seeding, which in turn depends on the effective combination between duration and intensity of ultrasonic burst, and cooling profile.

8.2 Experimental

8.2.1 Materials

Adipic acid (> 99.5% pure) was supplied by Sigma Aldrich. Deionized water was used as solvent.

8.2.2 Apparatus and operating procedure

Conventional seeded experiments and insonated experiments were both carried in a 300 mL jacketed vessel (ID = 80 mm) thermostated using a Haake thermostatic bath (accuracy of ± 0.5 °C). Stirring was provided by means of a cylindrical magnetic stir bar (length = 60 mm, breadth = 10 mm) and the stirrer speed was set at 200 rpm to ensure well mixed crystal suspension and avoid vortexing and bubble formation. The vessel temperature profile was controlled by means of Labview-National Instrument hardware.

An undersaturated aqueous undersaturated solution of adipic acid was cooled down to 20 °C by linear cooling, and aged for at least 1h to ensure stable conditions, in terms of particle size distribution, were achieved. The concentration of the initial solution was chosen between 5 and 18 g of solute/ 100 g of solvent, corresponding to a solubility temperature of 40 and 60 °C respectively. The initial temperature was set at 5 °C above the saturation temperature.

The volumetric particle size distribution (PSD) was measured using a long bench Malvern Mastersizer S. The instrument detects particle size values in the range between 4.8 and 3500 μm, where the size refers to the diameter of a sphere with the same volume of the detected particle. Each sample was analysed three times and measurements were made on wet material (crystals collected just after filtration). A saturated aqueous solution of adipic acid at room temperature was used as dispersant for size measurements; given the low solubility (no more than 1.9 g of adipic acid will dissolve in 100 g of water at 20 °C), dissolution can be neglected during measurements. Furthermore, the use of wet crystals offers the advantage of evenly dispersed particles in the measurement cell, an adequate obscuration value, and avoids floating of finest crystals on the top of the liquid in the instrument stirred cell (as observed when measurements were carried on dried crystals).

The shape of crystals was investigated using a Hirox KH-7700 Digital optical microscope, selecting magnification between 100× and 400×. The surface properties at nanometre scale were investigated using an atomic force microscope (AFM). Measurements were made using a Park Systems XE-120 AFM. Non contact silicon cantilevers with a nominal spring constant of 42 N/m, 125 μm nominal length, and nominal thickness of 4 μm were used for imaging in air with nominal resonant frequency value of 330 kHz. The radius of curvature of the pyramidal tip was lower than 10 nm. Images were processed by XEI software.

A 750 W ultrasonic processor with the frequency of 20 kHz (Cole-Parmer Instruments, Illinois, USA) was used to produce *in situ* crystals acting as seeds, at the beginning of unseeded batch experiments. The ultrasonic transducer is a tapered type with a tip diameter of 12 mm; the nominal power amplitude was set at 21% or 40%.

Conventional seeding was achieved by inoculating spherical shaped crystals from the crop of batch cooling crystallization experiments run under continuous insonation at a nominal power of 8.47 W/100 g slurry, as presented in chapter 6. Ultrasound is deemed to induce secondary nucleation by mechanically disrupting crystals or loosely bound agglomerates (Ruecroft et al., 2005). Furthermore, particles suspended in an insonated medium have an increased opportunity to collide with each other because of microstreaming induced by cavitation and high kinetic energies. These phenomena have been proven to evenly shape the habit of crystals; in fact, rounded shaped particles were also obtained when supplied material, with a poor and uneven crystal habit, was continuously insonated in a saturated aqueous solution.

Seeds were inoculated in a hot solution using a carrier-slurry at room temperature to ensure they were added close to the stirrer and easily dispersed, therefore avoiding the segregation on the top of the liquid surface likely experienced with dried seeds. The seed loading was set at 10% of the total mass of adipic acid dissolved before inoculation to achieve a growth dominated operation. It is suggested that fine particles tend to agglomerate and that agglomeration is less important or negligible above a certain critical size estimated around 50 μm (Mersmann, 2001); therefore, crystals were firstly sieved and selected from the range between 100 and 250 μm so that even a decrease of 50% in the lower size due to dissolution (caused by the increase of temperature after inoculation) does not cross the limit for agglomeration. Seeding temperatures were

reached by cooling at 0.5 K/min, and then the temperature was held for 45-60 minutes before resuming the cooling down to the final temperature (20 °C) at a linear rate.

The idea of using ultrasound to achieve comparable benefits with seeding was based on generating the amount of crystals acting as direct seeds within the system, by means of activated and controlled nucleation. In order to compare with conventional seeding procedures, the amount of solute dissolved at the beginning of the experiment with ultrasound was increased by 10% and cooling was operated from an accordingly higher temperature. As an example, a conventional seeding, where 54 g of solute/ 300 g of water (18 g of solute/100 g of water corresponding to a solubility temperature of 60 °C) was dissolved, cooled from 65 °C, with inoculation of 10% of seeds (5.4 g adipic acid crystals) at 59 °C, was compared with an initially insonated experiment with 60 (≈ 54 + 5.4) g of solute dissolved/ 300 g of water and cooling from 70 °C (without inoculation of seeds).

The percentage of crystals generated *in situ* under ultrasonic treatment is defined in this work as the ratio of the total quantity of crystals produced (at the temperature of seeding chosen for the corresponding seeded experiment) to the quantity of solute still dissolved in the mother liquor at the end of insonation; the value of both quantities has been estimated referring to the imaginary case that solubility conditions are reached at the considered temperature.

Generating seed crystals *in situ* using ultrasound was simply operated by cooling down, at a linear rate, an initially hot undersaturated solution, with ultrasonic irradiation turned on a sufficient time before the beginning of cooling to allow the adjustment in temperature control and ensure the heat release due to insonation did not alter the defined cooling profile. The ultrasonic burst was stopped a few minutes after the onset of nucleation was visibly detected. Two different cases were distinguished: in the first, cooling was interrupted as in conventional seeding runs, at the same temperature value selected for the corresponding conventional seeded case; in the latter there was no interruption of cooling until the final temperature was reached.

8.3 Results and Discussion

Figure 8.1 shows a comparison between the particle size distribution (PSD) of inoculated seeds and the final crystals. In the seeding experiment, 18 g of solute/100 g of water was cooled at 0.5 K/min from 65 °C. Seeds were inoculated at 59 °C (corresponding to an estimated supersaturation ratio of 1.05), and cooling was

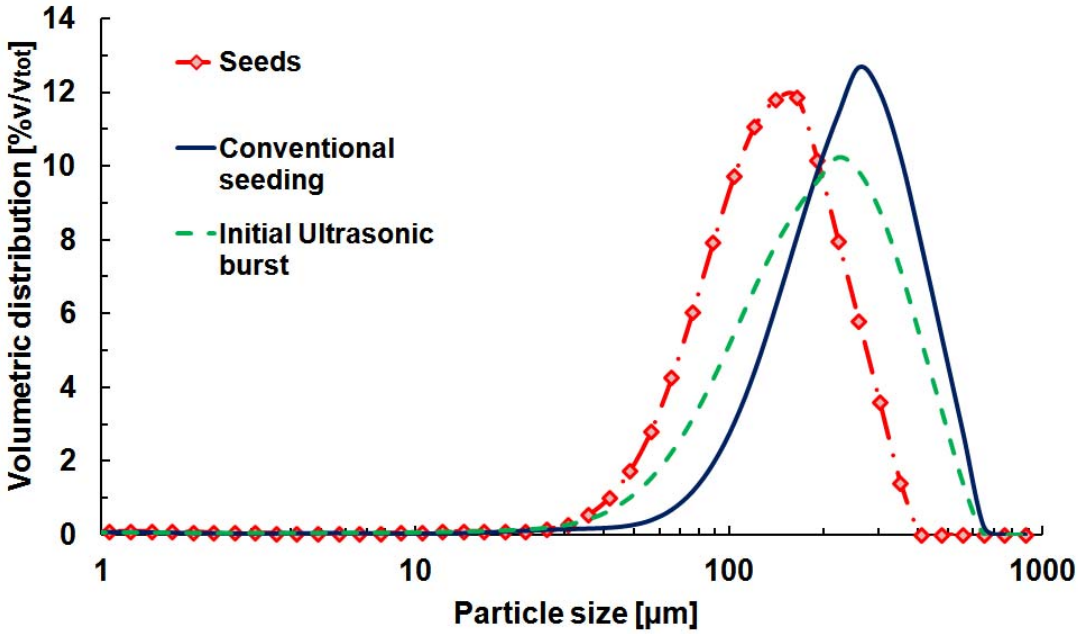

Figure 8.1 Comparison of the product particle size distribution of conventional seeding with the size distribution of inoculated seeds, and with the final particle size distribution after short ultrasonic burst applied at the beginning of cooling to seed the system in situ with 10% of seeding load.

interrupted for 45 min before being resumed at 0.3 K/min until 20 °C. PSD results show that 10% of seed loading provides a growth dominated process; the final PSD appears shifted toward bigger size values than the size distribution of inoculated seeds. Results were compared with the product of unseeded experiments, whereas 20 g of solute/100 g of water was cooled down at 0.3 K/min from 67 °C and a short ultrasonic burst was applied since the beginning of cooling. Insonation was stopped when the system reached 59 °C, and already formed crystals were tested as potential "seeds" for the following uninsonated stage of crystallization. At this temperature, the mass of solute turned into crystals is estimated to be 10% of the mass of adipic acid that remained in solution. The nominal value of ultrasonic intensity was set at 83 W/100 g of slurry (40% power amplitude), and the profile of temperature over time was set equal as in the conventionally seeded case (interruption of cooling at 59°C followed by cooling at 0.3 K/min until a temperature of 20 °C).

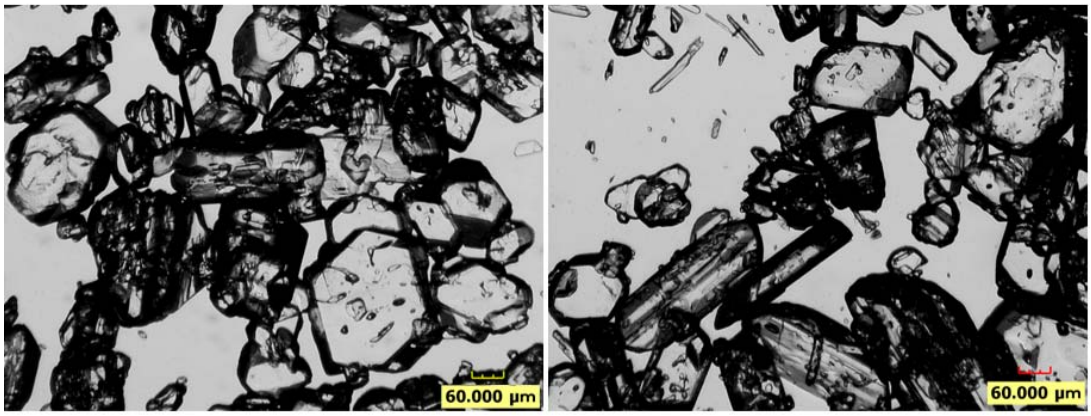

Figure 8.2 Final product of conventional seeding (left) and of seeding *in situ* using ultrasound with an equivalent l0 wt% of seeding load (right).

The final product from conventional seeding showed larger sizes and a narrower size distribution than the final product from a short insonation burst. The photomicrographs in Figure 8.2 reveal much more regular and evenly distributed shapes after conventional seeding than after the corresponding unseeded experiment with ultrasonic burst.

Unseeded experiments with a brief initial insonation were also operated with 21.7 g of solute/100 g of water cooled down from 70 °C at 0.3 K/min. In these cases, the total amount of crystals produced (under ultrasonic irradiation) when 59 °C was reached was 20 wt% of the still dissolved quantity. Two different cooling profiles have been applied. In one case, cooling was interrupted at 59 °C for 45 min; in the other one, no interruption was operated before reaching the final temperature of 20 °C. In both cases, final crystals presented more regular shapes than in the case of 10% crystals mass generated under insonation. The habit of crystals appeared more regular and symmetrical, with less elongated hexagonal particles than after conventional seeding, especially when cooling was not interrupted after the ultrasonic irradiation was stopped. Finally, the product PSD was comparable with the PSD obtained from conventional seeding (Figure 8.3).

Analogous results were observed at reduced concentration of 5 g of solute/100 g of water. The unseeded test, where a 10 wt% of dissolved solute turned into crystals under ultrasonic irradiation (at the beginning of crystallization), produced a widespread size distribution and crystals with poorer habit than the output of conventional seeding (10% of seeding load). On the contrary, when 40 wt% of dissolved solute turned into first crystals under ultrasonic control, both particle size and size distributions were improved

in the final product, and final results were comparable with the product of seeding (less than 1% difference in size uniformity).

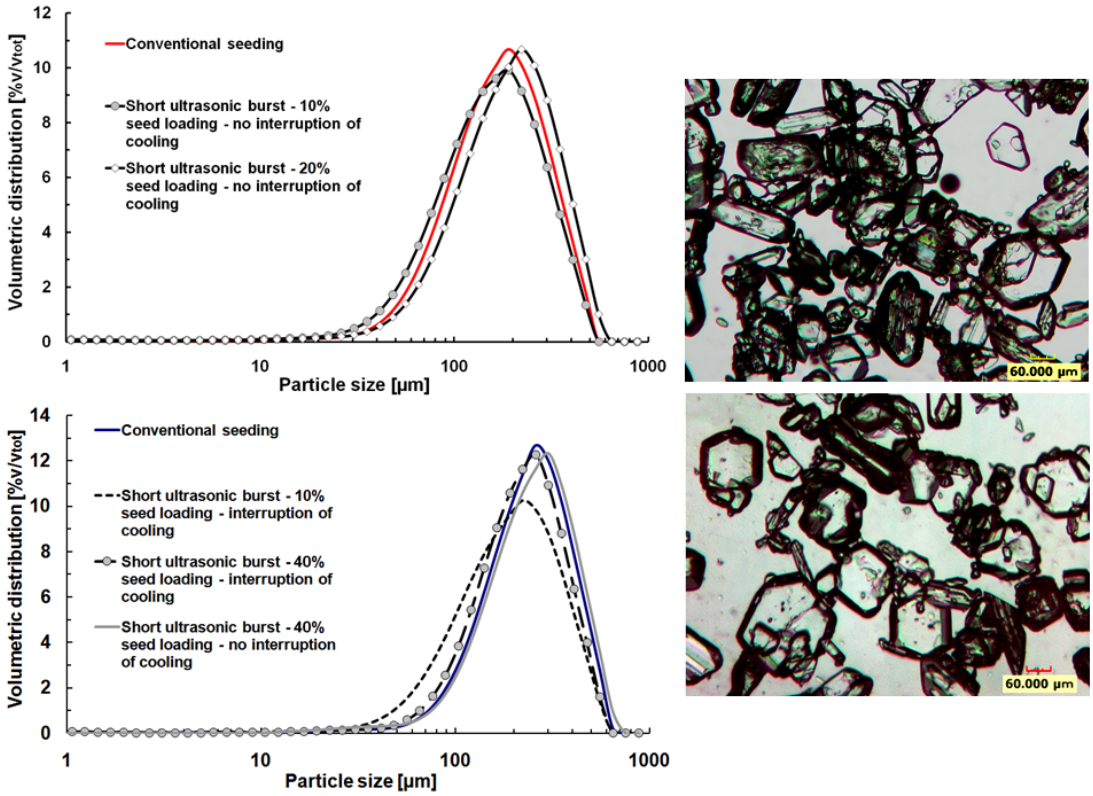

Figure 8.3 Comparison between the final PSD of conventional seeding and seeding in situ with ultrasound at 10% and 20% of seeding load at 18 g of solute/100g of water (top) and 5 g of solute/100 g of water (bottom).Optical photomicrographs refer to 18 g of solute/100g of water: product crystals of conventional seeding (top) and seeding with 20% of seeding load generated *in situ* with ultrasound (bottom).

The benefit of an uninterrupted cooling after the use of short burst insonation was finally confirmed when the experiments were repeated at a lower power amplitude. 9 g of solute/100 g of water was cooled down at 0.3 K/min from 55 to 20 °C; ultrasound at a nominal power of 48.16 W/100 g slurry (21% power amplitude) was started just before the beginning of cooling and stopped 6 min (2 °C) after the nucleation onset was detected. Cooling was interrupted for 30 min, after ultrasound was stopped, only in one case. PSD plots in Figure 8.4a and optical photomicrographs in Figure 8.4b show increased particle sizes and more regularly shaped crystals when the short ultrasonic burst was combined with an uninterrupted cooling, whereas a massive presence of small particles was produced when cooling was interrupted. The results suggest that initial crystals generated under ultrasonic treatment possess highly activated surfaces that favours growth processes, acting as seeds generated *in situ*. Keeping the temperature

constant after stopping ultrasound "deactivates" the surface, thereby reducing the effectiveness in controlling the following stages. Future works need to be addressed to

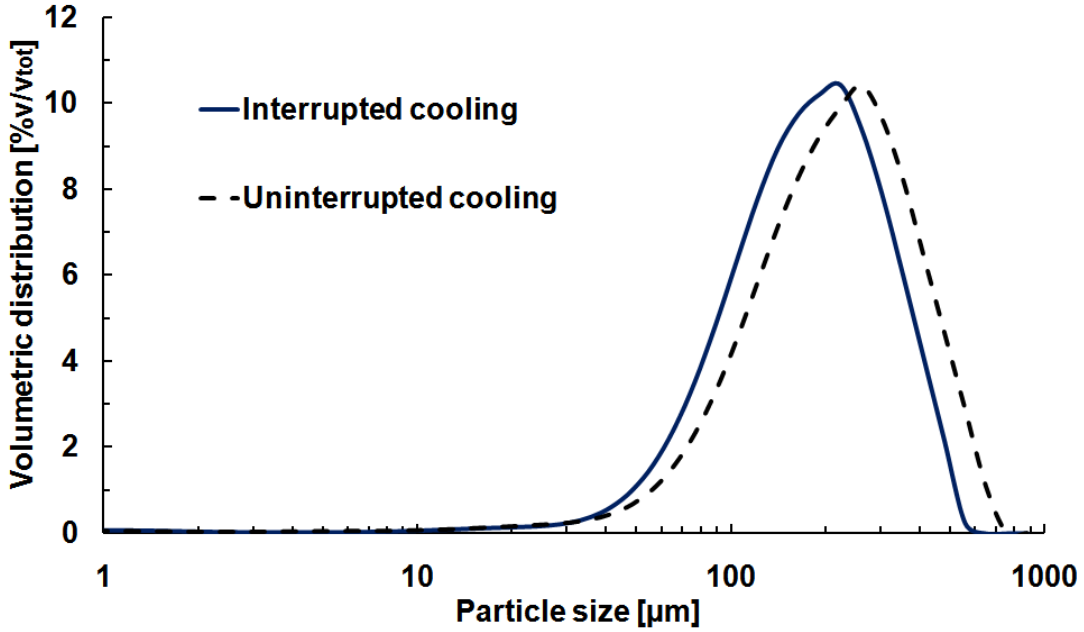

Figure 8.4a Effect of interruption of cooling after stopping the ultrasonic burst on the final particle size distribution. Operating conditions: cooling at 0.3 K/min of 9 g of solute/100 g of water at from 55 °C to 20 °C. Ultrasonic burst at nominal power of 48.16 W/100 g of slurry was stopped 6 min (2 °C) after the nucleation onset was visibly detected.

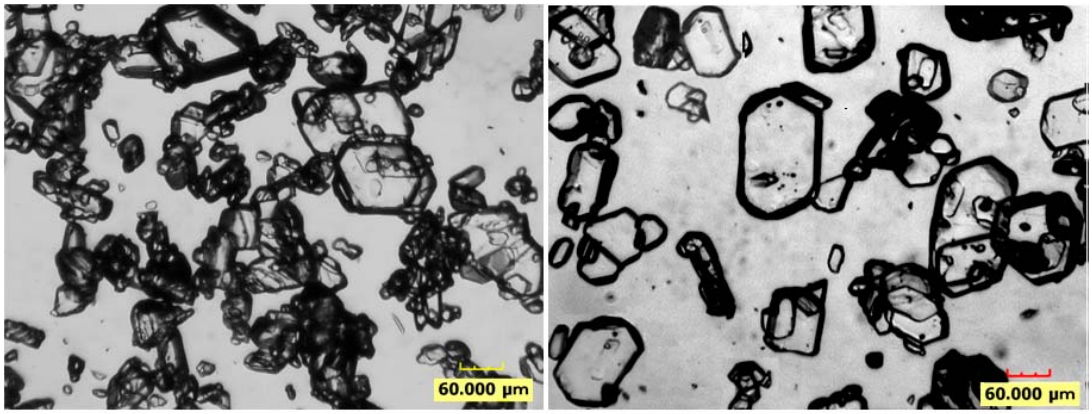

Figure 8.4b Effect of interruption of cooling after stopping the ultrasonic burst on the habit of final crystals (product of uninterrupted cooling in the right figure). Operating conditions as in panel (a).

investigate the effect of surface activation (due to insonation) on agglomeration, particularly after the source of energy is stopped. The interruption of ultrasonic irradiation seems to favour the growth of crystals rather than their agglomeration because of the well mixed conditions. The low density of crystals, at the time insonation

was stopped, reduced the probability of contact among crystals, which could further explain why agglomeration was not favoured.

8.3.1 Effect of cooling rate, intensity and duration of the ultrasonic burst

21.7 g of AA/100g of water was cooled down from 65 to 20 °C at three different cooling ramps (0.1, 0.3, 0.5 K/min), without the interruption of cooling. Ultrasound, set at 82.20 W/100 g of slurry (40% of power amplitude), was stopped after a subcooling of 2°C after the onset nucleation was visibly detected. As shown in Figure 8.5, large particles with regular habit were produced in the case of cooling at 0.3 K/min, while the slowest cooling provided more elongated crystals and particles with irregular shapes. The activation of the surface of crystals nucleated under ultrasonic action, as suggested before, is considered to favour an isotropic growth process; however, it requires a sufficient de-supersaturation rate, hence sufficiently high cooling rates, to achieve effective results. On the opposite, the fastest cooling provided regular particle shapes but smaller sizes than in the case of 0.3 K/min; highest cooling rates imply higher supersaturation values and secondary nucleation phenomena providing smaller sizes, while the application of ultrasound ensured regular shapes avoiding agglomeration.

A specific experiment was carried out to investigate the effect of interruption of ultrasonic irradiation on the Ostwald ripening. As mentioned in Chapter 3, localized hotspots related to cavitational phenomena are supposed not to induce ripening of crystals during uninterrupted insonation because of their transient and local nature; in fact, the duration of cavitational events has been estimated on the order of microseconds (Suslick et al., 1990) and to occur within the liquid phase. Furthermore, the reason for the Ostwald ripening lies in the tendency of the solid phase to adjust itself to minimize the total surface energy (Mullin, 2001) while ultrasonic irradiation provides energy (Mason and Lorimer, 2002) and favors a system of separate particles as previously documented. Continuous insonation can, in fact, be used to reduce the particle size under macroscopically saturated conditions, as proved in chapter 6. In this case, the investigation has been addressed to the evolution of particle size and habit after the interruption of insonation. 20 g of crystals/100 g of water was kept at 20 °C under continuous insonation at 43.75 W/100 g of slurry (nominal value corresponding to 21% of power amplitude). Ultrasonic irradiation was stopped after stable PSD conditions were achieved. Malvern analysis data shown in Figure 8.6 reveal that, even though stable PSD conditions were achieved before insonation was stopped, particle sizes

started increasing after stopping the ultrasonic irradiation to reach new stable conditions. The mean particle diameter increased by around 40% after 30 min (with a negligible further increase recorded in the following 12 h).

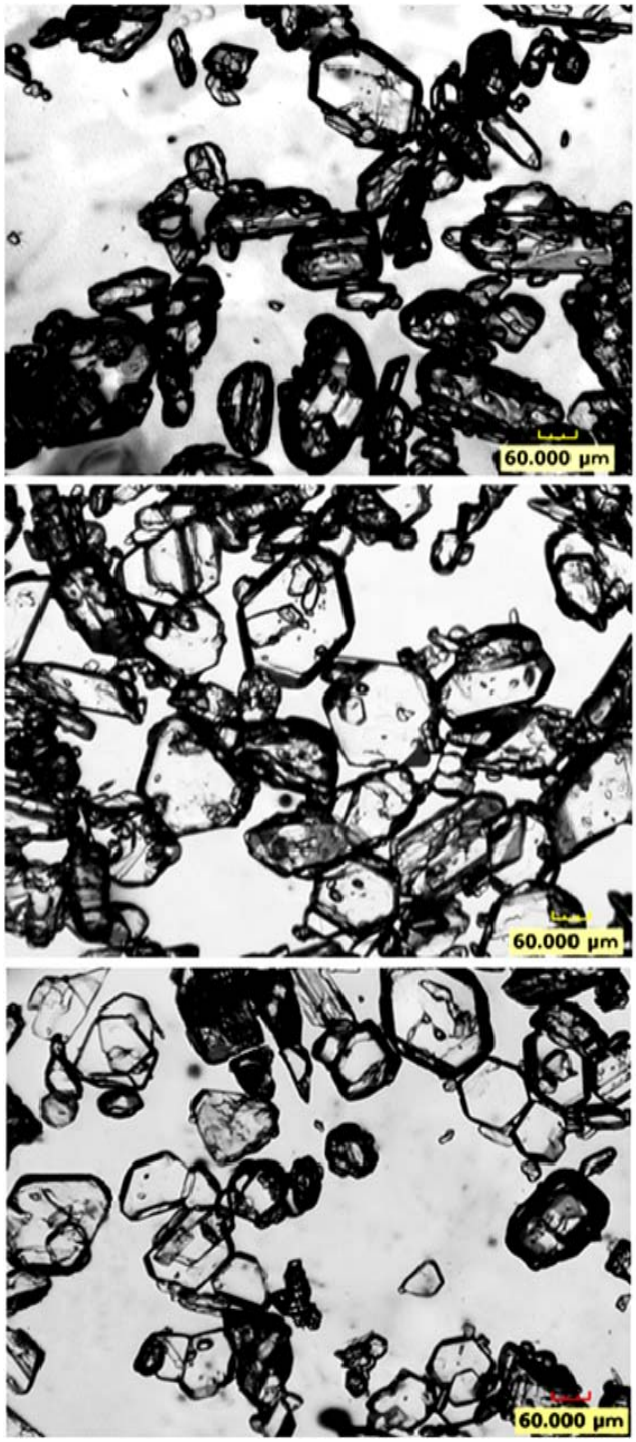

Figure 8.5 Effect of cooling rate on the habit of final crystals in seeding with an initial ultrasonic burst (top: 0.1 K/min; centre: 0.3 K/min; bottom: 0.5 K/min).

The effect of both power ultrasound and duration of the ultrasonic burst is shown in Figure 8.7; 21.7 g of solute/100 g of water was cooled down from 65 to 20 °C at 0.3

K/min, without interruption of cooling. The system was irradiated from the beginning of cooling until a subcooling of 2 °C (6 min) after nucleation was firstly detected. Experiments were carried out at 82.20 and 43.15 W/100 of g slurry. Decreasing the power ultrasound leads to a widespread particle size distribution (uniformity of 39.7 % at 82.20 W/100 g of slurry and 41.3% at 43.15 W/100 g of slurry from Malvern Mastersizer S measurements), while increasing the duration of ultrasonic irradiation shifts the size distribution toward smaller sizes. Microscope images indicate more uniform particle shapes and sizes when the level of power was increased (top image in Figure 8.7). Consequently, a longer period of irradiation is required to exert a more effective control at the reduced ultrasonic intensity values.

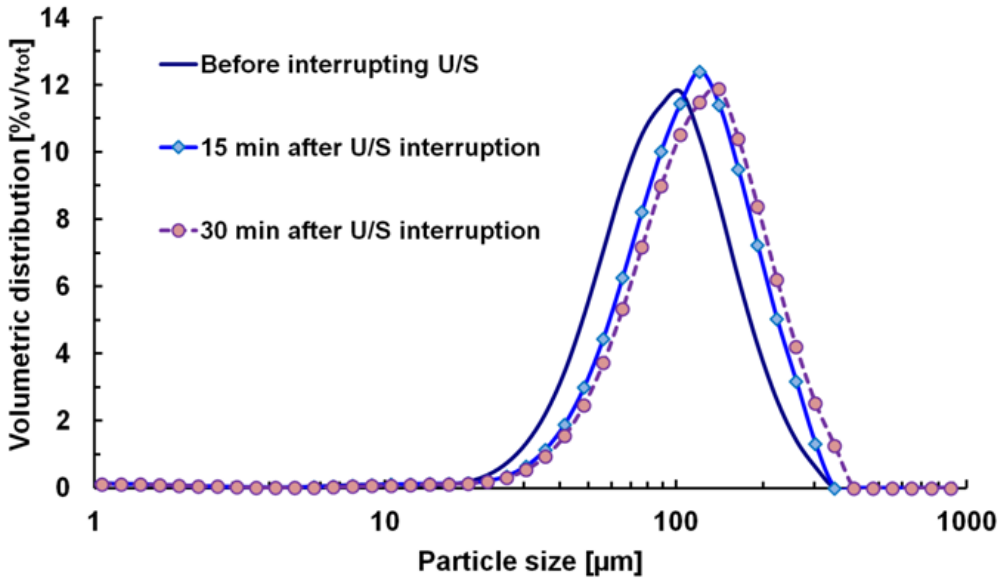

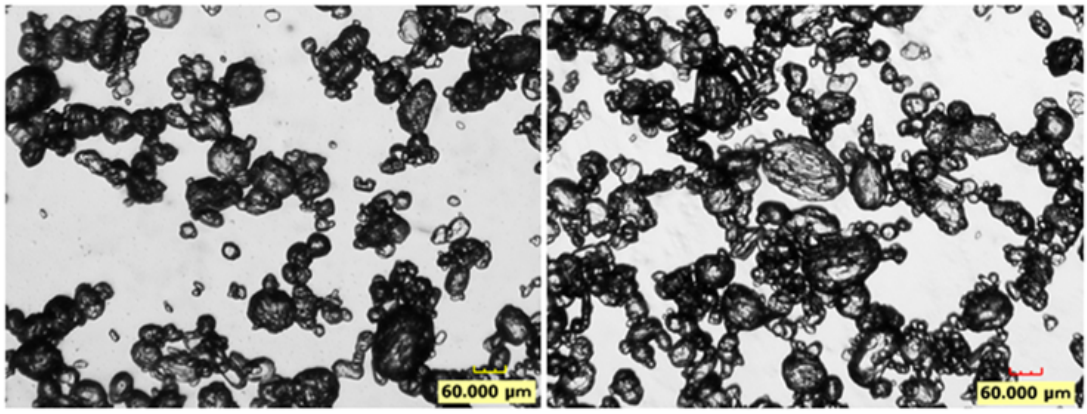

Figure 8.6 Effect of ripening, after interruption of insonation, on the particle size distribution and habit of final crystals (left picture: before interruption of insonation; right picture: 30 min after the interruption of insonation).

8.4 Comparison with intermittent insonation

The effect of a short ultrasonic burst was compared with an intermittent insonation applied throughout the duration of the experiment. 18 g of solute/ 100 g of solvent was

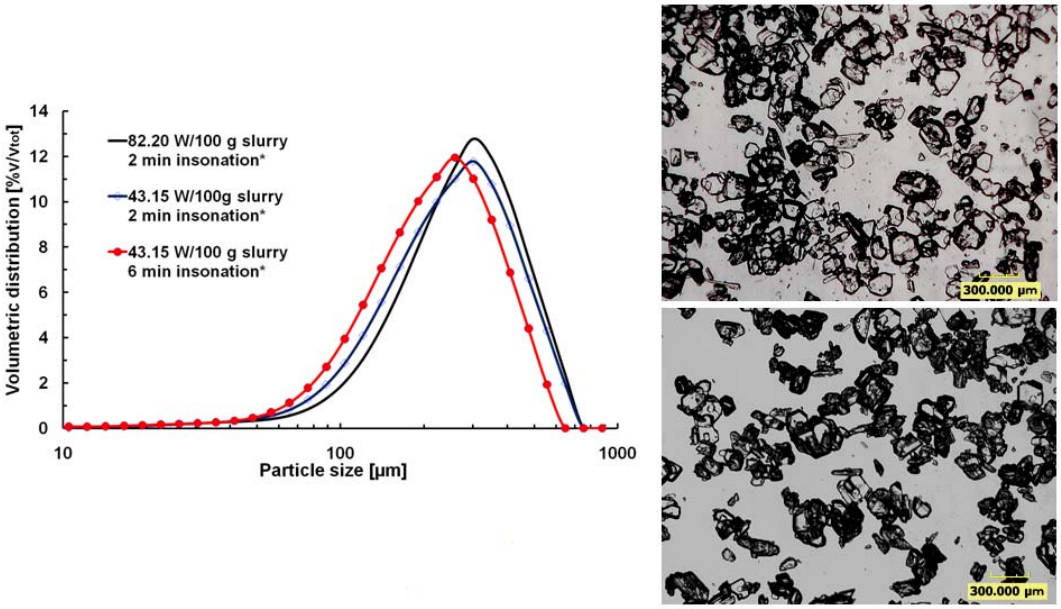

Figure 8.7 Effect of power ultrasound and duration of ultrasonic burst. Top picture: 43.15 W/100g of slurry - 6 minutes insonation*. Bottom picture: 43.15 W/100g of slurry - 2 minutes insonation*.
*after the onset of nucleation (at cooling rate of 0.3 K/min).

cooled down at 0.3 K/min under intermittent insonation at 84.75 W/100 g of slurry; the ratio between insonated and not-insonated period was varied between 5 s on/59 s off and 10 s on/59 s off, corresponding to a total insonation duration of 8 and 15 minutes respectively. PSD plots were compared with the case of an initial burst stopped 15 min after the onset of crystallization, as shown in Figure 8.8. The same duration of ultrasonic burst leads to smaller particles if the sonication was distributed throughout the cooling as short regular periods of 10 s alternated with 59 s of non-insonation, with a size reduction over 47% (based of mean particle size L_{43}). The final product of intermittent insonation presents elongated particles with rounded edges in the case of 5 s on/59 s off (top Figure 8.8) and spherical particles when the insonation period was doubled (bottom Figure 8.8).

8.5 AFM results

The crystal surface morphology was analysed to compare the growth mechanism after seeding and after a short burst insonation. The analysis is based on amplitude images over a square window of 20 nm × 20 nm and the results are shown in Figure 8.9. In both cases AFM images present a typical birth and spread crystal growth mechanism;

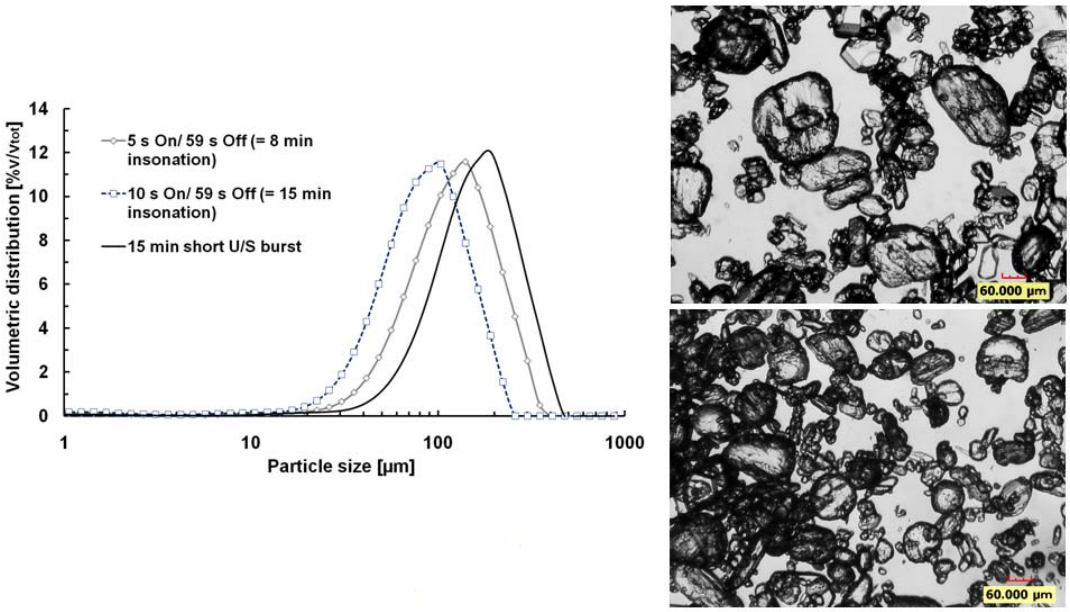

Figure 8.8 Effect of intermittent insonation on the particle size distribution and habit of final crystals. Right panels: top picture: 5 s on/59 s off; bottom picture: 10 s on/59 s off.

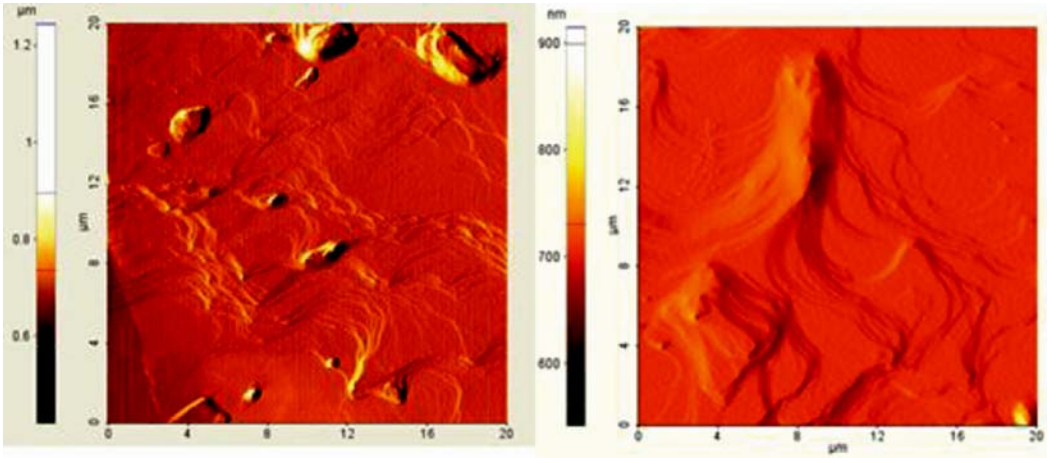

Figure 8.9 AFM surface images of crystals produced after conventional seeding (left) and using short ultrasonic burst to seed *in situ* (right).

however the surface presents narrower terraces after conventional seeding (left AFM images) than in the case of the initial ultrasonic burst. A multilayer structure with larger terrace widths is observed when nucleation was controlled using ultrasound (right AFM

images). Mersmann (2001) indicates that “at increased level of supersaturation the spreading of the nuclei loses ground compared to new nuclei continuously roughening the crystal growing surface in a polynuclear mechanism”. Therefore, the dominance of the polynuclear growth mechanism in the conventional seeded case can suggest a growth process that proceeds at higher supersaturation levels than in the case of ultrasonic action. AFM images reveal also the presence of surface discontinuities, considered traces left by the evaporation of trapped solvent after drying. These discontinuities dominate on the surfaces of crystals produced after conventional seeding.

8.6 Conclusions

A short ultrasonic burst was applied at the beginning of a batch cooling crystallization of adipic acid from aqueous solution to produce large crystals with regular particle size distributions. The effectiveness of the initial ultrasonic burst was investigated by comparison with seeded experiments with 10% of seed loading, in terms of particle size distribution, habit of crystals, and crystal surface morphology in the final product.

A few minutes insonation at the beginning of crystallization can provide comparable results with seeding in terms of regular shape and size distribution, eliminating the need of : i) preparation of seeds; ii) control quality of seeds; iii) operator intervention. However, while conventional seeding can be effectively achieved by inoculating 10% by weight of seeding load, the mass of crystals generated *in situ* under ultrasonic irradiation has to be more than 10 wt% to achieve comparable size and regular crystal shapes. The results showed that when the total mass nucleated under insonation was 20-40% of the quantity remaining dissolved at the time sonication was stopped, final crystals presented regular shapes, with less elongated hexagonal particles that after conventional seeding, and the product PSD was comparable with the PSD obtained from conventional seeding.

In conventional seeding operations, the temperature is held constant after the inoculation of the seeds to get effective results; on the contrary, using ultrasound at the beginning of cooling crystallization provided more effective results without interruption of cooling after sonication was stopped, with the further benefit of reduced operational times. In fact, insonated experiments without interruption of cooling produced more regular hexagonal shapes, with reduced elongation compared to experiments where

cooling was interrupted after the ultrasonic burst was stopped. We suppose that the initial crystals generated under ultrasonic treatment possess activated surfaces, and the increased surface energy favours growth processes; keeping the temperature constant after stopping ultrasound reduces the possibility to control the following unisonated stages of crystallization.

The effect of cooling rate was studied carrying out experiments where the ultrasonic burst was stopped after the same subcooling value. Faster coolings provided more regular particle shapes and reduced size. The effect of the duration of sonication was tested without interruption of cooling. Short insonation periods can be ineffective in avoiding a massive production of irregular shaped particles, while prolonged application of ultrasound after the nucleation onset (at same cooling rate value) improved the control over the final crystals shape and produced reduced sizes.

Crystal surface morphology analysed using atomic force microscopy revealed a birth and spread mechanism of growth after both conventional seeding and use of short ultrasonic burst. Crystal surfaces presented narrower terraces in the former case and a multilayer structure with larger terrace widths in the latter suggesting a growth process at higher supersaturation levels in conventional seeding than in the case of ultrasonic action.

CHAPTER 9

CONCLUSIONS AND FUTURE WORK

9.1 Conclusions

Crystallization is a technique which involves the formation of an ordered solid phase from a homogeneous gas, liquid or amorphous phase. The application of power ultrasound to crystallizing systems appears to offer significant potential for controlling and improving both processes and products. The main reason why ultrasound can bring such a significant influence to crystallization process is on account of its effects on crystallization kinetics. Ultrasound can influence nucleation, both primary and secondary, crystal growth, agglomeration and breakage processes. However the works presented in the literature refer to batch crystallization operations and focus principally on the ultrasonic impact on the kinetics of primary nucleation.

This thesis focuses first on the ultrasonic effect on a continuous crystallization process. Continuous crystallization is an attractive method for large-scale preparation of crystalline materials and promising in terms of improved economic performance and of controllability on the physical properties of the product for industrial processes.

The case study is cooling crystallization of adipic acid, a compound mainly used for production of nylon 6,6 but also with large application in food and pharmaceutical industry, from aqueous solution.

An experimental investigation has been carried out to probe the effect of continuous insonation on the physical properties of crystals and solid recovery at steady state operating conditions. Particle properties investigated include both the size distribution, determined using Malvern MasterSizer-S, and the crystals' habit at steady state, investigated using an optical microscope and scanning electron microscopy.

Experiments have been carried out at bench scale of 300 ml, comparing results produced in silent conditions with those achieved under continuous ultrasonic irradiation. In the first case, mixing was provided by a marine type propeller set at the maximum rotational speed to prevent any visible formation of bubbles, in the latter, with mixing enhancement induced by insonation, by a magnetic stirrer, set at the minimum rotational speed value to ensure a visible suspension of crystals in the slurry and minimize the fragmentation caused by impact with the stirring bar. This precaution allows distinguishing the eventual breakage effect of ultrasound and the maximum breakage conditions under silent conditions with the selected propeller.

Insonation was provided by means of ultrasonic processor with the frequency of 20 kHz and maximum nominal power of 750W.

In both silent and insonated conditions, experiments were carried out at three different mean residence time values. Sonicated experiments were carried regulating the ultrasonic power at 40% or 60% of power amplitude. Two different inlet concentration values were adopted for sonocrystallization experiments at the maximum selected sonication power, corresponding to a solubility temperature of 40 and 50 °C according to Mullin (2001). The study assessed the influence of these three input parameters on the time required to reach steady state conditions in terms of particle size distribution, relative supersaturation at the steady state hence yield, crystal size distribution (CSD) and crystal habit.

It was found that a continuous insonation throughout the continuous crystallization operation significantly affects both the process and the final product. Ultrasonic treatment shortens the time to attain steady state conditions in terms of particle size distribution, reduces the final concentration (and supersaturation) leading to increased yield values.

The influence of ultrasound on the crystal morphology and particle size distribution appears significant. SEM photomicrographs and PSDs of adipic acid crystals produced with and without sonication were compared to recognize eventual agglomeration and/or fragmentation phenomena. The micrograph clearly indicated that crystals produced under non sonicated conditions tend to form agglomerates while PSD measurements revealed a wide span in the particle size distribution. Crystals produced under continuous sonication present superior crystal habit and an even distribution of sizes with reduced agglomerative phenomena, and the presence of fragments suggests attrition phenomena. The corresponding size distribution curves are narrowed and shifted towards smaller size values. The explanation for the ultrasonic influence on the habit and size distribution of final crystals can be ascribed to the mechanical disruption of crystals or de-agglomeration caused by the shock wave released after transient cavitation collapse, results already documented in the case of batch operating conditions.

Finally, the crystal encrustation on baffles, propeller and probes resulted significantly reduced in insonated experiments, while the fouling on cooling surfaces

appeared comparable in silent and sonicated experiment, although insonated experiment needed lowers cooler liquid temperatures, with temperature gradient up to 20°C at the walls, to keep the system thermostated at isolation temperature. The liquid jet resulting by cavitational collapse near an extended solid surface, producing "cleaning" effects, can explain this phenomenon.

In the second section of this thesis, the population balance, in terms of equation of moments, has been used to estimate the kinetics of both nucleation and growth crystallization processes in order to extrapolate the effect of residence time, ultrasound power amplitude, and inlet concentration. The kinetic investigation has been carried under the assumption of Mixed-Suspension and Mixed-Product-Removal operating conditions for the continuous system. The results reveal a decrease in both the growth rate and the nucleation values occurs as the residence time is increased in every considered condition. This result can be easily explained considering that the driving force for both processes, the supersaturation at steady state, decreases with increasing values of τ. The effect of residence time on kinetic of growth appears more relevant in the case of non-sonicated conditions. The results indicate a reduction of the growth rate as continuous insonation is applied, with increasing extent as the power ultrasound increases. In addition, higher values of the inlet concentration leads to slightly increased values for the linear growth rate.

The application of ultrasound resulted in more significant effects on the nucleation process, in fact the nucleation rate values are increased up to 13 fold comparing the results without sonication with those with ultrasound. The effect of residence time on the nucleation rate appears more marked in the case of non-sonicated conditions, where the nucleation rate appears reduced by 3.4-3.7 fold for every increase of 10 min in τ. The estimated values of B^0 under continuous sonicated conditions result one order of magnitude higher than those achieved without sonication.

Increasing the power ultrasound leads to a slight increase in the nucleation rates values while the effect of solute content in the feed stream appears more marked than in the growth rate case: that could be linked to the higher solute content in the solution, resulting in higher steady state supersaturation and nucleation rates throughout the continuous run. However the influence of inlet concentration has been recognized only for the lowest residence time values investigated.

In the second part of the kinetic investigation, the correlation between both the rates of nucleation and growth and the supersaturation has been examined. The values of the apparent order of growth g estimated under non sonicated conditions are close to the unity indicating a diffusion controlling mechanism for crystal growth. The values for the g coefficient for insonated applications result higher but still in the range 1-2, suggesting an enhancement of the diffusional mass transfer of additional units from the bulk to the surface of growing crystals under ultrasonic irradiation. Ultrasound noticeably enhances the apparent order of nucleation almost redoubled from a value 1.49 without sonication to a value between 2.81 and 3.35 with sonication, whilst the effect on the apparent order of growth seems to be less remarkable. The results indicate a negligible effect of power amplitude and inlet concentration.

The Midlarz and Jones three parameters (MJ3) model for size dependent growth has been considered to fit the non-linearity in the population density distribution plot, presenting a sharp upward curvature for small crystal size values. The comparison resulted revealing only in the case of sonication at 40% of maximum power input and for crystal size value under 10 μm. As a result, the crystal growth could be deemed strongly size-dependent for smaller crystal sizes (under 10 μm), while for bigger crystals it could be evaluated from the slope of the linear population density plot as size independent rate. Attrition fragments can act as secondary nuclei and grow at different rates.

The commercial software package PARSIVAL (PARticle SIze eVALuation) has been used to estimate the kinetic of nucleation and growth at steady state in the continuous crystallization of adipic acid from aqueous solution. The population balance equation has been modeled with a secondary nucleation term, depending on supersaturation and magma density, and a growth rate depending from the supersaturation and the crystal size dependent. The growth rate expression has been tailored according to the Mydlard-Jones three parameter model. In the case of 40% power amplitude (the lowest ultrasonic intensity in this investigation), the model satisfactorily reproduce the experimental data points in the whole size range, both in the non-linear portion of the population density plot and in the linear part, where a size independent growth rate can be considered. It should be noted that the model tend to overestimate the experimental

data produced at higher ultrasound intensity values for $L > 20$ μm, predicting population density values up to 10 times bigger than the experimental ones.

The use of ultrasound in the particle engineering of micrometer scale adipic acid crystals has been implemented first with batch cooling crystallization of adipic acid from aqueous solution carried under continuous ultrasonic irradiation. The effect of ultrasound on the final product habit, size distribution and surface roughness was investigated. The results were compared with the product characteristics of industrial particle size reduction techniques consisting of either wet or dry grinding processes.

Among different types of dry milling operations commonly established, it was chosen Micronization, a fluid energy impact milling technique, and Hammer milling, where milling is achieved by mechanical impact.

The product characteristics were furthermore compared with the output of High Shear Wet Milling (HSWM), with particle size reduction operated directly into the product slurry of a batch crystallization, and of batch reverse antisolvent crystallization (RAS).

High power ultrasound combined with low initial solution concentrations resulted in the production of particle sizes comparable with the product of micronization, but with narrower size distribution and highly reproducible results.

Scanning electron photomicrographs of the particles produced showed that spherical habits are always obtained from continuously insonated crystallization. Furthermore, spherical particles were obtained even after insonation, under isothermal conditions, of supplied commercial material with poor and irregular habit. Conversely, micronization and hammer milling yielded irregular crystal habits and a massive presence of rod-shaped particles.

High Shear Wet Milling at the end of batch crystallization produced rounded shaped elongated particles and provided significant particle reduction; however, final particles were larger than those obtained after micronization and batch sonocrystallization at the highest power input investigated.

Reverse antisolvent crystallization of adipic acid in acetone (solvent) and heptane (antisolvent) provided the smallest particles, but of undefined shape. Aggregation was favoured by smallest produced sizes resulting in a bi-modal population in the final product.

The application of ultrasonic waves with batch and continuous crystallization produced micron sized spherical particles in a single-step operation from solution to particles. By removing the need of milling, the process avoids associated problems of dusting and reduction of yields, saves the time and expenses required for milling, eliminates the personnel contact with the produced agent and provides highly reproducible results. Surface analysis and roughness measurements revealed an increased surface roughness in crystals produced after continuously insonated batch crystallization compared to those from micronization and high shear wet milling, again with higher reproducibility in the results. Ultrasonic energy can be used in crystallization to yield advantageous control of the mean size and size distribution of resulting crystals, providing regular shapes and even distribution of crystal surface roughness in a single operation.

The assessment of the use of ultrasound in the particle engineering of adipic acid from aqueous solution was also addressed to the production of large crystals. Inoculation of seeds in supersaturated solutions is commonly employed for a growth dominated crystallization: the control of the final product characteristics is achieved by acting on the nucleation process and circumventing uncontrolled spontaneous primary nucleation. The effects of seed preparation method on the final product of the batch cooling crystallization of adipic acid in aqueous solution was analysed. Seeds were prepared by cooling crystallization with and without ultrasound and by grinding commercial crystals. The effects of cooling rate, initial concentration, seeding load, and supersaturation at the point of seeding on the crystal size distribution and crystal habit of the final product were studied as well, to characterize the conditions for the achievement of a growth-dominated operation.

A seed loading at 10% of the total mass of dissolved material ensured a near unimodal distribution of product crystal particles for any type of seed source investigated, while the largest sizes were achieved by cooling at 0.1 K/min. Higher values of initial concentration/temperature required slower cooling rates to maintain growth predominantly within the metastable zone. A slow cooling (0.1 K/min) applied exclusively during the first 10 °C subcooling and followed by a higher rate (0.5 K/min) provided large product crystal particles with reduced secondary nucleation, shortening the operation times.

Seeding with rounded shaped crystals, produced from a continuously insonated crystallization, resulted in a product of more regular crystal habit, with higher thickness than the product of seeding with conventionally ground material.

Finally, the use of a short ultrasonic burst at the beginning of a cooling crystallization has been investigated to achieve a growth dominated process and produce crystals with regular habit without the requirement of inoculation of seeds. The results of conventionally seeded crystallization experiments were compared with unseeded experiments where a short ultrasonic burst was applied before the beginning of cooling and was stopped a few minutes after the visible detection of the nucleation onset. A 10% of seed loading was chosen for conventionally seeded experiments, providing a unimodal size distribution and regular habit in the final product. Unseeded experiments where adipic acid was initially crystallised under insonation produced crystals with irregular habit and widespread size distributions. However, a short ultrasonic burst applied at the beginning of the cooling crystallization of adipic acid offered comparable advantages than conventional seeding, in terms of size distribution and a regular crystal shape, when approximately 20-40%wt of solute initially crystallizes under insonation. Furthermore, the use of a short ultrasonic burst offered the advantage of regular hexagonal particle shapes in the final product, with reduced elongation than after conventional seeding, especially when cooling was not uninterrupted after the insonation was stopped. Increasing the sonication power

provided more regular crystal habits and narrowed particle size distributions. Finally, a short ultrasonic burst applied exclusively at the beginning of the cooling was compared with an intermittent insonation regularly operated throughout the cooling. The same duration of an ultrasonic burst leaded to smaller particles when distributed throughout the cooling.

9.2 Future work

The literature reviewed in the second chapter documents that ultrasound can influence, among several mechanism involved in crystallization, secondary nucleation, crystal growth rate, agglomeration and breakage. Monitoring such processes strongly contributes in controlling the product quality of crystallization processes; however, successful application of ultrasound on crystallization processes is still difficult, mainly because the lack of understanding the influence of ultrasonic field on the physical and chemical processes involved.

Ultrasonic effects on nucleation have been compared in the available literature (Kordylla et al., 2009) with gassing, based on bubble expansion rather than on bubble implosion effects, showing comparable product characteristics. The mentioned work, however, shows agglomerated particles similar to those produced in this thesis work under silent conditions and uses ultrasonic devices at higher frequency levels. A future work is suggested to assess the effect of frequency on the physical characteristics of the final product in terms of habit and particle size distribution and on the pitting generated on metallic testing elements. It is recommended to distinguish the case of frequency values below 100 kHz from those at higher frequency values (300-400 Hz).

Average nucleation and growth rate values at steady state operating conditions in the continuous crystallization of adipic acid from aqueous solution have been evaluated by simultaneous contribution of secondary nucleation and size dependent growth. The combination of MJ3 model with secondary nucleation could be compared with other different size dependent growth models available in the literature. In Chapter5, PARSIVAL has been used to estimate the kinetic of nucleation and growth at steady

state in a continuous crystallization process under continuous insonation. According to the visual analysis of SEM photomicrographs showed in Chapter 3, agglomeration has been neglected and the population balance equation has been modeled by combining a secondary nucleation term with a size and supersaturation dependent growth model. A further work is recommended to estimate the kinetics of nucleation and growth for non insonated continuous operations, taking agglomeration into account and comparing different kernels available in the literature. In fact, microscope pictures in chapter 3 show a noticeable difference between the silent case and the insonated one in terms of crystal agglomeration and disruption.

Future works can be addressed to investigate the effect of surface activation (due to insonation) on agglomeration and crystal growth, particularly after the source of energy is stopped, by selecting different levels of magma concentration and different values of power ultrasound.

Finally, this work can be implemented with an experimental campaign to assess the effect of ultrasonic irradiation on both batch and continuous crystallization of compounds exhibiting polymorphisms and compounds characterized by wider metastable zone regions.

NOMENCLATURE

a	Solute activity
a^*	Solute activity in a saturated solution
A	Surface of growing crystal (§1.5)
A	Surface area of a layer of medium (2.2.3)
A_i	interfacial area of dissolving solute, cm^2cm^{-3}
A_T	Specific surface area of crystals
b	Apparent order of nucleation
B	Birth density function
B^0	nucleation rate, # $m^{-3}s^{-1}$
c	Propagation velocity of the sound wave
C	Steady state concentration of solute
C^*	Solubility concentration at operating vessel temperature
C_1	Concentration of inlet solution
C_2	Concentration of outlet mother liquor
c_{MJ}	Growth rate coefficient, μm
C_A	Solute concentration, $mol \cdot cm^{-3}$
C_i	Solute concentration at the interface between the layer dominated by diffusion and integration in the crystal growth process
C_p	Heat capacity at constant pressure, $J \cdot kg^{-1}K^{-1}$
C_S	Concentration of solute
C_S^*	Equilibrium concentration
C_{seed}	Mass fraction of seeds (mass of seeds/ total mass of dissolved adipic acid before seeding), %
c.v.	Coefficient of variation of the particle size distribution
C_v	Heat capacity at constant volume, $J \cdot kg^{-1}K^{-1}$
D	Death density function
D_t	Diameter of the transducer
d	Distance from radiation source

d_p	Propeller's blade diameter
E	Ultrasonic power input
E_w	Energy of the whole sound wave
f	Frequency of ultrasonic wave
g	Order of the overall crystal growth process
G	Linear growth rate, m/s
G_{feed}	Inlet mass in the interval Δt
G_{ml}	Product mother liquor mass in the interval Δt
ΔG	Free energy of cluster
ΔG_S	Surface free energy of cluster
ΔG_V	Volume free energy of cluster
ΔG_{crit}	Free energy of critical cluster
ΔG_s	Surface excess free energy
ΔG_v	Volume excess free energy
H_{40}	Liquid level for 40 ml solvent, mm
H_{50}	Liquid level for 50 ml solvent, mm
L	Characteristic crystal size
I	Sound wave intensity
k	Kinetic energy of an element of insonated medium
k	Numeric index of input and output streams
k_a	Dissociation constant (§3.2.1)
k_a	Surface shape factor
K_d	Diffusional mass transfer coefficient
K_G	Overall crystal growth coefficient
K_m	Intrinsic mass transfer coefficient, cm/s
K_N	Nucleation rate coefficient
K_p	Coefficient of inverse proportionality between induction time and nucleation rate

K_r	Integration reaction rate constant
k_v	Volume shape factor
L_T	Cumulative length of the particle distribution
$\overline{L}_{10}$	Mean size of particle size distribution
L_{43}	Volume mean diameter
L_s	Characteristic size of seeds, μm
L_{sp}	Characteristic size of final particles, μm
L_{wp}	Effective mean mass size of final particles, μm
m	Deposited solid mass
m_c	Mass concentration in the product stream
m_{feed}	Mass concentration in the inlet stream
m_g	Mass of a growing particle
m_j	j^{th} moment of the particle distribution
m_{ml}	Mass concentration in the mother liquor
m_0	Zero-th moment of he particle distribution
M_T	Specific mass of crystals
m_1	First moment of the particle distribution
m_2	Second moment of the particle distribution
m_3	Third moment of the particle distribution
n	Crystal population density
N	Distance of near field (Chapter 2)
N	Number of crystals per unit volume of slurry
N_f	Near field distance
n_0	Population density of nuclei
N_T	Total number of crystals in the system
P_a	Acoustic pressure

P_A	Acoustic pressure amplitude
P_i	Initial pressure of an adiabatically compressing gas
P_f	Final pressure of an adiabatically compressing gas
Q_f	Inlet mass flowrate, g/min
Q_k	Input and output streams to the volume V
r	Characteristic radius of cluster (assumed as spherical)
R	Volume of a sub-region in the particle phase space
r_c	Characteristic size of critical nucleus
r_i	Order of the integration reaction
R	Ideal gas constant
R_G	Mass deposition growth rate ($kg \cdot m^{-2}s^{-1}$)
S	Supersaturation ratio
S_C	Surface of cluster
S_e	Total particle fluid interface
S_m	Moving Surface of $V(t)$
S_S	Free surface of liquid in the vessel
t	Time
t_{ind}	Induction time
T_{feed}	Inlet temperature
T_i	Initial temperature in an adiabatically compressing gas, Chapter 2
T_i	Isolation temperature, Chapter 3
T_f	Final temperature of an adiabatically compressing gas
T_j	Temperature in the jacket
T_r	Temperature in the reactor
U	Uniformity, %
v	Vector particle phase-space velocity
v_s	Molar volume of the solute
V	Bulk volume

v_i	Internal component of the vector particle phase-space velocity
v_e	External component of the vector particle phase-space velocity
V_e	Volume occupied by the solid in the suspension
V_C	Volume of cluster
V_f	Final volume of an adiabatically compressing gas
V_i	Initial volume of an adiabatically compressing gas
v_N	Average particle velocity normal to the surface S_m
V_S	Solids-free volume of liquid
V_t	Volume of a layer of insonated medium swept by ultrasonic wave
w_{feed}	Mass fraction of Adipic acid at the inlet
w_{ml}	Mass fraction of Adipic acid in the product mother liquor
W_f	Mass of produced crystals, g
W_s	Mass of seeded crystals, g
x_0	Displacement amplitude
$Y\%$	Crystal yield
$Y_{max}\%$	Maximum allowable crystal yield, %
Y_t	Mass theoretical yield, g
α	Attenuation coefficient for the intensity
σ	Relative supersaturation
σ^2	variance of the particle size distribution
ρ	Density of an insonated medium element
ρ_c	Crystal density
ρ_s	Solid crystals density
γ	Heat capacity ratio
γ_i	Interfacial tension between the solid crystalline phase and the surrounding liquid
λ	Wavelength of sound

τ	Mean residence time

REFERENCES

AACA Pre-conference Workshop Perioperative Ultrasound, Nov. 5-6th 2006.

Abbas A., Nobbs D., and Romagnoli J.R., (2002) Investigation of on-line optical particle characterization in reaction and cooling crystallization systems. Current state of the art. *Measurements Science and Technology*, Vol. 13**,** 349-356.

Beckmann W., Nickisch K., Buddle U., (1998) Development of a Seeding Technique for the Crystallization of the Metastable A Modification of Abecarnil. *Organic Process Research & Development*, Vol.2, 298-304.

Beckmann W., (2000) Seeding the Desired Polymorph: Background, Possibilities, Limitations, and Case Studies. *Organic Process Research & Development*, Vol. 4, 372-383.

Biscans, B. (2004) Impact attrition in crystallization processes. Analysis of repeated impacts events of individual crystals. *Powder Technology*, Vol.143-144, 264-272.

Boussu K., Van der Bruggen B., Volodin A., Snauwaert J., Van Haesendonck C., Vandecasteele C., (2005) Roughness and hydrophobicity studies of nanofiltration membranes using different modes of AFM. *Journal of Colloid and Interface* Science, Vol. 286, 632–638.

Cains, P. W., McCausland L.J., and Martin P.D., (1999) "Sonocrystallization." *SPS Crystallization Manual*. Section 5.2. SPS, AEA Technology.

Cains, P. W., Martin, P. D., and Price, C. J., (1998) The use of ultrasound in industrial chemical synthesis and crystallization. 1. Application to synthetic Chemistry. *Organic Process Research & Development*, Vol.2, 34-48.

Caputo, G., Adami, R., Reverchon, E., (2008) Supercritical fluid crystallization of adipic acid using urea as habit modifier. *Crystal Growth & Design*, Vol. 8, No. 8, 2707-2715.

Clydesdale, G., Thomson, GB., Walker, EM., (2005) A Molecular Modeling Study of the Crystal Morphology of Adipic Acid and Its Habit Modification by Homologous Impurities. *Crystal Growth & Design*, Vol. 5, No. 6, 2154-2163.

Costa, CBB; Da Costa, AC; Maciel, R., (2005) Mathematical modeling and optimal control strategy development for an adipic acid crystallization process. *Chemical Engineering and Processing*, Vol. 44, 737-753.

Cristensen, J. J., Hansen, C. D. and Izatt, R. M., (1976) Handbook of Proton Ionization Heats and Related Thermodynamic Quantities. J. Wiley, New York.

Devarakonda S., Evans J. M. B. and Myerson A.S., (2003) Impact of Ultrasonic Energy on the Crystallization of Dextrose Monohydrate. Crystal Growth & Design, Vol. 3, 741-746.

Dhumal R.S., Biradar S.V., Paradkar A.R., York P., (2008) Ultrasound Assisted Engineering of Lactose Crystals. Pharmaceutical Research, Vol.25, 2835-2844

Doctycz S.J. and Suslick K.S., (1990) Interparticle collision driven by ultrasound. Science, Vol. 247, 1067- 1069.

Dodds J., Espitalier F., Louisnard O., Grossier R., David R., Hassoun M., Baillon F., Gatumel C., and Lyczko N., (2007) The Effect of Ultrasound on

Crystallisation-Precipitation Processes: Some Examples and a New Segregation Model. *Particle & Particle System, Characterization*, Vol. 24, 18-28.

Doki N., Sato A., Yokota M., (1999) Scaleup experiments on seeded batch cooling crystallization of potassium alum. *AICHE Journal*, Vol.45, No.12, 2527 -2533.

Doki N., Yokota M., Nakamura H., Sasaki S., Kubota N., (2003) Seeded batch crystallization of Adipic Acid from Ethanol Solution. *Journal of Chemical Engineering of Japan*, Vol.36, No.8, 1001-1004.

Dong C, Sharma S.K.. and Mudhoo A.., (2012) Handbook on Application of Ultrasound: Sonochemistry for Sustainability. CRC Press.

Eckart C., (1948) Vortices and Streams Caused by Sound Waves. *Physical Review*, Vol.73, No.1, 68-76.

Eksteen J.J., Pelser M.,. Onyango M.S, Lorenzen L., Aldrich C. , Georgalli G.A., (2008) Effects of residence time and mixing regimes on the precipitation characteristics of CaF2 and MgF2 from high ionic strength sulphate solutions. *Hydrometallurgy*, Vol. 91 104–112.

Fun H. and Chantrpromma S., (2009) A triclinic polymorph of hexanedioic acid. Acta Crystallographica Section E- Structure Reports Online, Vol. 65, 624.

Garside J. and Davey R.J. (1980) Secondary Contact Nucleation: Kinetics, Growth and Scale-up. *Chemical Engineering Communication*, Vol. 4, 393-424.

Gracin S. and Åke C. R., (2004) Polymorphism and Crystallization of p-Aminobenzoic

Acid. *Crystal Growth & Design*, Vol. 4, 1013-1023.

Gracin S., Uusi-Penttilä M. and Åke C. R., (2005) Influence of ultrasound on the nucleation of polymorphs of p-aminobenzoic acid. *Crystal Growth & Design*, Vol. 5, 1787 -1794.

Guo Z., Zhang M., Li H., Wang J., and Kougoulos E., (2005) Effect of ultrasound on anti-solvent crystallization process. *Journal of Crystal Growth*, Vol.273, 555-563.

Guo Z., (2007) Ultrasonic effects on Crystallization Processes, PhD Thesis, University College London.

Hajratwala B.R., (1982) Particle Size Reduction by a Hammer Mill I: Effect of Output Screen Size, Feed Particle Size, and Mill Speed. *Journal of Pharmaceutical Science*, Vol. 71, 188–190.

http://pdf.directindustry.com/pdf/silverson-machines/silverson-corporate-brochure/15561-163714-_4.html

Hulburt H. M., Katz S., (1964) Some Problems in Particle Technology - A Statistical Mechanical Formulation. *Chemical Engineering Science*, Vol. 19, 555-574.

J. am Ende D. and Rose P. R., Strategies to Achieve Particle Size of Active Pharmaceutical Ingredients, in *Fundamentals of early clinical drug development*, Abdel-Magid A.F. and Caron S. Eds., Wiley-Interscience (2006), 254-260.

Johnson K.C. and Swindell A.C., (1996) Guidance in the Setting of Drug Particle Size Specifications to Minimize Variability in Absorption. *Pharmaceutical Research*,

Vol.13, 1795 -1798.

Jones A.G.., (1974) Optimal operation of a batch cooling crystallizer. *Chemical Engineering Science*. Vol. 29, 1075-1087.

Kaerger J.S and Price R., (2004) Processing of Spherical Crystalline Particles via a Novel Solution Atomization and Crystallization by Sonication (SAXS) Technique. *Pharmaceutical Research*, Vol.21, 372-380.

Kempkes M., Vetter T., Mazzotti M. (2010) Monitoring the particle size and shape in the crystallization of paracetamol from water. Chemical Engineering Research and Design, Vol. 88 , 447–454.

Kordylla A., Krawczyk T., Tumakaka F., Schembecker G. (2009) Modeling ultrasound-induced nucleation during cooling crystallization. *Chemical Engineering Science*, Vol. 64, 1635-1642.

Li H., Wang J., Bao Y., Guo Z., Zhang M., (2003) Rapid sonocrystallization in the salting-out process. *Journal of Crystal Growth*, Vol. 247, 192–198.

Li X., Song X., Liu G., Yu J., (2009) Size-dependent nucleation and growth kinetics model for potassium chloride—Application in Qarhan salt lake. *Journal of Crystal Growth*, Vol.311, No 11, 3167-3173.

Louhi-Kultanen M., Karjalainen M., Rantanen J., Huhtanen M. and Kallas J., (2006) Crystallization of glycine with ultrasound. *International Journal of Pharmaceutics*, Vol. 320, 23 -29.

Lyczko N., Espitalier F., Louisnard O., Schwartzentruber J., (2002) Effect of ultrasound on the induction time and the metastable zone widths of potassium sulphate. *Chemical Engineering journal*, Vol. 86, 233-241.

Luque de Castro M.D., Priego-Capote F., (2007) Ultrasound-assisted Crystallization. *Ultrasonics Sonochemistry*, Vol. 14, 717–724.

Martell, A. E.; Smith, R. M., (1976) *Critical Stability Constants*, Vol. 1 - 4, Plenum Press: New York.

Mason T.J., (1997) ***Ultrasound in synthetic organic chemistry.*** Chemical society reviews, Vol.26, 443-451.

Mason T.J., Lorimer J.P., (2002) ***Applied sonochemistry: the uses of power ultrasound in chemistry and processing***. Wiley-WCH, pp.25-32.

McCausland L.J., Cains P.W., Martin P.D., (2001) Use the power of sonocrystallization for improved properties. *Chemical engineering progress*, 56-61 – www.alpha.aiche.org.

Mersmann A., (2001) ***Crystallization Technology Handbook***. Marcel Dekker, Inc. New York Basel, 2nd edition.

Michaels A. S., Colville A. R., (1960) The effect of surface active agents on crystal growth rate and crystal habit. *The Journal of Physical Chemistry*, Vol.64, No.11, 13-17.

Mydlarz J., Jones A.G., (1993) On the estimation of size-dependent crystal growth rate functions in MSMPR crystallizers. *The Chemical Engineering Journal*, Vol.53,

125-135.

Mydlarz J. and Jones A.G. (1993) On the estimation of size-dependent crystal growth rate functions in MSMPR crystallizers. *The Chemical Engineering Journal*, Vol.53, 125-135.

Mydlarz J. and Jones A.G. (1994) An assessment of MSMPR crystallization kinetics data for systems modelled by size-dependent crystal growth rate functions. *The Chemical Engineering Journal*, Vol.55, 69-80.

Midler, M., Paul, E. L., Whittington, E. F., Futran, M., Liu, P. D., Hsu, J., Pan, S.-H. *U.S. Patent* 5,314,506, 1994.

Miers H.A and Isaac F., (1907) The spontaneous crystallization of binary mixtures. Experiments on Salol and Betol. *Proceedings of the Royal Society of London*. Vol.79, 322-351.

Mosharraf M. and Nystrom C., (1995) The effect of particle size and shape on the surface specific dissolution rate of microsized practically insoluble drugs**.** *International journal of Pharmaceutics*, Vol.122, 37-47.

Mullin, J. W. (2001) ***Crystallization***, Paperback edition, Butterworths London.

NIST ChemistryWebBook, National Institute of Standards andTechnology (NIST), USA, http://webbook.nist.gov/chemistry/.

Owens E.P.K. and De Jong E.J., (1973) A Model for Secondary Nucleation in a Stirred Vessel Cooling Crystallizer. Industrial and Engineering Chemistry fundamentals,

Vol.12, 179-184.

Patist A. and and Bates D., (2008) Ultrasonic innovations in the food industry: From the laboratory to commercial production. Innovative Food Science & Emerging Technologies, Vol.9, 147-154.

Pellek A. and Arnum, P.V. (2008) Continuous processing: Moving with or against the Manufacturing Flow. Pharmaceutical Technology, Vol.9, 52-58.

Paul E.L., Atiemo-Obeng V.A., Kresta S.M., (2004) ***Handbook of industrial mixing***, Chapter 10, Wiley Interscience, 2004.

Paul, E. L., Tung, H. and Midler, M. (2005) Organic crystallization processes. Powder Technology, Vol.150, 133-143.

Randolph A.D., Larson M.A., (1988) ***Theory of Particulate Processes. Analysis and techniques of continuous crystallization***, Academic Press Inc San Diego, 2nd edition.

Rauls M., Van Gelder R., Wagner K., Bernard H.,(2003) Small particle-adjustment crystallization process .U.S. Patent 2003/0051659 A1.

Ristic R.I., Finnie S., Sheen D. B., and Sherwood J. N., (2001) Macro- and Micromorphology of Monoclinic Paracetamol Grown from Pure Aqueous Solution. *Journal of Physical Chemistry*, Vol. 105, 9057-9066.

Ruecroft G., Hipkiss D. , Ly T., Maxted N., Cains P. W., (2005) Sonocrystallization: The Use of Ultrasound for Improved Industrial Crystallization. *Organic Process Research & Development*, Vol. 9, 923-932.

Santos H.M., Lodeiro C., and Capelo-Martinez J.L. The Power of Ultrasound, from http://www.wiley-vch.de/books/sample/3527319344_c01.pdf

Shekunov B.Y. and York P., (2000) Crystallization processes in pharmaceutical technology and drug delivery design. *Journal of Crystal Growth*, Vol. 211, 122-136.

Sommer M., Stenger F., Peukert W., Wagner N.J., (2006) Agglomeration and breakage of nanoparticles in stirred media mills-a comparison of different methods and models. *Chemical Engineering Science*, Vol. 61, 135 – 148.

Srinivasa Gopalan R., Kumaradhas P., and Kulkarni G.U. (1999) Structural Phase Transition in Adipic Acid. *Journal of Solid State Chemistry*, Vol.148, 129-134.

Suslick K.S., Doktycz S.J., and Flint E.B., (1990) On the origin of sonoluminescence and sonochemistry. *Ultrasonics*, Vol.28, 280-290.

Suslick K.S., (1990*) Sonochemistry*. Science, Vol.247, 1439-1069.

Swarbrick J. (2007) ***Encyclopedia of Pharmaceutical Technology***, 3rd Ed., Informa Healthcare USA, Inc.

TaiC.Y. and Chen P-C., (1995) Nucleation, Agglomeration and Crystal Morphology of Calcium Carbonate. *AIChE Journal*, Vol.41, 68 -77.

Thompson L.H.and Doraiswamy L. K., (2000) The rate enhancing effect of ultrasound by inducing supersaturation in a solid-liquid system. *Chemical Engineering Science*, Vol. 55, 3085-3090.

Yang C-L., Randolph A. D., (1999) Crystallization of sodium nitrate from aluminum

and cesium containing liquors. *Chemical Engineering Communications*, Vol. 171, 135-149.

Young F.R, (1989) *Cavitation*. Imperial Collge press, 6.

Ward J.D., Mellichamp D.A., Doherty M.F., (2006) Choosing an operating policy for seeded batch crystallization. *AICHE Journal*, Vol.52, No.6, 2046-2054.

White E.T., Bendig L.L., Larson M.A., (1976), The effect of size on the growth rate of potassium sulphate crystals. *AIChE J. Symposium*. Ser. 153, 41-47.

Wulkow M., Gerstlauer A., and Nieken U., (2001) Modeling and simulation of crystallization processes using parsival. *Chemical Engineering Science*, Vol. 56, 2575-2588.

Wulkow M. (2007) Simulation Package for Particle Balances. Parsival Tutorial manual.

www.gec.jp/JSIM_DATA/WASTE/WASTE_2/html/Doc_363_1.html

www.innocalsolutions.com/catalog/product_view.asp?sku=0471140

www.jetpharma.com

www.olympus-ims.com/en/ndt-tutorials/transducers/characteristics/

www.pharmpro.com: Alpine Product Manager Hosokawa Micron Powder Systems,

Advances in Powder micronization Tecnology for the Pharmaceutical industry, *The Journal of Pharmaceutical Processing*.

www.sonicsystems.co.uk/tech_paper.html

www.sonochemistry.info/Research.htm

www.sreenex.com/html/double-cone-blender-suppliers-delhi-india-bulk_airjetmill.htm

http://www.wiley-vch.de/books/sample/3527319344_c01.pdf)

Zauner R., and Jones, A.G., (2000) Determination of nucleation, growth, agglomeration and disruption kinetics from experimental precipitation data: the calcium oxalate system. *Chemical Engineering Science*, 55, 4219-4232.

Zauner R., (1999) Scale-up of Precipitation Processes, *PhD Thesis*, University College London.

PUBLICATIONS

Refereed journals publications

1. Narducci O., Jones A.G., Kougoulos E. (2011) Continuous crystallization of adipic acid with ultrasound. *Chemical Engineering Science*, Vol. 66, 1069–1076 (Chapter 3).
2. Narducci O., Jones A.G., Kougoulos E. (2011) An Assessment of the Use of Ultrasound in the Particle Engineering of Micrometer-Scale Adipic Acid Crystals. *Crystal Growth & Design*, Vol. 11, 1742–1749 (Chapter 6).
3. Narducci O., Jones A.G., Kougoulos E. (2011) Crystal Product Engineering in the Seeded Cooling Crystallization of Adipic Acid from Aqueous Solution. *Organic Process Research & Development*, Vol. 15, 974–980 (Chapter 7).
4. Narducci O., Jones A.G. (2012) Seeding In Situ the Cooling Crystallization of Adipic Acid using Ultrasound. *Crystal Growth & Design*, ASAP (Chapter 8).

Conferences

1. 2009 Annual Conference of the British Association for Crystal Growth
6-8 September 2010, Bristol
Oral Presentation: Continuous Crystallization of Adipic acid with Ultrasound

2. 9th International Workshop on Crystal Growth of Organic Material (CGOM9)
4-7 August 2010, Singapore
Oral Presentation: Effect of Ultrasound in the Particle Engineering of Adipic acid Crystals

3. 2010 Annual Conference of the British Association for Crystal Growth
5-7 September 2010, Manchester
Poster Presentation: Seeding the cooling crystallization of adipic acid with Ultrasound